

DESIGN OPTIMIZATION OF AN
ELASTICALLY SUPPORTED MULTI-BEAM ROTORDYNAMIC SYSTEM
TO MINIMIZE FLEXURAL RESPONSE
WITH CONSIDERATIONS FOR ROBUSTNESS

by

BRET R. HAUSER

Presented to the Faculty of the Graduate School of
The University of Texas at Arlington in Partial Fulfillment
of the Requirements
for the Degree of

DOCTOR OF PHILOSOPHY IN MECHANICAL ENGINEERING

THE UNIVERSITY OF TEXAS AT ARLINGTON

May 2020

Copyright © by Bret R. Hauser 2020

All Rights Reserved



Dedication

To my wife, Karen

Acknowledgements

I am most grateful for the wisdom and guidance shown to me by my Supervising Professor, Dr. Bo P. Wang. His interest, critique and encouragement have been a source of inspiration for me and have made this research effort a very valuable process.

I would also like to express my appreciation to the following professors within UTA's Department of Mechanical and Aerospace Engineering for serving on my Dissertation Committee; Dr. Kent Lawrence, Dr. Alan Bowling, Dr. Brian Dennis and Dr. Daejong Kim.

My deepest gratitude goes to my wife, Karen. Without her daily love, support and sacrifice this work could not have been attempted.

Abstract

DESIGN OPTIMIZATION OF AN ELASTICALLY SUPPORTED MULTI-BEAM ROTORDYNAMIC SYSTEM TO MINIMIZE FLEXURAL RESPONSE WITH CONSIDERATIONS FOR ROBUSTNESS

Bret R. Hauser, PhD Candidate

The University of Texas at Arlington, 2020

Supervising Professor: Bo P. Wang, PhD

Modern rotating machines are often required to operate with a small physical footprint and/or overall weight; necessitating that they utilize wide-ranging shaft speed to accomplish needed power levels. It is not uncommon that these designs also be required to support operation through a speed range encompassing multiple Critical Speeds while also limiting flexural vibrations to acceptable levels. Design optimization of this class of problem can be particularly difficult in that responses can be highly multi-modal and, when coupled with Finite Element (FE) solvers meet the conditions of a High Dimensional, Computationally Expensive Black Box (HEB) system. Because of this, some conventional optimization methodologies have limited effectiveness or efficiency due to challenge with 'crossing' local maxima in search of the optimal solution. Additionally, conventional optimization methods that might be employed for HEB functions do not provide information regarding the Robustness of the identified solution.

An efficient 2-step method is developed using a modification of the conventional first-order method of Steepest Descent followed by a more efficient Sequential Quadratic Programming method to identify optimal solutions. A deterministic penalty method as well as programmatic considerations make the modified first-order method applicable to constrained searches. A Rotordynamic FE code is developed as part of this work leveraging both Eigenanalysis and Component solutions of the EOM as efficient methods for identifying Critical Speed frequencies and flexural responses. With the addition of considerations for Robustness during the optimization process, an efficient and practical tool is developed to guide the user regarding solutions to the HEB Rotordynamic design problem.

Table of Contents

Acknowledgements	iv
Abstract	v
List of Illustrations	ix
List of Tables	xii
Chapter 1 Introduction.....	1
Background and Motivation	1
Objectives, Scope and Significance of the Research.....	3
Unique Aspects and Contributions Resulting from the Research	4
Rotordynamic Example Problem	5
Variable Definitions.....	5
Objective Function	7
Constraints	7
Discretized Mapping Survey of Design Space	8
Literature and State of the Art	12
Fundamentals of Rotordynamic Systems.....	12
Rotordynamic Principle of Mass Inversion	15
Rotary Inertia and Gyroscopic Coupling.....	18
Mitigation Methods for Flexural Vibration of Rotordynamic Systems.....	22
Optimization Methods for Rotordynamic Systems	24
Optimization Methods for HEB Problems.....	28
Robustness and RBDO of Rotordynamic Systems	30
Chapter 2 Approach	32
Finite Element Model Development.....	32
Significant Model Features and Capabilities	32
General Programmatic Flow.....	33
Shape Function, EOM and Matrix Development.....	33
Eigenvalue Analysis – Critical Speed Characteristics.....	40

Steady-State Component Analysis – Flexural Response Characteristics	43
Optimization Method Development	44
General Programmatic Flow.....	45
Search Vector direction – Finite Difference and Magnitude Sensitivity	46
Search Vector Limitation within Feasible Design Space.....	47
Line search – Considerations for Constraints and High Modality Response	48
Use of a Single Objective Tool for Multi-Objective Optimization.....	51
Robustness Assessment	51
Chapter 3 Confirmation Challenges for Developed Software and Results	57
Rotordynamic Finite Element Model.....	57
Correctness Checks - Shape Function Equations:	57
Correctness Checks - EOM Matrix Equations:.....	57
Correctness Checks - Linearly Varying Geometry:	58
Correctness Checks - Assembled FEM Results – Static Deformations:.....	60
Correctness Checks - Non-Rotating Natural Frequencies and Mode Shapes:.....	61
Correctness Checks - Rotordynamic Results vs. Literature:.....	62
Optimization Methodologies	64
Deterministic Functionality – Non-Rotating Structural Dynamic Model.....	64
Deterministic Functionality - Rotordynamic Model	65
Deterministic Functionality – Proposed Method with Rotordynamic Model	66
Robustness Assessment	76
Optimization of Equation Coefficients	77
Identification of Local Minima / Maxima in the Toleranced Design Space.....	79
Confirmation – Challenge against Rotordynamic Problem	84
Conclusions – Robustness Code Challenges	86
Chapter 4 Demonstration of Practical Uses of Design Tool	89
Description of Demonstration Studies	89
Extension of Deterministic Optimization Study.....	89

Optimization of Systems with Internal Material Damping.....	91
Optimization of Systems with Internal Material Damping and Non-Isotropic Supports.....	93
Optimization of Systems with Negative Stiffness	95
Results of Demonstration Studies	98
Extension of Deterministic Optimization Study.....	99
Optimization of Systems with Internal Material Damping.....	102
Optimization of Systems with Internal Material Damping and Non-Isotropic Supports.....	109
Optimization of Systems with Negative Stiffness	115
Chapter 5 Summary and Conclusions	123
Chapter 6 Recommendations for Further Work	129
Appendix A Technical Paper – Hauser, Wang, <i>Structural and Multidisciplinary Optimization</i> , 2018	130
Appendix B Technical Paper – Hauser, Wang, <i>Structural and Multidisciplinary Optimization</i> , 2019	144
Appendix C EOM Development and Steady-State Solution for Jeffcott Rotor System	164
Appendix D EOM Development for Modified Jeffcott Rotor System	170
Appendix E EOM Development for Finite Element Program – MATLAB Source Code	174
Appendix F EOM Matrix Integration, Linearly Varying Geometry – MATLAB Source Code	188
Appendix G Shape Functions and EOM Matrices	192
Appendix H Robustness Evaluation – MATLAB Source Code (Toy Problem).....	197
Appendix I System Data File – Parallel Beam Example Problem.....	205
Appendix J Equation Development – Solution of EOM via Steady-State Component Analysis.....	209
Appendix K FEM Confirmation Test Results – Static Loading.....	215
Appendix L FEM Confirmation Test Results – Non-rotating vibration	218
Appendix M FEM Confirmation Test Results – Rotordynamic Code Comparison Output Plots	234
Appendix N Mode Shape Plots – Non-Isotropic Supports with Internal Material Damping	241
Biographical Information	246
References.....	247

List of Illustrations

Figure 1-1 Illustration of problem under study	1
Figure 1-2 Rotordynamic system responses	2
Figure 1-3 Schematic of rotordynamic model	5
Figure 1-4 Discretized Mapping Survey Results and GUO with Feasibility Bounds.....	9
Figure 1-5 Mapping Survey GUO Result with Refined Discretization.....	10
Figure 1-6 Discretized Mapping Survey Results with GCO with Feasibility Bounds	11
Figure 1-7 Mapping Survey GCO Result with Refined Discretization.....	12
Figure 1-8 Jeffcott (de Laval) Rotor and Free Body Diagram.....	14
Figure 1-9 Synchronous Whirl Critical Speed Inversion	15
Figure 1-10 Force Vector Polygon – Jeffcott Rotor	17
Figure 1-11 Amplitude and phase response of Jeffcott Rotor to Frequency Ratio.....	18
Figure 1-12 Modified Jeffcott Rotor with Extended Rotor	19
Figure 1-13 Campbell Plot	21
Figure 1-14 Eigenvalue relationship to frequency ratio – modified Jeffcott rotor.....	22
Figure 2-1 Nodal DOF (XY plane only).....	34
Figure 2-2 Steepest Feasible Descent Methodology.....	46
Figure 2-3 Flowchart – Feasible S_n Selection	48
Figure 2-4 Use of Penalty Function in 1-D Line Search	50
Figure 2-5 Pseudo-code – Robustness Application to Proposed SFD/SQP Optimization Process.....	52
Figure 2-6 Pseudo-code – Programmatic Term Expansion – Response Equation	55
Figure 3-1 Linearly varying conic element used for correctness checks – Creo	59
Figure 3-2 Example Beam Loading for Static FEM Confirmation	61
Figure 3-3 FEM models from literature used for code confirmation.....	63
Figure 3-4 Optimization test functions in 2D	65
Figure 3-5 Start Locations for Optimization	67
Figure 3-6 Start Locations 100-Pt Haltonset Trials (Test ID # 7).....	69
Figure 3-7 Optimization Paths – SFD & Proposed Hybrid (Test ID #1a, 1c).....	75

Figure 3-8 Optimization Paths – SQP (Test ID #1b).....	75
Figure 3-9 Optimization Path Summary – PSO and GA Methods	76
Figure 3-10 Pseudo-code – Optimization of Multinomial Expansion Coefficients	78
Figure 3-11 Robustness Code Response – Equation Fit to Rastrigin Centered on Local Minima	82
Figure 3-12 Robustness Code Response – Equation Fit to Rastrigin Centered on Local Maxima	83
Figure 3-13 Robustness Code Response – Equation Fit to Rastrigin in Transition Region	84
Figure 4-1 Mode Shape Plots – Non-Isotropic Behavior – Start Point #5	94
Figure 4-2 Illustration of Negative Stiffness Element Applied to Rotordynamic System	96
Figure 4-3 Design Variable Convergence Paths – Test ID #8c, Hysteretic Damping	104
Figure 4-4 FRP Bearing 2 Reaction Force – Test ID #8c, Hysteretic Damping – Start.....	106
Figure 4-5 FRP Bearing 2 Reaction Force – Test ID #8c, Hysteretic Damping – Optimum.....	106
Figure 4-6 FRP Shaft Tip Deflection – Test ID #8c, Hysteretic Damping – Start	107
Figure 4-7 FRP Shaft Tip Deflection – Test ID #8c, Hysteretic Damping - Optimum.....	107
Figure 4-8 Mode Shape Plots – Optimization Results for Non-Isotropic Support Stiffness.....	114
Figure 4-9 Optimization Convergence Paths – Negative Stiffness Study	117
Figure 4-10 Mode Shape Comparisons – Negative and Positive Stiffness Influence	120
Figure 4-11 FRP Plot Comparisons – Negative and Positive Stiffness Influence	121
Figure App-K-1 Static load FEM confirmation response – SS end conditions	216
Figure App-K-2 Static load FEM confirmation response – CS end conditions	216
Figure App-K-3 Static load FEM confirmation response – CC end conditions	217
Figure App-K-4 Static load FEM confirmation response – CF end conditions	217
Figure App-L-1 Non-Rotating FEM confirmation response – CC end conditions, mode 1	223
Figure App-L-2 Non-Rotating FEM confirmation response – CC end conditions, mode 2	223
Figure App-L-3 Non-Rotating FEM confirmation response – CC end conditions, mode 3	224
Figure App-L-4 Non-Rotating FEM confirmation response – CC end conditions, mode 4	224
Figure App-L-5 Non-Rotating FEM confirmation response – CC end conditions, XY mode shapes	225
Figure App-L-6 Non-Rotating FEM confirmation response – CC end conditions, XZ mode shapes.....	225
Figure App-L-7 Non-Rotating FEM confirmation response – CS end conditions, mode 1	227

Figure App-L-8 Non-Rotating FEM confirmation response – CS end conditions, mode 2	227
Figure App-L-9 Non-Rotating FEM confirmation response – CS end conditions, mode 3	228
Figure App-L-10 Non-Rotating FEM confirmation response – CS end conditions, mode 4	228
Figure App-L-11 Non-Rotating FEM confirmation response – CS end conditions, XY mode shapes.....	229
Figure App-L-12 Non-Rotating FEM confirmation response – CS end conditions, XZ mode shapes.....	229
Figure App-L-13 Non-Rotating FEM confirmation response – CF end conditions, mode 1	231
Figure App-L-14 Non-Rotating FEM confirmation response – CF end conditions, mode 2	231
Figure App-L-15 Non-Rotating FEM confirmation response – CF end conditions, mode 3	232
Figure App-L-16 Non-Rotating FEM confirmation response – CF end conditions, mode 4	232
Figure App-L-17 Non-Rotating FEM confirmation response – CF end conditions, XY mode shapes.....	233
Figure App-L-18 Non-Rotating FEM confirmation response – CF end conditions, XZ mode shapes.....	233
Figure App-M-1 Zorzi/Nelson - Non-Rotating Mode Shapes – Undamped Case.....	235
Figure App-M-2 Zorzi/Nelson – Campbell Plot – Undamped Case	235
Figure App-M-3 Zorzi/Nelson – Damped Eigenvalue Mode Shape Plots – Undamped Case	236
Figure App-M-4 Zorzi/Nelson – Frequency Response Plots – Undamped Case	237
Figure App-M-5 Vance - Non-Rotating Mode Shapes – $k=1.751e6$ N/m	237
Figure App-M-6 Vance – Campbell Plot - $k=1.751e6$ N/m	238
Figure App-M-7 Vance – Damped Eigenvalue Mode Shape Plots – $k=1.751e6$ N/m.....	239
Figure App-M-8 Vance – Frequency Response Plots – $k=1.751e6$ N/m.....	240
Figure App-N-1 Demonstration Mode Shape Plot – Starting Point 5	242
Figure App-N-2 Demonstration Mode Shape Plot – SFD Optimum	243
Figure App-N-3 Demonstration Mode Shape Plot – SQP Optimum.....	244
Figure App-N-4 Demonstration Mode Shape Plot – Hybrid (SFD+SQP) Optimum.....	245

List of Tables

Table 1-1 Fixed and variable model parameter definitions	6
Table 2-1 Nodal displacement vector definition	34
Table 3-1 Literature references used to confirm shape function equation correctness.....	57
Table 3-2 Literature references used to confirm EOM matrix correctness	58
Table 3-3 Confirmation Data – Geometric Mass Calculations.....	59
Table 3-4 Error Results – Geometric Mass Calculations	60
Table 3-5 Confirmation data – rotordynamic results vs literature	63
Table 3-6 Starting Region Definitions	68
Table 3-7 Deterministic Functionality – Rotordynamic Optimization Test Cases	70
Table 3-8 Deterministic Functionality – Rotordynamic Optimization Test Results	71
Table 3-9 Deterministic Functionality – Rotordynamic Optimization Result Comparisons.....	72
Table 3-10 Robustness Challenge Results (Rastrigin) – Equation Coefficient Determination.....	79
Table 3-11 Robustness Challenge Results (Rastrigin) –Minima / Maxima Locations	80
Table 3-12 Robustness Challenge Results (Rastrigin) –Minima / Maxima Response Values	81
Table 3-13 Robustness Challenge Results (Rotordynamic).....	85
Table 4-1 Robustness Input Parameters from Test ID #1c Results	90
Table 4-2 Model Parameter Definitions – Negative Stiffness Demonstration.....	97
Table 4-3 Design Space Definition Considering Feasible Space	99
Table 4-4 Results of Extended Robustness Study for Test ID #1c.....	101
Table 4-5 Design Variable Definition for Material Hysteretic Loss Factor Demonstration.....	103
Table 4-6 Optimization Results of Material Hysteretic Loss Factor Demonstration	104
Table 4-7 Objective Function Movement of Material Hysteretic Loss Factor Demonstration.....	104
Table 4-8 Robustness Results of Material Hysteretic Loss Factor Demonstration	108
Table 4-9 General Optimization Results of Non-Isotropic Support Stiffness Demonstration	109
Table 4-10 Objective Function Change - Non-Isotropic Support Stiffness Demonstration	111
Table 4-11 Robustness Results of Non-Isotropic Support Stiffness Demonstration	112
Table 4-12 Design Space Definition Considering Feasible Space	115

Table 4-13 General Optimization Results of Negative Stiffness Demonstration	116
Table 4-14 Robustness Results of Negative Stiffness Demonstration	118
Table 4-15 Negative vs Positive Stiffness Comparison	119
Table App-L-1 Non-Rotating FEM confirmation response – CC end conditions	222
Table App-L-2 Non-Rotating FEM confirmation response – CS end conditions	226
Table App-L-3 Non-Rotating FEM confirmation response – CF end conditions.....	230

Chapter 1

Introduction

Background and Motivation

Rotating machines are among the most common application of mechanical engineering¹, and designers are often required to create machines both increasing power output and constraints regarding decreased size, weight and cost. As a result, rotating equipment is often required to operate through large speed ranges, potentially incorporating one or more Critical Speeds. Such challenges exist across many industries including aerospace, mining, machine tools, medical devices, consumer appliance and others. Although very different in their application, these industries sometimes share the need to minimize one or more aspects of flexural deformation given some time-variant input load and with consideration for a set of design constraints. Although some of these problems can be solved with traditional 'planar' structural dynamics methods, the inclusion of a rotating degree of freedom (DOF) adds complication in that gyroscopic moments, cross-coupled forces and the possibility of whirling instability must be considered.¹ These factors serve to make the systems non-self-adjoint in that system matrices are asymmetric^{2,3,4,5} and optimization methods appropriate to non-rotating structural dynamic applications may not be appropriate.⁶

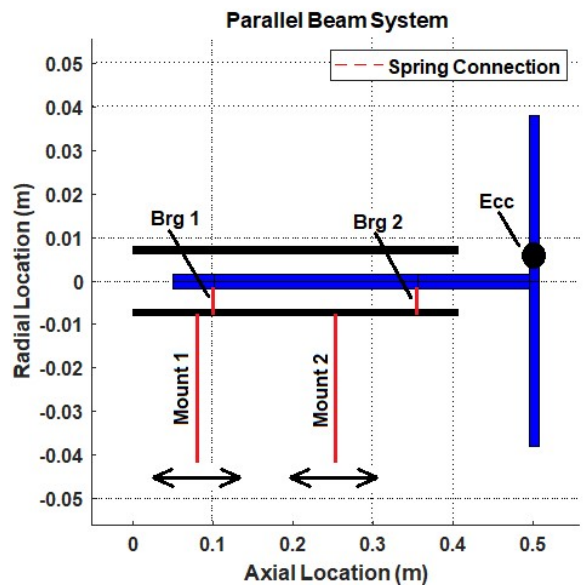
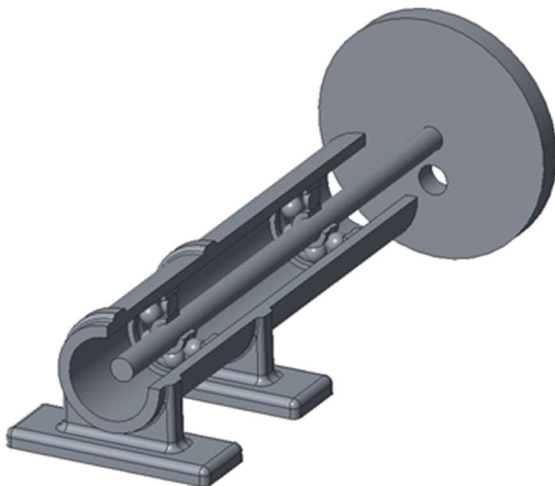


Figure 1-1 Illustration of problem under study

The previous figure illustrates a problem under study as a simple example of the Rotordynamic system; a rotating shaft housed within a non-rotating outer housing with elastic bearings and external mounting supports. Loading to the structure for this example is limited to a mass eccentricity on the end-mounted disk of the rotating shaft. To ensure that the system can operate safely across a wide speed range, flexural responses including bearing reaction forces and lateral shaft deformations are often identified as key parameters. For this academic example, the figure below provides a Frequency Response Plot of both tip deflection and bearing reaction force across a range of operating speeds, as well as a 3-dimensional representation of a sum of these parameters as might be used to optimize the location of the 2 non-rotating housing support locations.

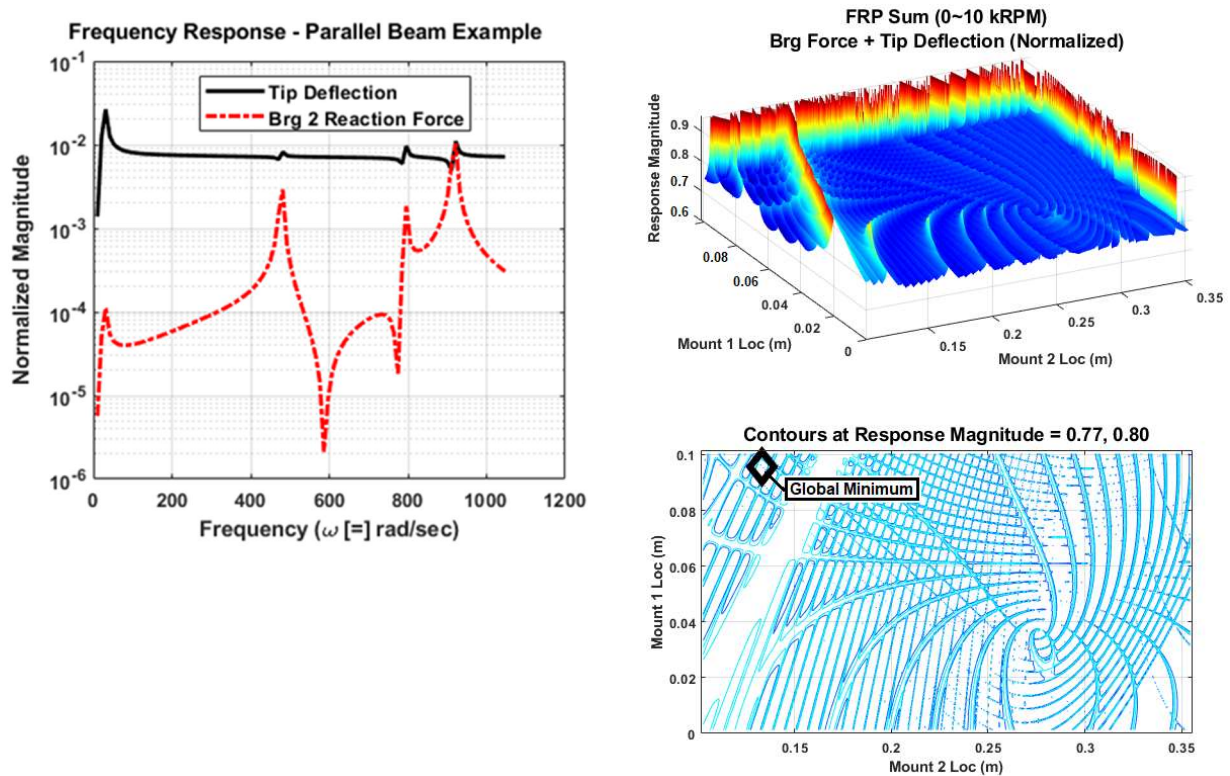


Figure 1-2 Rotordynamic system responses

As shown, these 'simple' responses can create a very challenging design problem. That is, the high modality response requires that the optimization method cross local maxima in search of a global, or even an acceptable, minimum. Although these challenges are not unique, the need is exaggerated here in comparison to many 'ordinary' design optimization problems. The high modality also underscores the

designer's need to consider effects of input variation on the response to identify an acceptably robust solution. Although some potential optimums may have more attractive values, the design space surrounding that solution may be more limiting with respect to input variation than a different solution with slightly higher function values. Further, if Finite Element Analysis (FEA) or a similar technique is used to evaluate the system then gradient information is not available to the Optimization process and the problem meets the criteria of a Black-Box system. When coupled with (potentially) high computational costs for each solve, then the system meets the classification of a High Dimensional, Computationally Expensive Black Box (HEB) system.

Robustness-Based Design Optimization (RBDO) has been explored in the context of Rotordynamic and HEB systems to solve this challenge. However, these optimization methods are often computationally intensive and therefore challenging to implement for multi-modal problems.

The result of these existing methods then is that designers of rotating machinery are limited to analysis and optimization methods that too-often are impractically lengthy and do not address business needs to find attractive, robust design solutions in a time-efficient manner.

Objectives, Scope and Significance of the Research

The key objective for this work is to develop and demonstrate a practical method for machine designers to efficiently optimize rotating systems with consideration for robustness. The proposed work focuses on 3 main areas:

- *Development of a special purpose Finite Element tool*
Provide efficient prediction of Critical Speed frequencies and flexural responses with consideration for Consistent Matrix development, Timoshenko shear theory, and internal material damping.
- *Development of an Optimization method*
Provide effective and efficient identification of multiple potential global optimums appropriate to constrained optimization for an HEB system.
- *Develop an efficient method of advising Robustness*

For each of the potential global optimums, effectively and efficiently provide a description of solution Robustness with respect to input variation with which the designer can subsequently identify preferred system solutions.

In addition to development of these tools, the scope of this project evaluates effectiveness and efficiency of the proposed methods. More specifically, the developed Rotordynamic code will be used with the proposed Optimization method for the example problem and results compared to other 'conventional' optimization methods identified in literature, as well as a discretized mapping of the 2-D design space. Further, the Robustness statements for various endpoints of the proposed Optimization method will be compared against the mapped response of the 2-D design space for practicality and usefulness to the Rotordynamic designer.

A successful conclusion to this work will develop and confirm that the tools are useful to designers of Rotordynamic machinery. Practicing engineers and scientists are commonly faced with the challenge of providing effective, safe solutions that can be implemented quickly to meet business objectives. As discussed previously, tools to accomplish this are limited in the field of rotating machinery; particularly when it comes to timely, optimized solutions. The work identified in this proposal holds the potential for significant business impact that can be both useful to Rotordynamic designers to achieve technical goals in a way that can be identified on the bottom line of a company's financial Income Statement.

Unique Aspects and Contributions Resulting from the Research

The primary unique contribution resulting from this work is the development of an Optimization method, that effectively considers Robustness for rotating systems where high modality and black-box function generators are used. A common practice in industry is to utilize optimization methods such as response-surface, genetic algorithm, particle swarm or the like to identify an optimal solution. These methods are not ideal for HEB systems and commonly lack the ability to provide robustness information. Commercial FE codes are commonly used to evaluate the system, but are normally written generically, to solve a variety of types of problems. As a result, they are often less efficient than a special purpose code;

carrying significant overhead with respect to file management, etc. This work then creates software tools in both of these areas that when combined, provide the rotordynamic system designer with an effective and efficient tool with which to meet both technical and business objectives.

Rotordynamic Example Problem

As illustrated previously, the example problem is a simplified form of a class of problem familiar to Rotordynamic designers. It features a single, rotating shaft with end-mounted disk supported by elastic bearings within a non-rotating (cylindrical) outer housing, in turn supported on elastic mounts to ground. The mass eccentricity of the end-mounted disk provides the source of excitation to the system. Schematically, the example problem is represented in the figure below. Note that the 'X' dimension is identified as the axial dimension. The 'Y' (shown) and 'Z' (not shown) dimensions are lateral and follow the conventional Right-Hand Rule. Although relatively simple in its academic form, this example problem is illustrative of Rotordynamic problems meeting the definition of an HEB function.

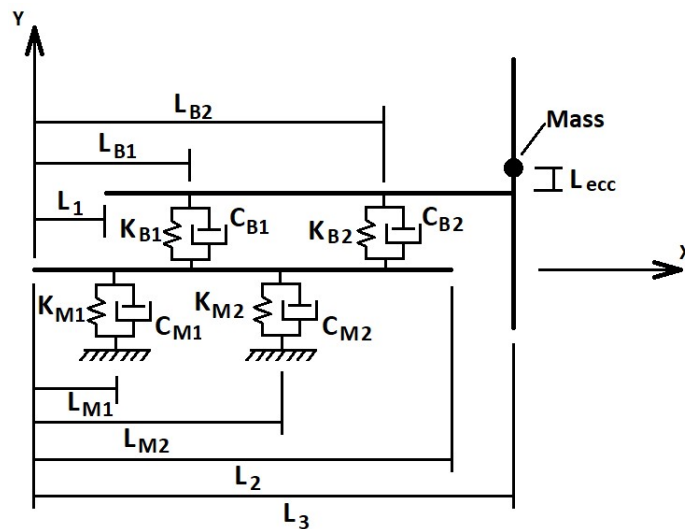


Figure 1-3 Schematic of rotordynamic model

Variable Definitions

The example problem of this work is limited to 2-DOF (design variables) ; location of the 2 'external' elastic mounts that constrain the outer housing to ground (L_{M1} and L_{M2}). In this way, a discretized mapping of the design space can be achieved for direct visualization and within a practical

time frame to map the objective response. The mapped response then is used as a means of comparison to evaluate the effectiveness of the optimization method developed under this work as well as responses from the other 'conventional' methods. Fixed and variable model parameters are defined in the table below. The rotating shaft is made of generic steel and the non-rotating housing from generic aluminum. Material damping is not considered for the initial example problem of this document, therefore both viscous damping coefficient and hysteretic loss factor values are set to '0'. (Material damping is included in the full/final 'demonstration of use' study as discussed later in this report.) Also, the example problem is defined with an operating speed range that encompasses multiple critical speeds.

Table 1-1 Fixed and variable model parameter definitions

		Fixed Parameter Value	Design Variable	
			Value	Tolerance ($\pm 0.25\%$)
L ₁	(m)	0.0508		
L ₂		0.4064		
L ₃		0.5080		
LM ₁			0 – 0.1016	± 0.00025
LM ₂			0.1016 – 0.3556	± 0.00025
LB ₁		0.1016		
LB ₂		0.3556		
L _{ecc}		1.27e-4		
OD _{Tube}	(m)	0.0080		
ID _{Tube}		0.0064		
OD _{Shaft}		0.0016		
OD _{Disk}		0.0381		
t _{Disk}		0.0127		
K _{M1} & K _{M2}	(N/m)	2.627e4		
K _{B1} & K _{B2}		2.627e6		
C _{M1} , C _{B2} , C _{B2} , C _{B2}	(N-s/m)	0		
Density _{steel}	(kg/m ³)	7833.4		
Density _{aluminum}		2698.8		
Modulus _{steel}	(N/m ²)	200e9		
Modulus _{aluminum}		69e7		
Poisson Ratio _{steel}	n/a	0.30		
Poisson Ratio _{aluminium}		0.33		
Speed Range	(RPM)	0 ~ 10 kRPM		

Objective Function

The example problem is defined to minimize both lateral deformation of the rotating beam's end-mounted disk and reaction force of bearing 'B2' (most distal shaft support); both as vector sums considering both 'Y' and 'Z' directions. Therefore, a 'single' objective function is defined for multi-objective use as shown in Eq. (1). Note that the portion of the objective function focused on the bearing reaction force (f_{obj_a}) is reduced by a factor of $1e4$ to create similar scale between the objective function components. Otherwise, the influence of tip deflection on the overall objective function would be minimized.

$$f_{obj} = f_{obj_a} + f_{obj_b}$$

where:

$$f_{obj_a} = \sum_{f=min}^{max} \frac{F_{Bearing\ B2\ Reaction}}{1e4} \quad (1)$$
$$f_{obj_b} = \sum_{f=min}^{max} \sqrt{(\delta_{UY})^2 + (\delta_{UZ})^2}$$

Constraints

Both input and output constraints are placed on the example problem. Input constraints include the side-bound limitation that the axial location for mounts 'M1' and 'M2' lie within the neighboring features. That is, mount 'M1' can move from the left end of the external housing to the axial location of bearing 'B1'. Similarly, mount 'M2' can range between bearings 'B1' and 'B2'. In addition, a minimum space of 0.0127 m is defined between support features to represent the physical width of the mounts and an assumption that they may not be superimposed for this example. These input constraints are provided in Eq. (2) below.

$$g_1 = 1 - \frac{L_{M1}}{0.0127}$$
$$g_2 = \frac{L_{M1}}{(L_{B1} - 0.0127)} - 1 \quad (2)$$
$$g_3 = 1 - \frac{L_{M2}}{(L_{B1} + 0.0127)}$$

$$g_4 = \frac{L_{M2}}{(L_{B2} - 0.0127)} - 1$$

An output constraint is also placed on the optimization to mitigate the potential for a solution that is ‘impractically flexible’. It is recognized that a theoretical solution to flexural vibrations (rotating or otherwise) might result in an optimum where the beam stiffness is insufficient for practical use. Therefore, this constraint function includes an evaluation of tip deformation to a static load as a means of assuring some minimally acceptable stiffness of the system. This output constraint is provided in Eq. (3) with a maximum static tip displacement of 0.0762 m allowed.

$$g_{result_i} = \frac{\sqrt{(\delta_{UY_st})^2 + (\delta_{UZ_st})^2}}{0.0762} - 1 \quad (3)$$

Discretized Mapping Survey of Design Space

The ‘Mapping Survey’ of Figure 1-2 is a discretized survey of the entire design space (without consideration for constraints), intended in part as a visual representation of the response to be solved. Key among the observations is the high modality of the response and significant ‘local’ and ‘transitory’ ridges; all providing significant challenge to the optimization of the system. It was conducted by evaluating the objective function of Eq. (1) with a small design space step size (2.54×10^{-4} m) as a compromise between being small enough to be practically useful in identifying a global minimum yet large enough to reduce computational burden of the mapping study. The selected discretization step size resulted in approximately 387,500 points across the 2D design space and, with an average function evaluation of approximately 2.2 sec, consumed approximately 3840 CPU-hrs.

The minimum unconstrained function value, or **Global Unconstrained Optimum (GUO)**, identified from the discretized mapping exercise is **0.721876 at the location $(L_{M1}, L_{M2}) = (0.095664, 0.133137)$** . The GUO is plotted for reference on Figure 1-2 and is used as a baseline for comparison among some optimization results discussed later in this report.

The input and response constraints of Eq. (2) and Eq. (3) can be applied to the discretized Mapping Survey. As shown in Figure 1-4, this results in large areas of infeasibility for the system (shown in red in the figure). The GUO (from Figure 1-2) is clearly illustrated as being within infeasible space.

Figure 1-5 is a 3D view of the local region surrounding the GUO bounded by the design variable tolerances ($\pm 0.00025\text{m}$ per Table 1-1). This 3D view uses a refined discretization (100 steps) within the applied tolerance bounds ($\pm 0.00025\text{m}$).

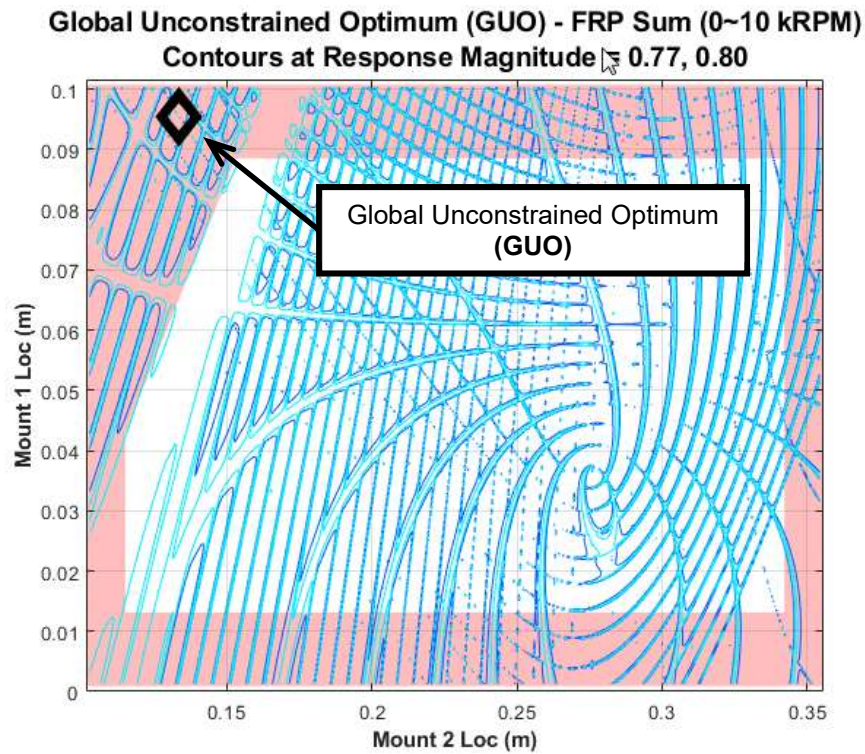


Figure 1-4 Discretized Mapping Survey Results and GUO with Feasibility Bounds

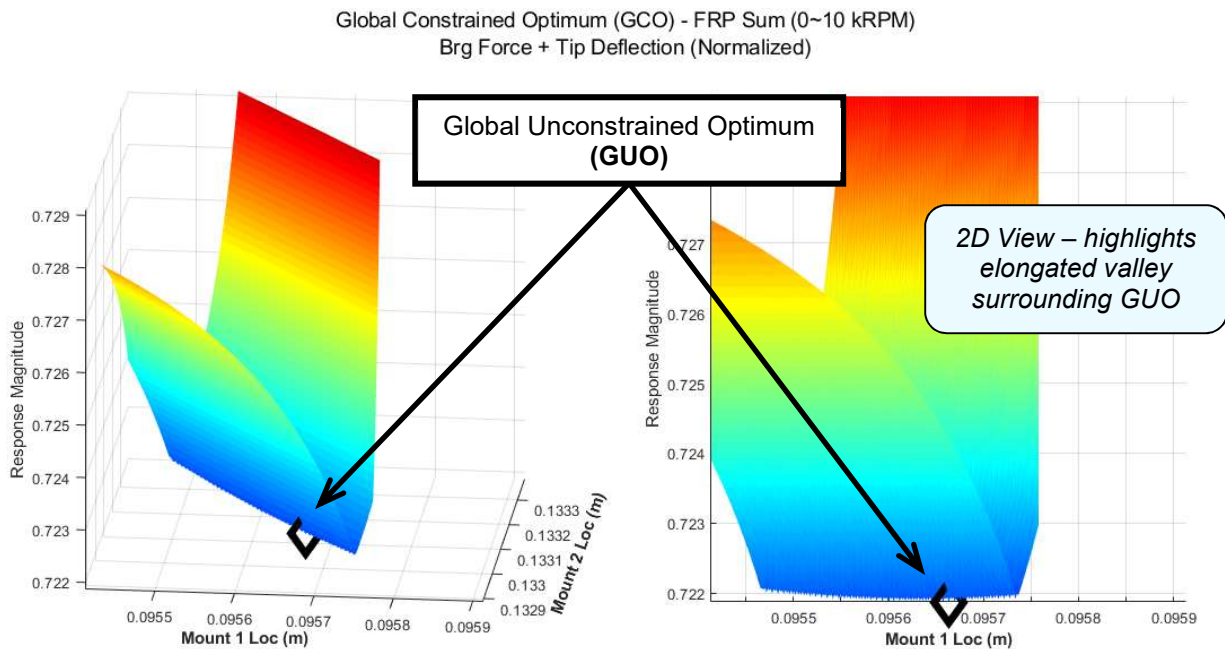


Figure 1-5 Mapping Survey GUO Result with Refined Discretization

Using constraints of Eq. (2) and Eq. (3), a **Global Constrained Optimum (GCO)** is identified from the discretized Mapping Survey as having a value of **0.730384** (*1.3% greater than the GUO*) **at the location $(L_{M1}, L_{M2}) = (0.073984, 0.197681)$** . This is illustrated in Figure 1-6 together with the constraint bounds. Also shown in Figure 1-6 is a 3D view of the local region surrounding the GCO bounded by the design variable tolerances ($\pm 0.00025\text{m}$ per Table 1-1) from the initial Mapping Survey. This 3D view illustrates the relative coarseness of the discretization steps of the initial Mapping Survey relative to the modality of the overall response. Figure 1-7 illustrates the GCO using a refined discretization (100 steps) within the applied tolerance bounds ($\pm 0.00025\text{m}$).

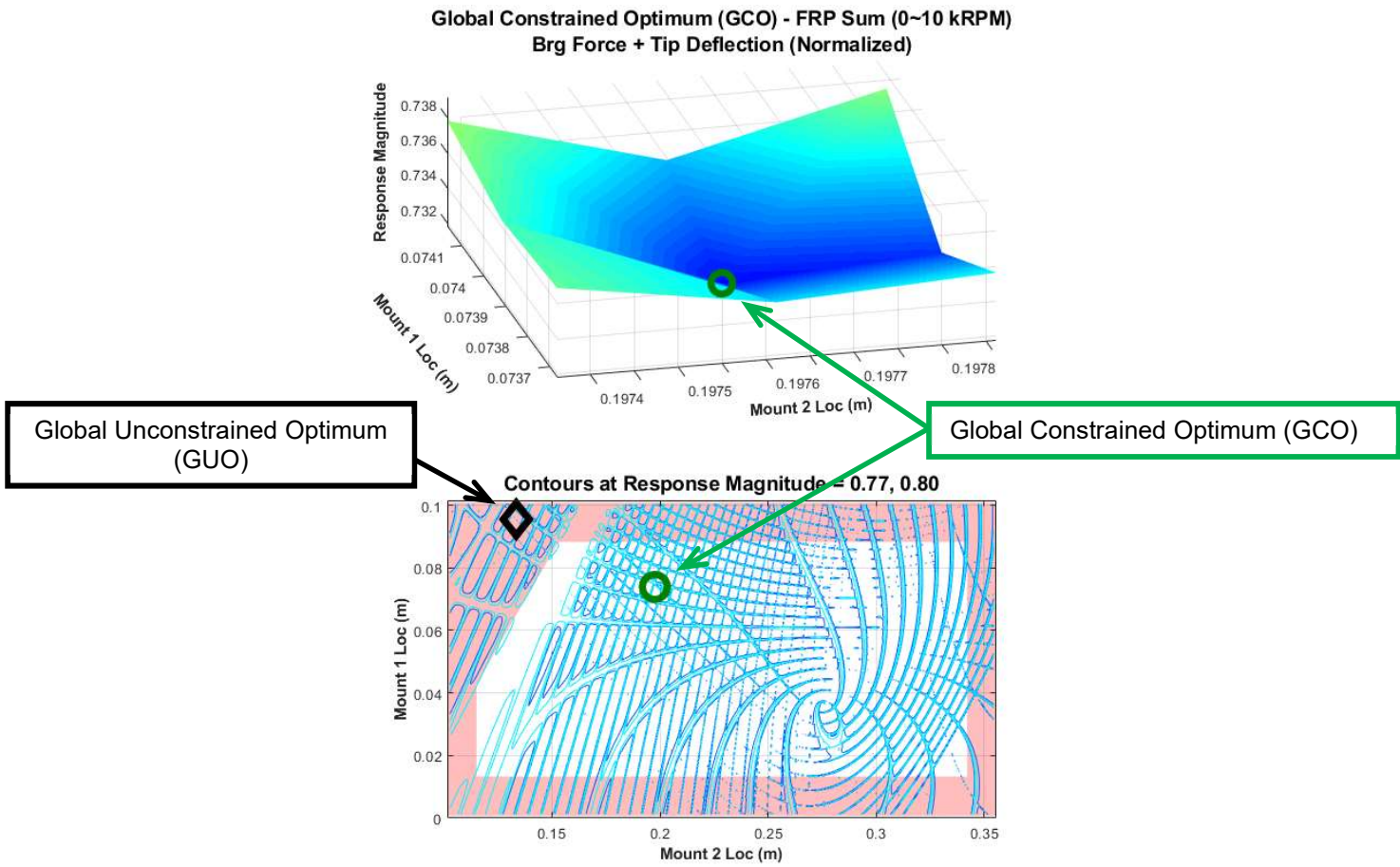


Figure 1-6 Discretized Mapping Survey Results with GCO with Feasibility Bounds

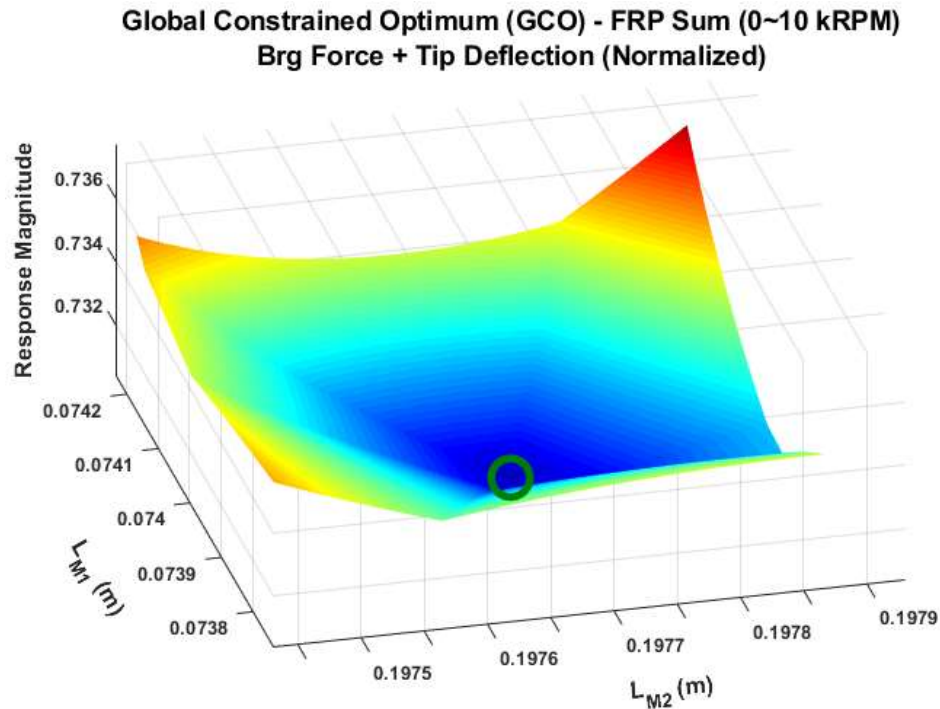


Figure 1-7 Mapping Survey GCO Result with Refined Discretization

Literature and State of the Art

The following summarizes key aspects from literature describing key learning and State of the Art as relevant to this study for rotordynamic modeling, mitigation options for lateral vibration of rotordynamic systems and optimization methods with relevance to both response minimization and robustness.

Fundamentals of Rotordynamic Systems

Vibratory response of rotating systems is, in many ways, analogous to the Structural Dynamic response of non-rotating systems. Both are governed heavily by the influence of mass, stiffness and damping.^{1,7,8} However, Rotordynamic systems include gyroscopic effects that non-rotating systems do not and the presence of damping in a Rotordynamic system can cause instability and increased vibration amplitude; as opposed to always providing reduced amplitude in non-rotating systems.¹

Two (2) types of vibration prevail in Rotordynamic systems, synchronous and self-excited.¹ Synchronous response is a forced response to unbalance forces and is among the most common

encountered in physical systems. These types of responses die out when the forcing function is removed and can also be limited by proper incorporation of damping. However, the use of damping in Rotordynamic systems can also be problematic in that, in certain circumstances, it can provide a source of instability to the system. For example, Gunter¹⁰ reports that, in response to a series of blast furnace compressor failures in the 1920's, Newkirk⁹ made a significant step to the study of rotordynamics by observing that all failures occurred above the first critical speed and were independent of the eccentricity of the rotors. Rather, he found that this 'non-synchronous' shaft whipping was ultimately due to the frictional interface of built-up rotors adding an instability force due to internal friction.

For purposes of this investigation, Rotordynamic events are limited to 'forced' or synchronous response given that this category represents most physical systems.¹

Gunter¹⁰ describes that the first recorded article about rotordynamics was created by Rankine¹¹ in 1869 where he investigated that rotating systems would produce large vibration amplitude at certain speeds but not at others; concluding that systems would remain stable below their first critical speed but would become unstable as speeds increased above that point. The state of the art advanced in 1894 when Dunkerley¹² provided a model based upon a flexible shaft with stiff bearing supports. In so doing, he showed that the problem of a whirling rotor could be replaced by the problem of finding natural frequencies of a non-rotating flexible beam on simple supports. Dunkerley supported Rankine's statements regarding stability by concluding that rotating imbalance of the rotor would excite natural frequencies (critical speeds), which in turn supported the general practice of increasing system stiffness to operate at higher speeds. Föppl and de Laval disproved this myth¹ in the latter-1890's by proving analytically and experimentally (respectively) that super-critical operation of a rotating shaft was possible. Vance¹ reports that in 1905 Stodola¹³ advanced the art further with respect to steam turbines as being the first to describe the possibility of dynamic interactions between rotors and the supporting foundation.

By 1919, supercritical operation of rotating machines was becoming commonplace, but vibration-related failures were frequent enough that The Royal Society of London commissioned H.H. Jeffcott to undertake an analysis of rotor whirling and critical speeds¹. Jeffcott's resulting work of 1919¹⁴ provides a clear description of rotordynamic response to unbalance with the inclusion of damping. Through this

work, Jeffcott is credited to making one of the first clear mathematical descriptions for rotordynamic phenomenon by modeling a flexible massless shaft on simple supports with an unbalanced disk mounted midspan between them and its translational velocity resisted by a viscous damping force.

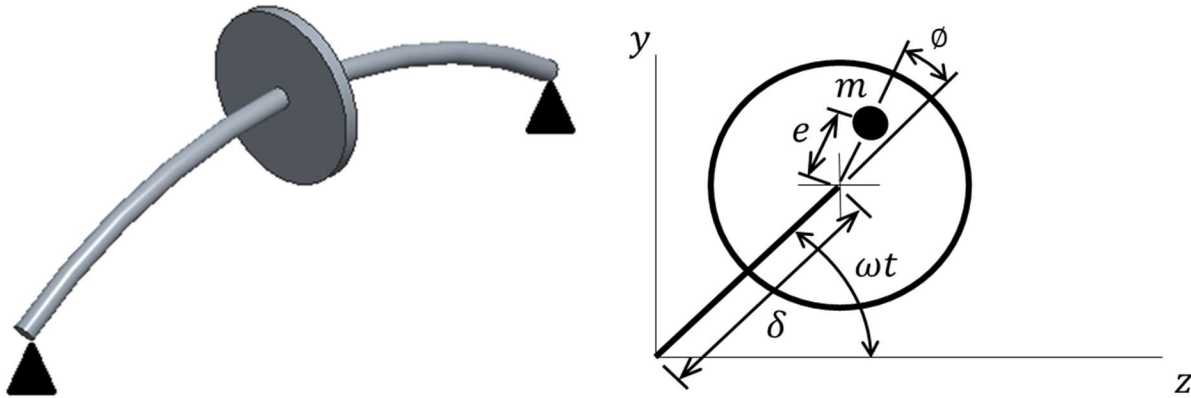


Figure 1-8 Jeffcott (de Laval) Rotor and Free Body Diagram

Jeffcott's model assumes a flexible, massless rotating shaft with mid-span unbalanced (rigid) disk supported on rigid end-mounted bearings without consideration for gravity. Jeffcott's study focused on the effects of rotor unbalance on rotor whirl with damping included. His analysis shows that unbalance leads the whirl vector by an increasing phase angle as rotational speed is increased, to a maximum at Critical Speed after which the phase is large enough that the unbalance is inboard of the disk center, reducing the effective imbalance force on the system. In so doing, he supported de Laval's work by showing mathematically how supercritical operation was advantageous in reducing vibration magnitudes, but in a smooth manner as opposed to the sudden jump predicted by de Laval.^{1,10} Jeffcott's analysis also shows that 3 main design elements are available to Rotordynamic designers to limit synchronous whirl amplitudes¹:

- Rotor balance
- Addition of damping (if near critical speed)
- Operating speeds further away from the critical speed

Rotordynamic Principle of Mass Inversion

A key Rotordynamic principle supported by study of a Jeffcott rotor is the principle of *critical speed inversion* or *mass center inversion*¹. Also described by Gunter¹⁰ as the concept of '*indifferent equilibrium*', this principle describes mathematically how operation above a critical speed can be attractive with respect to synchronous whirl vibration amplitude. The figure below illustrates this principle for a Jeffcott rotor with center-mounted rigid disk (with mass eccentricity) on a flexible and massless shaft (with rigid bearings).

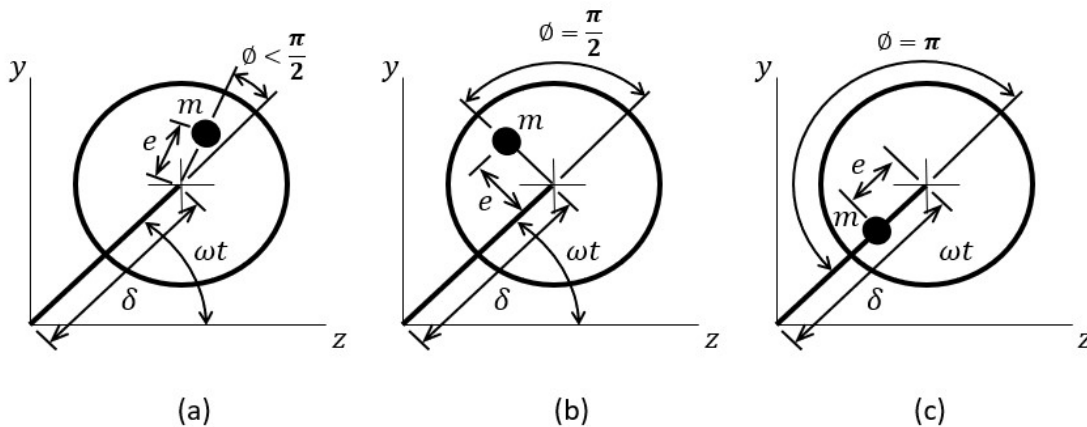


Figure 1-9 Synchronous Whirl Critical Speed Inversion

As shown, the center of mass is 'outboard' of the geometric center of revolution for slow shaft rotation speeds. That is, the centrifugal force of the mass eccentricity orients the rigid disk such that the mass eccentricity is 'outboard' of the natural bow of the flexible shaft (δ) and remains unchanged and 'in phase' with shaft rotation. As the shaft speed increases, the phase relationship between the mass imbalance and the whirl vector increases (a) until, at critical speed (b), the imbalance leads the whirl by 90 degrees. As the shaft speed further increases above Critical Speed, the phase relationship continues to increase as the mass imbalance leads the whirl vector by (approaching) 180 deg, causing the mass eccentricity to be 'fully inboard' of the center of rotation of the disk (c). In so doing, the distance between shaft center of rotation and mass center has reduced, resulting in reduced lateral vibration amplitudes.

This fundamental principal illustrates how 'precession balancing' of the rotor, to minimize the distance between mass center and geometric center of rotation, can result in the imbalance response being arbitrarily close to the static imbalance for operations significantly above critical speed. Further, it illustrates how the addition of damping is the most important aspect in limiting lateral vibrations at and near the Critical Speed. A mathematical description of this key concept follows.

The EOM for a Jeffcott rotor is shown as Eq. 4 with respect to the Free Body Diagram above. (Reference App. C for equation development). The total solution to this second-order ODE is the sum of the Homogeneous (transient) and Particular (steady state) components. However, for purposes of this study, interest is limited to the steady state portion of the solution. As derived in Appendix C, the Particular (steady state) solution to the EOM is provided in Eq. 5 with Real and Imaginary parts extracted as Eq. 6 and Eq. 7 (respectively) below. Note that for this discussion, the equation(s) are normalized by mass.

$$\ddot{\delta} + \frac{c}{m} \dot{\delta} + \frac{k}{m} \delta = e\omega^2 e^{i\omega t} \quad (4)$$

$$\left[\left(\frac{k}{m} - \omega^2 \right) D + \frac{c}{m} \omega D i \right] (\cos \phi - i \sin \phi) = e\omega^2 \quad (5)$$

$$\left(\frac{k}{m} - \omega^2 \right) D \cos \phi + \frac{c}{m} \omega D \sin \phi = e\omega^2 \quad (6)$$

$$-\left(\frac{k}{m} - \omega^2 \right) D \sin \phi + \frac{c}{m} \omega D \cos \phi = 0 \quad (7)$$

By manipulation of the Imaginary part of the solution (Eq. 7), the phase angle ' ϕ ' can be shown as Eq. 8 and the steady-state amplitude of the whirl radius (D) as Eq. 9.

$$\phi = \tan^{-1} \left(\frac{2\zeta R}{(1 - R^2)} \right) \quad (8)$$

$$\text{where: } R = \frac{\omega}{\omega_n} = \text{Frequency Ratio}$$

$$D = \frac{eR^2}{\sqrt{(1 - R^2)^2 + (2\zeta R)^2}} \quad (9)$$

where: e = Mass Eccentricity Distance from Shaft Center

The components of the Real part of the Particular solution (Eq. 6) can be plotted as a Force Vector Polygon to illustrate the relationships between stiffness and damping elements and the Phase angle ' ϕ ' between the mass imbalance and whirl vector. The figure below illustrates the force vector polygon for a) $\omega \ll \omega_{cr}$, b) $\omega = \omega_{cr}$ and c) $\omega \gg \omega_{cr}$. As shown in (b), the stiffness vector ($\frac{k}{m}D$) and mass vector ($\omega^2 D$) are of equal length. Therefore, the length of the force vector ($e\omega^2$) is determined solely by the damping vector ($\frac{c}{m}\omega D$) illustrating that, like non-rotating structural dynamics, the only influence over the magnitude of the force vector at resonance (critical) is the effect of damping.

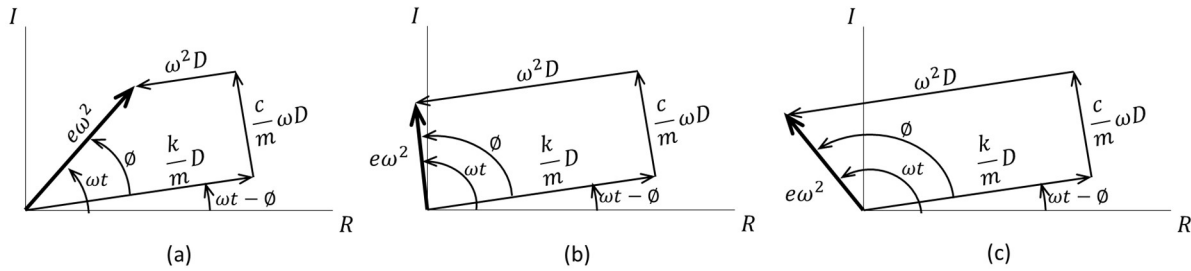


Figure 1-10 Force Vector Polygon – Jeffcott Rotor

As shown by Eq. 9, and by the force vector polygon, the presence of damping is the only limiting factor for displacement magnitude for a system at resonance ($R = \frac{\omega}{\omega_n} = 1$). This is essentially the same observation made for Single Degree of Freedom (SDOF) translational systems; the key difference here being that the Force Vector Polygon above describes Whirl characteristics of the system and the phase angle ' ϕ ' is the angle between the imbalance vector and the shaft restoring force (whirl) vector. The result of Eq. 8 and Eq. 9 for a Jeffcott rotor in synchronous whirl are illustrated below. This plot illustrates the principle of the Critical Speed Inversion in that at speeds significantly above the Critical Speed, the Amplitude approaches that of the static imbalance. Also, the plot illustrates that the phase angle between the mass imbalance and whirl vectors equates to 0 deg for a static condition, rises to pass through 90 deg at Critical Speed and then approaches 180 deg asymptotically for speeds significantly above critical (supporting the observations of the force vector polygon above). Also, shown is the effect of damping on these responses, which is comparable for non-rotating systems.

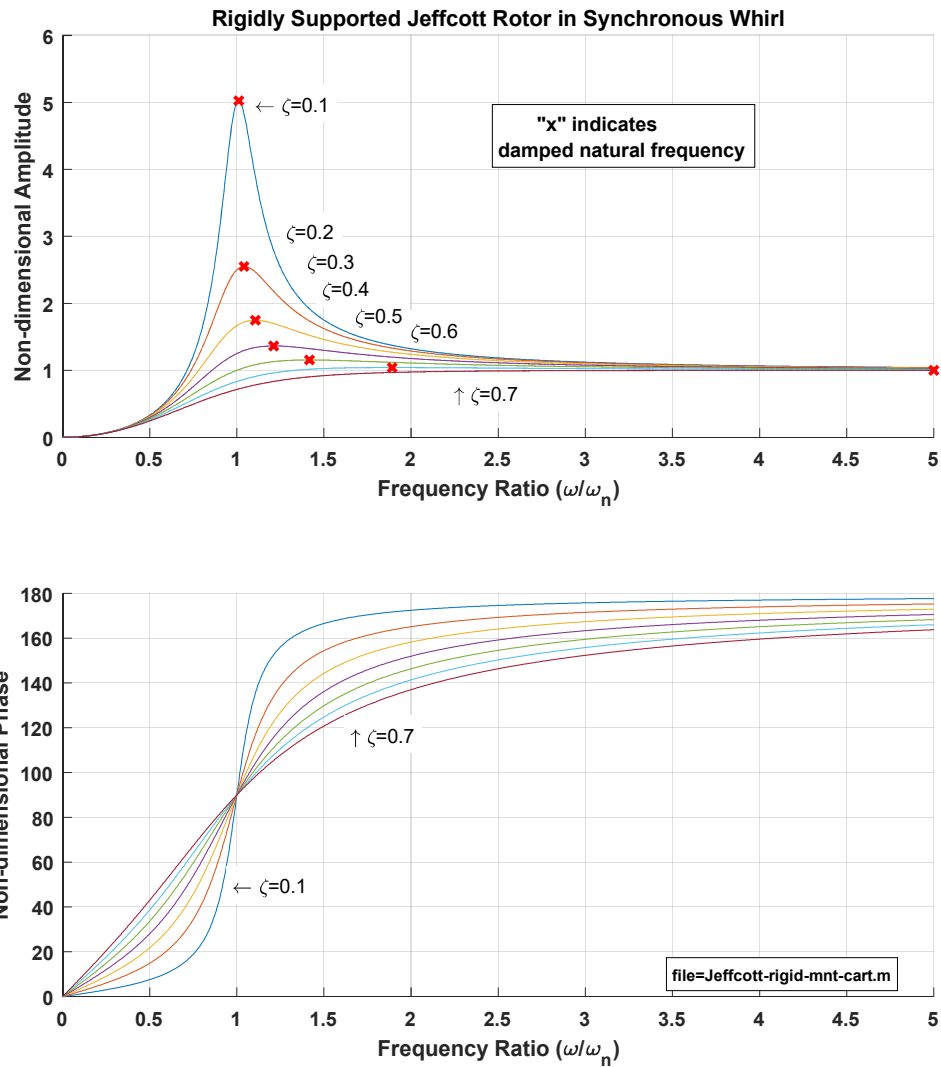


Figure 1-11 Amplitude and phase response of Jeffcott Rotor to Frequency Ratio

Rotary Inertia and Gyroscopic Coupling

A modified Jeffcott rotor, such that the shaft is rigid and the bearing supports are elastic, is useful to illustrate a second key Rotordynamic principle with respect to Synchronous Whirl; that of the influence that Inertia and Gyroscopic Coupling have to the shaft whirl response. Where the Jeffcott rotor is effectively a 'point mass' representation of a rotating system, this modification (also known as a Stodola-

Green model⁸) allows for the study of the effects of both polar and translational inertias on a simplified (rigid shaft) system. In the illustration below, the Jeffcott rotor is modified to include not only flexible bearing supports, but an extended rotor effectively serving to make the overall shaft design rigid.

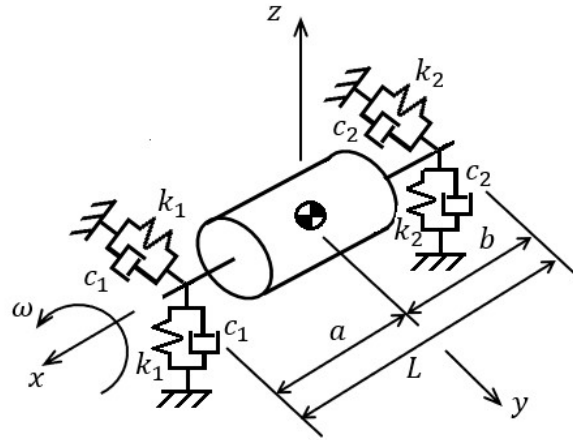


Figure 1-12 Modified Jeffcott Rotor with Extended Rotor

The mathematical development of the EOM for the modified Jeffcott rotor system is provided in Appendix D and the result is given as Eq. 10. The imaginary roots are the eigenvalues of the system and the first and second conical eigenvalues are given as Eq. 11 and Eq. 12 respectively^{1,15}. (For simplicity of this eigenvalue illustration, damping (C_1 and C_2 are defined to be '0') and the rotor is center-located in the shaft, resulting in $\gamma_{k=0}$.) Note that in Eq. 10 (assuming centrally-located rotor and damping=0), both Mass and Stiffness matrices are diagonal, and the Gyroscopic Matrix is skew-symmetric. Solutions of the EOM for both Cylindrical and Conical eigenvalues are also provided in Appendix D as guided by Yoon¹⁵.

$$\begin{aligned}
 & \begin{bmatrix} m & 0 & 0 & 0 \\ 0 & m & 0 & 0 \\ 0 & 0 & J_T & 0 \\ 0 & 0 & 0 & J_T \end{bmatrix} \begin{Bmatrix} \ddot{x}_G \\ \ddot{y}_G \\ \ddot{\theta}_{xG} \\ \ddot{\theta}_{yG} \end{Bmatrix} + \begin{bmatrix} \alpha_c & 0 & 0 & \gamma_c \\ 0 & \alpha_c & \gamma_c & 0 \\ 0 & \gamma_c & \delta_c & 0 \\ \gamma_c & 0 & 0 & \delta_c \end{bmatrix} \begin{Bmatrix} x_G \\ y_G \\ \theta_{xG} \\ \theta_{yG} \end{Bmatrix} + \begin{bmatrix} 0 & 0 & 0 & 0 \\ 0 & 0 & 0 & 0 \\ 0 & 0 & 0 & J_p \omega \\ 0 & 0 & -J_p \omega & 0 \end{bmatrix} \begin{Bmatrix} \dot{x}_G \\ \dot{y}_G \\ \dot{\theta}_{xG} \\ \dot{\theta}_{yG} \end{Bmatrix} \\
 & + \begin{bmatrix} \alpha_k & 0 & 0 & \gamma_k \\ 0 & \alpha_k & \gamma_k & 0 \\ 0 & \gamma_k & \delta_k & 0 \\ \gamma_k & 0 & 0 & \delta_k \end{bmatrix} \begin{Bmatrix} x_G \\ y_G \\ \theta_{xG} \\ \theta_{yG} \end{Bmatrix} = \begin{Bmatrix} F_x \\ F_y \\ M_x \\ M_y \end{Bmatrix} \quad (10)
 \end{aligned}$$

where:

$$\begin{aligned}
 \alpha_c &= C_1 + C_2 & \alpha_k &= K_1 + K_2 \\
 \gamma_c &= -aC_1 + bC_2 & \gamma_k &= -aK_1 + bK_2 \\
 \delta_c &= a^2C_1 + b^2C_2 & \delta_k &= a^2K_1 + b^2K_2 \\
 \pm J_p \omega &= \text{Gyroscopic terms}
 \end{aligned}$$

$$\omega_{n1_FW_con} = \frac{J_p}{2J_t} \left(\frac{\omega}{\omega_{nc0}} \right) + \sqrt{\left(\frac{J_p}{2J_t} \left(\frac{\omega}{\omega_{nc0}} \right) \right)^2 + 1} \quad (11)$$

$$\omega_{n2_FW_con} = \frac{J_p}{2J_t} \left(\frac{\omega}{\omega_{nc0}} \right) - \sqrt{\left(\frac{J_p}{2J_t} \left(\frac{\omega}{\omega_{nc0}} \right) \right)^2 + 1} \quad (12)$$

where:

$$\omega_{nc0} = \sqrt{\frac{(K_1 + K_2)L_b^2}{2J_t}} = \text{nonrotating conical natural frequency}$$

These first conical eigenvalues are instructive in 2 key ways. First, inspection of Eq. 11 (vs Eq. 12) illustrates that as the shaft rotating speed increases (ω), the magnitude of the Critical speed ($\omega_{n1_FW_con}$) increases as well. This (Eq. 11) is the Critical Speed associated with the first Forward Whirl where shaft precession (whirl) occurs in the same rotational direction as the shaft's spin. Eq. 12 illustrates the First Backward Whirl where the frequency reduces with increasing shaft speed (ω). Vance states that, although this relationship is generally true (FW whirl increasing and BW whirl decreasing with increasing shaft speed), the influence of other factors (e.g.; factors associated with non-synchronous whirl, etc.) that are not included in this simplified analysis may cause different results. The reason for this (Forward and Backward whirl changes to the Critical speed frequency with increasing shaft speed) is the Polar Inertia term (J_p) that appears in the Gyroscopic matrix acting together with the Shaft Rotating (Spin) speed (ω). Together, they provide a cross-coupled gyroscopic effect that acts with the damping matrix against the velocity vector. The result is that increasing shaft speed causes an effective 'increased stiffness' of the system due to the gyroscopic matrix for Forward Whirl and a 'softening' of the system for Backward Whirl.^{1,7,8} Also, it is reported^{1,8} that Forward (synchronous) Whirl sometimes results in unstable Critical Speeds, but Backward (synchronous) Whirl generally does not excite Critical Speed. The figure below illustrates the divergence of FW and BW whirl with increasing shaft speed in an exemplary Campbell plot.

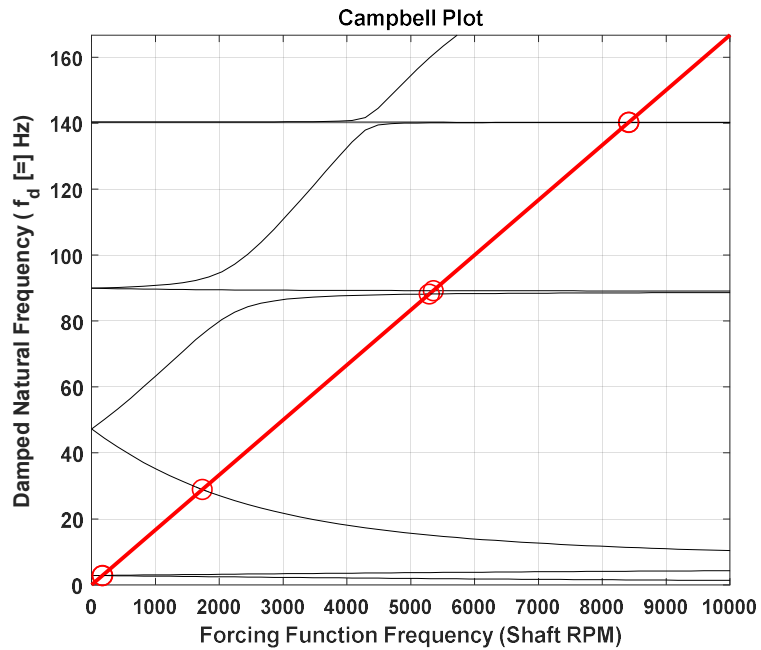


Figure 1-13 Campbell Plot

The figure below illustrates a second key Rotordynamic concept based on the First Forward Whirl Eigenvalue. The plot relates normalized natural frequency to the normalized frequency ratio for a range of Rotor Inertia Ratios ($\frac{I_p}{I_t}$) overlaid upon the synchronous whirl line^{1, 8, 15}. Both curves 'P=0.01' and 'P=0.5' cross the synchronous whirl (resonance) line and therefore Critical Speeds exist for shaft speeds corresponding to those intersections. Higher ratios of 'polar to transverse' inertia however do not cross the synchronous line and therefore do not excite a Critical Speed for the system. Note also that as the Polar Inertia approaches '0', the First Forward Whirl curve approaches a condition of insensitivity with respect to Frequency Ratio; indicating that the static (non-rotating) natural frequency can be used to approximate the Critical Speed of a rotating condition.

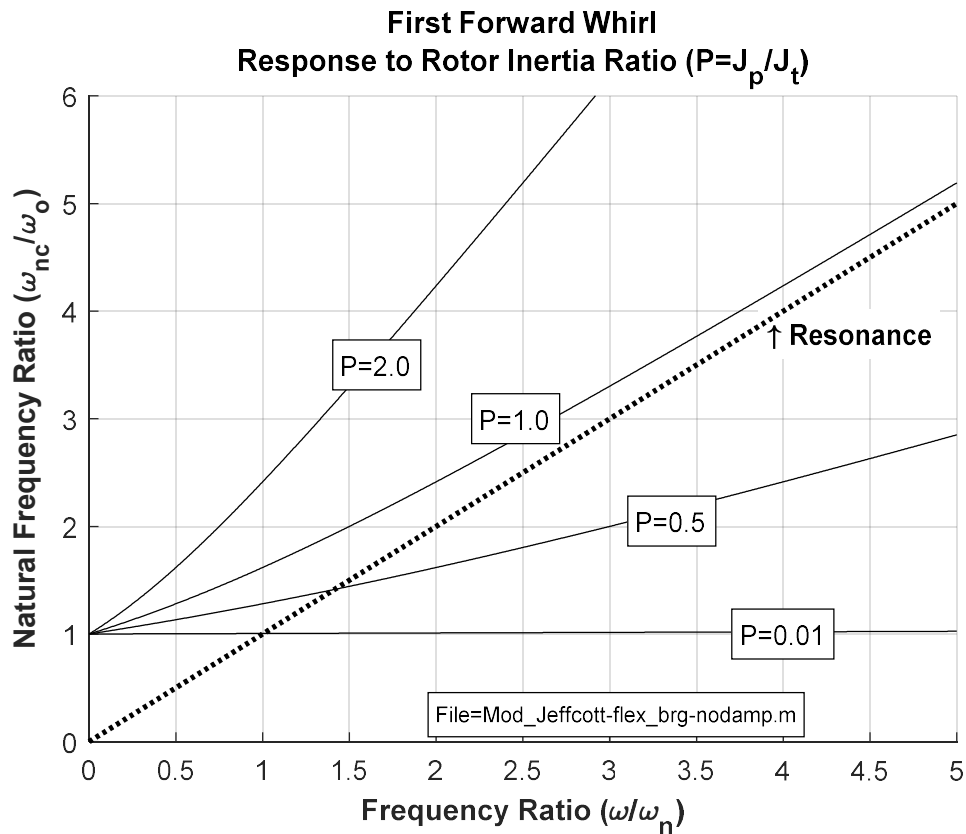


Figure 1-14 Eigenvalue relationship to frequency ratio – modified Jeffcott rotor

Mitigation Methods for Flexural Vibration of Rotordynamic Systems

A variety of methods have been studied as means of mitigation to vibrations experienced by Rotordynamic machines. Perhaps the earliest and most traditional method is to design the system such that the fundamental Critical Speed frequency is 'placed' above the operating speed.¹⁰

Since the early 1900's however, supercritical operation of machinery has been a preferred practice to achieve increasing power levels with minimal system weight or footprint.^{1,16} As a result, machine designers are faced with the challenge of minimizing flexural vibrations, particularly at the crossing of these Critical Speeds.

Optimal placement of bearing location is a method commonly used to influence Critical Speeds^{17,18,19,20,21} and was also recently explored using a Genetic Algorithm optimization method to maximize a first mode natural frequency for a motorized spindle-bearing system.²²

Incorporation of (appropriate) damping is key to reducing vibration amplitudes at resonant frequencies. Passive dynamic absorbers in the form of Tuned Mass Dampers (TMD) and Nonlinear Energy Sinks (NES) have been explored for application on flexible bladed Rotordynamic systems to reduce vibration levels.^{23,24,25} Supports using viscoelastic materials were explored as another passive control measure to add damping to the system.²⁶ Optimal placement of water lubricated rubber bearings, including damping effects, were also explored with application toward flexible, multistage rotor systems such as water pumps for fire protection, waste water treatment, etc.²⁷

Unfortunately, direct damping is too often difficult to implement explicitly into rotordynamic systems in practice. Therefore, alternate methods to minimize Rotordynamic vibrations have been researched. For example, geometry variation of the rotating shaft is explored as another passive mitigation alternative²⁸ for a Rotordynamic shaft where neither bearing location nor added damping are considered. Active Magnetic Bearings (AMBs) offer another alternative toward limiting amplitude at resonance and have been explored with application to vibration suppression in Rotordynamic systems.^{29,16,30,15}

Mechanisms designed to add Negative Stiffness to the system have been researched as an alternate way to dampen structural vibrations. The use of magnets to add negative stiffness have been explored directly for rotordynamic systems for aero-engine applications³¹ and as a Dynamic Vibration Absorber.³² More generally, multiple researchers have considered negative stiffness employing magnets for non-rotating structural vibration suppression.^{33,34} As an alternative to magnets, a honeycomb material structure has also been investigated for use as a negative stiffness element to suppress structural vibrations.³⁵

In general, implementation of these passive mitigation methods is often focused, at least to some extent, on suppressing vibration magnitudes at relatively narrow, targeted frequency bands; intended to avoid a particular Critical Speed. Active controls such as the use of magnetic bearings holds potential for much more broad-based frequency effects, but at the expense of increased complexity of the system through control and feedback systems.

Optimization Methods for Rotordynamic Systems

Various optimization methodologies have been reported by researchers with application to rotordynamic systems. Rotating structures are unique in the field of structural dynamics in that they are commonly non-self-adjoint systems.^{2,3,4,5} That is, due to gyroscopic and circulatory (cross-coupling stiffness) considerations, system matrices are asymmetric. Because of this, optimization methods appropriate to non-rotating structural dynamic applications may not be successful.⁶

One common area of focus is the optimization of imbalance in rotating machines to address physical, field-based systems. The Influence Coefficient (IC) balancing method is reported as an 'easily implemented' method for field balancing when used with Least Square (LS) methods.³⁶ Although the IC method assumes a linear correlation between lateral vibrations (at the measuring stations) of the rotating shaft and mass unbalance at the balancing planes, the authors explain that given the nonlinear nature of some constraints, the optimization problem can become non-linear. As a result, the semi-definite programming (SDP) technique, Convex Min-max methodology, is proposed using a linear matrix inequality (LMI) formulation to address the constraints.

Other optimization methods applied to rotordynamic systems include evolutionary and gradient-based algorithms.³⁷

A real coded Genetic Algorithm (GA) for use with mixed integer optimization is applied as part of a proposed Virtual Bearing method of optimization for rotordynamic systems.²⁰ In this work, a method is proposed which allows the placement of Critical Speeds for a rotordynamic system based on both optimal bearing quantity and location. It effectively identifies a priori a maximum number of potential bearings and their range of locations, and then turns the stiffness of the 'optional' bearings 'on' and 'off' as part of the optimization effort. The mixed integer optimization technique³⁸ then works in conjunction with other 'variables data' to identify the optimal solution.

A hybrid of GA together with the Nelder-Mead (NM) method is investigated by multiple researchers to leverage GA as a global search tool followed by Nelder-Mead as a more efficient local search method.^{26,39}

Although GA is reported as an efficient tool for identification of promising 'valleys' within the design space, it is also reported to suffer from slow convergence. A classical 'hill-climbing' algorithm, such as Nelder-Mead, can then be useful to investigate the 'promising' regions for the global optimum. Although Nelder-Mead is reported as 'extremely flexible and suitable for exploring difficult terrains'⁴⁰, it is limited as an unconstrained optimization technique.

A hybrid of PSO and Nelder-Mead is also researched⁴⁰ to leverage the benefits of an evolutionary algorithm with a 'hill-climbing' local search tool. Although not explicitly applied to a rotordynamic system, the hybrid GA-NM and PSO-NM methods are reported as being effective and efficient for nonlinear responses with multiple minimums.

Another evolutionary hybrid approach targeted to optimization of multi-modal response is a combination of GA and PSO.⁴¹ The resulting hybrid (GA-PSO) integrates the concept of evolving individuals (GA) with the self-improvement of PSO with superior ability to find the global optimum as compared with Continuous Genetic Algorithm (CGA), Continuous Hybrid Algorithm (CHA) and a hybrid NM-PSO. Data supports that although the proposed GA-PSO method may find a better optimum, it sometimes requires significantly more function evaluations to do so.

The commercial program ISIGHT was also used⁴² to evaluate 3 evolutionary-based optimization methodologies with respect to a 2-disk rotor system. In this work, the authors compare the performance of ISIGHT's Evolutionary Optimization (EVO) algorithm, Multi-Island Genetic Algorithm (MIGA) and 'Pointer', a hybrid of 4 methods including linear simplex, SQP, downhill simplex and GA. Goals of the analysis were to modify the locations of the 2 rotating disks to minimize their lateral deflections. It was found that the MIGA algorithm achieved the best result for one of the disks, but the worst result for the other. The hybrid Pointer method was similar. The EVOL evolutionary method was determined to perform best in terms of identifying the best overall global solution.

Pareto Optimality was investigated⁴³ to conduct a two-objective design optimization of an aircraft structural optimization with Rotordynamic effects. A challenge to use of Pareto Optimality⁵⁵ is that the technique is best used if the various objective functions are of the same general type and order of magnitude. This is not the case for the current example problem or of the anticipated extensions toward

Rotordynamic problems in general. Therefore, an alternative means of optimizing multiple responses is investigated.

Rather than Pareto Optimality, the proposed method utilizes a technique often incorporated within that and other MOO methods; that of Weighted Sums⁴⁴. Here, a single Objective Function (OF) is formed as a combination of multiple singular objectives with weighting factors serving to address both variances in orders of magnitude as well as objective priorities. The use of Weighted Sums is selected in consideration for the potentially high-modality response of the Rotordynamic system (as experienced in this example) and the potential for both quantity and cost of function evaluations. The specifics of the OF used in this example are described elsewhere in this manuscript, but the multi-modal nature of the response is illustrated in Figure 1-2 here as a function of variation in the 2 Design Variables.

Various gradient based optimization methodologies have been reported in literature. For example, a nonlinear rotordynamic system was successfully addressed as a linear optimization problem thru use of Sequential Linear Programming (SLP) to minimize system weight in consideration for eigenvalue constraints.⁴⁵

SLP is also used for the placement of Critical Speeds²⁸ in conjunction with the Method of Moving Asymptotes (MMA). Here, MMA⁴⁶ offers an ability to replace both objective and constraint functions of the original problem by approximating convex functions. It was observed that use of MMA increased the likelihood that the results would be identified within feasible design space and therefore was preferred to the linear SLP method alone.

Two gradient based methods, Gradient Projection Method (GPM) and Sequential Quadratic Programming (SQP) were compared for a rotordynamic system with stress, frequency and harmonic response constraints.⁴⁷ Although considered the more flexible and computationally advantageous of the two, the GPM method suffered on the non-self-adjoint rotordynamic application in that it was not always stable. The SQP method, although generally considered to be more sophisticated, was observed to sometimes get 'stuck' in a non-optimal solution due to the multi-modal nature of the response.

In continued research, SQP was coupled with hybrid analytical and numerical sensitivity analysis.⁴⁸ The authors used an internally developed FEA code and note that while sensitivity analysis of

the modal equation was beneficial to the SQP optimization in terms of convergence and stability, it increased the overall time required since a numerical analysis was necessary. Among the reasons cited for using the numerical method was that the skew-symmetric gyroscopic matrix for the rotordynamic system makes the generalized eigenvalue problem nonsymmetric, violating the assumption necessary for standard sensitivity analysis of linear eigenvalue problems.

A hybrid approach coupling DOE was investigated for sensitivity analysis with a modified GA approach.⁴⁹ In this 2-step optimization approach, the process first placed the Critical Speeds away from the operating range and then 'fine-tuned' the design to minimize flexural responses. The commercial program ISIGHT's DOE and Nondominated Sorting Genetic Algorithm II (NSGA-II) were used to identify sensitivities with respect to Critical Speeds and to perform the optimizations.

As an alternative to gradient based methods, a Golden Section search method was studied as a means of optimizing a Rotordynamic system with constraints based primarily on minimization of strain energy.⁵⁰ By incorporating a penalty function method with Powell's conjugate direction method, the problem was defined as a one-dimensional optimization, suitable for the Golden Search method. The use of strain energy as an objective function was concluded to be particularly advantageous due to its global ability to describe the severity of the conditions for flexible rotor systems where deflections are difficult to control.

A procedure for eigenvalue reanalysis is proposed⁵¹ for application with Rotordynamic systems with particular usefulness in improving the computational efficiency of iterative optimization schemes. It is based on use of a receptance formula⁵² useful to predict damped natural frequencies of the system, which particularly increases efficiencies for repeated analyses during optimizations. The authors report that the method improves convergence characteristics when only an incomplete set of modes is available.

As described previously, optimization methods applied to Rotordynamic systems include a wide variety of methods. A common theme in the literature, is that Rotordynamic optimizations often include multiple design variables including component size, support location, stiffness and/or damping and other material-related values. In addition, responses are sometimes multi-modal. This is particularly true for the present example where, even for only 2 design variables, the requirement of a wide operating speed

range encompassing multiple Critical Speeds results in a highly multi-modal objective function. Therefore, an optimization methodology is needed that is particularly appropriate for this environment. In addition, the selected methodology is desired to be appropriate to EBBF functions so that it may be enjoyed with FE analysis, either custom or commercial.

Optimization Methods for HEB Problems

The term High Modality, Computationally Expensive Black Box (HEB) problems is associated with the intent of the current example. It is reported⁵³ that HEB is an area that is less well researched than optimization strategies for 'low modality' problems and recommendations are made that future research would benefit from methods taking advantage of the natures of the underlying functions, including dimensionality, linearity and nonlinearity and interactions of terms. Currently however, it is recommended that 2 methods exist with particular promise for HEB problems; mapping and decomposition.

At least 2 groups of mapping methods are described with respect to HEB problems⁵³; dimensionality reduction and mapping aiming at optimization. Dimensionality reduction is focused on the reduction of the problem to those parameters with sensitivity toward the objective function to simplify the problem. Techniques such as Analysis of Variance (ANOVA) or others can be useful in this regard. A technique for space mapping is proposed as a method for 'mapping aimed at optimization'.⁵⁴ Here, the authors propose a hybrid approach consisting of 2 models; a first 'course' surrogate model which is not computationally expensive and can be surveyed with less accuracy for potential areas of optimum followed by a 'fine', more computationally expensive model, suitable for more accurate exploration in the identified candidate areas of the design space. An advantage given to mapping methods is simplification of the model through reduction of dimensionality and subsequent reduced computational burden. A stated disadvantage is the potential to miss the global optimum through optimization of a model with reduced dimensionality.

Decomposition is the reformulation of the original problem into a set of independent or coordinated, smaller-scaled problems.⁵³ As applied to engineering problems, the authors describe decomposition as categorized in terms of product, process and problem decomposition; 'product'

separating the problem by physical component, process by the flow of element or information and problem decomposition separating a complex problem into simpler elements. Decomposition also holds the potential for improved computational efficiency and a related expansion of applicable optimization methodologies with the recognition that decomposability may be limited for some problems.

Although not always used in conjunction with systems of high-modality, 'First-Order' methods, including the method of Steep Descent (SD)⁵⁵ may be useful for the problem at hand. These gradient-based methods are known to be initially productive but become inefficient as the solution approaches the optimal result. They are typically useful for single objective and unconstrained searches; neither of which applies to the example problem at hand. A proposed approach using the method of SD for multicriteria optimization⁵⁶ together with the method of feasible directions⁵⁷ for use in constrained cases is recommended as having potential. Given that it is a first-order method, the authors recommend that it should be considered only as a 'first step' toward efficiency rather than an efficient method unto itself.

An attribute shared by many of the 'natural computing' paradigm's such as described previously is the ability to deal with noisy or incomplete data.⁵⁸ These authors cite that PSO can find solutions near optima faster than GA but is more prone to premature convergence than Evolutionary Algorithms (EA). In another work, the effectiveness of EA, PSO and Differential Evolution (DE) was compared⁵⁹ and it was concluded that, in general, the DE algorithm outperforms both PSO and EA in terms of consistent speed of convergence and ability to find the optimum. However, the authors note that PSO was particularly problematic with noisy functions.

Separately, PSO is compared as a means of optimizing minimax problems to SQP.⁶⁰ The authors conclude that for Black Box functions where gradient information is not available (as with HEB's) that PSO may be a good alternative as an initial search tool with continued optimization performed by more efficient methods such as SQP.

All Direct Methods, including GA, PSO, and SQP are applicable to constrained functions and are also known to potentially require a high number of function evaluations, especially for multi-modal responses.⁵⁵ This makes them undesirable as 'stand-alone' optimization tools for EBBF's and HEB functions.

The previous observation regarding potential for SQP as an effective follow-on to an initial global search⁶⁰, together with potential for use of Steepest Descent as an initial search tool⁵⁶ is the inspiration for the proposed method. That is, that the best overall method for a HEB function may be to initially investigate the design space using a first-order method and then, from the region of most promising minimum response, continue the search using local SQP. A first order method, when limited to a few jumps and modified for use with constraints, is theorized to be more efficient for the initial (global) search than direct methods. In addition, the use of a polynomial approximation during the steepest descent's 1-D search is theorized to be effective in identifying 'global' minima in a multi-modal environment. This theory was considered in a previous work Hauser, Bret R. "Optimal Design of a Parallel Beam System with Elastic Supports to Minimize Flexural Response to Harmonic Loading." (2015).⁶¹ (Appendix A) where optimization of a non-rotating structural dynamic (parallel beam) system was considered. It was concluded that for the example problem of that work, the combined method of Steepest Feasible Descent (SFD) followed by local SQP search found the same global optimum (as compared with the component methods alone) but with approximately 44% fewer function evaluations.

Robustness and RBDO of Rotordynamic Systems

Some researchers have explored the use of Robustness-Based Design Optimization (RBDO) techniques as means to effectively identify optimal designs with consideration for variation inherent to Design Variables. For example, Robustness was considered in the design optimization of a multi-stage rotor shaft⁶² by optimizing for minimal weight as constrained by flexibility with respect for variation in residual unbalances and journal bearing stiffness. The authors used a Latin-Hypercube (LH) DOE construct on an assumed trust region to develop a Kriging Response Surface model of both objective and constraint functions. The constrained optimum was then identified using a deterministic optimization algorithm, verifying the solution thru additional LH sampling, and if necessary, repeating the iterative process by successively reducing the size of the trust region and repeating. The effort required 4 iterations of a 2000 sample LH evaluation, supporting that the approach may have efficiency challenges for high-modality responses.

Although not a Rotordynamic analysis per se, RBDO was used in the optimization of a NASA Stage 37 axial compressor for maximal efficiency and minimized weight⁶³. The process involved use of an Artificial Neural Network approximation model of the objective function upon which Monte Carlo simulation was performed. Multiobjective RBDO was then used with the uncertainty model by Parato-Optimal analysis to identify a solution.

RBDO was used to optimize the design of a NASA rotor67 transonic blade⁶⁴. This application also did not involve a rotordynamic evaluation directly but is useful in evaluating a use of RBDO for an optimization involving 'complex engineering calculations'; in this case the combined results of CFD and structural FEA. The authors constructed a Response Surface model of the objective and constraint functions based on LH DOE sampling, with Monte Carlo simulation used to extract the probability sufficient factor, and then applied a Real-Coded Genetic Algorithm for Multiobjective optimization. Although the authors experienced good result, significant discussion is given to the challenges of use of both Moment-based and Monte Carlo methods. Moment-based methods are reported as relatively efficient but exhibit accuracy challenges when the function is highly non-linear. Monte Carlo methods are frequently used due to their robustness and simplicity but require high numbers of function evaluations due to the nature of the approach; normally being applied to a surrogate function such as a Response Surface. This also provide challenge to the balance between accuracy and efficiency for highly nonlinear responses.

Reliability sensitivity estimation was applied to a Rotordynamic problem for studying failure modes including oil whip and resonance⁶⁵. Although not an optimization effort, the authors discuss that the use of Monte Carlo simulation techniques, although popular in statistical evaluations, have low computational efficiency resulting in large numbers of (potentially) costly analyses.

In general, these investigations support that, although beneficial at identifying the robustness of the solution, RBDO optimization methods are often computationally intensive and/or inefficient and therefore challenging to implement for EBBF functions.

Chapter 2

Approach

Finite Element Model Development

Significant Model Features and Capabilities

To support the needs of this research effort, a method is needed to model a Rotordynamic system including a shaft with both flexibility and distributed mass, the influence of elastic and asymmetric bearing supports, damping, geometric variance along the length of the system, multi-body connections and the addition of point masses and rigid disks. The prediction of the following criteria is sought:

- Critical speed frequencies
- Stability and direction of whirl for critical speed events
- Flexural deformations
- Reaction force response of spring and damper elements

The Rotordynamic Equation of Motion (EOM) is fundamental to all these outputs. As discussed elsewhere in this document, 2 primary analysis methods are used: 1) eigenanalysis to predict the Critical Speed frequencies, stability and whirl directions and 2) transformation of the EOM to a Steady-State component equation (in sin and cos) to determine flexural characteristics. A 'fully featured' and correct definition of the EOM then is key to developing a Rotordynamic model capable of supporting the needs of this study. Since this analysis includes a rotating shaft within a non-rotating housing, a fixed reference frame is required.⁶⁶ Other key considerations for this model include:

- Model based on 3-dimensional beam elements
- Rotatory effects on system stiffness
- Gyroscopic effects of the rotating elements including lumped mass and disk parameters
- Consistent mass, stiffness and damping models
- Timoshenko shear effects
- Axial force effects on system stiffness
- Symmetric / asymmetric bearing stiffness and damping effects
- Internal material damping effects (viscous coefficient and hysteretic loss factor)

- Consideration for both stepped and linearly varying (conic) hollow / solid shaft elements
- Multi-body connectivity such as rotating shaft supported within an exterior housing

It should be noted that although not all features are included in the subsequent optimization study of this project, the presence and capability of these features were believed to be important for potential future applications and therefore included as part of this development work.

General Programmatic Flow

As described later in this section, various resources were consulted in the development of the Rotordynamic EOM. However, multiple of these resources had conflicts (likely typographical errors) that raised concern in their direct usage. Therefore, the EOM was derived in this work 'from scratch' by deriving shape functions and implementing them to obtain the EOM with guidance from the various references. The mathematical process was conducted using MATLAB and the source-code is presented in Appendix E of this document. Key variable definitions are identified in the header of that code listing.

Shape Function, EOM and Matrix Development

As described later in this section, various resources were consulted in the development of the Rotordynamic EOM. However, multiple of these resources had conflicts (likely typographical errors) that raised concern in their direct usage. Therefore, the EOM was derived in this work 'from scratch' by deriving shape functions and implementing them to obtain the EOM with guidance from the various references. The mathematical process was conducted using MATLAB and the source-code is presented in Appendix E of this document. Key variable definitions are identified in the header of that code listing.

Shape Function Equation Development:

In general, shape functions were derived with consideration for Timoshenko Shear effects and used as input to a Lagrangian derivation for the EOM. Consideration for the various elements of the model (rotatory, gyroscopic, internal material shear, etc.) are defined as part of the kinetic and potential energy functions. A 2-node element model was incorporated for this work and, although some references

utilized a 6-DOF model (by separating nodal rotations due to bending and shear effects), a 4-DOF model (combining rotational effects) was selected for this work to improve computational efficiency while retaining the needed functionality of 2 translational and 2 rotational DOF per node. The nodal deformations are illustrated in the figure below with definitions provided in the following table. In the illustration, total nodal rotation (θ_z) is the sum of bending effects (v') and shear effects (β_y).

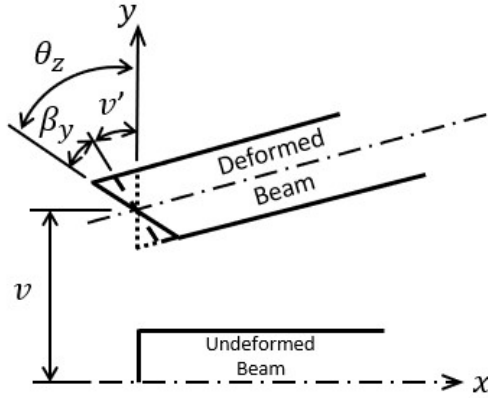


Figure 2-1 Nodal DOF (XY plane only)

Table 2-1 Nodal displacement vector definition

$$\{q\} = \begin{Bmatrix} v \\ w \\ \theta_y \\ \theta_z \end{Bmatrix} = \begin{Bmatrix} \text{Translation} - UY \\ \text{Translation} - UZ \\ \text{Rotation about } y - \text{axis} \\ \text{Rotation about } z - \text{axis} \end{Bmatrix}$$

Shape function development is made for a 3D beam element with inclusion of Timoshenko shear effects⁶⁷. The functions are built upon a 3rd order translational displacement equation (Eq. 13) to support interelement continuity of slope (C¹ element).⁶⁸

$$v(x) = a_0 + a_1x + a_2x^2 + a_3x^3 \quad (13)$$

Shear strain is assumed to be independent of 'x' and constant along the element length ($\gamma_{xy} = \text{const} = \gamma_o$) and combines with the bending rotation to establish the total slope at the node per Eq. (14).⁶⁷ The bending rotation can then be shown as Eq. (15). The bending moment (M_z) is related to the shear force (Q_y) as shown in Eq. (16) and the moment-curvature relation by Eq. (17). Shear force is

related to transverse shear strain by Eq. (18) where the shear correction factor (k) represents the Timoshenko shear coefficient and accounts for the non-uniform distribution of shear stress over the cross-section.⁶⁷

$$\frac{\partial v}{\partial x} = \frac{\partial v_b}{\partial x} + \frac{\partial v_s}{\partial x} = \theta_z + \gamma_o \quad (14)$$

such that:

$$\theta_z = a_1 + 2a_2x + 3a_3x^2 - \gamma_o \quad (15)$$

$$\frac{\partial M_z}{\partial x} - Q_y = 0 \quad (16)$$

$$M_z = -EI_{zz} \frac{\partial \theta_z}{\partial x} \quad (17)$$

$$Q_y = kGA\gamma_{xy} \quad (18)$$

By manipulation of these equations, a definition for Shear Strain can be developed as shown in Eq. (19) and, given definition of a shear ratio term (Λ_z) per Eq. (20), can be simplified and substituted into Eq. (13) and Eq. (15) together with the 4 fundamental (deformation) boundary conditions to develop the system of equations shown in Eq. (21). These simultaneous equations can then be solved to determine the values of the four coefficients.

$$\gamma_o = -\frac{EI_{zz}6a_3}{kGA} \quad (19)$$

$$\Lambda_z = \frac{EI_{zz}}{kGA} \quad (20)$$

$$\begin{bmatrix} v(x=0) = 1 = a_0 + a_1(0) + a_2(0)^2 + a_3(0)^3 \\ \theta(x=0) = 0 = a_1 + 2a_2(0) + (3(0)^2 + 6\Lambda_z)a_3 \\ v(x=L) = 0 = a_0 + a_1(L) + a_2(L)^2 + a_3(L)^3 \\ \theta(x=L) = 0 = a_1 + 2a_2(L) + (3(L)^2 + 6\Lambda_z)a_3 \end{bmatrix} \quad (21)$$

The coefficients (a_0 thru a_3) are then substituted into the deformation equations (Eq. 13 and 15) and coefficients extracted for the nodal DOF (v, w, θ_y, θ_z) to obtain the coefficients ($\psi_1, \psi_2, \psi_3, \psi_4$) for each respectively. Upon mathematical simplification, the shape functions for translation and rotation for a single element (nodes ' i ' and ' j ') is as shown in Appendix G.^{67, 69, 8} Note that the sign of translation in ' v ' and ' w ' and rotation in ' β ' and ' Γ ' are adjusted to account for the right-hand rule according to the plane of

action. The term Φ used in the development of these equations (Appendix G) represents the ratio between bending and shear stiffnesses.⁶⁷ It should be noted that axial warping during torsion is neglected in the development of these shape function equations.⁶⁷

The (Timoshenko) shear effects upon bending strain are included in the model to accommodate that plane cross-sections not be constrained to remain planar and perpendicular to the neutral axis under bending for beams of low aspect ratio.⁶⁷ In addition, the shear correction is useful in extending the theory of flexural vibration of beams to accommodate higher frequencies than possible with Euler-Bernoulli theory.^{70, 71, 72} The shear correction factor ' k ' is described as 'a ratio of average shear stress on a section to the product of shear modulus and angle of shear at the neutral axis'.⁷⁰ Numerical values for the shear correction factor are described as a function of the cross-sectional shape in multiple references with a numerical value of approximately 0.85~0.93 cited as appropriate for circular beams.^{70, 73, 74, 75} Note that by using a shear correction factor (k) value of '1.0', the Timoshenko shear effects can be removed from the model (Eq's. 18-20).

EOM Development:

The EOM was derived from the shape functions using the Lagrangian approach (Eq. 22) (MATLAB source code provided in Appendix E). Through this process, consistent matrices were developed for mass, damping and stiffness characteristics. Consistent matrices were desired to create a more accurate model than is possible with a 'lumped parameter' model.

$$\frac{\partial}{\partial t} \left(\frac{\partial KE}{\partial \dot{x}_i} - \frac{\partial PE}{\partial \dot{x}_i} \right) - \left(\frac{\partial KE}{\partial x_i} - \frac{\partial PE}{\partial x_i} \right) = 0 \quad (22)$$

The Kinetic Energy term is assembled in Eq. (23) with consideration for mass translation and rotary inertia (1st term), gyroscopic coupling (2nd term) and rotatory (spin-axis) effects(3rd term).^{8, 69, 76}

$$KE = \frac{1}{2} \{\dot{q}\}^T \{ [M_T] + [M_R] \} \{\dot{q}\} - \Omega \{\dot{q}\}^T [G] \{\dot{q}\} + \frac{1}{2} \dot{\Omega}^2 I \rho \quad (23)$$

The Potential Energy term is assembled in Eq. (24) with consideration for internal damping due to elastic bending (1st term), Timoshenko shear (2nd term) and axial load (3rd term) effects.^{8, 69, 76, 77, 78}

$$\begin{aligned}
 PE = \frac{1}{2} \{q\}^T & \left\{ \left[EI \left(\frac{\eta_H + 1}{\sqrt{1 + \eta_H^2}} \right) \int_0^L B_b^T B_b ds \right] + \left[\int_0^L kAG B_s^T B_s ds \right] + \int_0^L P B_a^T B_a ds \right\} \{q\} \\
 B_b &= \frac{\partial \begin{Bmatrix} \Gamma(s) \\ \beta(s) \end{Bmatrix}}{\partial s} \\
 B_s &= \begin{Bmatrix} \Gamma(s) \\ \beta(s) \end{Bmatrix} - B_a \\
 B_a &= \frac{\partial \begin{Bmatrix} v(s) \\ w(s) \end{Bmatrix}}{\partial s}
 \end{aligned} \tag{24}$$

In addition to the 'basic' EOM developed thru the Lagrangian process above, material effects known to add instability to the system are incorporated. Both factors are added directly to the EOM after Lagrangian operations. The Internal damping circulation matrix provides for instability associated with internal material damping and is given by Eq. (25).^{79, 76}

$$K_c = \int_0^L EI \begin{bmatrix} 0 & -1 \\ 1 & 0 \end{bmatrix} B_b \Big]^T B_n ds \tag{25}$$

Internal viscous material damping also provides energy dissipation and is accounted for as a Dissipation Energy term applied to the EOM as part of the overall Damping matrix. The Dissipation Energy term is given by Eq. (26).⁷⁶

$$ED = \frac{1}{2} \eta_v \{\dot{q}\}^T \left[\int_0^L EI B_b^T B_b ds \right] \{\dot{q}\} \tag{26}$$

An additional feature desired of this project is the ability to model geometries that vary linearly along the length (such as conical features); including consideration for hollow elements. In this way, more realistic models can be developed, and non-linear variations can be approximated using the linear elements by faceting with appropriate element lengths. This was accomplished with guidance from Greenhill⁷⁶ and is an additive step to the EOM derivation described above. However, as described above, Greenhill's approach used a nodal model with 6-DOF (2 translational, 2 rotational due to bending effects and 2 rotational due to Timoshenko shear effects). A decision was made to reduce the model to

4-DOF per node (to improve computational efficiency), therefore the geometric equations provided in Greenhill⁷⁶ were re-derived for this 4-DOF approach. Appendix F contains the MATLAB source codes used to both develop and integrate the linearly varying geometry considerations into the distributed matrices developed above.

A challenge was encountered in efficiently using these geometric equations as input to the matrices developed in the 'EOM_derivation' code (of Appendix F). This was due to the complexities involved in the integrations with respect (primarily) to the Λ_z function (shear ratio term for Timoshenko properties). The problem is that, due to the size of the equations being integrated, an error occurred within the MATLAB process. A solution was identified to simplify the equations by maintaining key properties (A, I, J_p, J_t and Λ_z) as independent variables during the equation and matrix development (Appendix F and G). These terms are then computed numerically during the FEA matrix 'build' within the main code based on the elemental geometry and then implemented during the global matrix assembly. In this way, the equations are dramatically simplified, and the MATLAB error avoided.

The resulting EOM then is shown in its assembled form in Eq. (27) and includes all the desired effects described above. Note that this EOM does not include external damping or stiffness considerations from bearing and other system supports. These external elements are added to the EOM during matrix assembly for the full model. A full listing of the matrices is provided in Appendix G.

$$[M]\{\ddot{q}\} + [[ED] + \Omega[G]]\{\dot{q}\} + [[K] + \Omega[K_{dcmv}]]\{q\} = \{Q_F\} \quad (27)$$

where:

ED = Dissipation Energy Matrix due to material internal viscous damping

G = Gyroscopic Matrix

K = 'Basic' Stiffness Matrix (bending, axial, shear, material damping effects)

K_{dcmv} = Stiffness Damping Circulation Matrix

q = nodal displacement vector

The above development of the EOM and consistent matrices considers a single element with 2 end nodes. A final step then toward creating a useable EOM is the matrix assembly with respect to a multi-element model, including external damping and stiffness considerations due to system supports.

System definition is provided by the user in a formatted 'System Data' file. Appendix I contains an example System Data file for the dual-shaft example problem described previously. Definition of the

system is made through a ‘Super Node’ and ‘Super Element’ description process. That is, geometry is defined in terms of major (axial) geometric events and then later subdivided to ‘actual’ nodes and elements within the main code to the desired level of discretization. The ‘Super Node’ definition method is useful to minimize complexity in general model definition while allowing for a convenient method to identify varying geometry, material properties, application of loads and boundary conditions, support connections, etc.

Each Super Element is discretized to FEA elements according to the user-defined parameter in the System Data file. System matrices are developed per above on an elemental level and standard matrix assembly techniques are used to develop the Global Matrices.⁸⁰ As part of this process, mass eccentricities defined for each Super Element in the System Data File are converted to nodal force inputs according to the element discretization. The eccentricity is assumed to act at the center of mass of the FEA element and nodal forces (normalized by rotational speed) are calculated based on the center of mass location for the element with respect to the end nodes as shown in Eq. (28). The resulting normalized nodal forces (F_{ecc}) are applied against the shaft rotational speed during execution of the main program to obtain true load values.

$$\begin{aligned} F_{ecc_i} &= (m_e e) \left(1 - \frac{\bar{y}}{L_e}\right) \\ F_{ecc_j} &= (m_e e) \left(\frac{\bar{y}}{L_e}\right) \end{aligned} \quad (28)$$

where:

m_e = mass of the element

e = radial mass eccentricity of the element

\bar{y} = location of element CG with respect to node i

L_e = axial length of element

System definition allows for the addition of lumped mass parameters (Mass and Rigid Disk); defined by Super Node location and each with a specified mass-eccentricity. For each, values of mass and inertia (both polar and transverse) are either specified directly in the System Data file by the user (lumped mass) or calculated based on specified diameter and thickness (Rigid Disk). Normalized eccentricity forces are applied to the nodal locations of the lumped feature in a manner like that described previously for elemental mass eccentricity.

Supports to the system are defined by Super Node location in the System Data file with user-specified stiffness and damping properties. Bearing and stiffness properties are assumed constant; however, non-isotropic properties are accepted with values specified in both 'y' and 'z' lateral directions as well as ' θ_y ' and ' θ_z ' rotations. Stiffness and damping parameters are added to the elemental matrices directly for rollup to the Global matrices.

External forces acting on the system are applied in 2 parts; loads derived from mass eccentricities (applied radially as function of rotating speed) and steady-state loads (forces and torques applied directly against a DOF) directly applied to a Super Node. These loads are used only for the computation of Frequency Response characteristics since Eigenanalysis leading to Critical Speed characteristics does not consider external loading.

Boundary Conditions (constraints) are applied to the model in the System Data file in 2 ways; explicit constraints on given Super Nodes (against any or all the 4-DOF) and constraints to all nodes against planar motion. Both work in the same way but allow convenience to the user in the identification of nodes involved. Constraint application is 'standard' in that matrix calculations are based on 'Free' or unconstrained nodes only.⁶⁸

Eigenvalue Analysis – Critical Speed Characteristics

As discussed previously, this work requires the prediction of both Critical Speed frequencies and Whirl stability and direction characteristics. As an alternative to a computationally intensive time-based solution of the EOM, Eigenvalue analysis provides an efficient means of obtaining these parameters as reported by multiple researchers. For general matrix structural analysis, Przemieniecki describes the use of Eigenvalue analysis to evaluate vibration based on stiffness and mass matrices⁸¹ and more generally for a geared set of parallel shafts with coupled torsional and lateral loads.⁸² Whirl analyses were also conducted using Eigenvalue techniques.^{77, 76} In addition to Critical Speed values, Eigenvalue analysis is used to obtain whirl stability and whirl direction information.¹ As a result, Eigenvalue analysis is incorporated in this work to predict Critical Speed characteristics and the major steps involved are identified below:

1. Eigenvalue analyses of the system EOM are conducted for a user-defined speed range and steps to define natural frequencies and Lambda values.^{1, 8} The complex eigenvalue is shown in Eq. (29) and provides 2 key pieces of information; the damped circular natural frequency (ω_d) and the reciprocal of the time constant of decay (λ).

$$s = \lambda + i\omega_d \quad (29)$$

2. Non-rotating natural frequencies and mode shapes (if allowed by the speed range set by the user) are extracted. Mode shapes are plotted and useful for supporting correctness of boundary conditions applied to the model.
3. Eigenvalue analysis results from Step 1 are used to develop 'mode curves' as a function of shaft speed. Mode curves relate the natural frequency response of the system at each of the operational speeds in preparation for identification of Critical Speeds and graphical display (Campbell plots).
4. The mode curves of Step 1 and 3 are evaluated against the synchronous curve to identify the speed range studied that 'spans' the synchronous curve. Additional points are then evaluated (Eigenvalue analysis) within this range so that a polynomial of user-specified order can be fit and compared to the synchronous curve to identify the Critical Speed. Quality of the polynomial fit is evaluated and reported in terms of both correlation coefficient (R^2) value and Normalized Root Mean Square Error (NRMSE-%). Eq. (30) and Eq. (31) identify these evaluations.

$$R^2 = 1 - \frac{\sum(f_{actual} - f_{curve})^2}{\sum(\Omega - \bar{\Omega})^2} \quad (30)$$

$$NRMSE = \frac{\sqrt{\sum(f_{actual} - f_{curve})^2}}{\bar{f}_{curve}} \quad (31)$$

where:

f_{actual} = frequency from Eigenvalue analysis

f_{curve} = frequency calculated from Polynomial

$\bar{\Omega}$ = mean of shaft speeds evaluated

\bar{f}_{curve} = mean of frequencies calculated from Polynomial

5. The Critical Speed is defined as the frequency at which the mode curve and synchronous curves intersect. This is accomplished algebraically, and the smallest real root identified as the Critical Speed. Re-evaluate the Eigenvalue analysis with the Critical speed value to obtain the appropriate λ value.^{1, 7}
6. Whirl direction is identified for each node along each beam through Eigenvalue analysis. As reported by Vance¹, the only way to definitively tell if a given shaft is whirling Forward, Backward, or both is through analysis. Mixed modes (both FW and BW whirl on a given shaft) frequently occur on rotors supported by fluid film bearings. At the transition, the rotor whirl 'orbit' becomes a straight line.¹ The whirl orbit analysis is based on the complex Eigenvalue result of Eq. (29) and the complex Eigenvector result for all nodal DOF at the selected CS. From the mode shape matrix, the UY and UZ deformations for each node (at the CS) are extracted and the phase angle and magnitude computed as the angle or vector sum of the real and imaginary components. The deformation magnitude then of the node (as a function of time through a single whirl orbit and for a given plane) is provided by Eq. (32).¹ Shape functions are used to convert these nodal results to more refined displacements for plotting.

$$x(t) = e^{\lambda t} X \cos(\omega_d t - \Phi) \quad (32)$$

where:

λ, ω_d are obtained from Eq. (30)

X, Φ are magnitude and phase from the complex eigenvector

7. The direction of whirl orbit rotation is evaluated per node and CS by computing the angular relationship of successive whirl orbit points. By means of Eq. (33) for each of the successive planar (UY, UZ) deformations of Eq. (32), the positive or negative direction of whirl (α) around the orbit can be identified. If some nodes on a given beam rotate in one direction and 1 or more in the opposite, then the beam's whirl direction is 'mixed'.

$$\alpha = \tan^{-1} \left(\frac{UY}{UZ} \right) \quad (33)$$

Steady-State Component Analysis – Flexural Response Characteristics

A computationally expensive time-based solution of the EOM can also be used to evaluate the flexural response of the beams. However, a more efficient method is to convert the EOM to a Steady-State Component analysis equation (in sin and cos) and solve the determinant for both Eigenvalue and Eigenvector complex results.^{8, 83} Development of equations to convert a generic EOM to the Component equation is presented in Appendix J. The solution for a n-DOF problem is developed and shown as Eq. (34).

$$\begin{Bmatrix} X_{1s} \\ \vdots \\ X_{Ns} \\ X_{1c} \\ \vdots \\ X_{Nc} \end{Bmatrix} = INV \begin{bmatrix} [-\omega^2[M] + [K]]_{NxN} & -\omega[C]_{NxN} \\ \omega[C]_{NxN} & [-\omega^2[M] + [K]]_{NxN} \end{bmatrix} \begin{Bmatrix} F_{1s} \\ \vdots \\ F_{Ns} \\ F_{1c} \\ \vdots \\ F_{Nc} \end{Bmatrix} \quad (34)$$

where:
s = sin components
c = cosine components

FRP results are calculated for both beam (nodal) lateral deformation (UY and UZ) and support reaction force for a user-defined frequency step across the range of shaft speeds studied. The load vector (as discussed previously) is composed of both mass-eccentricity and externally-applied constant forces.

Bearing reaction forces are defined as a function of nodal displacement, support spring stiffness and damping parameters and shaft spin speed as shown in Eq. (35).¹

$$F_{support} = \sqrt{\left(UY^2 \left(K_{support_y}^2 + (\omega C_{support_y})^2\right)\right) + \left(UZ^2 \left(K_{support_z}^2 + (\omega C_{support_z})^2\right)\right)} \quad (35)$$

Optimization Method Development

A second key part of the research supporting this work is development of an optimization methodology that meets the following requirements:

- Appropriate for expensive, black-box function generators with high-modality responses
- Appropriate for non-self-adjoint systems including Rotordynamic EOM's
- Appropriate for systems with both input- and results-based constraints
- Ability to consider multiple design objectives
- Ability to provide robustness information about the identified optimums

Literature describes RBDO optimization solutions that meet several of these requirements (discussed previously), including the ability to provide robustness information about the optimums. However, these methods are also described as computationally intensive and with limited appropriateness to HEB functions and therefore not identified as an optimal solution to the needs of this work. Rather, this research effort focuses on adaptation of a deterministic method shown to be effective for HEB systems to also provide robustness information useful to the designer.

A deterministic optimization method focused on HEB systems was developed as part of the author's work toward the degree of Master of Science in Mechanical Engineering at UTA (2015), toward optimization of non-rotating structural dynamic systems. Specifically, that work derived a deterministic, hybrid methodology useful for constrained optimization of HEB systems. In addition to the Master of Science (MSME) Thesis⁸⁴, the work also resulted in the peer-reviewed, published paper⁶¹ of Appendix A.

The deterministic methodology of that previous effort is leveraged toward this Ph.D. research and the requirements listed above. A second paper⁸⁵ published by the author (Appendix B) discusses this and compares the its effectiveness and efficiency with a Rotordynamic system (non-self-adjoint system with high response modality) against other, more conventional methodologies. In addition to the Journal publication (Appendix B), this work was also accepted for poster presentation to the World Congress of Structural and Multidisciplinary Optimization in 2019 (WCSMO13).

This deterministic method then is further expanded under this research to include the desired ability to provide robustness information as part of the optimization process. The remaining sections of

this Chapter provide 1.) a summary of key elements of the deterministic hybrid methodology from Appendix A and B and 2.) added methodologies to address robustness as part of the solutions.

The deterministic aspect of the proposed optimization method is a Combined or Hybrid Optimization Algorithm; comprised of an initial survey of the entire design space using a Global Optimization tool followed by a more efficient Local Optimization tool to refine the potential solutions for a more accurate Global Optimum. The proposed method then first uses a derivative of the first-order method of Steepest Descent (SD), termed Steepest Feasible Descent (SFD), making it effective for constrained searches, and useful for the global survey. Once identified, the solution(s) of the global search become the starting point for local search(es) using the more efficient SQP methodology. Key aspects of the proposed hybrid methodology are summarized in the following sub-sections. For more detail, the reader may reference the MSME Thesis⁸⁴ or the published papers of Appendix A⁶¹ and Appendix B⁸⁵.

General Programmatic Flow

The general functionality starts with (potentially many) user-defined start points throughout the design space. From each start point, a Search Vector (direction) is identified via Finite Difference (FD) methodology as the steepest descent vector into feasible design space based on finite difference methodology. Using this vector orientation, the distance to the nearest input constraint bound is computed and used as the length of a 1-D line search. A Polynomial 1-D line search identifies and evaluates points along the vector to derive an optimum. The process from start point evaluation to ID of the 1-D line search optimum is identified as a 'jump'. The 1-D optimum from the first 'jump' then is used as the start point for a second 'jump' and so on until either convergence is achieved or a maximum user-defined number of 'jumps' is achieved. This process is illustrated for a 2-DOF design space in the figure below. MATLAB's 'fmincon' implementation of the SQP process is then used from the final SFD 1-D optimum to conclude the process.

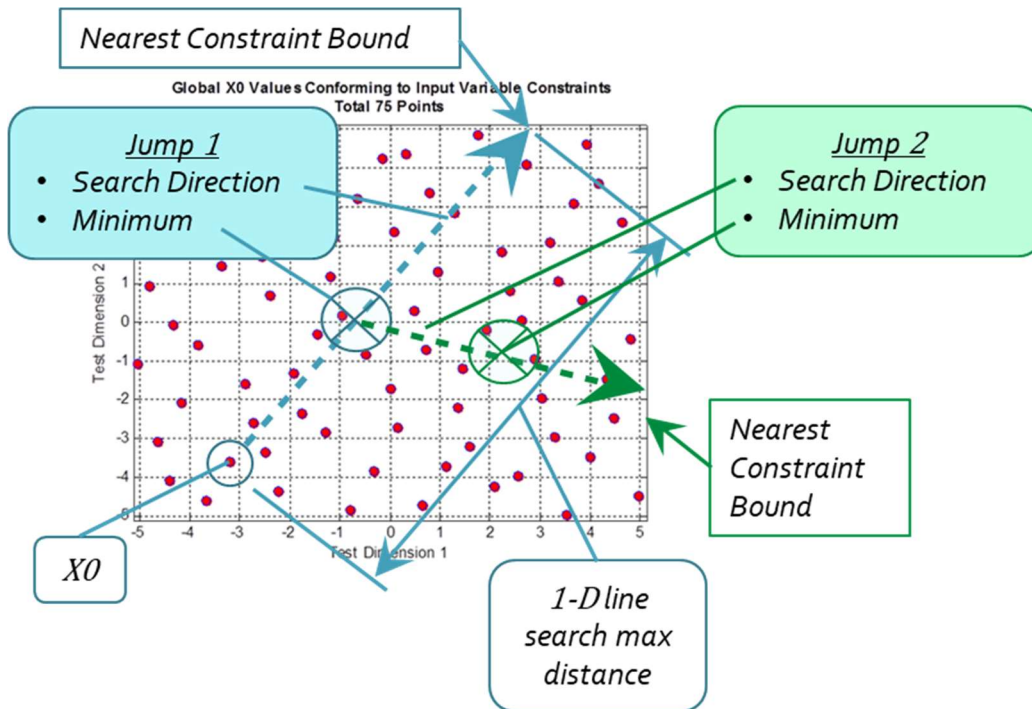


Figure 2-2 Steepest Feasible Descent Methodology

Search Vector direction – Finite Difference and Magnitude Sensitivity

The gradient for the search vector definition is based on a Finite Difference approach because of the use of FEA as a BB function generator. It is recognized that analytical methods, such as the Adjoint method^{86, 87, 88} and others offer significant computational efficiencies to the proposed FD technique. However, as with Othmer⁸⁹, the problem to be solved involves the use of FEA as a Black Box function generator which precludes use of the Adjoint method. It is recognized by the author that the special purpose FEA tool developed in this research could be modified to export data useful to an Adjoint method. However, a goal of the optimization methodology is intended to be representative of (and useful with) a commercial FEA program. For commercial FEA programs, the source code is commonly unavailable to the optimization routine; precluding effective use of the Adjoint method. Therefore, the FD approach is utilized with modifications for orientation to feasible space, etc. as discussed in this section.

A challenge to the FD method is that the Rotordynamic problem under study demonstrates a class of problems where the design variables may have significantly different orders of magnitude (length

vs. spring stiffness for example). This can lead to sensitivity error in the search vector when this method is employed. That is, if a common step size were computed as appropriate to a variable with smaller magnitude, and subsequently applied to all design variables, then the step size could be so small as to have an insignificant effect upon a variable of larger magnitude.

An option (to the common step size) explored here is to define the step size for each design variable individually based upon the magnitude of the variable at its lower and upper (side) bounds. In this way, the step sizes used in the FD evaluation of the Search Vector would be more numerically appropriate to each variable. This is given in equation below and provides both a numerical solution to this challenge and the benefit of a ‘generalized’ nondimensionalization technique within the code for user convenience.

$$\Delta_x = \alpha_a \left(\frac{x_{Upper\ Bound} - x_{Lower\ Bond}}{2} \right) \quad (36)$$

Where:

α_a = percentage of average

A numerical example of this technique is presented in the published paper of Appendix B which illustrates the benefits of the method.

Search Vector Limitation within Feasible Design Space

A common method of constraint handling with respect to search vector direction is the Method of Feasible Directions (MFD)⁵⁵. Here, an offset of ‘push-off factor’ is applied to the search vector to avoid a constraint bound. In cases of nonlinear constraint bounds however, this process is less effective and an additional ‘optimization exercise’ is needed to avoid infeasible space.

The proposed method of SFD is intended to be used in circumstances where multiple linearities exist including the high modality responses and other effects. Therefore, a programmatic implementation of MFD is incorporated to avoid a potentially large subproblem for a more conventional implementation of MFD. In general, the methodology evaluates the distance from the start point to the nearest (input) constraint bound against a user-defined minimum (as a percentage of distance across the design space). If shorter than allowable, that vector component that ‘points’ most directly into the nearest constraint

bound is converted to '0' in order to reorient the vector more directly into feasible space. The figure below illustrates this process in a conventional flowchart format.

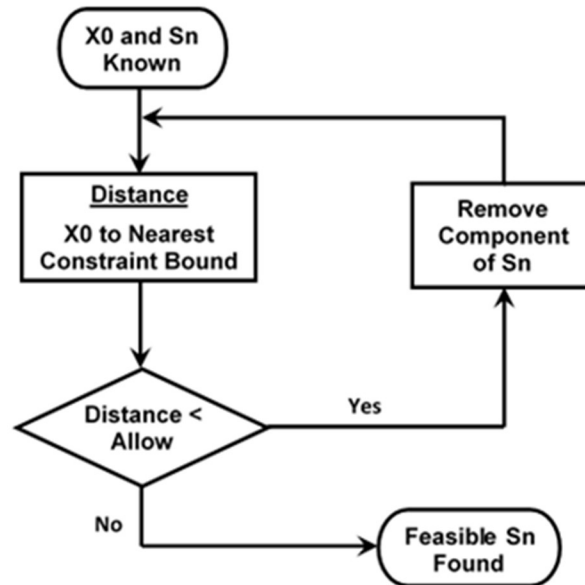


Figure 2-3 Flowchart – Feasible Sn Selection

Line search – Considerations for Constraints and High Modality Response

As with conventional SD methods, the proposed SFD method uses a 1-D line search along a given S_n vector to identify a given iteration's optimum. Various methods for such searches have been developed over the years but given consideration for use with high modality responses a polynomial search is implemented in the proposed SFD method.

Conceptually, the polynomial 1-D search is computed based on an initial sampling of points along the length of the S_n vector, from which a regression coefficient is computed and compared to a predetermined acceptance criterion. If unacceptable, additional points are programmatically selected near the anticipated minima and the order of the polynomial increased (up to a user-defined maximum) to improve the curve fit. For responses of low or moderate modality, acceptance by this method can generally be achieved relatively quickly. However, for high modality responses convergence can be challenging. In this event, the strategy shifts from that of adding points near the anticipated minima to

that of eliminating points far from the observed minimum (along the 1-D search). In this way, the quality of the curve fit can (potentially) be improved near the observed minimum.

As with determination of the descent vector S_n , constraints (both input and results-based) must be considered in the line search algorithm. Multiple methods exist to apply penalties to an unconstrained search methodology and make it useful as a constrained tool. Chen and Chi⁹⁰ for example utilize a penalty function to improve their particle swarm algorithm by applying a penalty to particles that are at the upper or lower bound of the design variable definition. Another researcher explored an interior penalty (IP) method⁹¹ as a type of discontinuous Galerkin method for the spatial discretization of elliptic partial differential equations. As discussed by that author however, a notable drawback of the IP method is that if the user-selected penalty parameter is not sufficiently large, the approximate solution is unstable.

In the development of the proposed SFD method, feasibility with respect to constraint(s) is considered during the execution of the line search in multiple ways. First, the length of the line search is limited by design variable constraint bounds (both side bounds and other, discussed previously). Secondly, as proposed by Vanderplaats⁵⁵, an external penalty term is combined with the function value $f(x)$ to form a penalized function value $f(x)_{pen}$ to be used as the objective function. This is shown in the equation below.

$$f(x)_{pen} = f(x) + \alpha_p \sum_{j=1}^n \left(\max [0, g_j(x)]^2 \right) \quad (37)$$

As shown, the penalty function is a second-order function. This is selected so that the penalty value at the constraint bound has a slope of zero; ensuring a continuous slope of the penalized function value through this region. If only a linear form were used, a discontinuity is possible at the constraint bounds adding risk of numerical ill-conditioning. Additionally, a penalty multiplier (α_p) is included to aid the 1-D line search by scaling the effect of the penalty to preclude minima from being identified within infeasible space. That is, a multiplier value that is too weak can limit the penalty value such that the penalized function value remains as infeasible. If too strong however, the minima could artificially be 'pushed' away from the constraint bound. The figure below illustrates these concepts.

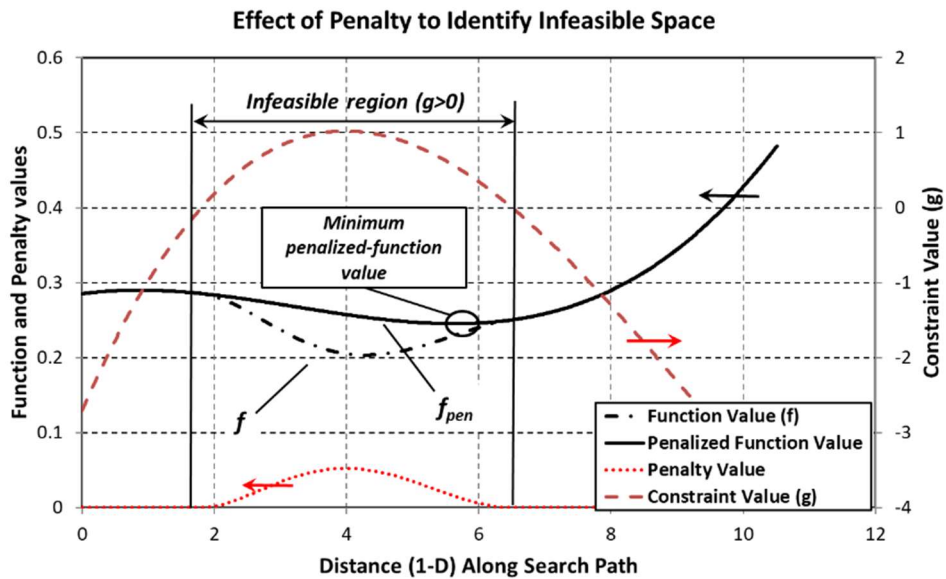


Figure 2-4 Use of Penalty Function in 1-D Line Search

Although helpful in tailoring the penalty function, optimal selection of the penalty multiplier can be problem dependent; the risk of an improperly selected value being that the resulting minima could either remain within infeasible space or be pushed artificially ‘far’ from the constraint bound.

To address this, a programmatic element is incorporated to the SFD method in the event that the penalized minimum (f_{pen}) is identified as being infeasible. In this case, the function values at the bounding constraints are evaluated and the appropriate minimum identified (such as the right-most constraint bound of Figure 2-4). In this way a minimum $f(x)_{pen}$ is precluded from being identified within infeasible space during the line search; allowing that a penalty value can be selected conservatively small while avoiding excessive ‘pushout’ without risk of finding an infeasible result. It is recognized that this programmatic search could be avoided by incorporating a sub-problem to optimize the penalty multiplier such that the ‘0’ of the penalized function value’s derivative coincides with the constraint bound. However, this requires computations potentially adding significant encumbrance to the overall problem. The proposed combination of penalty multiplier and programmatic consideration then is theorized to achieve the desired constraint-handling effects acceptably with improved computational efficiency.

Use of a Single Objective Tool for Multi-Objective Optimization

The algorithms described here (both Steepest Feasible Descent and SQP) are Single-Objective Optimization tools. That is, they are appropriate for optimization of a single objective. They can, however, be utilized for Multi-Objective Optimization by combining the elements of various 'individual' single objectives into a single 'combination' objective function⁵⁵. One method of 'consolidating' these objectives is to create one objective function is to simply scalar versions of the component results. As described by Vanderplaats however it may also be necessary to consider weighting factors for the components of this multi-faceted optimization function; especially if the magnitudes of the components are significantly different⁵⁵. Otherwise, the optimization algorithm would disproportionately 'focus' its efforts to minimize the larger magnitude response at the expense of the other. Normalization of constraint functions should also be considered for similar reasons.

Robustness Assessment

Robustness, in terms of this discussion, is defined in the classical sense as the quantified variation in response(s) as a function of variation in the input. It can be argued that by identifying and minimizing sensitivity (of the response) as part of the optimization process then robustness is thereby inherently addressed. Although this is true and is inherently included in the deterministic optimization processes described in this work, it does not address the goal with regards to the classical definition of robustness given above. That is, by including sensitivity in the Objective Function, it is actually addressing the sensitivity in a deterministic fashion rather than addressing Robustness over the full design space. Therefore, an additional function to address Robustness is needed beyond minimization of sensitivity.

The literature review discussed previously describes a direct application of RBDO methods towards rotordynamic and HEB systems as being effective at considering robustness in the optimization process (with respect to the design space), but at the same time being computationally intensive and/or inefficient. Because of this, an alternate approach is identified in this Rotordynamic work. That is, rather than a direct application of RBDO methods as part of the optimization process, the approach pursued in

this work attempts compute the robustness of interim solutions over the design space and add that to consideration for the Optimal Result as part of the overall process. The following Pseudo-Code describes this at a high level for the proposed Hybrid SFD/SQP search methodology.

- a) Identify a discrete starting point '**X0**'
- b) Perform a search using SFD with defined number of 'jumps'
 1. Establish **search vector 'Sn'** (maximum descent = maximum design variable sensitivity)
 2. Compute distance along Sn from X0 to nearest constraint bound
 3. Compare distance to user-defined min allowable (%)
 4. If distance < min allowable, identify Sn vector component that points most directly to the constraint bound & convert Sn component to '0'
 5. Compare distance along new Sn to nearest constraint bound – repeat #4 as needed to achieve min allowable search distance (%)
 - If successful, conduct line search with revised Sn to identify a **potential 'optimum'** for this **SFD 'jump'**
 - If not successful, report search as 'in a constraint corner' and stop – point becomes a **potential 'optimum'** for this **SFD 'jump'**
 6. After the defined maximum number of 'jumps', **assess the Robustness** of the potential optimum
 - Discretize each DOF (input variable) using stated +/- tolerance around the potential optimum to form a 'grid' in n-DOF.
 - Evaluate the response at each of the grid points.
 - Compute a response function thru the grid points using multinomial expansion with optimization of least squares response to create term coefficients.
 - Use the response equation to iteratively evaluate the design space surrounding the potential optimum to identify a maximum and minimum response value.
 7. Report the Robustness for each potential Optimum as an aid to identifying the Optimal Solution among the various X0 potential Optimums. ***The overall result with the minimal deterministic Objective Function result and minimal result variation over the tolerated design space (Robustness about the potential Optimum) is identified as the overall Optimal Solution from the SFD process.***
- c) From the SFD's Optimal Solution, conduct an SQP search as described elsewhere for the proposed Hybrid methodology.
 1. Assess the Robustness of the resulting SQP search and report.
 2. The user may select from the potential optimums for the desired Optimal Solution as a function of trade-off between Objective Function value and Robustness at each point.

Figure 2-5 Pseudo-code – Robustness Application to Proposed SFD/SQP Optimization Process

A key aspect of the proposed Robustness assessment is the ability to compute a polynomial response equation through discretely evaluated Response Points with acceptable accuracy and with acceptable computational burden. Doing so for linear responses or for non-linear responses limited to 1- or 2-DOF is somewhat trivial. However, the goals of this study require that a response be formulated for an n-DOF problem with high modality. Unfortunately, at the time of this study MATLAB (the programmatic language used for these algorithms) does not include a function to directly fit a nonlinear response to more than 2 independent variables. Therefore, a methodology is created based on multinomial expansion of a sinusoidal response that is continuously differentiable as shown in the following equation.

$$y = \left(\sum_{i=1}^m A_i (\cos x_i * \sin x_i) \right)^n \quad (38)$$

Where:

- $n = \text{polynomial order}$
- $m = \text{DOF}$
- $A = \text{term coefficient}$

The classical Multinomial Theorem describes how to expand a power of a sum of terms to yield a summation of powers of the terms in that sum as given by the following equation.

$$(x_1 + x_2 + \dots + x_m)^n = \sum_{k_1+k_2+\dots+k_m=n} \binom{n}{k_1 + k_2 + \dots + k_m} \prod_{t=1}^m x_t^{k_t} \quad (39)$$

Where:

$$\text{multinomial coefficient} = \binom{n}{k_1 + k_2 + \dots + k_m} = \frac{n!}{k_1! * k_2! * \dots * k_m!}$$

The result is a complete polynomial (as might be obtained using Pascal's Triangle for 2DOF or Pascal's Pyramid for 3DOF) for a power 'n' of a collection of 'm' DOF. Application of the Multinomial Theorem for expansion in this study however differs in that the multinomial coefficients need to be computed alternatively in order to fit the resulting polynomial to the observed responses. This is accomplished by formulating an optimization problem to identify a set of term coefficients (A_i) for Eq. (38) according to the Least Squares method where the Sum of the Squared Residuals is used to formulate the

Objective Function. Accuracy of the response equation is assessed as the classical Root Mean Square Error (RMSE), normalized on the mean of the responses to produce the classical Normalized Root Mean Square Error (NRMSE) as given by the following equation.

$$NRMSE (\%) = \frac{\sqrt{\frac{\sum_{i=1}^N (y_f - y_o)^2}{N}}}{\bar{y}_o}$$

Where:

y_o = observed responses

y_f = forecast responses

\bar{y}_o = mean of observed responses

N = sample size

(40)

An alternative to the multinomial expansion technique may be to use a Taylor series expansion to approximate the response. An advantage of this approach is that Taylor series is known to approximate the response with very small error in the local area of the point where it is computed. However, as distance extends from that point, the error grows. In this way, a Taylor series can be thought of as a 'local' approximation method. By comparison, this work seeks a polynomial that will represent the response over a defined design space whose size may vary considerably from problem-to-problem or use-to-use. Therefore, the multinomial expansion is deemed to be more appropriate for this application than Taylor series expansion.

MATLAB features a variety of curve and surface fitting tools as part of their Curve Fitting Toolbox including Linear and Nonlinear Least Squares, Weighted Least Squares and Robust techniques to produce polynomial equations to fit known data points. Unfortunately, none of these methods allow the use of more than 2 independent variables and are therefore insufficient to fit the needs of the n-dimensional design spaces of this study. Therefore, a programmatic solution is included in this work based on the Multinomial Expansion theorem of Eq. (39).

Application of the Multinomial Expansion theorem to this problem requires a 2-step approach; a programmatic method for determining the terms (variables and powers involved) and a means of determining the various term coefficients necessary to predict the response. A goal of the expansion is to produce a complete polynomial that includes all combinations of variables as would be produced by a

'manual' expansion. By Eq.(39), it is known that a component of this is that the sum of the powers among the variables of any given term equates to the raised power of the base equation. The process for programmatic expansion of the terms of Eq. (38) then is provided in the Pseudo-Code of the Figure below.

a) Create a matrix of powers for each variable by term for numerical expansion.
 'exp' = [rows = terms, columns = powers for each independent variable]

$$y = (\sum_{i=1}^m A_i (\cos x_i * \sin x_i))^n = A_1^2 (\cos x_1 * \sin x_1)^2 (\cos x_2 * \sin x_2)^0 + 2[A_1 (\cos x_1 * \sin x_1)^1 A_2 (\cos x_2 * \sin x_2)^1] + (\cos x_1 * \sin x_1)^0 A_2^2 (\cos x_2 * \sin x_2)^2$$

$$\text{exp} = \begin{bmatrix} 2 & 0; \\ 1 & 1; \\ 0 & 2; \end{bmatrix};$$

b) Create a vector of coefficients for each term

- For convenience, redefine coefficients such that $\text{coef}_1 = A_1^2$, $\text{coef}_2 = 2A_1A_2$, $\text{coef}_3 = A_2^2$, etc.

c) Optimize vector of coefficients by minimizing Least Square residuals

Figure 2-6 Pseudo-code – Programmatic Term Expansion – Response Equation

Optimization of the coefficients to complete the multinomial response fit is an unconstrained problem in that neither side bounds or other constraints apply to the coefficient values being optimized nor are there constraints on the result. Therefore, optimization tools within MATLAB hold potential for use including fminunc and fmincon. Since both fmincon and GA can consider multiple types of constraints, each is setup for this problem without consideration for constraints. A side-by-side comparison of the use of these tools is explored in a later section in order to identify which is most appropriate in terms of both effectiveness and efficiency.

Once the vector of coefficients is identified to complete the numerical equation, the design space surrounding the potential optimum is surveyed using this equation and MATLAB's Optimization function to determine a maxima and minima in addition to the value for the proposed optimum (at the center of the local design space). These values subsequently are used to form the Robustness statement for the design space (within declared DOF tolerances) surrounding the potential optimum. Since this search is

within a bounded design space, MATLAB's fmincon (only) is considered. As with the optimization routine to define the equation coefficients, a side-by-side comparison of both effectiveness and efficiency of these 2 tools is presented in a later section; supporting a decision as to which is more appropriate to include in the Optimization program.

The resulting source code for the robustness evaluation as applied to a 'toy problem' using Rastrigin's function (in n-DOF) is presented in Appendix H. Performance of the code, appropriateness of the Rastrigin's function as an evaluation tool and key conclusions are presented in a later section of this report.

Chapter 3

Confirmation Challenges for Developed Software and Results

Rotordynamic Finite Element Model

At the time that this document is written, a working draft of the Rotordynamic FEA code is completed at version 1.5 (Flexible_Rotordynamics_v1_5.m). Correctness checks of the various elements supporting development of that code as well as high-level functionality of the FEA code are discussed in this Chapter.

Correctness Checks - Shape Function Equations:

Shape function equations were derived with particular guidance from Bazoune and Khulief.⁶⁷ In addition, the developed shape functions were compared against the following resources and found to be consistent. These references were selected because of their included reference to Timoshenko shear coefficients and other pertinent commonalities:

Table 3-1 Literature references used to confirm shape function equation correctness

Nelson and McVaugh ⁷⁷	Kosmatka ⁹²	Bazoune and Khulief ⁹³
Zorzi and Nelson ⁷⁹	Choi et. al. ⁷⁸	Dong and Taciroglu ⁷³
Nelson ⁶⁹	Yokoyama ⁹⁴	Mindlin and Deresiewicz ⁷⁰
Greenhill et. al. ⁷⁶	Friedman and Kosmatka ⁹⁵	Labuschagne et. al. ⁷²
Childs ⁸		

Correctness Checks - EOM Matrix Equations:

Matrix confirmations are implemented against published literature within the MATLAB code used to develop the equations 'EOM_derivation_01Sep.m' (Appendix E). As noted, the Matrices provided by the various references provide 'components' of the assembled matrices used in this work. That is, some references might include Timoshenko shear effects, but not internal material damping characteristics, etc. The comparison to a given reference then is made by setting the features not considered by the reference to '0' in the developed matrix and then subtracting the reference matrix from the developed matrix. For example, in the case that internal material damping is not considered in the reference matrix, the appropriate material damping constants are set to '0' in the developed matrix prior to the matrix

comparison. A result of '0' from the matrix comparison (subtraction) supports that the developed matrix matches the reference matrix. A list of the references used to evaluate the correctness of the developed matrices, together with the features included in each is provided in the Table below. All comparisons support that the developed matrices match the reference matrices. Note that some typographical errors were identified in the references. Correctness of the developed matrices with respect to the identified typo are confirmed by inspection of the matrix development via Lagrangian technique and comparison with other references with similar features. Comments detailing these observations and confirmations are embedded within the EOM development code provided in Appendix E.

Table 3-2 Literature references used to confirm EOM matrix correctness

Reference	Matrices Confirmed	Key Components
Nelson and McVaugh ⁷⁷	Mass Gyroscopic Stiffness	Euler-Bernoulli Beam
Zorzi and Nelson ⁷⁹	Mass Dissipation Energy Gyroscopic Stiffness Internal Damping Circulation	Euler-Bernoulli Beam Internal Material Damping
Nelson ⁶⁹	Mass Gyroscopic Stiffness	Timoshenko shear
Greenhill et. al. ⁷⁶	Mass Dissipation Energy Gyroscopic Stiffness Internal Damping Circulation	Euler-Bernoulli Beam Internal Material Damping

Correctness Checks - Linearly Varying Geometry:

Correctness of the equations for mass properties of the linearly varying geometry features were confirmed both by comparison of the developed equations to conventional closed form equations (limited to solid cylinders and cones) and numerically to results for a set of example models using the commercial CAD software Creo 3.0 (PTC, Inc.). Equation comparisons were embedded within the MATLAB code used to develop the inertia equations (Appendix F). Additionally, numerical confirmation tests for non-prismatic geometries are presented in this section and include definition of a (single) linearly-varying element with both solid and hollow, conic and cylindrical configurations and with variation in the direction

of taper applied to both ID and OD. The figure below illustrates a typical element modeled in Creo. The tables below summarize results of the comparison. As shown, a maximum error of 0.00153% was measured. This result confirms for the intended use of this software that the equations adequately predict the geometric mass properties of linearly varying solid and hollow, cylindrical and conic elements.

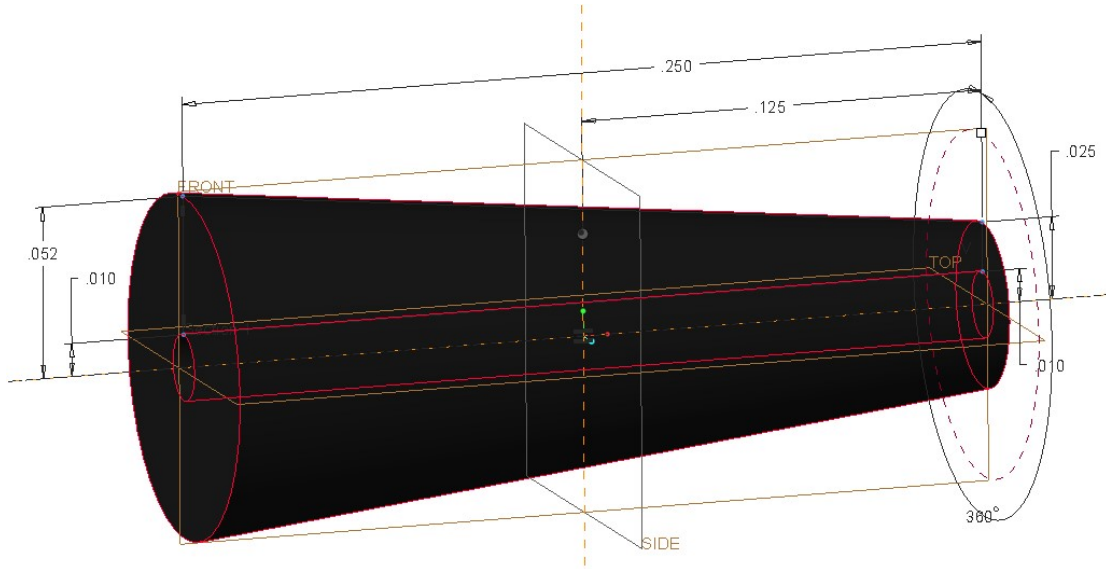


Figure 3-1 Linearly varying conic element used for correctness checks – Creo

Table 3-3 Confirmation Data – Geometric Mass Calculations

Interior (r) and Exterior (R) Radii				Creo			Code Calculations		
r_i (m)	r_j (m)	R_i (m)	R_j (m)	Mass (kg)	I_p (kg*m ²)	I_t (kg*m ²)	Mass (kg)	I_p (kg*m ²)	I_t (kg*m ²)
0	0	1.32E-03	1.32E-03	2.7261E-04	2.3779E-10	1.0349E-09	2.7261E-04	2.3779E-10	1.0349E-09
0	0	6.35E-04	1.32E-03	1.5556E-04	8.9240E-11	5.0472E-10	1.5556E-04	8.9240E-11	5.0473E-10
2.54E-04	0	6.35E-04	1.32E-03	1.5220E-04	8.9175E-11	4.8143E-10	1.5220E-04	8.9175E-11	4.8144E-10
0	2.54E-04	6.35E-04	1.32E-03	1.5220E-04	8.9175E-11	4.9698E-10	1.5220E-04	8.9175E-11	4.9699E-10
2.54E-04	2.54E-04	6.35E-04	1.32E-03	1.4548E-04	8.8915E-11	4.6520E-10	1.4548E-04	8.8915E-11	4.6521E-10
2.54E-04	2.54E-04	1.32E-03	1.32E-03	2.6253E-04	2.3746E-10	1.0009E-09	2.6253E-04	2.3746E-10	1.0009E-09
2.54E-04	0	1.32E-03	6.35E-04	1.5220E-04	8.9175E-11	4.9698E-10	1.5220E-04	8.9175E-11	4.9699E-10
2.54E-04	5.08E-04	1.32E-03	1.32E-03	2.4909E-04	2.3577E-10	9.5158E-10	2.4909E-04	2.3577E-10	9.5159E-10

Note: all cases $L_e=6.35e-3$ m, Density=7833.4 kg/m³

Table 3-4 Error Results – Geometric Mass Calculations

Interior (r) and Exterior (R) Radii				Error		
r_i (m)	r_j (m)	R_i (m)	R_j (m)	Mass (%)	I_p (%)	I_t (%)
0	0	1.32E-03	1.32E-03	0.00054%	0.00054%	0.00150%
0	0	6.35E-04	1.32E-03	0.00054%	0.00054%	0.00152%
2.54E-04	0	6.35E-04	1.32E-03	0.00054%	0.00054%	0.00152%
0	2.54E-04	6.35E-04	1.32E-03	0.00054%	0.00054%	0.00153%
2.54E-04	2.54E-04	6.35E-04	1.32E-03	0.00054%	0.00054%	0.00151%
2.54E-04	2.54E-04	1.32E-03	1.32E-03	0.00054%	0.00054%	0.00149%
2.54E-04	0	1.32E-03	6.35E-04	0.00054%	0.00054%	0.00152%
2.54E-04	5.08E-04	1.32E-03	1.32E-03	0.00054%	0.00054%	0.00149%

Correctness Checks - Assembled FEM Results – Static Deformations:

The correctness of the FE code, including the shape function equations, was confirmed in part through a static load-case analysis of a simple cylindrical beam. Four load cases were evaluated; Simply Supported - Simply-Supported, Clamped – Simply Supported, Clamped - Clamped and Clamped - Free. The beam is illustrated in the figure below. For these static load tests, the beam was defined to be OD=0.00127 m, Length=0.1270 m and constructed of steel (E=200 MPa). Loading is applied to the model including both a vertical force and moment at a midspan node (as illustrated below) in both the XY and XZ planes. Magnitude and direction of both force and moment are indicated in the header of the output plots. The static load FEM results are compared against deformations calculated via Castigliano's theorem. Results for the 4 boundary conditions are shown in the figures of Appendix K and support good subjective correlation of the results. Therefore, the FEM code is determined to be acceptable with respect to static deformations and interpolation of deformations via the shape function equations.

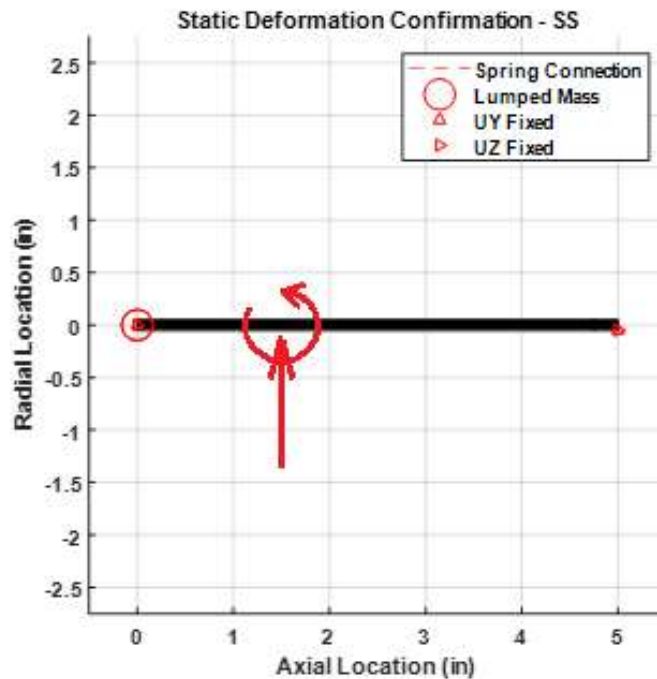


Figure 3-2 Example Beam Loading for Static FEM Confirmation

Correctness Checks - Non-Rotating Natural Frequencies and Mode Shapes:

The non-rotating natural frequencies and mode shapes were used to test the FEM code results to known values. As with the static deflection tests, multiple end configurations were evaluated for a prismatic cylindrical beam. The baselines for the evaluation were based on equations provided by Blevins⁹⁶ for Clamped-Free, Clamped-Simply Supported and Clamped-Clamped configurations. Calculations for natural frequency using Blevins' data are provided in Appendix L as are tabular results of frequency for the first 4 modes for a range of beam lengths; yielding beam aspect ratios ranging from 5:1 to 50:1. Also provided in Appendix L are the tabulated results from the FEM code for frequencies including a range of Timoshenko shear coefficients ranging from 0.85 to 1.0 as well as error values with respect to Blevins equations. Note that the shear coefficient value of 1.0 effectively inactivates shear compensation and is useful as a direct comparison to Blevins' equations since the Blevins reference is for Euler-Bernoulli beams only. Also provided in Appendix L are representative mode shape plots produced by the FEM code for shear coefficient values of 1.0.

This non-rotating natural frequency data (provided in Appendix L) supports 3 conclusions as follows.

- First, the FEM results (with shear factor of 1.0) compare favorably to Blevins equations for all aspect ratios greater than approximately 10:1 for fundamental modes and greater than 30:1 for all modes through mode 4. This indicates that for 'long' aspect ratio beams, appropriate to Euler-Bernoulli theory that the developed FEM code provides appropriate prediction of non-rotating natural frequencies.
- Secondly, natural frequency values show significant sensitivity to Timoshenko shear coefficient variation for beam aspect ratios less than approximately 30:1, with increased error with respect to a Euler-Bernoulli beam for the higher modes. This illustrates that the developed FEM code is sensitive to the additional shear influence in a manner consistent with expectations from literature (discussed previously).
- Finally, inspection of the mode shape plots compares favorably (from a subjective evaluation) to mode shapes commonly understood for prismatic beams with these 3 end configurations.

These results support that the FEM code performs acceptably with respect to prediction of non-rotating natural frequencies and mode shapes.

Correctness Checks - Rotordynamic Results vs. Literature:

Confirmation of high-level functionality of the Rotordynamic FEM code is evaluated by comparison to results published in literature. Two key works were used to study the code's ability to predict both damped and undamped system behavior; Zorzi & Nelson⁷⁹ and Vance et al¹. Both involve 'single-shaft' models and are illustrated in the figure below. Among the 2 models, a total of 5 case comparisons are made. Results are provided in the table below. Sample output plots are provided in Appendix M.

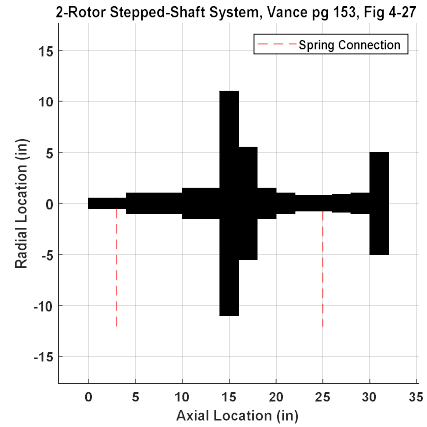
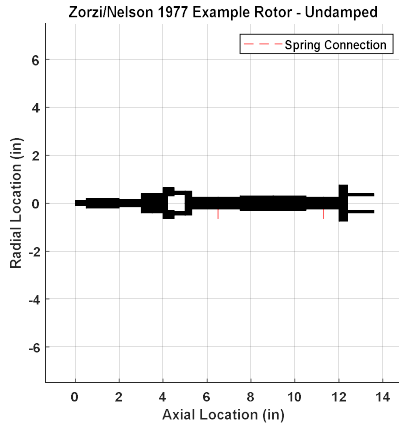


Figure 3-3 FEM models from literature used for code confirmation

Table 3-5 Confirmation data – rotordynamic results vs literature

Reference	Test Case	CS Mode 1 (RPM)		CS Mode 2 (RPM)		CS Mode 1 FW (RPM)	CS Mode 2 FW (RPM)
		BW	FW	BW	FW		
Zorzi, Nelson ⁷⁹	1) Undamped	Literature					
		16512	18200	46900	50500		
		FEM Code					
		17702	18004	58447	65887		
	Error (%)						
	+ 7.2%	-1.1%	+24.6%	+30.5%			
	2) Damped	Literature					
		17070	18600	48300	51800		
FEM Code							
17707		18010	58953	67067			
Error (%)							
+ 3.7%	-3.2%	+22.1%	+29.5%				
Vance et al ¹	1) K=1.751e6 N/m	Literature				1400	3100
		FEM Code				1354.6	3189.2
		Error (%)				-3.2%	+2.9%
		Literature				3900	4900
	2) K=1.751e7 N/m	FEM Code				3884.0	4857.7
		Error (%)				-0.4%	-0.9%
		Literature				5100	8000
		FEM Code				5304.0	7909.0
	Error (%)				+4.0%	-1.1%	
	3) K=1.751e8 N/m	Literature				5100	8000
		FEM Code				5304.0	7909.0
		Error (%)				+4.0%	-1.1%
Literature				5100	8000		
FEM Code				5304.0	7909.0		
Error (%)				+4.0%	-1.1%		

All the Vance comparisons and the Mode 1 comparisons against Zorzi & Nelson showed error of less than $\pm 7.5\%$ with most being less than $\pm 4\%$ and the Mode 2 results against Vance showed error of less than $\pm 3\%$. The Mode 2 results from Zorzi & Nelson however showed higher error with the FEM code overpredicting the frequencies in all cases.

The reason for this increased error is attributed to a tendency of the FEM code to overpredict higher modes for short L/D ratios. As noted with the non-rotating natural frequency evaluations described above (data in Appendix L), short L/D ratios are noted to produce errors in this range. Given that the focus of this work is on rotating equipment of long aspect ratios, this is determined to be acceptable. Therefore, these results support that the FEM code performs acceptably with respect to prediction of Critical Speed frequencies, FW/BW CS relationships and damped/non-damped performance with respect to literature comparisons.

Optimization Methodologies

Deterministic Functionality – Non-Rotating Structural Dynamic Model

The Deterministic Optimization method is evaluated for both effectiveness and efficiency against other common optimization methodologies researched and reported in literature. Fundamentally, the Optimization code is tested against 4 test functions from literature ranging from unimodal to highly modal and including an example of the Rosenbrock's Valley function which challenges optimization methods regarding convergence. These mathematical test functions are illustrated in the figure below.

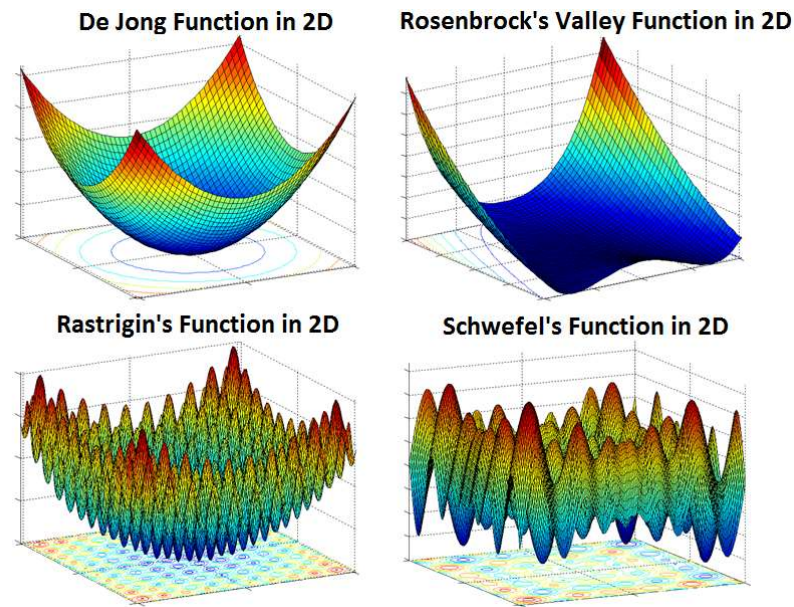


Figure 3-4 Optimization test functions in 2D

Both effectiveness and efficiency of the Deterministic code for non-rotating systems are discussed in the technical paper⁶¹ presented in Appendix A. These challenges confirm that the proposed method identifies appropriate global optimum values for both unconstrained and constrained systems for a variety of modalities and does so with acceptable efficiency.

Deterministic Functionality - Rotordynamic Model

The Deterministic code is evaluated with Rotordynamic systems as reported in the technical paper⁸⁵ presented in Appendix B (also accepted for poster presentation to WCSMO13). This work challenges the code against additional 'common' optimization methods including Genetic Algorithm and Particle Swarm, concluding that the proposed method has comparable effectiveness and significantly improved efficiency in identifying a global optimum for Rotordynamic, HEB functions.

As noted in the technical paper of Appendix B, both GA and PSO are potentially useful both as singular optimization solutions and as part of hybrid solutions. The investigations reported (Appendix B) are for use of GA and PSO as 'singular' methodologies. Considerations for use as part of a Hybrid methodology are discussed in a later section of this report.

Also, both GA and PSO as used in this report (and the investigation reported in Appendix B) are for constrained problems. MATLAB's 'ga' tool is used for this study 'as is' in that it includes capability to consider constraints. However, MATLAB's particle swarm tool is limited to unconstrained searches, therefore, an alternative PSO routine⁹⁷ was used which allows for nonlinear constraints. In this way, PSO can be compared directly with the other methodologies for the constrained searches of this study.

Deterministic Functionality – Proposed Method with Rotordynamic Model

Hybrid optimization methodologies are well researched with references discussed both in other areas of this report and in the author's journal paper provided in Appendix B. An advantage of hybrid methods is that they potentially can be used to leverage the benefits of the component methodologies while limiting key disadvantages. This is the intent behind the proposed combined (or hybrid) methodology (SFD followed by SQP) of this work.

To challenge the functionality of the proposed hybrid methodology against other methods (including both individualistic and hybrid methods) in terms of deterministic effectiveness and efficiency, a suite of comparisons is made and discussed in this section. These comparisons are identified in Table 3-7, each attempting to solve the constrained Rotordynamic problem of Figure 1-3 (defined by Table 1-1) by minimizing the Objective Function of Eq. (1) subject to the Constraints of Eq. (2) and Eq. (3).

The optimization methods of Table 3-7 involve different starting point schemes. The Proposed Hybrid, SFD and SQP searches for example require specification of discrete start point locations from which to begin the study whereas both GA and PSO require definition of design space regions and a quantity of start points (which the program distributes across the specified region) due to the evolutionary nature of their algorithms. In order to challenge the various methods for effectiveness (given the multi-modal nature of the response) with consideration for computational efficiency, the design space is divided into 9 regions (shown in Figure 3-5) to facilitate survey of the full design space. For the Proposed Hybrid, SFD and SQP methods, 1 start point in the approximate center of each region (or 9 total start points) are used.

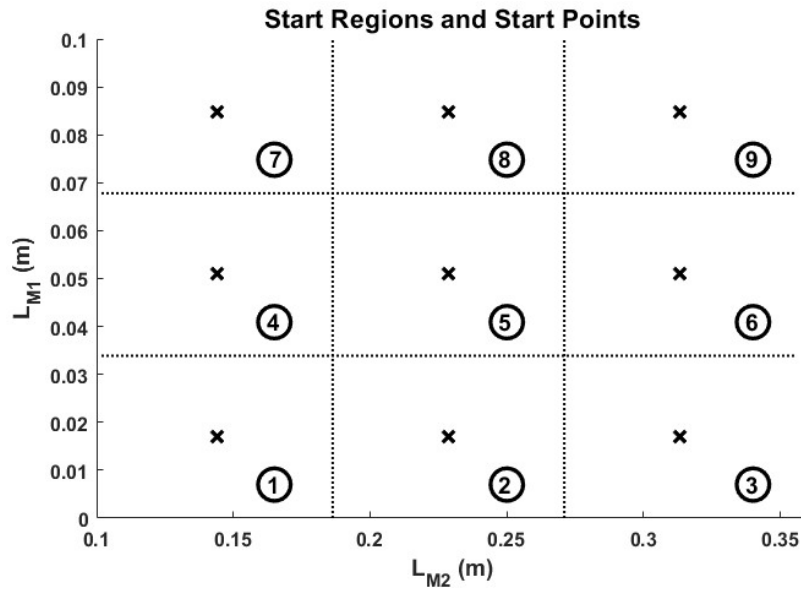


Figure 3-5 Start Locations for Optimization

Rather than an array of discrete starting points, both GA and PSO utilize identified starting regions and a defined quantity of points to apply to each region. The same start regions then (Figure 3-5) are used for GA and PSO evaluations with a total of 9 points being utilized per region. Definition of these starting regions is given in Table 3-6. For GA and PSO alike, this start region strategy results in an effective starting population across the entire design space of 81 points (9 regions x 9 points per region) whereas only 9 discrete starting points are specified for the Proposed Hybrid, SFD and SQP methods. In order that this variation does not inadvertently skew the study (either toward excessive function evaluations for the GA/PSO routines or reduced probability of success for the others, additional studies were made with GA and PSO utilizing 9 points across a single region spanning the entire design space. In this way, the (previously unstated) assumption that results of an optimization are to some degree influenced by the start point location strategy is equally challenged for all methods.

Table 3-6 Starting Region Definitions

Start Region	L_{M1} (m)	L_{M2} (m)
1	0.0 – 0.0339	0.1016 – 0.1863
2	0.0 – 0.0339	0.1863 – 0.2710
3	0.0 – 0.0339	0.2710 – 0.3556
4	0.0339 – 0.0678	0.1016 – 0.1863
5	0.0339 – 0.0678	0.1863 – 0.2710
6	0.0339 – 0.0678	0.2710 – 0.3556
7	0.0678 – 0.1016	0.1016 – 0.1863
8	0.0678 – 0.1016	0.1863 – 0.2710
9	0.0678 – 0.1016	0.2710 – 0.3556

Test ID #1 (Table 3-7) then is the Proposed Hybrid method and component methods (SFD & SQP), each using 9 start points distributed across the 2-DOF design space (per Figure 3-5). Test ID #2 and #3 use GA and PSO (respectively) to identify the optimum as individualistic methods each starting from 2 scenarios; a) 9 regions each with 9 starting points and b) a singular region over the entire design space with 9 starting points.

Test ID #4 and #5 convert the individualistic GA and PSO methods (of Test ID #2 and #3) into hybrid searches by adding subsequent searches using a) SFD, b) SQP and c) the Proposed Hybrid starting from the local design space surrounding the optimum identified from the GA (or PSO) base routine. In this context, the ‘local design space’ is defined as the region surrounding the base method’s optimum bounded by the design tolerances for each input variable (per Table 1-1). A total of 5 start points are used then for the subsequent study including the center point and 4 corner points.

Test ID #6 is a hybrid leveraging the optimal result (GCO) of the Constrained Mapping Survey (Figure 1-6) with subsequent searches using a) SFD, b) SQP and c) the Proposed Hybrid. As with the GA and PSO hybrids (ID #4 and 5), the subsequent searches start from the local region surrounding the GCO and include a total of 5 start points each.

Finally, Test ID #7 is similar to #1 except that the Design Space is initially surveyed by 100 randomly generated points, the best 10 of which are used as discrete start points for a) SFD, b) SQP and

c) the Proposed Hybrid searches. (This as compared to Test ID#1 where 9 starting points are used, each defined as the approximate center of the 9 evenly divided regions.) In this case, only the discrete 10-best solutions are used as subsequent start points to mimic the process of Test ID #1, but with starting points established from a more complete initial survey of the design space. The 100 randomly generated survey points (x's) and resulting 10 best results used as start points (o's) for Test ID #7 are illustrated in Figure 3-6 along with the Response Contours, GUO and GCO as presented previously (Figure 1-4 and Figure 1-6).

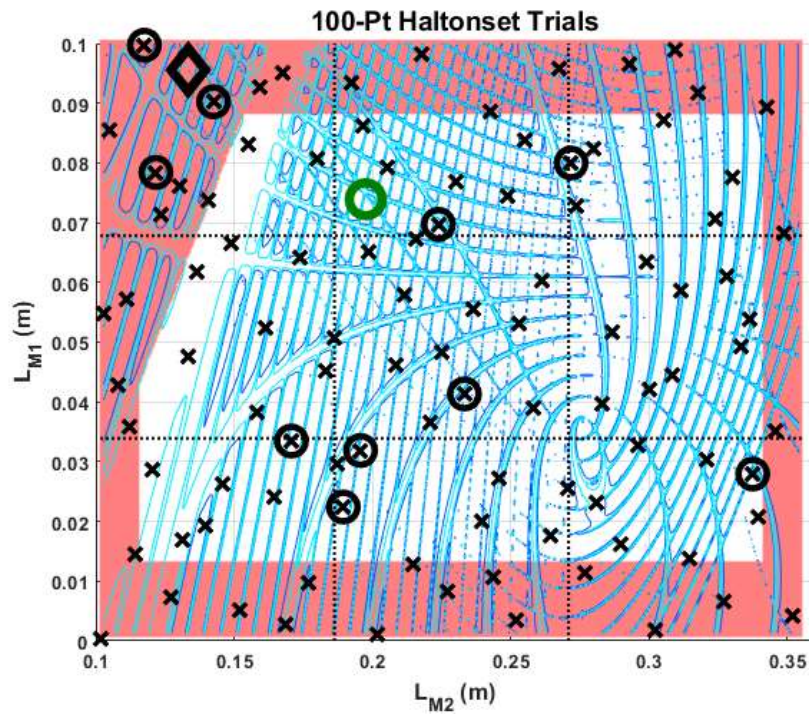


Figure 3-6 Start Locations 100-Pt Haltonset Trials (Test ID # 7)

Table 3-7 Deterministic Functionality – Rotordynamic Optimization Test Cases

Test ID	Optimization Method		Initial Search	Subsequent Search		Start Points (Ttl - Design Space)	
1	(a)	SFD Only	SFD			9	
	(b)	SQP Only	SQP			9	
	(c)	Proposed Hybrid	SFD	SQP		9	
2	GA Only		GA			(a)	9 regions / 81 pts Ttl
						(b)	1 region / 9 pts Ttl
3	PSO Only		PSO			(a)	9 regions / 81 pts Ttl
				(b)	1 region / 9 pts Ttl		
4	GA-Based Hybrid		GA (Test 4)	(a)	SFD	<i>5-pt Tol Bounds</i> ¹ surrounding best result of GA (Test ID 4)	
				(b)	SQP		
				(c)	SFD/SQP Hybrid		
5	PSO-Based Hybrid		PSO (Test 5)	(a)	SFD	<i>5-pt Tol Bounds</i> ¹ surrounding best result of PSO (Test ID 5)	
				(b)	SQP		
				(c)	SFD/SQP Hybrid		
6	Mapping Survey Based Hybrid		Constrained Mapping Survey (Figure 1-6)	(a)	SFD	<i>5-pt Tol Bounds</i> ¹ surrounding GCO of Constrained Mapping Survey (Figure 1-6)	
				(b)	SQP		
				(c)	SFD/SQP Hybrid		
7	Random Start Points		Random 100 points over design space	(a)	SFD	Best 10 results of initial random 100 points	
				(b)	SQP		
				(c)	SFD/SQP Hybrid		

1.) *'5-pt Tol Bounds'* equals 5 points defined as design space center plus min/max corners of each of 2-DOF.

Results of the Deterministic Optimization Challenge tests are provided in Table 3-8. Comparison of the results against baseline values are presented in Table 3-9. More specifically, effectiveness comparisons are made for each method against the Global Constrained Optimum (GCO) function value and efficiency comparisons relate the Total Function Evaluations against the function evaluations required by the Proposed Hybrid (Test ID #1c) method.

Table 3-8 Deterministic Functionality – Rotordynamic Optimization Test Results

Test ID	Optimization Method	Optimum Location		Minimum Function Value	Total Function Evaluations ²
		L _{M1} (m)	L _{M2} (m)		
GCO from Mapping Survey (Figure 1-6)		0.07398	0.19768	0.730384	387500
1	a) SFD Individually	0.07759	0.20384	0.740436	304
	b) SQP Individually	0.08890	0.31270	0.750859	484
	c) Proposed Hybrid (SFD + SQP)	0.07828	0.20411	0.735935	358
2	a) GA Individual – 9 regions / 81 Ttl start points	0.07398	0.19768	0.730406	4824
	b) GA Individual – 1 regions / 9 Ttl start points	<i>No Feasible Result Found</i>			
3	a) PSO Individual – 9 regions / 81 Ttl start points	0.04806	0.19613	0.734185	3446
	b) PSO Individual – 1 regions / 9 Ttl start points	0.08593	0.19469	0.736278	666
4	a) GA opt + SFD from '5-pt Tol Bounds'	0.07398	0.19768	0.730406	4933
	b) GA opt + SQP from '5-pt Tol Bounds'	0.07397	0.19770	0.730586	5086
	c) GA opt + Proposed Hybrid from '5-pt Tol Bounds'	0.07399	0.19768	0.730492	4954
5	a) PSO opt + SFD from '5-pt Tol Bounds' ¹	0.04806	0.19613	0.734186	3546
	b) PSO opt + SQP from '5-pt Tol Bounds' ¹	0.04798	0.19625	0.731987	3689
	c) PSO opt + Proposed Hybrid from '5-pt Tol Bounds' ¹	0.04805	0.19611	0.735492	3574
6	a) GCO opt + SFD from '5-pt Tol Bounds'	0.07400	0.19771	0.731033	387169
	b) GCO opt + SQP from '5-pt Tol Bounds'	0.07398	0.19768	0.730430	387760
	c) GCO opt + Proposed Hybrid from '5-pt Tol Bounds'	0.07395	0.19769	0.730741	387659
7	a) 100 pt. + SFD from 10 best survey results	0.06947	0.22255	0.736935	299
	b) 100 pt. + SQP from 10 best survey results	0.02837	0.33764	0.743008	870
	c) 100 pt. + Proposed Hybrid from 10 best survey results	0.06947	0.22257	0.736989	320

1) Optimum from PSO with 9 regions (81 total start points) used as starting point for Test ID # 7.

2) Total Function Evaluations of Hybrid include both Initial and Follow-on searches

The results of Table 3-8 illustrate that all methodologies which completed successfully identified a function value within approximately 2.8% of each other. However, the location of the optimal value (L_{M1} & L_{M2}) differed among the solutions. A subjective inspection of the Constrained Mapped results (Figure 1-6) supports that several locations across the design space have similar objective function values with respect to the various local maximas of the system. It is not surprising then that the different numerical optimization schemes might identify multiple locations with similar, minimal function values; particularly with consideration for the different start position schemes.

Table 3-9 Deterministic Functionality – Rotordynamic Optimization Result Comparisons

Test ID	Optimization Method	Minimum Function Value (Baseline = GCO = 0.730384)	Total Function Evaluations (Baseline = Proposed Hybrid SFD+SQP)
1	a) SFD Individually	+ 1.38%	- 15.1%
	b) SQP Individually	+ 2.80%	+ 35.2%
	c) Proposed Hybrid (SFD + SQP)	+ 0.76 %	Baseline
2	a) GA Individual – 9 regions / 81 Ttl start points	< 0.01%	+ 1247.5%
	b) GA Individual – 1 regions / 9 Ttl start points	<i>No Feasible Result Found</i>	
3	a) PSO Individual – 9 regions / 81 Ttl start points	+ 0.52%	+ 862.6%
	b) PSO Individual – 1 regions / 9 Ttl start points	+ 0.81%	+ 86.0%
4	a) GA opt + SFD from '5-pt Tol Bounds'	< 0.01%	+ 1277.9%
	b) GA opt + SQP from '5-pt Tol Bounds'	+ 0.03%	+ 1320.7%
	c) GA opt + Proposed Hybrid from '5-pt Tol Bounds'	+ 0.01%	+ 1283.8%
5	a) PSO opt + SFD from '5-pt Tol Bounds'	+ 0.52%	+ 890.5%
	b) PSO opt + SQP from '5-pt Tol Bounds'	+ 0.22%	+ 930.4%
	c) PSO opt + Proposed Hybrid from '5-pt Tol Bounds'	+ 0.70%	+ 898.3%
6	a) GCO opt + SFD from '5-pt Tol Bounds'	+ 0.09%	+ 108173.5%
	b) GCO opt + SQP from '5-pt Tol Bounds'	+ 0.01%	+108212.8%
	c) GCO opt + Proposed Hybrid from '5-pt Tol Bounds'	+ 0.05%	+108184.6%
7	a) 100 pt. + SFD from 10 best survey results	+ 0.90%	- 16.5%
	b) 100 pt. + SQP from 10 best survey results	+ 1.73%	+ 143.0%
	c) 100 pt. + Proposed Hybrid from 10 best survey results	+ 0.90%	- 10.6%

Table 3-8 identifies that the lowest function values (fobj) were produced by the GA-based processes (Test ID #2 and 4) using 9 starting regions each with 9 start points per region (total 81 start points). Here, the lowest function value was achieved with the standalone GA process (Test ID #2a) and then replicated with follow-on SFD search (Test ID #4a). For these, the function value was approximately equal to the GCO result (0.7304). The GA method using a starting population of 9 across a single region (full design space) failed to identify feasible options from which to continue and therefore failed in-process. It is recognized that an initial starting population of 9 is lower than considered 'normal' for GA but is comparable to the 9 start points used with the SFD, SQP and proposed Combination methods studied here.

The least effective results were obtained with the SFD and SQP methods applied independently (Test ID 1a & 1b); with errors of 1.38% and 2.80% respectively to the GCO.

The 2 PSO methods (Test ID #3a & 3b) and the proposed Combined (Test ID #1c) method were similar in their objective function accuracy with errors of 0.52%, 0.81% and 0.76% respectively.

Optimization searches starting with the 100-pt survey of the design space (Test ID #7) had similar effectiveness to the Proposed and SFD/SQP methods applied independently (Test ID #1) with error ranges of 0.90~1.73% and 0.76~2.80% respectively. This is attributed to the fact that the 100-pt survey searches are basically the same as those of Test ID#1 except that more start positions are considered from which to begin the searches. The additional starting points is attributed to the lower 'maximum error' of the 100-pt survey (1.73% - SQP) as compared to that of Test ID #1 (2.80% - SQP).

Test ID #6 effectively addresses the accuracy of the discretized mapping survey's GCO due to the selected step size. As shown, the 3 searches (Test ID #6a-6c) resulted in very similar results to the GCO with only improvements of between 0.01~0.09% identified.

Efficiencies of the methods (in terms of the number of function evaluations required) provide the greatest variability among the results. For this metric, all methods are compared against the proposed Combined method which required 358 function evaluations.

Although the GA method found the most accurate function value (< 0.01% error) it required significantly more function evaluation than the proposed Combination method (+1247%). GA-based hybrid methods (Test ID #4a-c) similarly required high function value counts ranging from 1278%~1321% above that of the proposed Hybrid method (Test ID #1c).

Both PSO individual methods (Test ID #3a, b) and hybrids (Test ID #5a-c) also required significantly greater function evaluations than the Proposed Hybrid method ranging from +86% to +930% among the variations. These data support statements made in literature^{55, 58, 59} that GA and PSO methods can require a high number of function evaluations, causing challenges when applied to multi-modal responses.

When used individually, the SQP solution identified an optimum with approximately 2.8% error to the GCO but required approximately 35% more function evaluations than the proposed combined method.

The SFD method when used individually found an optimum a little closer to the GCO (+1.4%) and used the fewest function evaluations of any tested method compared to the proposed Combination method (-15.1% for the 9-point start of Test ID #1a and -16.5% for the 100-pt start of Test ID #7a). Another interesting comparison from Table 3-8 is that the individual SFD and proposed Hybrid (Test ID #1a & 1c) found optimums with locations very close to each other and the GCO with L_{M1} and L_{M2} within 3.1~5.8% of the GCO. The individual SQP (Test ID #1b) identified an optimum significantly more distant.

These results support that the use of SQP is more effective as a local search tool (as with the Proposed Hybrid method) as compared to SQP used alone. That is, SQP is less effective as a global search tool in terms of both efficiency and effectiveness.

The SFD routine when used individually (for either 9-pt or 100-pt start scenarios) found an optimum that differs by 0.6% or less from the proposed Combined solution, yet improved efficiency by 15.1~16.5% (by omitting the 'follow-on' SQP local search). This supports that the SFD routine as an individual technique has merits when compared with SQP, GA and PSO for use on BB functions where evaluations are expensive, and response modality is high.

Figure 3-7 and Figure 3-8 provide a graphical view of the convergence behavior of the methods of Test ID #1; illustrating their ability to travel across a design space with high-modality response. Figure 3-7 illustrates the results of the SFD (individual) and proposed Hybrid methods. Given that the proposed Hybrid method and SFD are identical except for the addition of a single SQP optimization at the end of the SFD, both results are plotted together. (As shown in Table 3-8, the resulting optimum location from SFD and the proposed Hybrid are slightly different, but close enough for common illustration in Figure 3-7.) This data shows that the SFD / proposed Hybrid and SQP process from some start points travelled significantly across the design space and local maxima/minima in search of a global optimum. Importantly, the methods are observed to 'jump' the major local ridge. As evidenced by the number of

function evaluations (Table 3-8), the SQP process is observed to ‘wander’ more than the SFD / proposed Hybrid methods.

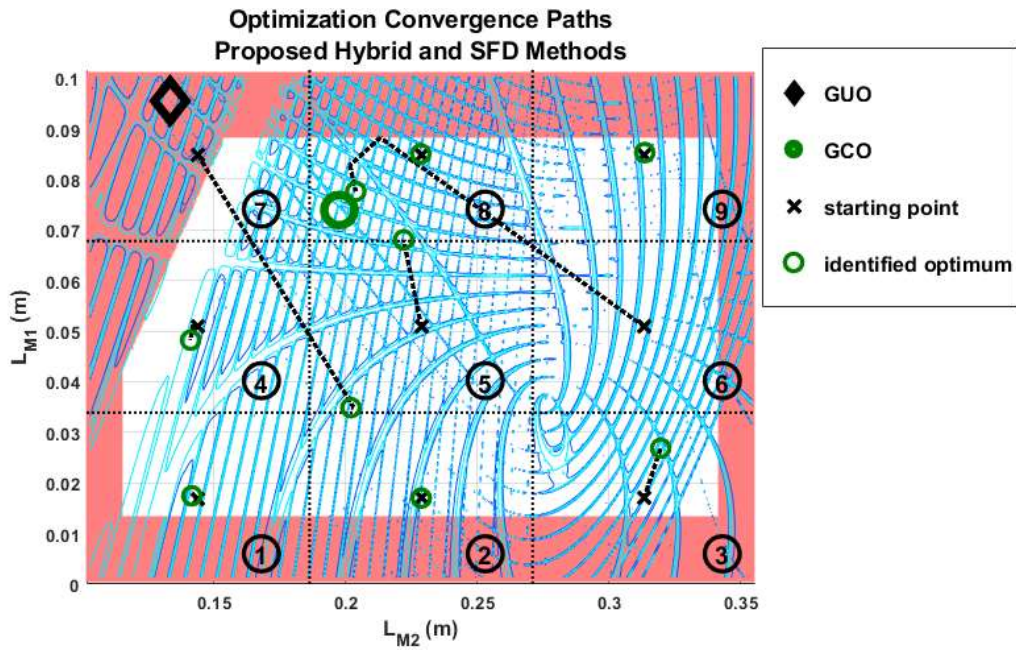


Figure 3-7 Optimization Paths – SFD & Proposed Hybrid (Test ID #1a, 1c)

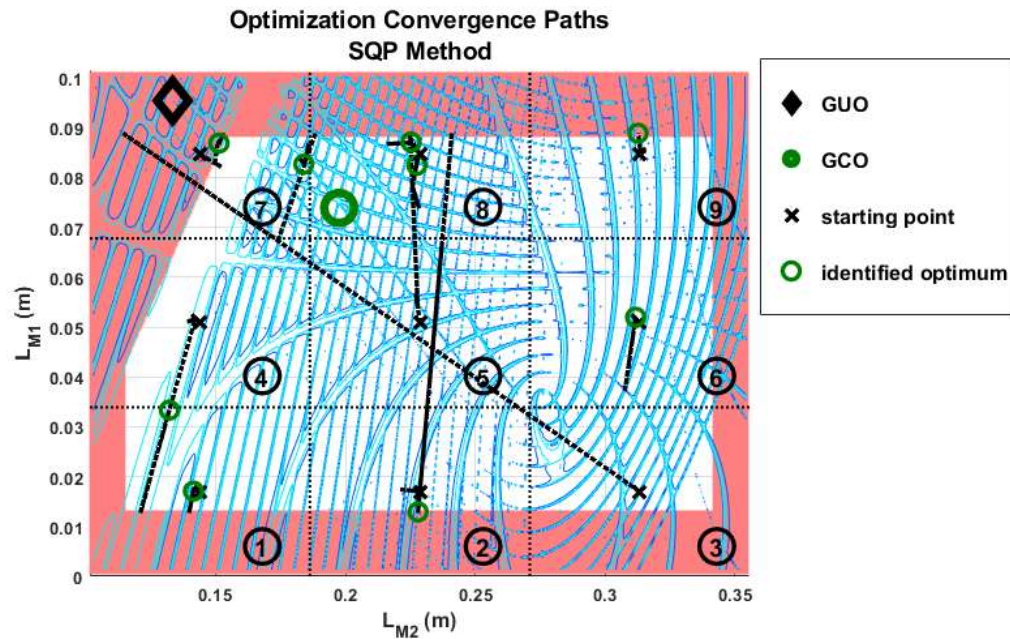


Figure 3-8 Optimization Paths – SQP (Test ID #1b)

Figure 3-9 illustrates summary information for both GA and PSO searches. Both are observed to traverse significant distance over the design space, but none are observed to jump the major ridge in search of a feasible optimum.

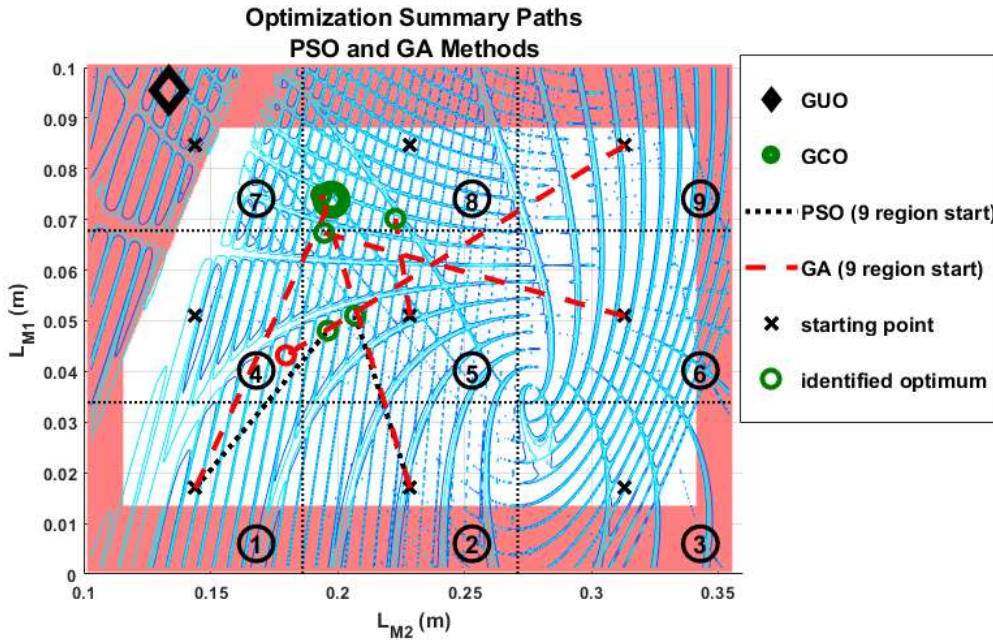


Figure 3-9 Optimization Path Summary – PSO and GA Methods

Robustness Assessment

The Robustness code (described in a previous section of this report and provided in Appendix H) is challenged for both effectiveness and efficiency in this section against 2 function generators. The initial challenge uses Rastrigin function⁶¹, a well-known test function for optimization algorithms at 3 different locations to test different regions of the response modality. Rastrigin function is a non-convex function in n-DOF with high modality that has similarity to the Rotordynamic response of the problem at hand. The response for Rastrigin function in 2-DOF is illustrated in Figure 3-4 as compared to the mapping results for the Rotordynamic problem illustrated in Figure 1-2. A second challenge tests the Robustness code against the Rotordynamic function generator at both the GCO (Figure 1-7) and GUO (Figure 1-5) locations.

In general, the challenges described in this section are focused on comparisons of performance for different optimization methodologies using the Rastrigin equation as a ‘toy problem’ or ‘test bed’, and then confirmation of the selected method using the actual Rotordynamic FEA code for the problem at hand at both GCO and GUO locations. The challenges are as follows:

- Optimization of coefficients for the multinomial expansion equation
- Identification of local minima/maxima in the tolerated design space using the resulting equation

Both effectiveness (accuracy) and efficiency aspects are considered as discussed in the remainder of this section.

Optimization of Equation Coefficients

This first-aspect of the Robustness code seeks to optimize the multinomial expansion equation for accuracy to the known data thru Least Squares Regression of the term coefficients. The ‘known data’ is established by direct solution of the function solver for a variety of input points. In the case of this challenge (‘toy’) problem, Rastrigin’s equation is used as the function solver for the ‘known’ data. In the eventual application of this code to the Rotordynamic optimization, the FEA code is used as the function solver. In either case, the input points are distributed about the potential optimum point (resulting from the deterministic optimization routine) and span the tolerance bounds established by the user for each DOF. The routine searches from among a user-defined range of maximum polynomial orders, optimizing the term coefficients via Least Squares to achieve either a user-defined threshold for equation quality (NRMSE, Eq. (40)), or if not achievable within the orders surveyed a minimum NRMSE. The number of points used along each DOF is dependent upon the equation order and is user-specified to be at least one greater than the polynomial order of that optimization loop. This process is described in the following Pseudo Code.

- a) Create input data matrix centered on potential optimum and spanning range of symmetric tolerances.
- b) Create vector of responses (knowns) for input data matrix using function solver
- c) Loop thru user-defined vector of maximum multinomial orders, optimizing coefficients via Least Squares Regression to define the coefficients for each multinomial order.
- d) Compare among the responses for the minimum and/or acceptable equation quality (NRMSE).
- e) Use selected equation order and coefficients in subsequent evaluations of the design space to identify minima / maxima for robustness statement.

Figure 3-10 Pseudo-code – Optimization of Multinomial Expansion Coefficients

This challenge considers the response of multiple optimization tools (MATLAB's `fminunc` and `fmincon`) in terms of equation fit (quality achieved) and efficiency of the process (number of function evaluations required). In this case, the term 'function evaluations' refers to the Least Squares objective function comparing the quality of the curve fit for a given set of equation coefficients (X_0 values) to the known (exact) responses. Since the location of a potential optimum with respect to the multimodal response in an actual Rotordynamic use case is likely to vary (not always exactly at a local minima), the challenge considers response equation scenarios for 3 different regions of Rastrigin's equation, centered on a local minima, local maxima or transition region. For each, the DOF tolerances are set large enough so as to span more than a '2nd-order response'. In this way, the ability of the Robustness code to fit the coefficients to the various shapes is challenged. Also, 2-, 3- and 4-DOF design spaces are considered. The `fminunc` algorithm was set to 'quasi-Newton' and `fmincon` to 'sqp' for these challenge trials and the point discretization is set to '1' more than the equation order under evaluation.

Three key output parameters are considered in this challenge; the selected multinomial order (that either achieves the user-desired NRMSE threshold or minimum among the equation orders considered), the total number of function evaluations (Least Squares computations) in the optimization effort, and the resulting equation quality (NRSME) of the selected multinomial order and coefficients. The following table summarizes these results. Note that all runs were conducted with a 16c, Xeon E5-2667 v3,

3.20 GHz CPU. Parallel processing was enabled for both optimization functions and key calculation loops.

Table 3-10 Robustness Challenge Results (Rastrigin) – Equation Coefficient Determination

Design Space	Number of DOF	Optimization Method	Selected Equation		Total Function Evaluations
			Equation Order	NRMSE (%)	
Local Minima ^{1,4}	2 (Figure 3-11)	<i>fminunc</i>	12	0.3985	4661
		<i>fmincon</i>	12	0.0840	3493
	3	<i>fminunc</i>	14	0.4576	68846
		<i>fmincon</i>	10	0.0924	10217
	4	<i>fminunc</i>	8	0.7488	38003
		<i>fmincon</i>	9	0.1206	27600
Local Maxima ^{2,4}	2 (Figure 3-12)	<i>fminunc</i>	15	34.7530	10584
		<i>fmincon</i>	15	34.7396	7133
	3	<i>fminunc</i>	11	28.9200	76940
		<i>fmincon</i>	15	28.3850	25852
	4	<i>fminunc</i>	9	22.8923	55878
		<i>fmincon</i>	9	22.1325	25813
Transition ^{3,4}	2 (Figure 3-13)	<i>fminunc</i>	2	2.6832	10808
		<i>fmincon</i>	15	2.2158	7787
	3	<i>fminunc</i>	2	0.7725	71534
		<i>fmincon</i>	2	0.7725	31103
	4	<i>fminunc</i>	2	0.2038	40415
		<i>fmincon</i>	2	0.2038	24352

Notes:

1. Local Minima design space centered at (0,0), (0,0,0), (0,0,0,0)
2. Local Maxima design space centered at (0.5,0.5), (0.5,0.5,0.5), (0.5,0.5,0.5,0.5)
3. Transition design space centered at (0.25,0.25), (0.25,0.25,0.25), (0.25,0.25,0.25,0.25)
4. All DOF tolerances = ±0.50

Identification of Local Minima / Maxima in the Toleranced Design Space

The second challenge to the Robustness code evaluates the ability of the code to use the defined equation and identify the local minima / maxima of the toleranced design space. This is an extension of the challenge described previously for equation accuracy using Rastrigin's equation. Key output includes the DOF-location of both Exact and Equation-based minima / maxima, the value of the response at these locations, response error and the time (mins) required by the code to conduct the searches. For purposes of this evaluation, Response error is normalized against the average of Exact Minima and Exact

Maxima responses. Data is provided in the following tables. In addition, Figure 3-11 thru Figure 3-13 illustrate the minima / maxima determined from the response equation as compared to the Exact Rastrigin surface.

Table 3-11 Robustness Challenge Results (Rastrigin) –Minima / Maxima Locations

Design Space	Number of DOF	Coefficient Optimization Method	Location	
			Exact	Calculated
Local Minima ^{1,4}	2 (Figure 3-11)	<i>fminunc</i>	(0, 0)	(0, 0) (-0.5000, -0.5000)
		<i>fmincon</i>	(±0.50, ±0.50)	(0, 0) (+0.5000, +0.5000)
	3	<i>fminunc</i>	(0, 0, 0)	(-0.4e-3, -0.4e-3, -0.4e-3) (+0.50, +0.50, +0.50)
		<i>fmincon</i>	(±0.50, ±0.50, ±0.50)	(0.5e-3, 0.5e-3, 0.5e-3) (-0.50, -0.50, -0.50)
	4	<i>fminunc</i>	(0, 0, 0, 0)	(-4.6e-3, -4.6e-3, -4.6e-3, -4.6e-3) (+0.50, +0.50, +0.50, +0.50)
		<i>fmincon</i>	(±0.50, ±0.50, ±0.50, ±0.50)	(+6.6e-3, +6.3e-3, +6.3e-3, +4.9e-3) (-0.50, -0.50, -0.50, -0.50)
Local Maxima ^{2,4}	2 (Figure 3-12)	<i>fminunc</i>	(0, 0)	(0, 0.7854) (+0.4054, +0.4054)
		<i>fmincon</i>	(±0.5025, ±0.5025)	(0.7854, 0.7854) (+0.4065, +0.4065)
	3	<i>fminunc</i>	(0, 0, 0)	(+4.3e-3, +4.3e-3, 0.7854) (+0.4149, +0.4149, +0.4149)
		<i>fmincon</i>	(±0.5025, ±0.5025, ±0.5025)	(0.7584, 0.7584, 0.7584) (+0.4068, +0.4071, +0.4071)
	4	<i>fminunc</i>	(0, 0, 0)	(+3.0e-3, +5.2e-3, 0.7854, 0) (+0.4173, +0.4342, +0.4316, +0.3991)
		<i>fmincon</i>	(±0.5025, ±0.5025, ±0.5025, ±0.5025)	(0, 0, 0, 32.6e-3) (+0.3989, +0.4727, +0.727, +0.3478)
Transition ^{3,4}	2 (Figure 3-13)	<i>fminunc</i>	(0, 0)	(-0.6e-3, -0.6e-3) (+0.4859, +0.4859)
		<i>fmincon</i>	(±0.5025, ±0.5025)	(+4.5e-3, +4.5e-3) (+0.5032, +0.5032)
	3	<i>fminunc</i>	(0, 0, 0)	(5.5e-3, 2.3e-3, 2.5e-3) (+0.4844, +0.4802, +0.4805)
		<i>fmincon</i>	(±0.5025, ±0.5025, ±0.5025)	(-9.8e-3, -9.7e-3, -9.9e-3) (+0.4944, +0.4943, +0.4944)
	4	<i>fminunc</i>	(0, 0, 0, 0)	(+1.7e-3, +1.7e-3, +1.7e-3, +1.7e-3) (+0.4577, +0.4577, +0.4578, +0.4577)
		<i>fmincon</i>	(±0.5025, ±0.5025, ±0.5025, ±0.5025,)	(+1.1e-3, +0.9e-3, +0.8e-3, +0.8e-3) (+0.4791, +0.4786, +0.4789, +0.4791)

Notes:

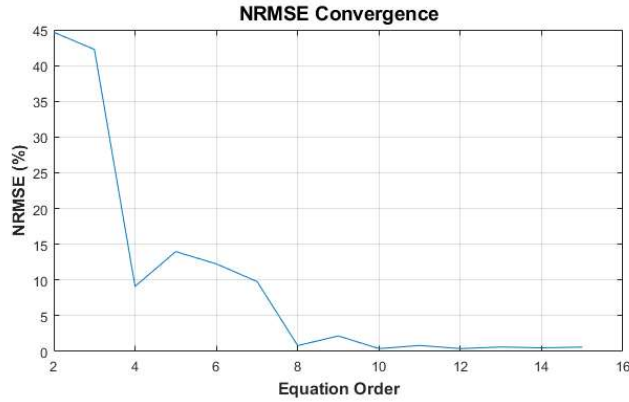
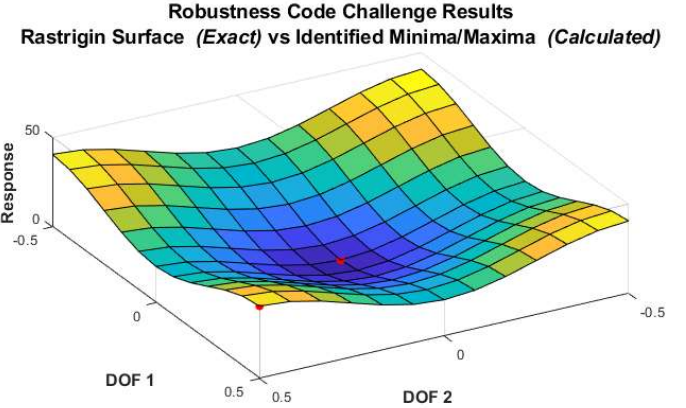
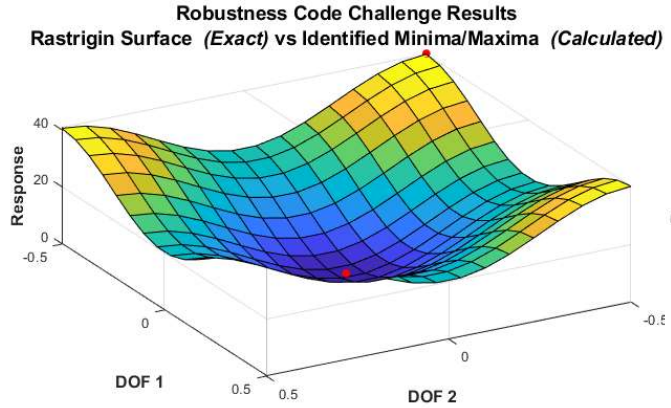
1. Local Minima design space centered at (0,0), (0,0,0), (0,0,0,0)
2. Local Maxima design space centered at (0.5,0.5), (0.5,0.5,0.5), (0.5,0.5,0.5,0.5)
3. Transition design space centered at (0.25,0.25), (0.25,0.25,0.25), (0.25,0.25,0.25,0.25)
4. All DOF tolerances = ±0.50

Table 3-12 Robustness Challenge Results (Rastrigin) –Minima / Maxima Response Values

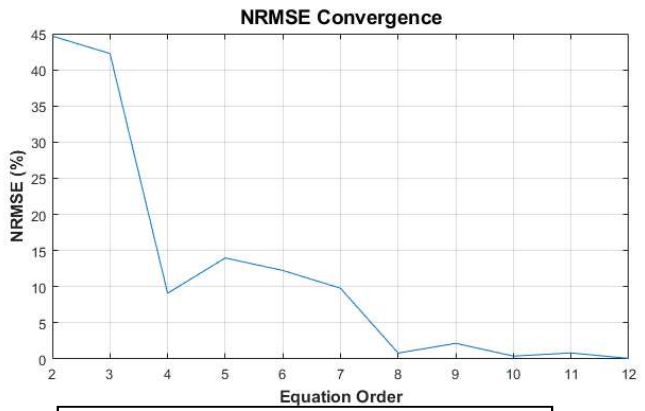
Design Space	Number of DOF	Optimization Method ⁵	Response Value		Error (%) ⁶	Min/Max Search Time (mins)
			Exact	Calculated		
Local Minima ^{1,4}	2 (Figure 3-11)	U / C	0.0000	-0.1314 40.6101	- 0.65 % + 0.54 %	0.0048
		C / C	40.5000	0.0292 40.5105	+ 0.14 % + 0.05 %	0.0051
	3	U / C	0.0000	-0.2747 61.0654	- 0.90 % + 1.04 %	0.0157
		C / C	60.7500	0.0188 60.7588	+ 0.06 % + 0.03 %	0.0170
	4	U / C	0.0000	-0.5191 81.6050	+ 1.28 % + 1.48 %	0.0189
		C / C	81.0000	- .0522 81.0288	- 1.288 % + 0.07 %	0.0182
Local Maxima ^{2,4}	2 (Figure 3-12)	U / C	0.0000	7.2508 37.7369	+ 35.80 % - 13.66 %	0.0043
		C / C	40.5025	15.8816 37.7881	+ 78.43 % - 12.95 %	0.0043
	3	U / C	0.0000	6.2634 52.3805	+ 20.62 % - 27.56 %	0.0188
		C / C	60.7538	23.4575 56.4086	+ 77.22 % - 7.72 %	0.0189
	4	U / C	0.0000	6.4860 68.7501	- 16.01 % - 30.26 %	0.0221
		C / C	81.0051	-0.6546 71.9199	- 1.62% - 22.43 %	0.0212
Transition ^{3,4}	2 (Figure 3-13)	U / C	0.0000	0.6631 41.1643	+ 3.27 % + 3.27 %	0.0035
		C / C	40.5025	-0.3561 41.3298	- 1.76 % + 4.09 %	0.0046
	3	U / C	0.0000	0.9891 61.5237	+ 3.26 % + 2.53 %	0.0205
		C / C	60.7538	-0.1933 62.0072	- 0.64 % + 4.13 %	0.0242
	4	U / C	0.0000	-2.8752 78.6041	- 7.10 % - 5.92 %	0.0485
		C / C	81.0051	1.2383 82.1205	+ 3.10 % + 2.75 %	0.0206

Notes:

1. Local Minima design space centered at (0,0), (0,0,0), (0,0,0,0)
2. Local Maxima design space centered at (0.5,0.5), (0.5,0.5,0.5), (0.5,0.5,0.5,0.5)
3. Transition design space centered at (0.25,0.25), (0.25,0.25,0.25), (0.25,0.25,0.25,0.25)
4. All DOF tolerances = ±0.50
5. Optimization method = 'Coefficient method / Design Space Search method', 'U'=fminunc, 'C'=fmincon
6. Error normalized to mean of Exact values (Exact mean = (Exact Max – Exact Mean)/2)



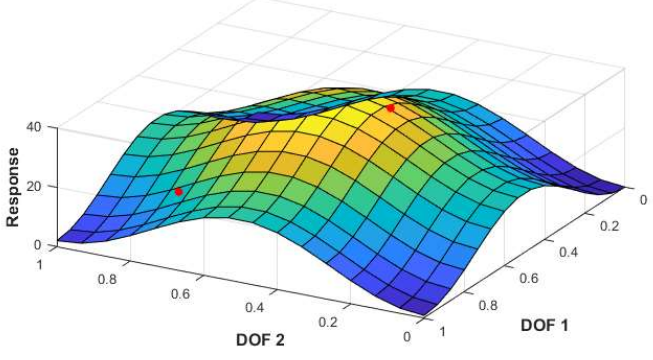
fminunc coefficient search



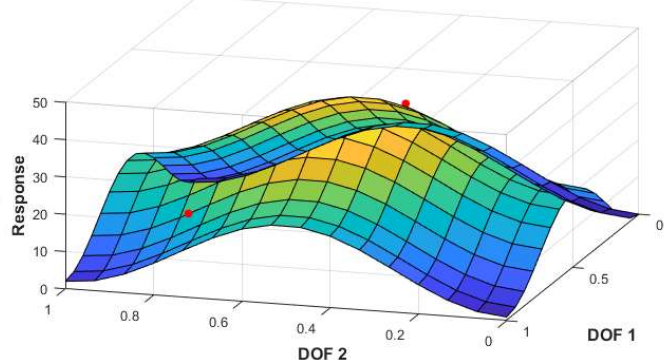
fmincon coefficient search

Figure 3-11 Robustness Code Response – Equation Fit to Rastrigin Centered on Local Minima

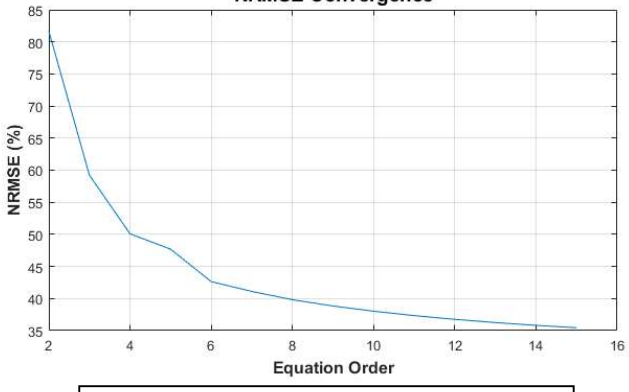
Robustness Code Challenge Results
Rastrigin Surface (Exact) vs Identified Minima/Maxima (Calculated)



Robustness Code Challenge Results
Rastrigin Surface (Exact) vs Identified Minima/Maxima (Calculated)

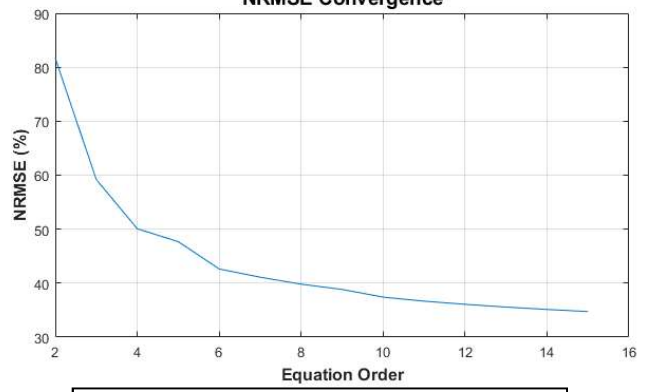


NRMSE Convergence



fminunc coefficient search

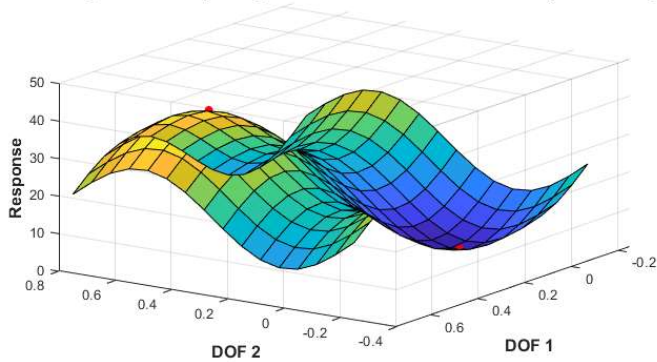
NRMSE Convergence



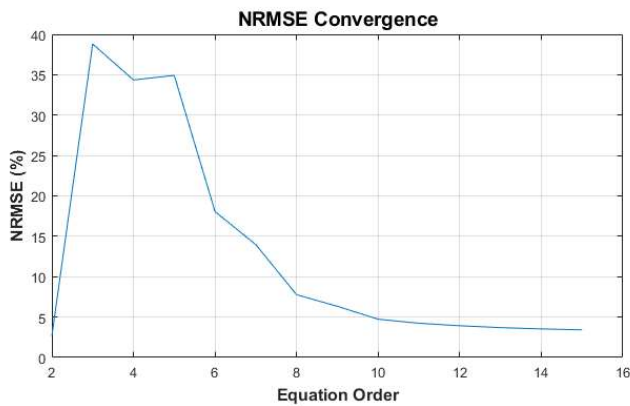
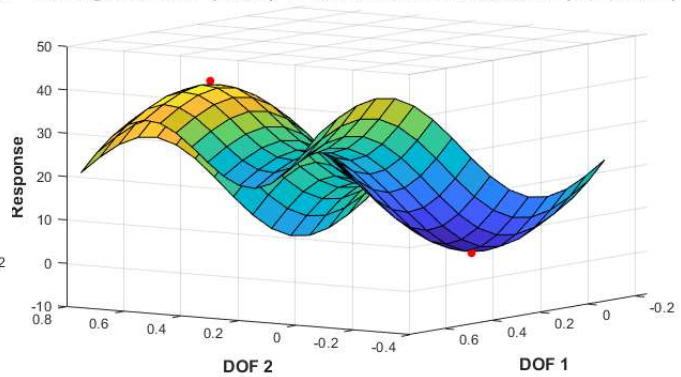
fmincon coefficient search

Figure 3-12 Robustness Code Response – Equation Fit to Rastrigin Centered on Local Maxima

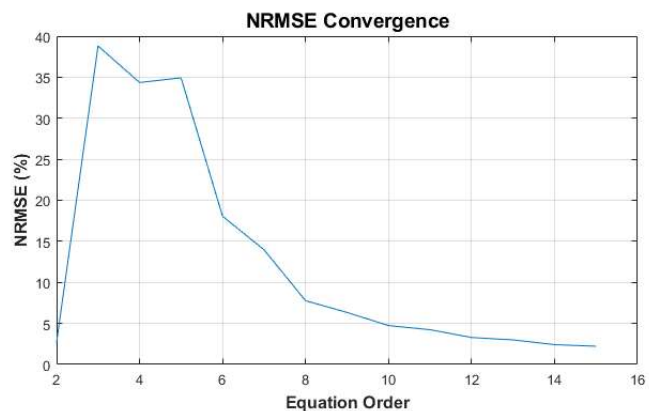
Robustness Code Challenge Results
Rastrigin Surface (Exact) vs Identified Minima/Maxima (Calculated)



Robustness Code Challenge Results
Rastrigin Surface (Exact) vs Identified Minima/Maxima (Calculated)



fminunc coefficient search



fmincon coefficient search

Figure 3-13 Robustness Code Response – Equation Fit to Rastrigin in Transition Region

Confirmation – Challenge against Rotordynamic Problem

In addition to the Rastrigin’s test function, a confirmation challenge of the Robustness code is conducted using the Rotordynamic FEA code developed under this work as an example of the intended use. The purpose of this challenge is to determine if the Robustness code can effectively predict the maxima and minima of the response within the tolerated design space surrounding a defined optimum. Key output includes accuracy assessment of the Robustness Response Equation and also that of the local maxima / minima predictions themselves. Response Equation accuracy is determined by comparing

the actual (FEA solve) and predicted (Robustness Equation) values of the response at each of the locations used to create the Response Equation as normalized to the actual (FEA solve) values. Accuracy of the maxima / minima predictions is determined by comparison of the predicted values from the Robustness process against results from a Mapped Survey of the design space, normalized against results of the Mapped Response Survey. Both GCO (Figure 1-7) and GUO (Figure 1-4) locations are included for this challenge and both 'fminunc' and 'fmincon' optimization routines are considered as part of the Robustness methodology. Data resulting from the evaluations is presented in Table 3-13.

Table 3-13 Robustness Challenge Results (Rotordynamic)

Design Space	Method	Points Greater than Equation Order	Total Function Evals	Selected Equation Order	Equation Accuracy		Robustness Prediction vs FEA Solve ²	
					NRMSE (%)	Max Equation Error (%) ¹	Maxima (%)	Minima (%)
GCO	fminunc	1	604	8	0.25	- 0.80	+ 0.73	- 0.15
		2	573	7	0.24	- 0.80	- 0.15	+ 0.24
		3	496	6	0.24	- 0.80	-0.16	+ 0.26
		4	470	5	0.25	- 0.77	- 0.12	+ 0.21
	fmincon	1	1204	8	0.11	- 0.36	+ 0.30	+ 0.15
		2	1020	7	0.11	- 0.36	+ 0.29	+ 0.15
		3	851	6	0.11	- 0.36	+ 0.30	+ 0.15
		4	603	5	0.11	- 0.41	+ 0.24	+ 0.19
GUO	fminunc	1	1205	4	1.77	- 98.98	- 196.68	- 3.20
		2	960	3	1.77	- 77.63	- 195.54	- 2.05
		3	740	2	1.96	- 98.28	- 196.67	- 3.14
		4	503	3	4.74	- 78.34	- 195.56	- 2.12
	fmincon	1	1265	4	1.77	- 98.96	- 196.68	- 3.20
		2	1076	3	1.77	- 77.60	- 195.53	- 2.05
		3	799	2	1.82	+ 3235.06	- 89.00	+ 104.23
		4	506	3	4.74	- 78.32	- 195.56	- 2.12

1) Computed as max error among data points used to develop response equation – predicted value from resulting equation vs actual (function solve) value normalized to function solve value.
2) Computed as error of maxima/minima predicted within tolerated design space using equation developed from Robustness effort vs maxima/minima obtained from FEA mapping survey of tolerated design space, normalized to maxima/minima from FEA mapping survey.

The data of Table 3-13 indicates good Robustness Equation Accuracy for the local design space centered on the GCO with NRMSE generally less than 0.25% and Maximum Equation Error less than $\pm 0.8\%$. The Equation Accuracy was poor however for the design space centered at the GUO with NRMSE as high as 4.74% but more importantly Maximum Equation Error up to $\pm 3235\%$. This is attributed to the form of the response surfaces at the 2 locations (Figure 1-7 for GCO and Figure 1-4 for GUO) where the GCO design space is more conducive to a multinomial fit than that of the GUO. This indicates a limitation of the Robustness methodology in that a local modality such as GUO may not be accurately modeled by the process. Effectiveness of the prediction of the local maxima / minima within the tolerated design space follows similarly with acceptable results for the GCO space (less than ± 0.73) and unacceptable results for the GUO space (error up to -197%).

Conclusions – Robustness Code Challenges

The data of Table 3-10 indicates that the Robustness code fits the case of a tolerated space on Rastrigin centered at a local minima the best of the 3 scenarios. For this case, a maximum NRMSE of 0.75% was achieved among the various DOF challenges. For a transition region spanning (potentially) both local minima and local maxima, the code results in reduced, but acceptable accuracy with maximum NRMSE of 2.68%. The code behaved worst for Rastrigin in the case of a tolerated space centered on a local maximum with a maximum NRMSE of 34.75% being achieved among the multiple DOF challenges. Inspection of the 2-DOF response surfaces (Figure 3-11 thru Figure 3-13) using Rastrigin illustrate that for the case where the design space is centered on a local maximum, the tolerances selected (± 0.50) are large enough to cause curvature of higher order than design spaces centered at either a local minimum or a transition. This infers that if the studied design spaces were smaller (i.e.; tolerances were $< \pm 0.50$) then the resulting fits would be more accurate. A separate study (results not presented here) confirms this and supports that a design space centered on a local minimum, local maximum or transition can be created with significantly improved accuracy simply by limiting the design tolerances and therefore the complexity of the response. This of course supports general expectations given that the code is attempting to fit the response to a multinomial of limited maximum order.

The data of Table 3-10 (Rastrigin) and Table 3-13 (Rotordynamic Problem) also supports that use of 'fmincon' (as an unconstrained tool) is, in general, more effective than use of 'fminunc' at deriving the appropriate multinomial coefficients. (This is, in large part, attributed to the use of the 'sqp' search algorithm available in MATLAB's 'fmincon' tool.) For both cases, the NRMSE achieved (for a particular design space and number of DOF) is the same or better when using 'fmincon' and for the Rastrigin challenges the Total Function Evaluations (optimization effort) are reduced where 'fmincon' is used. It should be noted here that 'Total Function Evaluations' is the effort given to optimization of the multinomial coefficients and not to the number of primary function evaluations (Rastrigin's Equation solves or FEA evaluations in the full embodiment). This is important because the optimization functions for the coefficient search occur quickly (on the order of milliseconds per evaluation) whereas the primary function evaluations to generate the known responses may take up to several minutes or longer depending on the FEA model being considered.

The data of Table 3-11 and Table 3-12 (Rastrigin) and Table 3-13 (Rotordynamic Problem) compare use of the selected (optimal) multinomial coefficients to identify the known maximum and minimum response within the tolerance bounds. As with the identification of coefficients (Table 3-10), the most accurate response with Rastrigin is for design spaces centered at a local minima (max error = 1.48%) with worst response for a design space centered on local maxima (max error = 78.4%). The transition space resulted in max error of 7.10%. The Rotordynamic Problem (Table 3-13) resulted in the most accurate prediction for the GCO design space (max error = 0.73%) but poor predictive capability for the GUO design space (max error = -197%). Both Rastrigin and Rotordynamic challenges support that use of 'fmincon' to search the design space using the selected multinomial coefficients is generally more effective than use of 'fminunc'. Some discrepancies do exist however with Rastrigin; most notably with the design space centered on a local maxima where the tolerances result in a more complex response than the other 2 cases. Also, the data indicates (not presented here) that the optimization effort to determine the multinomial coefficients can take on the order of a few minutes with the follow-on search of the design space (with optimal multinomial) happens quickly and within several milliseconds. This is

acceptable given the intended use of the robustness code as a periodic evaluation within the larger optimization.

As a result of these findings, the following key conclusions regarding the Robustness methodology are made.

- The multinomial method to develop a predictive equation of the Response within a local design space is acceptable in terms of accuracy and effectiveness for the intended application. 'Smooth' test functions using Rastrigin for local minima and transition regions and 'Actual' use for a bowl-shaped minima like GCO resulted in both acceptable equation accuracy and prediction of known maxima / minima.
- The local maxima (Rastrigin) and 'valley-shaped' response of GUO was not well predicted by the method. However, equation fit metrics correlate well to the ability to predict accurate maxima / minima. They can therefore be used as a flag to the user as to whether the Robustness prediction is acceptable for the local design space of the identified optimum.
- The 'fmincon' tool is selected for use in the Robustness code application to the full Optimization program for both multinomial coefficient search and search of the design space with the multinomial for minima and maxima.

Chapter 4

Demonstration of Practical Uses of Design Tool

Description of Demonstration Studies

The programmatic elements discussed earlier in this report are combined and used for a series of demonstration events in this section. The purpose of these studies is to demonstrate the capabilities of the Rotordynamic FEA and Optimization with Consideration for Robustness software programs toward the goal of demonstrating that they are a practical design tool for a Rotordynamic Designer. A total of 4 demonstrations are provided here as follows:

- a) Extension of one example from the Deterministic Optimization study (discussed in an earlier section) to demonstrate the results of Robustness evaluation.
- b) Optimization with Robustness considerations for a Rotordynamic system which includes the effects of **internal material damping**; as might prove detrimental to stability of the system.
- c) Optimization with Robustness considerations for a Rotordynamic system which includes **non-isotropic support parameters**; as might affect the precession characteristics.
- d) Optimization with Robustness considerations for a Rotordynamic system which includes **negative stiffness elements** (conceptually); as might prove beneficial to stability of the system.

For case (a), the purpose of the demonstration is to compare the study including effects of the Robustness evaluation against that of the (previous) study which did not include Robustness. For cases (b) thru (d), comparisons among the Optimization methods developed in this study are included (i.e.; SFD, SQP and SFD+SQP hybrid) including the effects of the Robustness study; this as a means of demonstrating and comparing the effectiveness and efficiencies of the developed full optimization method. Since GA and PSO methods do not include Robustness information, they are not included in this demonstration.

Extension of Deterministic Optimization Study

Table 3-7 through Table 3-9 present details regarding a number of deterministic optimization comparisons for the example Rotordynamic problem of this study (Figure 1-1). These comparisons are

made regarding both effectiveness and efficiency among the systems. None of these methods however provide information concerning Robustness of the solution(s) with respect to input variation.

In this section, one example from the deterministic optimization is extended to demonstrate the Robustness evaluation developed as part of this work. More specifically, Test ID #1c (Proposed Hybrid of SFD + SQP methods) is used to illustrate the benefits and costs of the Robustness study. Geometric input tolerances are applied to support locations L_{M1} and L_{M2} as specified in Table 1-1. Note that in the Deterministic results for this test (Table 3-8) only the optimal solution is reported to the user. The Robustness methodology however considers a Robustness evaluation of each of the potential optimums and reports all to the user. For this example (using Test ID #1c) the reported output is expanded to include the potential optimum identified from each of the 9 start points as well as that resulting from the follow-on SQP search. These 10 potential optimums then are used as the input to the Robustness study demonstrated in this section. The starting points and corresponding function values are shown in the following table. Results of the Robustness evaluation are presented and discussed later in this chapter.

Table 4-1 Robustness Input Parameters from Test ID #1c Results

Start Point	L_{M1} (m)	L_{M2} (m)	Minimum Function Value
1	0.01745	0.14162	0.7451
2	0.01700	0.22870	0.7510
3	0.02686	0.31961	0.7481
4	0.04821	0.14111	0.7788
5	0.06804	0.22200	0.7450
6	0.07759	0.20384	0.7404
7	0.03487	0.20199	0.7420
8	0.08501	0.22850	0.7441
9	0.08527	0.31356	0.7515
Post-SQP	0.07828	0.20411	0.7359

Optimization of Systems with Internal Material Damping

This section compares output of the developed optimization methods (including Robustness) where the model includes material damping; specifically, a hysteretic loss factor for the rotating shaft. The goal of this demonstration is 2-fold; 1) to illustrate that inclusion of a hysteretic loss factor can be detrimental to the stability of the system as discussed in literature and 2) that the optimization methodologies can be sensitive to stability as part of an overall Objective Function.

To accomplish this, input from Test ID #1a,1b and 1c (Table 3-7) are considered by adding stability as part of the Objective Function to form a new test series for this section termed Test ID #8a, 8b and 8c (SFD, SQP and Hybrid methods). Material Hysteretic Damping Loss Factor (η_H) ranging from 0.0 ~ 0.0500 is included for the rotating shaft to represent a range from 'no material loss factor' to an 'excessively large' material loss factor of 5% as applied to steel for this example problem. Literature varies significantly in the valuation of Loss Factor for steel, but a generally accepted bound is less than 1% depending upon the hardness of the steel.^{98, 79} The value of 5% is selected as a maximum bound for this exercise solely to test the responsiveness of the code to Hysteretic Damping. It is recognized that this range does not match the expected range for Hysteretic Damping of steel in 'the real world'.

The Objective Function is modified from the basic form of Eq. (1) to include Stability of the system as output by the Rotordynamic program. The stability output is provided to the user as a 'yes' or 'no' for each of the Critical Speeds within the operational range. This output is also provided to the user as part of the overall numerical output package as a '0' (not stable) or '1' (stable). For this demonstration, the stability values for all Critical Speeds, both Forward and Backward, are summed to optimize the system toward improved stability. Since the Optimization method seeks to minimize the Objective Function, the summed stability value is inverted so that a reduced value indicates improved convergence. Additionally, the inverted stability sum is normalized to a factor of '4.0' in order to adjust its overall magnitude such that it is of the same order of magnitude as the other components of the Objective Function. In this way, the added Stability term is neither overpowering nor lost in the overall Objective Function. The resulting Objective Function then is provided as Eq. (41).

$$f_{obj} = f_{obj_a} + f_{obj_b} + f_{obj_c}$$

where:

$$f_{obj_a} = \sum_{f=min}^{max} \frac{F_{Bearing\ B2\ Reaction}}{1e4}$$

$$f_{obj_b} = \sum_{f=min}^{max} \sqrt{(\delta_{UY})^2 + (\delta_{UZ})^2} \quad (41)$$

$$f_{obj_c} = \frac{\sum_{ii=C}^{CSend} Stability_{ii}}{4}$$

This demonstration then seeks to minimize the Objective Function of Eq. (41) subject to the ‘standard’ Constraints of Eq. (2) and Eq. (3) by modifying the Design Variables LM_1 and LM_2 (Table 1-1) plus the material Hysteretic Damping Loss Factor (η_H) ranging from 0.0 ~ 0.050. Note again that both this range of loss factor and this optimization demonstration are not intended to demonstrate a practical method of system optimization; since material loss factor is generally not a factor that can be adjusted in the way that it is being used here. Rather, this demonstration exercise is intended to illustrate that the Optimization method developed under this work is sensitive to material damping properties given a starting point of $\eta_H = 0.0002$ ⁽⁷⁹⁾ with a range varying from ‘no damping loss factor’ to an excessively large damping loss factor. As stated in literature, the addition of material Hysteretic Damping Loss Factor can cause instability⁷⁹ as opposed to reduced or no material Hysteretic Damping Loss Factor. Also, it is well known that the addition of damping to a vibrating system is the sole means of reducing resonant flexural values.

It is expected then that the optimization of Eq. (41) in this exercise may tend to favor designs minimizing flexural response (both bearing reaction force and tip deflection terms) due to increased system damping while potentially also influencing stability due to the inclusion of Hysteretic Damping Loss Factor for the rotating shaft.

Optimization of Systems with Internal Material Damping and Non-Isotropic Supports

This section demonstrates use of the developed Rotordynamic code where the model includes non-isotropic support stiffnesses as well as internal material damping as discussed in the previous section. The goal of this demonstration is 2-fold; 1) to illustrate the effects of non-isotropic supports upon precession characteristics using the developed Rotordynamic code and 2) illustrate potential influence over the precession characteristics using the developed Optimization methodologies with consideration for Robustness.

As with the material damping demonstration previously discussed, Test ID #8a,8b and 8c (Table 3-7) are expanded here to also include the effects of non-isotropic support stiffnesses. The new studies of this section then are termed Test ID #9a, 9b and 9c (SFD, SQP and Hybrid respectively). For all evaluations of this section, a constant Material Hysteretic Damping Loss Factor (η_H) of 0.02% is assumed. This is the 'start point' value of the 'damping optimization' conducted previously. As shown in Table 1-1 and discussed previously for the 'basic' problem in this report, the stiffness of support mounts K_{M1} & K_{M2} are symmetric, each with a stiffness of 2.627e4 N/m in both 'Y' and 'Z' directions. For the demonstration of this section however, the stiffness values are modified to be significantly non-isotropic where each mount has a stiffness in the 'Y' direction of 2.627e4 N/m (unchanged from the base model) and 2.627e7 N/m (increase of 3 orders of magnitude) in the 'Z' direction.

Non-isotropic support stiffnesses are anticipated from literature to create non-isotropic precession characteristics such as elliptical orbits^{1, 79}. In addition, it is possible that 'mixed' precession results might be achieved¹ where some Super Nodes of the beam(s) are observed to precess in the same direction as shaft spin (FW) and others (on the same beam) are observed to precess in the opposite direction (BW). Appendix N provides Damped Eigenvalue Mode Shape Plots resulting from this non-isotropic support stiffness exercise. As a baseline, Figure App-N-1 illustrates deflections for the first 4 Critical Speeds of both Beam 1 (tube) and Beam 2 (rotating shaft) for mount locations **L_{M1}** and **L_{M2}** located at the **geometric center of Region 5** (Table 3-6); the starting point resulting in optimums identified later in this section. As shown, multiple of the plots show 'mixed' precession. As an example, beam flexure of the rotating shaft is illustrated in Figure 4-1 for the 3rd Critical Speed of the rotating shaft (Beam 2). In this

particular response, the flexural shape of the rotating shaft is of a higher order and differs as the shaft rotates thru the (horizontal) X-Y plane (illustrated by solid Black mode shape line) as compared to the (vertical) X-Z plane (illustrated by dashed Red mode shape line). In this case, the precession at the distal end of the rotating shaft is near isotropic (circular) but is somewhat elliptical at the proximal end. At the proximal end ($x=0$) however the precession is Forward (red solid 'ellipse') whereas the distal end ($x = 0.5$ m) precession is in the Backward direction (red dotted 'circle'). The precession trace near midspan also shows Backward precession but in a more pronounced elliptical shape which is also in alignment with the non-isotropic mount stiffnesses.

**Damped Eigenvalue Mode Shape Plot
Beam-2, CS=3 (2058.4769 RPM)**

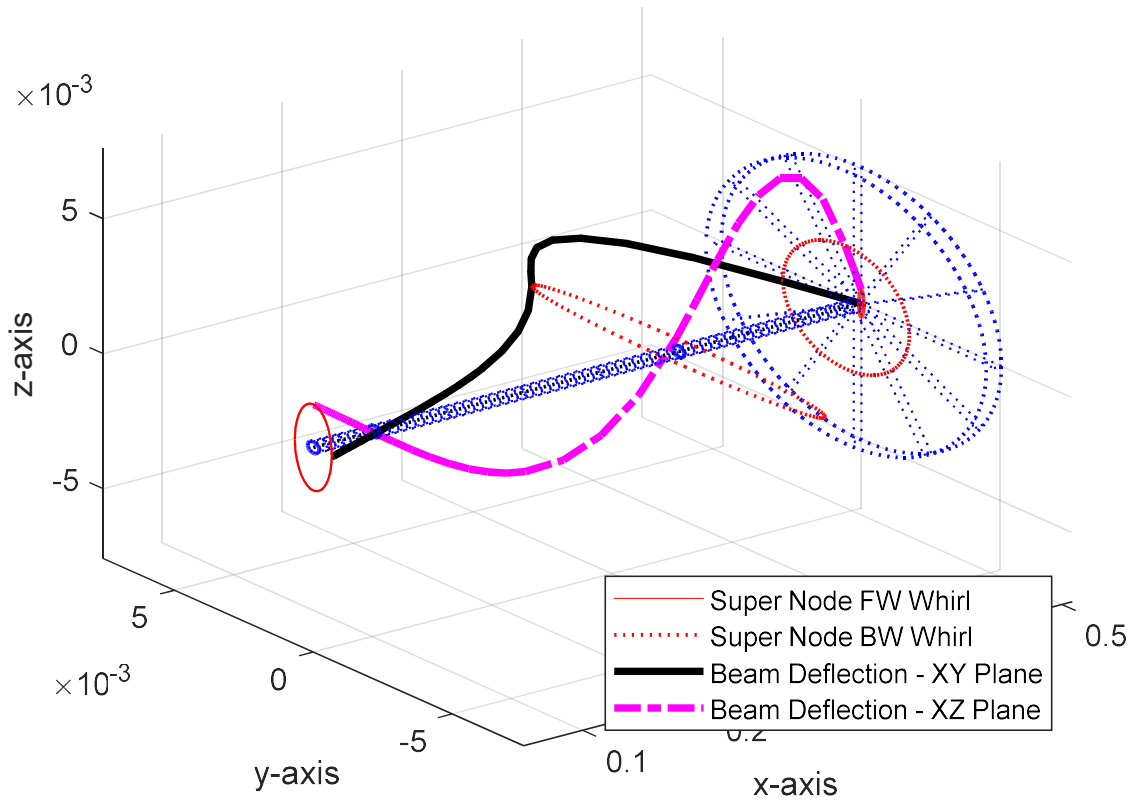


Figure 4-1 Mode Shape Plots – Non-Isotropic Behavior – Start Point #5

A key challenge offered by the system illustrated in Figure 4-1 is to reduce the radial deformations of the spinning shaft along its length and thereby reduce the reaction forces of the bearing supports. The developed Optimization code with considerations for Robustness is demonstrated for this purpose here by modifying the Objective function from that of Eq. (41), where Stability was added, to a form that focuses on bearing reaction force (Bearing B2 – of the base problem) plus deformation of the rotating shaft along its length. The resulting Objective Function is provided as Eq. (42) where bearing B2's reaction force (per Eq. (1)) is added to an average of the grand vector sum of nodal radial displacements along the rotating shaft.

$$f_{obj} = f_{obj_a} + f_{obj_b}$$

where:

$$f_{obj_a} = \sum_{f=min}^{max} \frac{F_{Bearing\ B2\ Reaction}}{1e4}$$

$$f_{obj_b} = \frac{\sum_{shaft_node=min}^{max} \sqrt{(\delta_{UY})^2 + (\delta_{UZ})^2}}{\quad}$$
(42)

This demonstration then seeks to minimize the overall rotating shaft deformation and distal bearing (B2) reaction force by minimizing the Objective Function of Eq. (42) subject to the 'standard' Constraints of Eq. (2) and Eq. (3), by modifying the Design Variables L_{M1} and L_{M2} (Table 1-1). Robustness information is based upon the local tolerated design space around the potential optimums based on the design tolerances of Design Variables L_{M1} and L_{M2} (Table 1-1). Note that this demonstration is not intended to explicitly tune the system to avoid 'mixed' precession, but rather to illustrate that the ability to improve key operating outcomes like rotating shaft deformation (magnitude) and bearing reaction force with consideration for Robustness.

Optimization of Systems with Negative Stiffness

This section demonstrates use of the developed Rotordynamic code where the model includes a negative stiffness element in combination with non-isotropic support stiffnesses and material Hysteretic

Damping Loss Factor in the rotating shaft. The use of negative stiffness elements is explored here as a potential mitigation for rotordynamic flexure as reported in some literature references discussed previously^{32, 31, 33, 34, 34}. The negative-stiffness configuration utilized in this section is based upon the concept presented by Yao, et. al.³² of a cylindrical magnet attached to the rotating shaft and positioned between 2 fixed, non-rotating cylindrical magnets (attached to the non-rotating tube). Figure 4-2 illustrates a 3D view of the system as well as a schematic view.

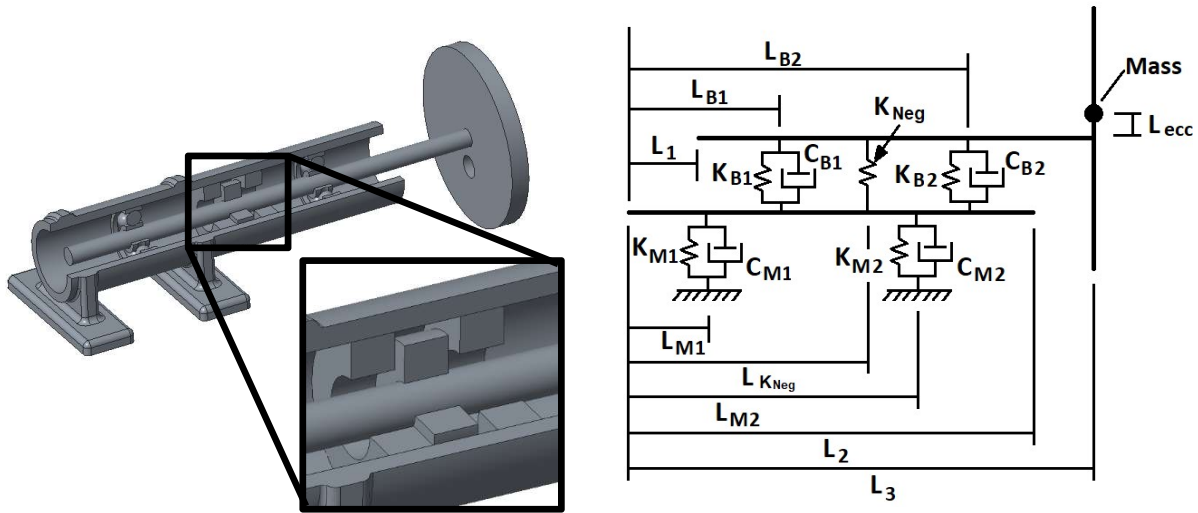


Figure 4-2 Illustration of Negative Stiffness Element Applied to Rotordynamic System

The purpose of this exercise is to demonstrate the usefulness of the developed software tools to the Rotordynamic Designer in exploration of 'unconventional design alternatives' as well as the more conventional design methodologies discussed thus far. It is recognized that in practice, the designer sometimes needs to explore conceptual solutions in order to determine whether it is appropriate to move forward with a more detailed, exacting study. The addition of Robustness information is intended to support this effort by providing sensitivity information to the designer regarding design influencers on the response. This demonstration exercise is conceptual only. The proposed configuration by Yao³² is that of a negative stiffness system that varies with distances between magnets and eccentricity and as such is nonlinear. A current limitation of the Rotordynamic code developed under this work is that stiffness characteristics remain linear. Therefore, this demonstration exercise is limited to a linearized evaluation of

a single magnet configuration (conceptual). From Yao³² and as applied to the system of this work, the additional elements of the negative system are defined as follows in addition to that of Table 1-1.

Table 4-2 Model Parameter Definitions – Negative Stiffness Demonstration

		Fixed Parameter Value	Design Variable	
			Value	Tolerance (± 0.25%)
L _{K_Neg}	(<i>m</i>)		0.1016 – 0.3556	± 0.00025
K _{Neg}	(<i>N/m</i>)	-1.751e4		
m _{magnet}	(<i>kg</i>)	7.072e-5		
I _{polar_magnet}	(kg-m ²)	1.114e-10		
I _{trans_magnet}		7.053e-11		

The Objective Function for this Demonstration exercise remains the same as for the non-isotropic stiffness study discussed previously. As defined in Eq. (42), this is a combination of the reaction force of the distal bearing 'B2' and the grand average of nodal lateral deformations of the rotating shaft over all frequencies studied. The Constraint functions are as defined previously with the exception that the negative stiffness element is constrained to be between bearing 'B1' and bearing 'B2'. As a result of the Super Node definition of the model then, 2 optimization runs are considered; a first with the negative stiffness element between bearing 'B1' and mount 'M2' and a second with it contained between mount 'M2' and bearing 'B2'. Two constraint equation sets are used to accomplish this and are provided as Eq. (43) (negative stiffness element between 'B1' and 'M2') and Eq. (44) (bounded by 'M2' and 'B2'). The Output Constraint remains unchanged as defined in Eq. (3).

$$\begin{aligned}
 g_1 &= 1 - \frac{L_{M1}}{0.0127} \\
 g_2 &= \frac{L_{M1}}{(L_{B1} - 0.0127)} - 1 \\
 g_3 &= 1 - \frac{L_{K_Neg}}{(L_{B1} + 0.0127)} \\
 g_4 &= \frac{L_{K_Neg}}{(L_{B2} - 0.0127)} - 1 \\
 g_5 &= 1 - \frac{L_{M2}}{(L_{K_Neg} + 0.0127)}
 \end{aligned} \tag{43}$$

$$\begin{aligned}
g_6 &= \frac{L_{M2}}{(L_{B2} - 0.0127)} - 1 \\
g_1 &= 1 - \frac{L_{M1}}{0.0127} \\
g_2 &= \frac{L_{M1}}{(L_{B1} - 0.0127)} - 1 \\
g_3 &= 1 - \frac{L_{M2}}{(L_{B1} + 0.0127)} \\
g_4 &= 1 - \frac{L_{K_Neg}}{(L_{M2} + 0.0127)} \\
g_5 &= 1 + \frac{0.0127 - L_{M2}}{(L_{K_Neg})}
\end{aligned} \tag{44}$$

For all evaluations of this section, a constant Material Hysteretic Damping Loss Factor (η_H) of 0.02% is assumed and non-isotropic support stiffnesses are defined for mounts K_{M1} & K_{M2} as 2.627e4 N/m in the 'Y' direction and 2.627e7 N/m in the 'Z' direction. These values are unchanged from the non-isotropic demonstration discussed in the previous section.

This demonstration then seeks to minimize the overall rotating shaft deformation and distal bearing (B2) reaction force by minimizing the Objective Function of Eq. (42) subject to the Input Constraints of Eq. (43) and Output Constraint of Eq. (3), by modifying the Design Variables L_{M1} , L_{M2} and L_{K_Neg} (Table 1-1 and Table 4-2). Robustness information is based upon the local tolerated design space around the potential optimums based on the design tolerances of the Design Variables.

Results of Demonstration Studies

Results of the Demonstration Studies include the effects of internal material damping and non-isotropic support parameters on the example Rotordynamic system as well as the (conceptual) effects of negative stiffness elements as a potential mitigation to Rotordynamic flexure. These results also demonstrate the usefulness of Robustness information in the Optimization process. Two primary types of output are provided by the Robustness study; design space definition and feasibility of the local

toleranced spaces studied and the range of function value variance across each space. These are discussed in the context of each of the 4 demonstration studies of this section.

Extension of Deterministic Optimization Study

The data of Table 4-3 provides the definition of the local design spaces studied in terms of the input variables. Here, support locations L_{M1} and L_{M2} define the system and the table provides both center point and symmetric tolerance definitions for each space. An important aspect of these space definitions is that potential optimum locations are the input to the Robustness evaluation. However, regions centered on these locations but bounded by the tolerances may not lie fully within feasible space. The Robustness code addresses this by first evaluating the toleranced design space for feasibility to input constraints, adjusting as needed to abut the feasibility bounds. In cases where the design space may not be as wide as the tolerances allow, adjustment to both center point and tolerance are possible for a given DOF. Consideration for results-based feasibility is given in the Robustness output (Table 4-4). As shown, all of the Local Design Spaces were feasible with respect to input conditions and therefore are unchanged from the Center Point input data of Table 4-1 and original tolerance specification of Table 1-1.

Table 4-3 Design Space Definition Considering Feasible Space

Start Point	Potential Optimum Center Location		Tolerances	
	L_{M1} (m)	L_{M2} (m)	L_{M1} (m)	L_{M2} (m)
1	0.01745	0.14162	0.00025	0.00025
2	0.01700	0.22870	0.00025	0.00025
3	0.02686	0.31961	0.00025	0.00025
4	0.04821	0.14111	0.00025	0.00025
5	0.06804	0.22200	0.00025	0.00025
6	0.07759	0.20384	0.00025	0.00025
7	0.03487	0.20199	0.00025	0.00025
8	0.08501	0.22850	0.00025	0.00025
9	0.08527	0.31356	0.00025	0.00025
Post-SQP	0.07828	0.20411	0.00025	0.00025

The data of Table 4-4 provides a summary of the data resulting from the Robustness study. Note that the data is sorted (top to bottom) from smallest to greatest 'Xopt' value; or potential optimum function (optimization results from each of the starting points). Note for example that the resulting 'Xopt' value of 'Post-SQP' (first row) matches that of the optimum for Test ID #1c in Table 3-8. The 'Solve Count' is the number of design space locations solved by the Rotordynamic FEA code to determine the coefficients for the response equation. NRMSE and Maximum Equation Error are quality metrics comparing the resulting response equation to FEA data and in general, those cases where higher function evaluations were needed resulted in poorer quality of the response equation. This is not unexpected since the algorithm loops in increasing complexity in search of a suitable equation. Note that most cases resulted in an acceptable fit with only 9 function evaluations, a minimum for this study including 2 input variables and minimum 2nd order polynomial (3 points required). Primary output of the Robustness routine is prediction of minimum and maximum function value within the toleranced design space. The 'Mid-Range' function value is also given in order to have a rough comparison against the Xopt value from the optimization conclusion for each start point. The function value range is also given as normalized to the Mid-Range as another indication of the variability of the response within the local space. Finally, a feasibility statement is made based upon FEA solves of the various points used for both input and output constraints of Eq. (2) and Eq. (3) respectively.

Table 4-4 Results of Extended Robustness Study for Test ID #1c

Start Point	Function Evaluations		NRMSE (%)	Max Equation Error (%)	Robustness Output				
	Xopt Function Value	Solve Count			Max	Mid Range	Min	Range (%)	Space Feasible
Post-SQP	0.7359	9	0.229	0.46	0.74111	0.73939	0.73768	0.47	yes
6	0.7404	9	0.178	-0.33	0.74320	0.74199	0.74077	0.33	yes
7	0.7420	9	0.033	0.06	0.74336	0.74185	0.74035	0.41	yes
8	0.7441	71	0.464	-2.40	0.75681	0.74989	0.74298	1.86	yes
5	0.7450	127	0.505	-2.74	0.75409	0.74819	0.74228	1.59	yes
1	0.7451	9	0.094	-0.18	0.74713	0.74614	0.74514	0.27	yes
3	0.7481	9	0.129	-0.22	0.75127	0.74901	0.74674	0.61	yes
2	0.7510	127	0.757	-4.98	0.77155	0.75926	0.74697	3.27	yes
9	0.7515	9	0.226	-0.39	0.75470	0.75197	0.74925	0.72	yes
4	0.7788	9	0.016	0.03	0.77932	0.77887	0.77841	0.12	yes

In general, the Robustness function values increase from top to bottom as do the Xopt values resulting from the Optimization studies. Subtle differences do exist however that may or may not be important to the Rotordynamic Designer. Of more importance perhaps is comparison of these Mid-Range function values in combination with the Range across the Toleranced space. For example, the optimum presented by the Optimization routine (row 1) does show the lowest Mid-Range value of the Robustness output; yet its Maximum value is only slightly below that of Start Point 1 which has a Range of 0.27% compared to the Row 1 'optimum's' range of 0.47%. Starting point 4 on the other hand has the highest Xopt function value, but also has the smallest Range. These comparisons are illustrative of the usefulness of Robustness information in the overall design of Rotordynamic systems even though the design differences may (or may not) be practically significant in this example.

In this example, the cost of the Robustness evaluation is significant with a total of 388 (FEA) function solves required for this purpose as compared to the 358 solves for the Optimization effort of Test ID #1c (Table 3-8). Table 4-4 identifies that approximately 68% of these Robustness function evaluations occurred in the study of just 2 of the 10 toleranced design spaces; and approximately 84% if a third space is considered as well. For these 3 design spaces, the data indicates that the response was more

complicated than for the other design spaces; requiring many more FEA solves in search of an acceptable equation fit but ultimately resulting in poorer equation error than the other 70% of tolerated spaces studied. The input data provided for this Robustness demonstration allowed for the algorithm to build and evaluate polynomials up to 10th order (as was done for the Rastrigin's-based challenges discussed earlier). The 3 tolerated spaces with lowest X_{opt} and Mid-Range function values were solved with only 9 FEA solves each for the Robustness effort as were the 2 tolerated spaces with the lowest Range. With experience, it may be shown that an upper limit of significantly lower equation order can be effective in the Robustness effort. In this approach, an unsuccessful equation fit (poor error) would identify more complicated areas of response and the user could then choose whether to disregard those areas or repeat the Robustness evaluation with more complicated polynomials in an attempt to more accurately describe them.

Optimization of Systems with Internal Material Damping

The data of Table 4-5 provides the definition of the starting locations for supports L_{M1} and L_{M2} (from starting region definitions of Table 3-6) as well as material Hysteretic Damping Loss Factor for the rotating beam. Also shown are the tolerances for each Design Variable used in the subsequent Robustness evaluation. Tolerances applied to the support locations are as given in Table 1-1. Tolerances applied to the Loss Factor however are artificial here but include a range of +/- 5% of the range's mean ($0 \sim 0.05 = \pm 0.0013$) for the purpose of this demonstration. Output for the Optimization studies are presented in Table 4-6 and Table 4-7. Robustness results are provided in Table 4-8.

Table 4-5 Design Variable Definition for Material Hysteretic Loss Factor Demonstration

Start Point	Starting Point Value			Tolerances ($\pm 0.25\%$ per Table 1-1)		
	L_{M1} (m)	L_{M2} (m)	η_H	L_{M1} (m)	L_{M2} (m)	η_H
1	0.01700	0.14400	0.00020	± 0.00025	± 0.00025	± 0.0013
2	0.01700	0.22870	0.00020	± 0.00025	± 0.00025	± 0.0013
3	0.01700	0.31330	0.00020	± 0.00025	± 0.00025	± 0.0013
4	0.05090	0.14400	0.00020	± 0.00025	± 0.00025	± 0.0013
5	0.05090	0.22870	0.00020	± 0.00025	± 0.00025	± 0.0013
6	0.05090	0.31330	0.00020	± 0.00025	± 0.00025	± 0.0013
7	0.08470	0.14400	0.00020	± 0.00025	± 0.00025	± 0.0013
8	0.08470	0.22870	0.00020	± 0.00025	± 0.00025	± 0.0013
9	0.08470	0.31330	0.00020	± 0.00025	± 0.00025	± 0.0013

The data of Table 4-6 illustrates that all test runs moved the Hysteretic Damping Loss Factor from a starting value of 0.0002 to at or very near the maximum allowed value of 0.05. However, the stability term result of the Objective Equation did not change as a result of the optimization (Table 4-7). Rather, the bearing force and tip deflection terms of Eq. (41) changed significantly, supporting the design's convergence. Comparison of the starting locations (Table 4-5) against the potential Optimum location (Table 4-6) shows that the location of L_{M1} and L_{M2} did not change at all for Test ID #8a and changed very little for Test ID #8b and 8c. Therefore, it can be concluded that the major contributor to the function value decrease for each run is due to increased Hysteretic Loss Factor and not change in location for the mounts. This is reinforced visually in Figure 4-3 where the convergence paths of the design variables are plotted for Test ID #8c.

Also, these data support that the 3 optimization techniques (SFD-Individually, SQP-Individually and the proposed Hybrid) perform very similarly in terms of the minimum function value achieved (0.7% total range), but SQP requires approximately 2x the number of function evaluations of either of the other 2 methods.

Table 4-6 Optimization Results of Material Hysteretic Loss Factor Demonstration

Test ID	Optimization Method	Start Point of Opt. Result	Optimum Location			Minimum Function Value	Total Function Evaluations ₁
			L_{M1} (m)	L_{M2} (m)	η_H		
8	a) SFD Individually	3	0.0170	0.3133	0.0500	0.368281	220
	b) SQP Individually	8	0.0117	0.2551	0.0494	0.365640	524
	c) Proposed Hybrid (SFD + SQP)	3	0.0192	0.3161	0.0499	0.368280	278

1) Total Function Evaluations of Hybrid include both Initial and Follow-on searches

Table 4-7 Objective Function Movement of Material Hysteretic Loss Factor Demonstration

Test ID	Optimization Method	Start Point of Opt. Result	Components of Eq. (41)					
			Starting Value			Potential Optimum		
			$f_{obj,a}$ (Brq F.)	$f_{obj,b}$ (Tip Defl)	$f_{obj,c}$ (Stability)	$f_{obj,a}$ (Brq F.)	$f_{obj,b}$ (Tip Defl)	$f_{obj,c}$ (Stability)
8	a) SFD Individually	3	1.02432	0.48738	0.35000	0.00853	0.00975	0.35000
	b) SQP Individually	8	0.76729	0.91464	0.35000	0.00757	0.01006	0.35000
	c) Proposed Hybrid (SFD + SQP)	3	1.02432	0.48738	0.35000	0.00828	0.00974	0.35000

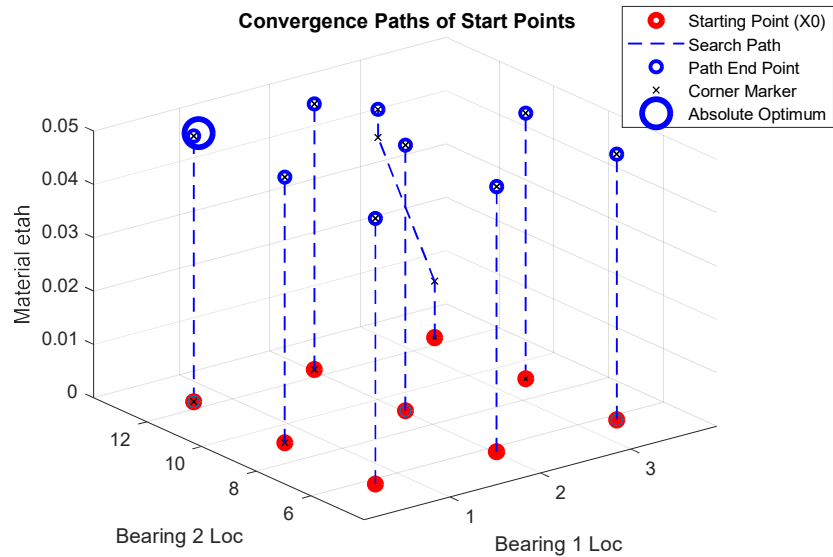


Figure 4-3 Design Variable Convergence Paths – Test ID #8c, Hysteretic Damping

Figure 4-4 through Figure 4-7 illustrate the frequency response plots of (distal) bearing 'B2' reaction force and the rotating shaft tip deflection for the starting and optimal points from Test ID #8c. As illustrated with the data of Table 4-7, a primary effect of the change in Hysteretic Loss Factor was the reduction in magnitude of rotating shaft flexure; resulting in more than 2 orders of magnitude reduction in bearing 'B2' reaction force and also the shaft's lateral tip deflection. These results support the general expectation that the addition of damping to the system is key to amplitude reduction at resonance conditions. **These results also support that the optimization attempt did not modify the stability characteristics among the Critical Speeds.** It would then be left to the designer to determine whether this resulting design was acceptable given frequency characteristics of the instable speeds, the degree of instability, ability to control a 'rapid' transition through those regions, etc.

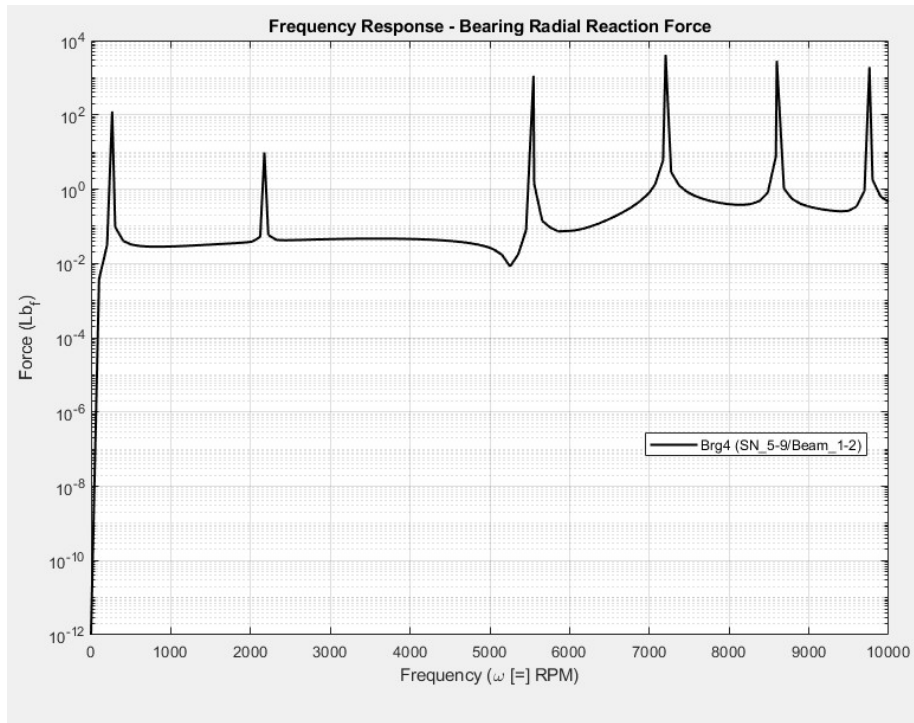


Figure 4-4 FRP Bearing 2 Reaction Force – Test ID #8c, Hysteretic Damping – Start

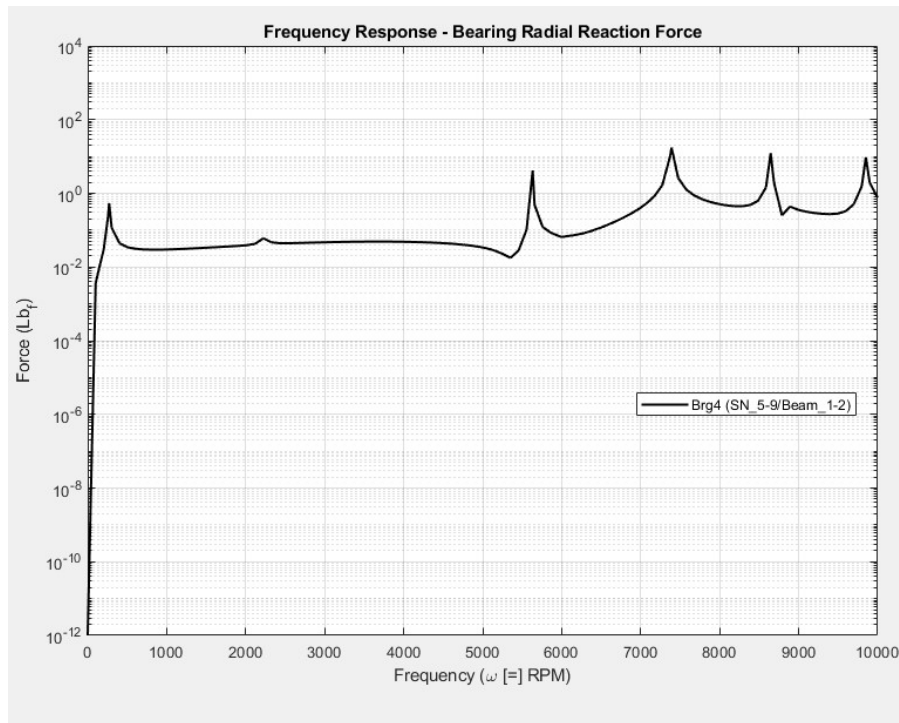


Figure 4-5 FRP Bearing 2 Reaction Force – Test ID #8c, Hysteretic Damping – Optimum

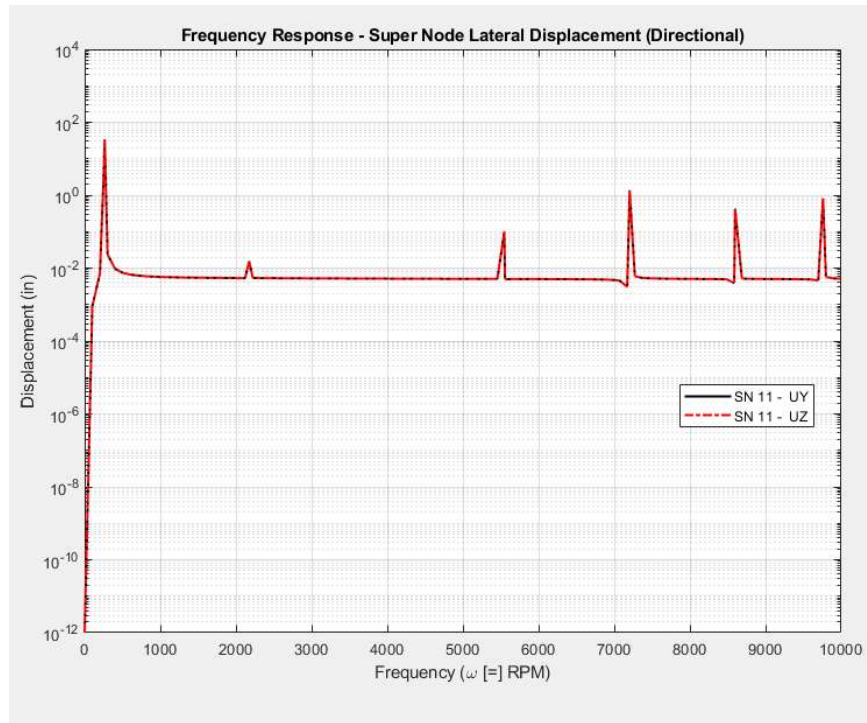


Figure 4-6 FRP Shaft Tip Deflection – Test ID #8c, Hysteretic Damping – Start

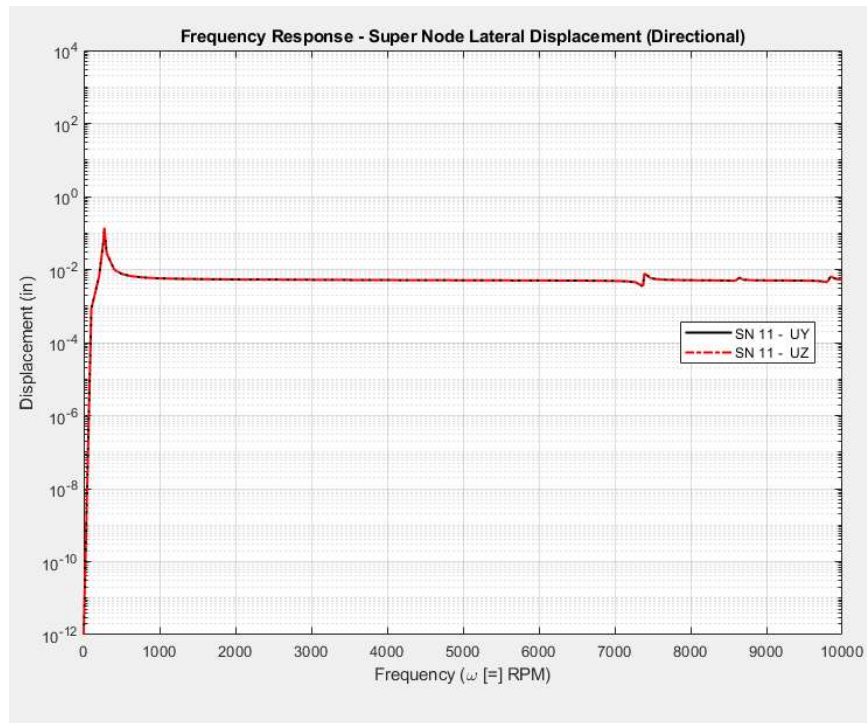


Figure 4-7 FRP Shaft Tip Deflection – Test ID #8c, Hysteretic Damping - Optimum

Table 4-8 Robustness Results of Material Hysteretic Loss Factor Demonstration

	Start Point	Function Evaluation Solve Count	NRMSE (%)	Max Equation Error (%)	Robustness Output				
					Max	Mid Range	Min	Range (%)	Space Feasible
SFD Only	3	28	0.008	-0.010	0.369200	0.368720	0.368240	0.260	yes
	9	27	0.006	-0.010	0.368720	0.368570	0.368410	0.083	yes
	8	28	0.002	0.000	0.369300	0.369030	0.368760	0.144	yes
	5	28	0.016	0.030	0.370900	0.370670	0.370440	0.123	yes
	2	28	0.009	-0.020	0.371880	0.371620	0.371360	0.141	yes
	6	28	0.024	-0.060	0.373690	0.372540	0.371400	0.616	yes
	4	28	0.004	-0.010	0.434970	0.434340	0.433710	0.292	yes
	1	28	0.006	-0.010	0.525270	0.524790	0.524300	0.185	yes
	7	28	0.124	-0.230	0.731610	0.721450	0.711300	2.82344	yes
		251							
SQP Only	8	27	0.005	0.010	0.365890	0.365760	0.365630	0.071	yes
	5	28	0.002	0.000	0.365950	0.365840	0.365740	0.059	yes
	9	28	0.011	-0.020	0.367800	0.367720	0.367640	0.042	yes
	7	27	0.014	-0.040	0.368320	0.368020	0.367730	0.160	yes
	2	28	0.007	-0.020	0.368180	0.367990	0.367800	0.102	yes
	3	28	0.008	0.010	0.368880	0.368430	0.367980	0.244	yes
	1	27	0.006	-0.010	0.373780	0.373250	0.372710	0.286	yes
	4	28	0.004	-0.010	0.375730	0.375330	0.374920	0.216	yes
	6	28	0.008	-0.020	0.392600	0.392330	0.392050	0.141	yes
		249							
Hybrid (SFD + SQP)	Post-SQP	28	0.008	0.010	0.368880	0.368430	0.367980	0.244	yes
	3	28	0.008	-0.010	0.369200	0.368720	0.368240	0.260	yes
	9	27	0.006	-0.010	0.368720	0.368570	0.368420	0.083	yes
	8	28	0.002	0.000	0.369300	0.369030	0.368760	0.144	yes
	5	28	0.016	0.030	0.370900	0.370670	0.370440	0.123	yes
	2	28	0.009	-0.020	0.371880	0.371620	0.371360	0.141	yes
	6	28	0.024	-0.060	0.373690	0.372540	0.371400	0.616	yes
	4	28	0.004	-0.010	0.434970	0.434340	0.433710	0.292	yes
	1	28	0.006	-0.010	0.525270	0.524790	0.524300	0.185	yes
	7	28	0.124	-0.230	0.731610	0.721450	0.711300	2.823	yes
		279							

Table 4-8 illustrates the Robustness results of this demonstration exercise. As with the study reported in Table 4-4, trade-offs exist between the Mid-Range function values and the Range of function values across the tolerated design space. Also, the cost of the Robustness exercise in terms of the number of function (FEA) evaluations is high when compared to the number of function evaluations of the basic optimization (Table 4-6). This of course can be significantly modified by not conducting a Robustness evaluation at the result from each starting point as was done in this demonstration.

In general, the data of Table 4-8 supports that the Robustness considerations provided by the program can provide significant input to the designer in selection of a 'preferred optimum', including those cases where internal material damping is included.

It should be reiterated that this demonstration exercise is not intended to suggest that an optimal outcome can be obtained by simply modifying the material's Hysteretic Loss Factor. Rather, this demonstration supports a conclusion that the Rotordynamic code and Optimization code can be effective at evaluating the effects of material Hysteretic Loss Factor among the considerations of a Rotordynamic System.

Optimization of Systems with Internal Material Damping and Non-Isotropic Supports

Starting locations for supports LM₁ and LM₂ (regions defined in Table 3-6) in this demonstration are the same as used for the previous Extension of Deterministic Optimization Study per Table 4-3. Optimization results are provided in Table 4-9 and Table 4-10. Robustness results are provided in Table 4-11.

Table 4-9 General Optimization Results of Non-Isotropic Support Stiffness Demonstration

Test ID	Optimization Method	Start Point of Opt. Result	Optimum Location		Minimum Function Value	Total Function Evaluations ¹
			LM ₁ (m)	LM ₂ (m)		
9	a) SFD Individually	5	0.08890	0.25579	1.113522	268
	b) SQP Individually	5	0.08538	0.29518	0.862283	523
	c) Proposed Hybrid (SFD + SQP)	5	0.08890	0.26331	1.034154	294

1) Total Function Evaluations of Hybrid include both Initial and Follow-on searches

The data of Table 4-9 illustrates that all 3 test runs found the optimal solution as coming from Starting Point #5 to minimize distal Bearing Reaction Force (Brg B2) and overall rotating shaft flexure per Eq. (42). As with previous results, the SQP method applied individually used significantly more function evaluations than did for either SFD Individually or the Hybrid. However, in this study, SQP applied Individually found an improved solution compared to the other 2; by 22.6% against SFD Individually and 16.6% against the Proposed Hybrid.

The data of Table 4-10 compares the degree of improvement from each Starting Point among the different optimization methods. For example, the SFD method applied individually (limited to 3 SFD 'jumps') resulted in improvements in the overall objective function (by starting point) ranging from 0~96.8%. Interestingly, improvement in the objective function components were similar; indicating that the objective function was well 'balanced' and that one objective component did not significantly overshadow improvements in the other. The SQP method applied individually resulted in improvements in the overall objective function ranging from 1.9~81.7% among the start points ,also having general 'balance' in the objective function components.

The proposed hybrid method (based on the SFD results and adding a follow-on SQP study from that interim optimum) resulted in an additional improvement in the objective function value of 7.1% over the SFD 'interim optimum', also generally balanced between the components.

These results support that for this demonstration exercise, the SQP method applied individually found a lower function value (16.6% compared to the Hybrid) but required approximately 78% more function solves than the Hybrid. The SFD applied individually was approximately 7.7% higher than the Hybrid but required 8.8% fewer function solves; and approximately 29.1% higher than the SQP (individually) but with 48.8% fewer function solves. **As with earlier conclusions, the proposed Hybrid and perhaps also the SFD may be a preferred approach compared to SQP applied individually; particularly for problems where the function evaluation is particularly costly.**

Table 4-10 Objective Function Change - Non-Isotropic Support Stiffness Demonstration

	Start Point	Starting Point			Potential Optimum			<i>Improvement (%)</i>		
		f_{obj_a} (Brg B2)	f_{obj_b} (δ_{vector_sum})	f_{obj} Eq. (42)	f_{obj_a} (Brg B2)	f_{obj_b} (δ_{vector_sum})	f_{obj} Eq. (42)	f_{obj_a} (Brg B2)	f_{obj_b} (δ_{vector_sum})	f_{obj} Eq. (42)
SFD Only	1	1.64351	1.04871	2.69222	1.63469	1.02879	2.66348	0.5%	1.9%	1.1%
	2	1.34671	6.29657	7.64328	1.07972	4.68707	5.76679	19.8%	25.6%	24.6%
	3	1.02432	1.08906	2.11338	0.61668	0.69825	1.31493	39.8%	35.9%	37.8%
	4	2.26682	1.64622	3.91303	1.74577	1.36466	3.11044	23.0%	17.1%	20.5%
	5	1.13791	1.41122	2.54912	0.52057	0.59295	1.11352	54.3%	58.0%	56.3%
	6	1.38920	2.12175	3.51095	0.97093	0.69144	1.66238	30.1%	67.4%	52.7%
	7	33.81421	25.02568	58.83989	0.88169	0.99009	1.87178	97.4%	96.0%	96.8%
	8	0.76729	0.84362	1.61091	0.69349	0.78142	1.47491	9.6%	7.4%	8.4%
	9	0.79632	0.58829	1.38461	0.79632	0.58829	1.38461	0.0%	0.0%	0.0%
SQP Only	1	<u>Same as SFD Only Above</u>			1.62883	1.01216	2.64100	0.9%	3.5%	1.9%
	2				0.89777	0.63602	1.53379	33.3%	89.9%	79.9%
	3				0.90590	0.91836	1.82425	11.6%	15.7%	13.7%
	4				0.78262	1.08158	1.86420	65.5%	34.3%	52.4%
	5				0.44745	0.41484	0.86229	60.7%	70.6%	66.2%
	6				0.89755	0.63619	1.53374	35.4%	70.0%	56.3%
	7				6.24818	4.49190	10.74008	81.5%	82.1%	81.7%
	8				0.44621	0.41624	0.86245	41.8%	50.7%	46.5%
	9				0.49740	0.43947	0.93687	37.5%	25.3%	32.3%
Hybrid (SFD + SQP)	1	<u>Same as SFD Only Above</u>			<u>Same as SFD Only Above</u>			<u>Same as SFD Only Above</u>		
	2									
	3									
	4									
	5									
	6									
	7									
	8									
	9									
	Post-SQP from SFD #5	0.52057	0.59295	1.11352	0.48159	0.55256	1.03415	7.5%	6.8%	7.1%

Table 4-11 Robustness Results of Non-Isotropic Support Stiffness Demonstration

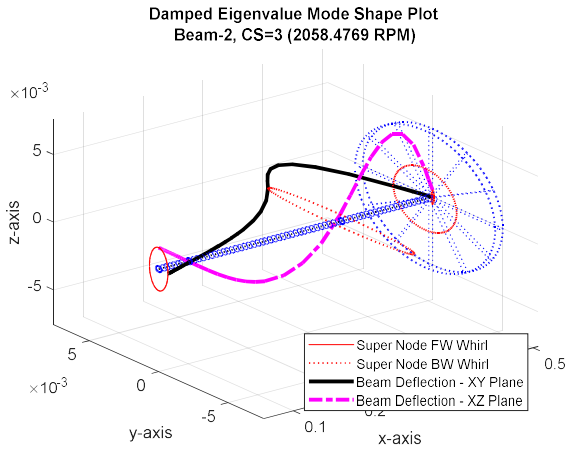
	Start Point	Function Evaluation Solve Count	NRMSE (%)	Max Equation Error (%)	Robustness Output				
					Max	Mid Range	Min	Range (%)	Space Feasible
SFD Only	5	9	0.007	-0.010	1.123900	1.113610	1.103320	1.848	yes
	3	9	0.006	-0.010	1.324790	1.315010	1.305220	1.488	yes
	9	127	0.532	921.330	*****	*****	*****	*****	yes
	8	9	0.196	-0.380	1.484150	1.475810	1.467480	1.130	yes
	6	9	0.002	0.000	1.670640	1.662440	1.654230	0.987	yes
	7	9	0.012	-0.020	1.873490	1.871980	1.870470	0.161	yes
	1	9	0.072	0.120	2.671810	2.663850	2.655890	0.598	yes
	4	9	0.021	0.030	3.129240	3.111540	3.093830	1.139	yes
	2	9	0.059	-0.100	5.857450	5.767130	5.676810	3.132	yes
		199							
SQP Only	5	21	0.449	0.660	0.876350	0.868880	0.861400	1.734	yes
	8	21	0.434	0.620	0.874120	0.868150	0.862180	1.384	yes
	9	43	0.432	-1.480	0.959280	0.948910	0.938530	2.215	yes
	6	127	11.867	-69.190	*****	*****	*****	*****	yes
	2	127	9.450	2550.920	*****	*****	*****	*****	yes
	3	9	0.034	0.070	1.826590	1.825840	1.825100	0.081	yes
	4	9	0.316	-0.770	1.887940	1.868500	1.849050	2.086	yes
	1	9	0.110	0.190	2.649390	2.641630	2.633880	0.587	yes
	7	127	1.884	-7.040	13.244210	11.340160	9.436110	35.457	yes
		493							
Hybrid (SFD + SQP)	Post-SQP	9	0.089	-0.180	1.041260	1.035160	1.029070	1.179	yes
	5	9	0.007	-0.010	1.123900	1.113610	1.103320	1.848	yes
	3	9	0.006	-0.010	1.324790	1.315010	1.305220	1.488	yes
	9	127	0.532	919.770	*****	*****	*****	*****	yes
	8	9	0.196	-0.380	1.484150	1.475810	1.467480	1.130	yes
	6	9	0.002	0.000	1.670640	1.662440	1.654230	0.987	yes
	7	9	0.012	-0.020	1.873490	1.871980	1.870470	0.161	yes
	1	9	0.072	0.120	2.671810	2.663850	2.655890	0.598	yes
	4	9	0.021	0.030	3.129240	3.111540	3.093830	1.139	yes
	2	9	0.059	-0.100	5.857450	5.767130	5.676820	3.132	yes
		208							

Table 4-11 illustrates the Robustness results of this demonstration exercise. As with other demonstrations discussed in this report, tradeoffs appear between the lowest absolute function value and the range in output values across the local toleranced design spaces. Also, the cost of the Robustness exercise in terms of the number of function (FEA) evaluations is generally high compared to the optimization effort if all potential optimums are studied. However, the data also supports (as did the previous demonstrations) that practical benefit from the Robustness evaluation may be obtained from a relatively few potential optimum studies; making it much more attractive with respect to the cost of function evaluations.

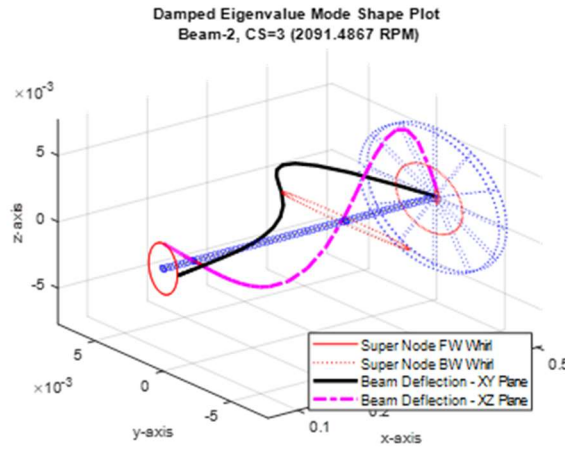
Damped Eigenvalue Mode Shape Plots for the optimums identified by the 3 techniques are illustrated in the figures of Appendix N as compared to the response of the starting point (#5) from which those optimums were identified. Other than differences in deformation magnitude, as evidenced by the data of Table 4-10, the most striking difference among the results is the mode shape of Critical Speed 3 for the rotating shaft.

Figure 4-8 illustrates Critical Speed 3 results for the rotating shaft (repeated here from Appendix N for convenience) for the 3 Optimization methods as well as that of Starting Point #5. Other than magnitude (per Table 4-10), the SFD result is generally similar to Starting Point #5 except for a slightly less elliptical FW orbit at the proximal end ($x=0$). The Hybrid result ('d' of Figure 4-8) also has improved magnitudes per Table 4-10 but retains the elliptical FW orbit at the proximal end like Start Point #5. However, the magnitude of the displacement at that location is increased such that the overall radial deformation is reduced along the length (per data of Table 4-10) for an improved Objective Function value. The SQP result however exaggerates these changes for a significantly more elliptical orbit at both proximal and mid-span nodes. Perhaps more significantly though, the SQP result changes the flexure of the rotating shaft such that it is no longer a 'mixed' precession result but a BW precession at all locations. In addition to the improved optimum (Table 4-10) magnitudes, this could potentially be beneficial to the design in terms of reduced flexural stresses along the shaft. This of course was not purposefully studied as part of this demonstration exercise since it was not part of Objective Equation Eq. (42), but certainly could be added as part of the overall optimization effort.

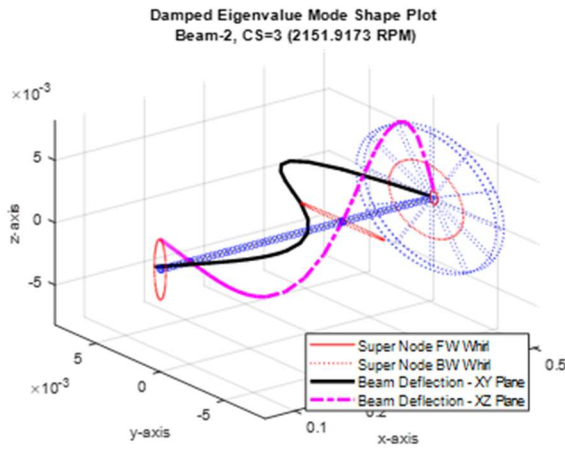
These data then support that the Rotordynamic model, Optimization method(s) and Robustness considerations provided by these tools can provide significant insight to the design behavior for cases where support stiffnesses are non-isotropic and the material includes non-zero Material Hysteretic Damping Loss Factor (η_H).



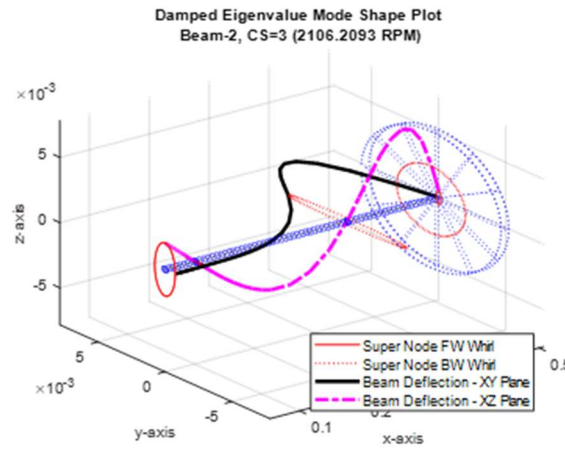
(a) Starting Point #5



(b) Optimum from SFD-Individually



(c) Optimum from SQP-Individually



(d) Optimum from Hybrid (SFD+SQP)

Figure 4-8 Mode Shape Plots – Optimization Results for Non-Isotropic Support Stiffness

Optimization of Systems with Negative Stiffness

Starting locations for supports L_{M1} and L_{M2} (regions defined in Table 3-6) in this demonstration are the same as used for the previous demonstration regarding non-isotropic stiffness and the starting point for the negative stiffness element location is either between bearing 'B1' and 'M2' or between 'M2' and 'B2' in order to cover the full range of negative stiffness element location between 'B1' and 'B2'. The starting points are shown in Table 4-12. Optimization results are provided in Table 4-13 and Robustness results in Table 4-14.

Table 4-12 Design Space Definition Considering Feasible Space

Start Point	L_{M1} (m)	L_{M2} (m)	L_{K_Neg} (m)	
			'B1' to 'M2'	'M2' to 'B2'
1	0.01700	0.14400	0.12700	0.20320
2	0.01700	0.22870	0.17800	0.25400
3	0.01700	0.31330	0.22860	0.33020
4	0.05090	0.14400	0.12700	0.20320
5	0.05090	0.22870	0.17800	0.25400
6	0.05090	0.31330	0.22860	0.33020
7	0.08470	0.14400	0.12700	0.20320
8	0.08470	0.22870	0.17800	0.25400
9	0.08470	0.31330	0.22860	0.33020

Table 4-13 General Optimization Results of Negative Stiffness Demonstration

Test ID	Optimization Method		Start Point of Opt. Result	Optimum Location			Minimum Function Value	Total Function Evaluations ₁
				L _{M1} (m)	L _{M2} (m)	L _{K_Neg} (m)		
10	a) SFD Individually	(B1 to M2)	3	0.01301	0.33525	0.17132	0.946008	228
		(M2 to B2)	1	0.01270	0.14133	0.20309	2.891052	208
	b) SQP Individually	(B1 to M2)	3	0.08686	0.28957	0.17395	1.202743	978
		(M2 to B2)	4	0.01270	0.17040	0.18310	1.597210	399
	c) Proposed Hybrid (SFD + SQP)	(B1 to M2)	3	0.01270	0.33513	0.16464	0.938098	291
		(M2 to B2)	1	0.01270	0.14922	0.21464	2.87720	249

1) Total Function Evaluations of Hybrid include both Initial and Follow-on searches

The data of Table 4-13 illustrates that all test runs found the optimal solution as coming from runs with the Negative Stiffness element constrained between bearing 'B1' and mount 'M2'. Of these, Starting Point #3 was common as the start point resulting in the minimum objective function. This is similar to the finding from the Non-Isotropic study (Table 4-9) except that Start Point #5 applied to that study whereas Start Point #3 applies here. This difference is attributed to the influence of the negative stiffness element in this study.

The minimum function value for both SFD and Hybrid was lower for the negative stiffness study than for the results of Table 4-9 by approximately 15% (SFD Individually) and 9.3% (Hybrid). The minimum function value from SQP Individually was approximately 39.5% higher for the negative stiffness study than for the non-isotropic. Overall, the minimum for this negative stiffness study was approximately 8.8% higher than for the non-isotropic study of Table 4-9. This data indicates that, on the surface, the linear negative stiffness application is not as effective at minimizing the bearing 'B2' reaction force and overall rotating shaft flexure as simply adjusting the mount locations alone.

As with previous studies, the SQP-Individual method (Test ID #10b) used many more function evaluations than either SFD-Individually or the Hybrid (Test ID # 10a and 10c), supporting earlier conclusions that SQP applied individually is less effective for high modality responses. The effectiveness of the SQP-Individual methods to find the lowest function value for the non-isotropic study (Test ID # 9b)

yet the poorest among the negative stiffness results is attributed to this same fact; that SFD is a good local search tool but not as effective when needing to cross significant local maximas. It is possible that for the non-isotropic study, the starting point was 'within local maxima borders' of the lower function value whereas that was not the case for the negative stiffness study. The increased number of function values for the negative stiffness study relative to the non-isotropic study (+87%) also supports this assertion; that the starting point location relative to local maximas was significant for the SQP method applied individually.

Even though the negative stiffness study included 3 design variables (as opposed to 2 for the non-isotropic study), the SFD and Hybrid methods required approximately the same number of function evaluations between the 2 studies. Figure 4-9 provides a graphical display of the convergence paths for the SQP Individual and Hybrid methods for the negative stiffness study. As shown, the SQP process did make major 'jumps' across the design space, but did so in a much less efficient and, what appears as a less direct effort, than did the Hybrid method.

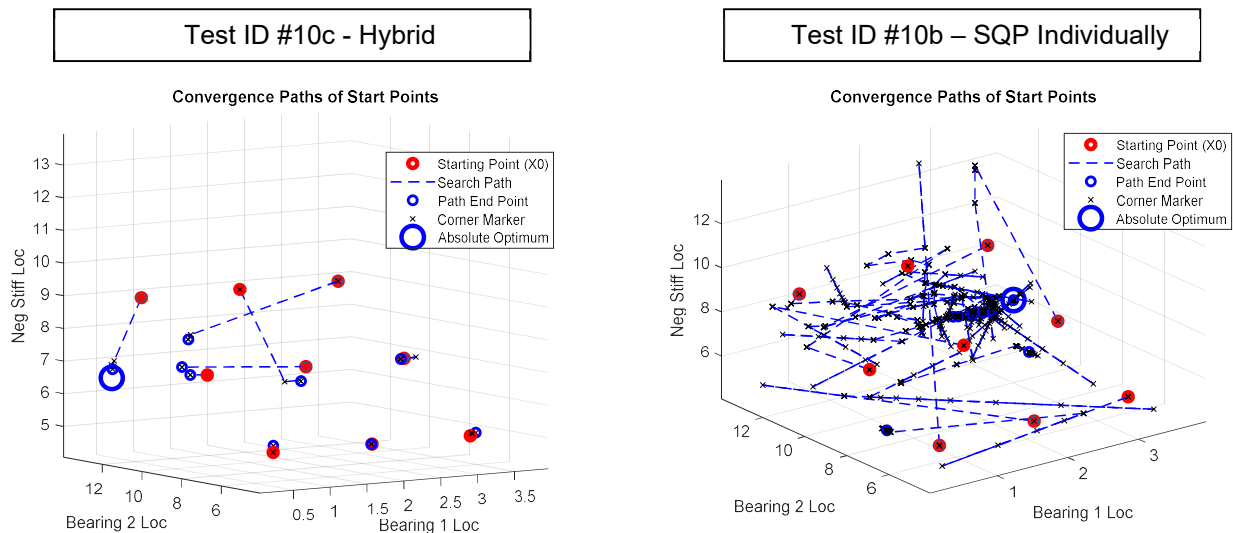


Figure 4-9 Optimization Convergence Paths – Negative Stiffness Study

These results support earlier assertions that the proposed Hybrid and perhaps also the SFD may be a preferred approach compared to SQP applied individually; particularly for problems where the function evaluation is particularly costly.

Table 4-14 Robustness Results of Negative Stiffness Demonstration

	Start Point	Function Evaluation Solve Count	NRMSE (%)	Max Equation Error (%)	Robustness Output				
					Max	Mid Range	Min	Range (%)	Space Feasible
SFD Only	3	27	0.124	0.200	0.952280	0.947750	0.943220	0.957	yes
	8	199	57.290	9999.000	*****	*****	*****	*****	yes
	6	27	0.004	-0.010	2.304990	2.300960	2.296930	0.350	yes
	9	27	0.222	-0.820	3.128720	3.125830	3.122950	0.185	yes
	1	181	0.670	292.990	*****	*****	*****	*****	yes
	5	27	0.058	-0.140	6.206880	6.166250	6.125620	1.319	yes
	2	27	0.007	-0.010	7.027750	6.994770	6.961800	0.943	yes
	4	27	0.403	0.650	11.140700	10.999920	10.859150	2.574	yes
	7	27	0.355	-1.010	11.685070	11.488320	11.291560	3.440	yes
		569							
SQP Only	3	83	21.920	61.000	*****	*****	*****	*****	yes
	6	27	0.008	-0.020	2.267340	2.266950	2.266570	0.034	yes
	8	27	0.045	-0.180	2.278040	2.276710	2.275370	0.118	yes
	5	27	0.328	-1.440	2.320510	2.311160	2.301800	0.811	yes
	9	27	0.319	-1.400	2.320300	2.311120	2.301930	0.796	yes
	2	27	0.059	-0.210	2.334200	2.332240	2.330270	0.168	yes
	1	27	0.078	-0.240	2.345960	2.343170	2.340380	0.238	yes
	7	181	46.807	-1407.400	*****	*****	*****	*****	yes
	4	27	0.276	0.460	5.744800	5.692380	5.639960	1.850	yes
		453							
Hybrid (SFD + SQP)	Post-SQP	27	0.025	-0.060	0.939450	0.938360	0.937260	0.233	yes
	3	27	0.124	0.200	0.952280	0.947750	0.943220	0.957	yes
	8	199	57.334	9999.000	*****	*****	*****	*****	yes
	6	27	0.004	-0.010	2.304990	2.300960	2.296930	0.350	yes
	9	27	0.222	-0.820	3.128720	3.125830	3.122950	0.185	yes
	1	181	0.670	292.990	*****	*****	*****	*****	yes
	5	27	0.057	-0.140	6.206910	6.166280	6.125650	1.319	yes
	2	27	0.007	-0.010	7.027750	6.994770	6.961800	0.943	yes
	4	27	0.403	0.650	11.140700	10.999920	10.859150	2.574	yes
	7	27	0.355	-1.010	11.685070	11.488320	11.291560	3.440	yes
		596							

Table 4-14 illustrates the Robustness results of the negative stiffness demonstration exercise. As before, tradeoffs appear between the lowest absolute function value and the range in output values across the local tolerated design spaces; although benefits of tradeoffs from this study are much more restricted than previous studies. The cost of the Robustness exercise for this 3-factor negative stiffness exercise is greater than for previous 2-factor studies, reinforcing that in practice a limited number of optimums are likely needed to gain the desired information.

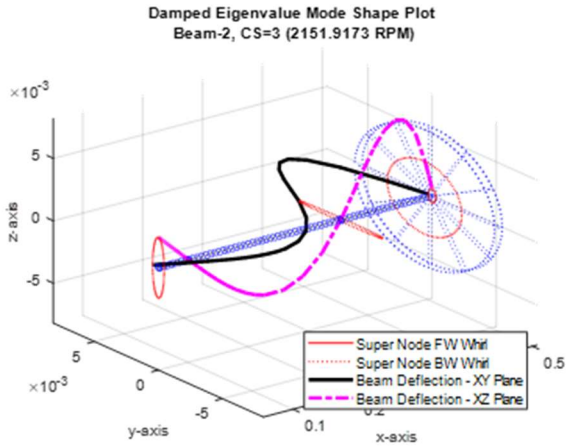
Another consideration in this study is the effectiveness of ‘negative stiffness’ as compared to conventional ‘positive stiffness’ for the added element. As means of quick evaluation, the influence of ‘negative stiffness’ as opposed to ‘positive stiffness’ (of the same absolute value magnitude and location) are evaluated by running the model with the 2 stiffness values (‘negative’ and ‘positive’) at locations as derived from the Hybrid optimization (Test ID #10c) above. The data is provided in Table 4-15 and supports that the effect of a ‘negative stiffness’ element is not the same as a ‘positive stiffness’ element ‘in reverse’. Rather, the effect of the linearized negative stiffness bearing shows significant improvement compared to a conventional support in the same location with positive stiffness.

Table 4-15 Negative vs Positive Stiffness Comparison

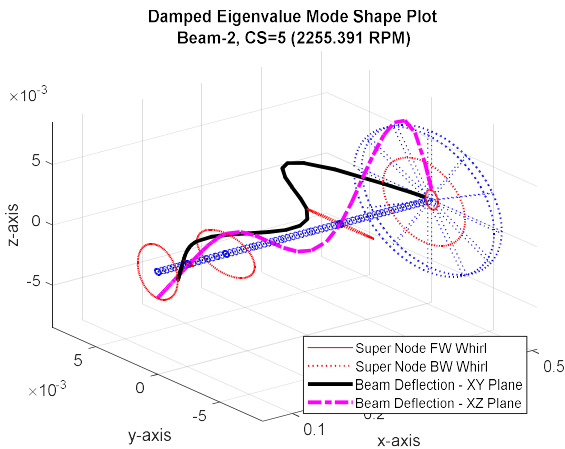
Optimum Location (Test ID #10c)			Stiffness of K _{Neg} (N/m)	Minimum Function Value
L _{M1} (m)	L _{M2} (m)	L _{K_Neg} (m)		
0.01270	0.33513	0.16464	- 1.751e4	0.938098
			+ 1.751e4	6.810846

Figure 4-10 illustrates a comparison among the mode shapes for the optimal Non-Isotropic Stiffness Study (Test ID #9b) as a baseline and the potential mitigations of an added element with Negative Stiffness and Positive Stiffness (per Table 4-15). Although the objective function values are within approximately 8.8% for the Non-Isotropic baseline and Negative Stiffness design, the mode shapes are considerably different as are precession patterns for the Critical Speed at approximately 2200 RPM. Both mode shape and precession pattern are subjectively much more similar between the baseline and

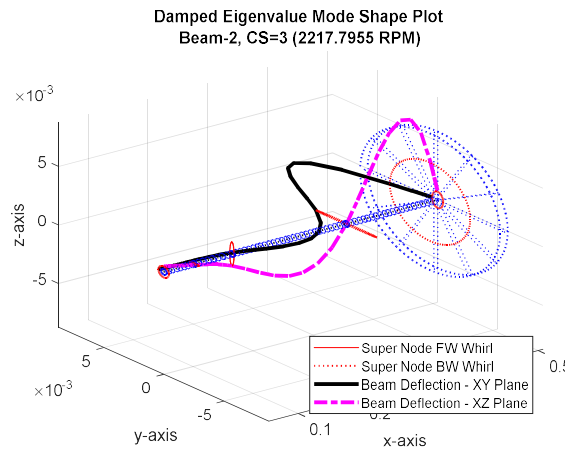
Positive Stiffness alternative (for CS~ 2200 RPM) yet the objective function value is significantly higher for the Positive Stiffness design. Note also that despite the Non-Isotropic stiffness properties of the moveable Mounts ('M1' and 'M2'), precession pattern of the shaft's distal tip appears round and symmetric. This despite precession patterns elsewhere on the models that are markedly elliptical or even linear.



Optimum from Test ID #9b ($f=0.8623$)
(Non-Isotropic Stiffness Study)



Optimum from Table 4-15 ($f=0.9381$)
(Negative Stiffness Element)



Optimum from Test ID #10c ($f=6.8108$)
(Positive Stiffness Element)

Figure 4-10 Mode Shape Comparisons – Negative and Positive Stiffness Influence

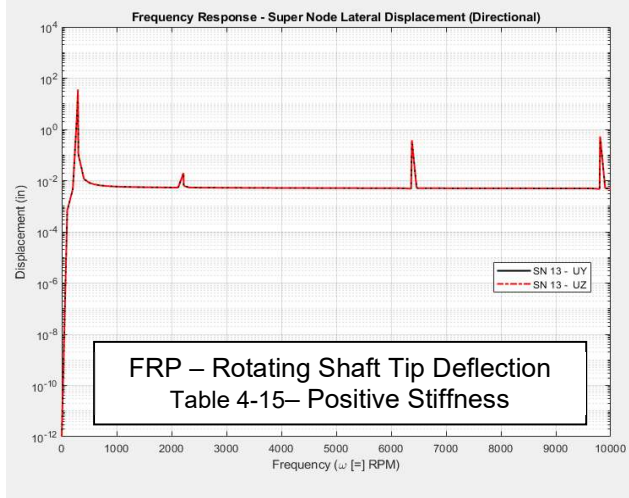
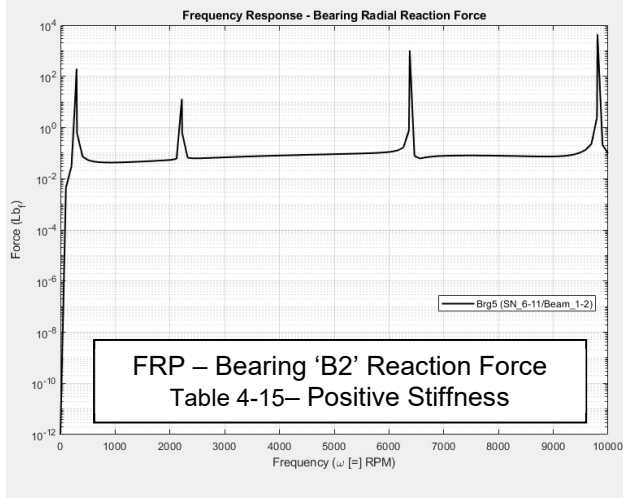
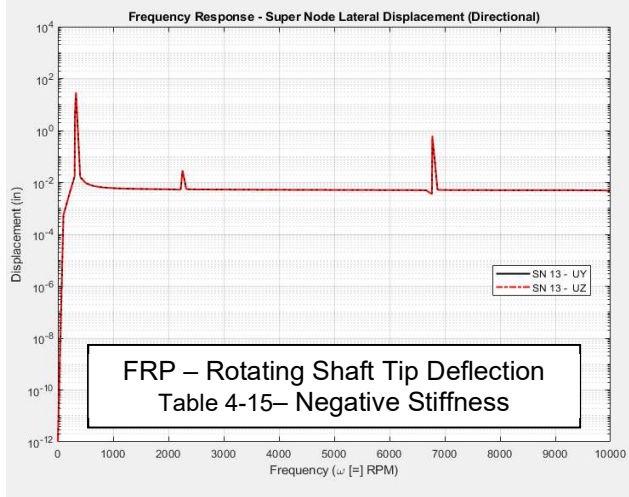
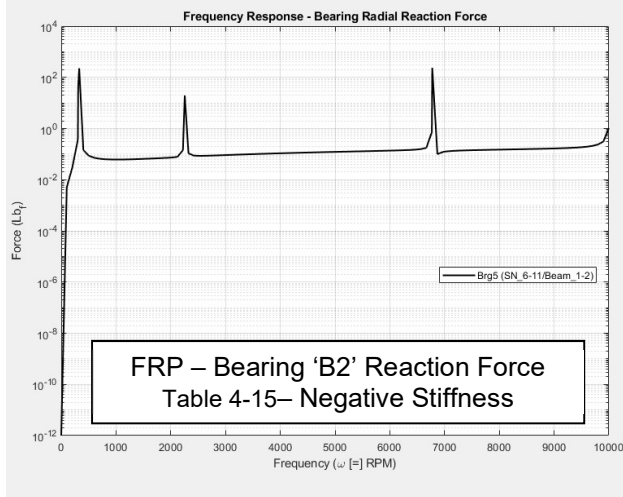
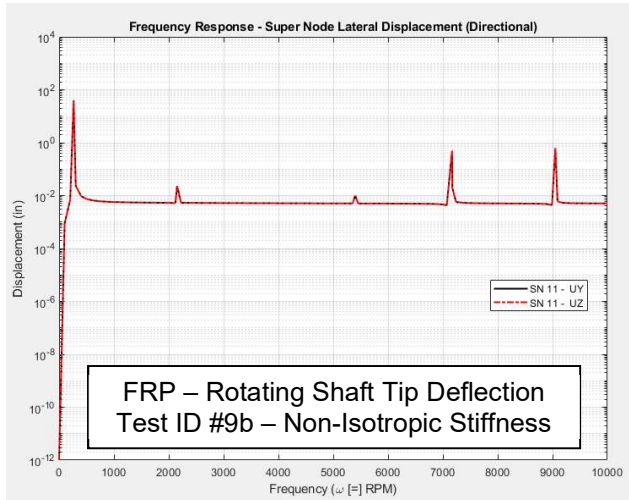
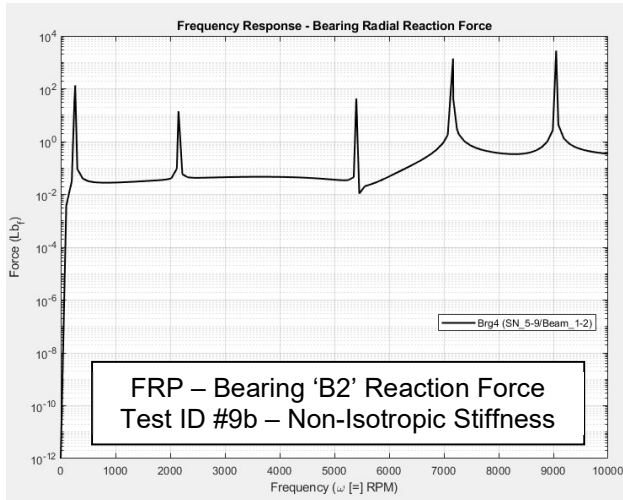


Figure 4-11 FRP Plot Comparisons – Negative and Positive Stiffness Influence

Figure 4-11 provides insight into these comparisons by confirming the appearance of 'round' or 'symmetric' shaft tip precession in that UY and UZ FRP traces effectively overlap for all 3 designs. The FRP trace for shaft tip displacement (right-most plots in Figure 4-11) are substantially similar among all 3 designs. However, the Bearing Reaction Force for 'B2' is significantly lower through the operating range for the Negative stiffness design compared to the Baseline; particularly in the upper 1/3 of the operating range.

These observations support that in this case, the selected objective function (bearing 'B2' reaction force plus overall rotating shaft deformation) may not fully describe an 'optimal' rotordynamic design and, because of this the Negative Stiffness design may be more attractive than the 8.8% difference might otherwise suggest. This supports that the developed Rotordynamic FEA code and Optimization code with Robustness can be a meaningful tool for the designer with respect to conceptual analyses where a decision to invest further time on investigation is needed.

Chapter 5

Summary and Conclusions

Rotating machines are among the most common application of mechanical engineering, yet tools and methods available to the Rotordynamic Designer are too often limited in their capability as compared to tools and methods available for non-rotating systems. This is particularly true when the rotating machine must operate through a wide speed range encompassing one or more resonant frequencies. This is increasingly the case given system requirements to minimize weight and footprint yet achieve high power densities; often as a result of increased speed range. As a result, system response can have high modality, causing challenge to conventional optimization methods. In addition, the inclusion of a rotating degree of freedom, gyroscopic moments, cross-coupled forces and the possibility of whirling instability all combine to make the systems non-self-adjoint where system matrices are asymmetric such that many Optimization methods appropriate for non-rotating systems are no longer appropriate.

Additionally, Robustness information is seldom available as an output Rotordynamic Optimization tools. This is important in that the Designer needs to understand the influence of input variation with respect to the responses of interest. As such, the appropriateness of an 'optimal' solution is often unknown considering known geometric, material and other variation causing reduced certainty in the appropriateness of an identified solution.

This work focuses on the development of tools to aid the Rotordynamic Designer in design evaluation and optimization, including Robustness considerations. An example of a rotating shaft housed within a non-rotating outer housing with elastic bearings and external mounting supports is used to illustrate both effectiveness and efficiency of the developed tools. **Key objectives of this work include:**

- Development of a special purpose Finite Element Tool able to predict Critical Speeds and Frequency Response characteristics of a Rotordynamic system including consideration for Consistent Matrix development, Timoshenko shear effects, material damping and non-isotropic stiffness effects.
- Development of an Optimization method that is effective for high-modality responses and efficient with respect to conventional methods such as GA, PSO and SQP.

- Development of an effective and efficient method of advising Robustness of the optimal design(s).

A primary unique contribution resulting from this work is the development of an effective and efficient Optimization method for rotating systems where high modality and black-box function generators are commonly used, and the ability to provide Robustness information about the optimum(s) with respect to variation in the design variables.

The significance of this work is development of design tools that allow for significant business impact by the Rotordynamic designer to achieve technical goals in a way that can be identified on the bottom line of a company's financial Income Statement.

Chapter 1 presents an Introduction for the work and includes description of the overhung rotor problem used as an example thru this work. A review of Literature and State of the Art with respect to Rotordynamic systems, the principle of mass inversion, gyroscopic effects and potential methods of mitigating flexural vibrations and related outputs. Optimization methods appropriate (and not appropriate) to Rotordynamic systems as well as Robustness and RBDO solutions are also discussed.

Chapter 2 presents the technical approach for both the Rotordynamic Finite Element solution and Optimization methodology developed under this work. Shape Functions, Consistent Matrix and EOM development are described as are the use of Eigenvalue analysis and Steady-State Component analysis in the development of Critical Speed and Flexural Response characteristics. Development of a Hybrid optimization methodology including modification of the well-known first-order Steepest Feasible Descent methodology for use as both a Constrained and multi-objective search tool. A method for Robustness assessment of the optimization results is also described.

Chapter 3 presents the results of various challenges to the developed software tools. Correctness checks for the Finite Element code include comparison of developed Shape Function, Matrix and EOM equations to literature as well as the ability to correctly characterize the physical properties of linearly varying geometry. Output of the FEA code with respect to static deformations under load, non-rotating natural frequencies and mode shapes and rotordynamic results are made as a high-level demonstration of the effectiveness of the developed code. In addition to mathematical test functions, the

Hybrid optimization methodology is challenged against non-rotating structural dynamic vibrations as well as Rotordynamic systems. Finally, the developed Robustness method is assessed using both a mathematical test function and Rotordynamic model.

Chapter 4 presents various demonstrations of the developed FE and Optimization codes including the effects of Robustness. These demonstrations 'build' on each other, starting with Optimization and Robustness evaluation of the example overhung rotor system, Optimization and Robustness when Internal Material Damping is included in the rotating shaft, the same when Non-Isotropic Supports are added, and finally the effects of a Negative Stiffness element as a potential mitigation to bearing reaction force and flexural deformations of the rotating shaft.

Key conclusions of this work include:

- The proposed Hybrid optimization methodology, comprised of a global SFD search followed by local SQP, is an effective tool in the search for global optimums of a constrained, high-modality response where cross-coupled matrices are asymmetric and non-self-adjoint as with the Rotordynamic problem.
- The developed Rotordynamic FEA code was confirmed against numerous challenges including:
 - Shape function equations – 13 literature comparisons
 - EOM / matrix equations – 4 literature comparisons
 - Stepped / linearly varying geometry – Closed form equations and CAD geometry
 - FEM for static deformations – direct calculations using Castigliano's (4 BC's)
 - FEM for non-rotating Structural Dynamics – literature comparisons (3 BC's)
 - FEM for rotating systems – literature comparisons (4 models)
- GA-based optimization methods produced the lowest (most optimal) function values in deterministic use with errors against results of a constrained, mapped survey optimum of less than 0.1%. The methods however used more than 1250% more function evaluations than the proposed Hybrid method.

- PSO-based optimization methods produced optimum function values in deterministic tests with errors between 0.2 ~ 0.8% against the Global Constrained Optimum from mapped survey results (GCO). They used between 86 ~ 930% more function evaluations than the proposed Hybrid method.
- The proposed Hybrid method (SFD + SQP) identified an optimum with 0.8% error to the mapped GCO.
- Hybrid component methods used individually found an optimum within 1.4% and 2.8% of the mapped GCO for SFD and SQP respectively. The SFD used individually however used 15% fewer function evaluations than the proposed Hybrid and SQP used individually used 35% more.
- When starting from the mapped GCO and followed with SFD Individually, SQP Individually and the proposed Hybrid method, resulting optimums were within 0.1% of the mapped GCO result.
- When using 100 'quasi-random' starting points rather than the 9 starting points used in previous deterministic evaluations, the SFD and SQP (each used individually) resulted in optimums within 0.9% and 1.7% (respectively) of the mapped GCO. The proposed Hybrid with 100 starting points also found a result within 0.9% of the mapped GCO. These results are little different from the tests using 9 starting points; indicating that the search methodology is effective as a Global search tool.
- Based upon deterministic search challenges, the SFD routine used as an individual technique has merits when compared with SQP, GA and PSO for use on functions with high modality results; particularly where the cost of function evaluations is high.
- The developed multinomial-based Robustness methodology was tested against Rastrigin's function in 2-, 3- and 4-DOF for ability to predict minima and maxima on a local design space centered on a local minimum, a local maximum and a transition space. The method identified results with error against exact results ranging up to 1.5% for design space centered on the local minima and up to 7% for transition space. Design

space centered on a local maxima produced the greatest error (up to 78%) due to limited ability of the multinomial method to appropriately fit the complex curvature of the tolerated space. Error predictions within the Robustness code accurately predict the fit of the multinomial to the function data and, when included with the Robustness output results in an effective Robustness indication to the user.

- When used against the mapped survey Global Constrained Optimum (a bowl-shaped section of the response), the Robustness methodology resulted in multinomial error of less than 0.5% between actual FEA data and the robustness response equation. When tested against the mapped survey Global Unconstrained Optimum (a valley-shaped section of the response), the Robustness response equation had error of up to 197% against actual FEA data. When coupled with predicted error values, the resulting Robustness output to the user is found to be effective for high modality use as with the example Rotordynamic system.
- When the Optimization method including Robustness elements was applied to the example rotor system, an optimum was identified 0.8% error to the mapped GCO (as with the deterministic test) and Robustness was predicted among 10 identified potential optimums with robustness equation error of 0.5% for the identified optimum and ranging up to 5% for the other potential solutions. This supports that the Robustness method can be effective for the intended use.
- Use of the tools for a Rotordynamic system including Material Hysteretic Loss Factor was conducted as a demonstration to evaluate the influence of Loss Factor on the system. In addition to Mount locations as with the basic example, Loss Factor was identified as a design variable with a modified objective function focused on improvement of system stability. Results support that design variable movement was significant for the Loss Factor and almost non-existent for location of the Mounts. Although not a practical study in that Loss Factor is not a 'variable', the demonstration does illustrate that the developed FEA code is sensitive to Loss Factor (in addition to 'component-level' equation

confirmations of code correctness against literature). The demonstration results also support that the optimization did not significantly modify the stability characteristics of the system.

- When demonstrated against a system including both Material Hysteretic Loss Factor and Non-Isotropic stiffness in the external mounts, the proposed Hybrid and perhaps also the SFD are shown to be preferred compared to the SQP applied individually. Here, the SFD (applied individually) found an optimum approximately 7.7% higher than the proposed Hybrid but with 8.8% fewer function solves. As with previous studies, the SQP (applied individually) found the lowest optimum (16.6% below the proposed Hybrid) but used 78% more function evaluations in the process.
- The effects of a Negative Stiffness element when applied to a system including Material Loss Factor and Non-Isotropic External Mount stiffness show potential as mitigation against distal bearing reaction force and flexural vibrations of the rotating shaft. The best optimum from this study was produced by the proposed Hybrid at approximately 9.3% higher than the best optimum (SQP individually) for the system without a Negative Stiffness Element, with a Robustness variation approximately 86.6% lower than that of the SQP solution without the Negative Stiffness element. When a conventional positive stiffness element was placed in the same location as the optimized Negative Stiffness element and with a stiffness value matching the absolute value, the objective function response grew by approximately 626%. Although purely conceptual, this demonstration exercise illustrates the intended significance of this work in the development of design tools that allow for significant business impact by the Rotordynamic designer to achieve technical goals in a way that can be identified on the bottom line of a company's financial Income Statement

Chapter 6

Recommendations for Further Work

Following are areas where further research may yield significant improvement to the current work.

- The current Robustness methodology involves the fit of a polynomial to known points developed from the FEA evaluations. The existing method of identifying coefficients to polynomial terms through optimizations for a variety of polynomial powers is effective in basic functionality but results in significant error for more complex response 'surfaces'. In addition, the influence of the number of design variables is significant in this method. An alternative equation-fit methodology could potentially be an improvement to this methodology. Both effectiveness (error) and efficiency (time or number of FEA solutions required) are to be considered in an alternate approach.
- The current Robustness methodology is currently not included as part of the optimization process. That is, Robustness information does not inform the optimization search but instead is an evaluation attributed to the identified solutions in an attempt to minimize the number of function evaluations of the overall process. A methodology that uses Robustness information to inform the optimization directly is preferred. However as with conventional RBDO solutions the potential to greatly reduce the efficiency is high. An efficient form of this solution is preferred.
- The Rotordynamic FEA code developed under this work is effective but limited to linear representations of stiffness and damping. In addition, the super-node concept aids simplicity of the user interface but serves as a challenge for optimizations where multiple super node configurations need to be considered. Both challenges are exemplified in the 'negative stiffness demonstration' of this work. A modification to both areas would increase the scope of effectiveness for the Rotordynamic code.

Appendix A

Technical Paper – Hauser, Wang, *Structural and Multidisciplinary Optimization*, 2018



Optimal design of a parallel beam system with elastic supports to minimize flexural response to harmonic loading using a combined optimization algorithm

Bret R. Hauser¹ · Bo P. Wang¹

Received: 3 December 2017 / Revised: 19 February 2018 / Accepted: 9 March 2018
© Springer-Verlag GmbH Germany, part of Springer Nature 2018

Abstract

Mechanical systems subject to vibration are prevalent across many industries. Although potentially different in application, they sometimes share the need to minimize aspects of flexural deformation given harmonic loading and the need to consider a variety of both input and response-based constraints in the process. Practical design efforts also sometimes include the need for consideration of the optimal response of a platform-style product, including responses of multiple design variants supported by a common base structure. Harmonic problems can be especially challenging to optimize due to the likelihood that the response will be multi-modal; influenced by system natural frequencies throughout the design space. Further, analysis of these systems often involves large and complex computer models which require significant resources to execute. A harmonically loaded, platform-style parallel beam system with multiple family variants is used as an example in this work to demonstrate a proposed method for identifying an optimum in a constrained, multi-modal response environment with consideration for Expensive Black Box Functions (EBBF). The presented method proposes a combined approach where the high modality, EBBF's domain is first surveyed for potential areas of optimal response using a method of Steepest Feasible Descent (SFD), followed by a local search in the optimal region using a more efficient direct search method. The method of SFD is a modification of the classical method of Steepest Descent, made useful for constrained models by a penalty system including both deterministic and programmatic methods. A sensitivity-based search vector method also helps to manage situations where significant difference in magnitude exists among the design variables. Evidentiary support for these key program elements is provided using standardized test functions. The effectiveness of the method is demonstrated by seeking a minimum flexural response for a parallel beam system subject to elastic support and response constraints.

Keywords Harmonic optimization · Parallel beam · Elastic supports

1 Introduction

Figure 1 illustrates the problem under study; a harmonically loaded parallel beam system with elastic supports and three (3) family variants, subject to harmonic loading through a range of frequencies. The objective of the study is to minimize flexural deformation of the tip mass (m) throughout the de-

finied frequency range, subject to location constraints of the elastic supports as well as a maximum allowable static deformation for the tip masses. A total of 10 design variables are considered for optimization, (2) lengths, (4) support stiffnesses and (4) viscous support dampers.

The family variants differ in upper-beam definition only, each constrained with a specified (and differing) length, tip mass and cross-sectional geometry. The location of intermediate supports (L_3 and L_4) are fixed with respect to system ground (A) and represent a design constraint often encountered in platform-style products; the need for common interface design. The objective function (flexural response) is multi-objective; being comprised of the summed effect of all family variants (upper beams) upon the integrated response across the prescribed frequency range as well as the maximum

✉ Bret R. Hauser
bret.hauser@tc.ttu.com

Bo P. Wang
bpwang@uts.edu

¹ University of Texas at Arlington, Arlington, TX, USA

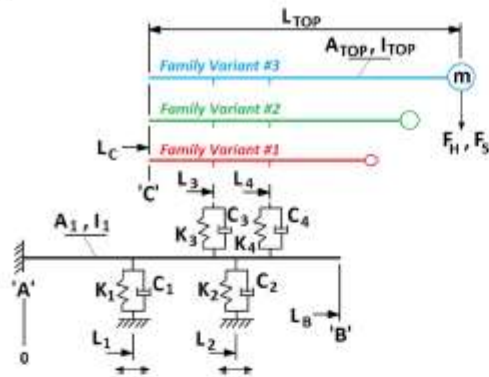


Fig. 1 Elastically supported parallel beam structure with 3 family variants

range of response across the frequency range. In this way, the response of the entire product family is optimized for both flexural response magnitude and variation; providing a familial design for the lowest, most consistent vibrational responses.

A common approach in the design of vibrating systems is to stiffen the structure such that the fundamental natural frequency is higher than the operating range. Akesson and Olhoff (1988) described that a minimum stiffness could be identified for optimally located intermediate elastic supports to maximize the fundamental frequency of a cantilever beam. Wang et al. (2004) attempt to devise an approach to programmatically optimize the location of support positions to maximize the fundamental frequency of structures regardless of their stiffness value. Wang also uses this general methodology to optimize support locations for the static deflection of structures due to force (Wang 2004) and moment (Wang 2006). Given consideration that it is impossible within a practical world to implement a support with infinite stiffness, Wang, Friswell and Lei (2006) use the closed form equation for design sensitivity proposed by Wang (2004) to investigate a minimum effective stiffness for intermediate supports of various end conditions. Similar results are demonstrated by Zhu and Zhang (2006) where a topology optimization method is implemented to maximize the fundamental natural frequencies of beams and plates using a Solid Isotropic Material with Penalty (SIMP) model.

Consideration for these works infers at least two (2) things: 1) that the maximization of a fundamental natural frequency for a beam system is enhanced by the fact that the response function (frequency) can be treated as a 'smooth surface', without significant mathematical discontinuity and 2) that the natural frequencies can be designed to be significantly above the operating range of the device(s). As is demonstrated later with this example, such a philosophy is not always possible. Therefore, an alternate method is needed.

In his text on the subject, Den Hartog (1985) discusses the use of a damped dynamic vibration absorber (DDVA) to reduce the magnitude of the response near to the natural frequencies. The DDVA is illustrated in Fig. 2 and the Equation of Motion given in (1) below.

$$\begin{aligned} \begin{bmatrix} m_1 & 0 \\ 0 & m_a \end{bmatrix} \begin{Bmatrix} \ddot{u}_1 \\ \ddot{u}_a \end{Bmatrix} + \begin{bmatrix} c & -c \\ -c & c \end{bmatrix} \begin{Bmatrix} \dot{u}_1 \\ \dot{u}_a \end{Bmatrix} \\ + \begin{bmatrix} k_1 + k_a & -k_a \\ -k_a & k_a \end{bmatrix} \begin{Bmatrix} u_1 \\ u_a \end{Bmatrix} \\ = \begin{Bmatrix} P_a \\ 0 \end{Bmatrix} \cos(\Omega t) \end{aligned} \quad (1)$$

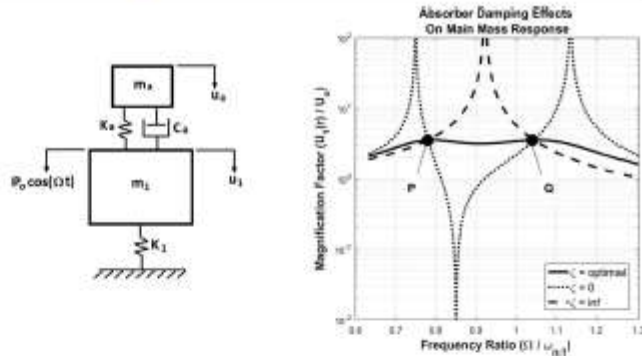
Also illustrated in Fig. 2 is the frequency response plot for the DDVA, illustrating the effect of damping coefficient upon the system. As described by Den Hartog (1985), an optimal response exists for some finite value of damping coefficient whereby the variation in response is minimized with the slope becoming horizontal at frequency points 'P' and 'Q'.

The use of DDVA's to aid vibrating systems is well known. For example, Ozguven and Cildir (1986) applied the use of DDVA's to a cantilever beam to suppress first and second responses. Yang et al. (2011) extended the application of a DDVA to application on a vibrating plate. Multiple 'practical' applications of DDVA's are reported in literature. Among them are Russell (2006) who investigated a novel use of a DDVA to a baseball bat to reduce the sensation of 'sting' experienced by a player, Hao et al. (2011) who investigate the application of a DDVA to an electric grass trimmer to suppress detrimental hand-arm vibration, and Pierson (2012) who addresses a tangential topic regarding magnetorheological fluids to serve as a 'controllable support mechanism' for support of feed stock in high-volume computer-numerically-controlled (CNC) turning machines.

The improved system behaviour resulting from the DDVA is sought for the parallel beam system to minimize flexural response among the family variants given that some resonant conditions may exist within the frequency range of interest. Since the parallel beam system is complex relative to the DDVA of Fig. 2, a closed form solution is not practical; so, a numerical approach is needed to identify the optimal values. Use of a numerical system then adds a requirement that the optimization method not rely upon a priori knowledge of the response equation as is typical for Black Box methods.

Multiple strategies exist for optimization of such a system. Among the simplest are 'First-Order' methods, including the method of Steep Descent (SD) (Vanderplaats 2007). These gradient-based methods are known to be initially productive but become inefficient as the solution approaches the optimal result. In addition, they are useful for single objective and unconstrained searches; neither of which applies to the

Fig. 2 Single DOF damped dynamic vibration absorber



parallel beam problem at hand. Fliege and Svaiter (2000) however, propose using the method of SD for multicriteria optimization as well as adaptation of Zoutendijk's (1960) method of feasible directions for use in constrained cases. They conclude that since the result is a first-order method, it should be considered only as a 'first step' toward efficiency rather than an efficient method unto itself.

'Second-Order' methods improve upon first-order methods by incorporating Hessian matrix information and result in a more efficient process (Vanderplaats 2007). This information however is not readily available for Black Box methods (Laskari et al. 2004). Since a goal of this effort is to find a method suitable to Expensive Black Box Functions (EBBF's), second-order methods are not considered further.

Direct Search methods are described by Kolda et al. (2003) as a class of methods traditionally best-known as unconstrained optimization techniques that do not explicitly use derivatives. These methods are sometimes also referred to as 'Gradient Free' methods. Kolda et al. (2003) recommend that these Direct methods may be particularly appropriate for Simulation Based Optimization where the process of obtaining derivatives for gradient-based methods are difficult, or potentially not possible, even when the underlying objective and constraint functions are smooth and continuously differentiable.

Direct (Gradient Free) methods include techniques such as Genetic Algorithm (GA) (Wang and Chen 1996 and Hajela 1990), Particle Swarm Optimization (PSO) (Laskari et al. 2004, Venter Sobieszczanski-Sobieski 2003, Banks et al. 2007 and Vesterstrom and Thomsen 2004) and Sequential Quadratic Programming (SQP) (Vanderplaats 2007). As stated by Banks et al. (2007), an attribute shared by many of the 'natural computing' paradigm's such as these is the ability to deal with noisy or incomplete data. They cite that PSO can find solutions near optima faster than GA but is more prone to premature convergence than Evolutionary Algorithms (EA). Vesterstrom and Thomsen (2004) compared the effectiveness

of EA, PSO and Differential Evolution (DE) and concluded that, in general, the DE algorithm outperforms both PSO and EA in terms of consistent speed of convergence and ability to find the optimum. However, Vesterstrom and Thomsen (2004) note that PSO was particularly problematic with noisy functions.

Vanderplaats (2007) states that although all Direct Methods are applicable to constrained functions, they are known to potentially require a high number of function evaluations, particularly for multi-modal responses. This makes them undesirable as 'stand-alone' optimization tools for EBBF's.

Given the objectives of this study, Direct or Gradient Free methods are not considered further. However, it is recognized that development of such a method with efficient application to EBBF's is an opportunity for future work with potentially exciting ramifications.

SQP is another alternative technique and known as a more efficient method than first-order methods. However, it is primarily a 'local' search tool with respect to multimodal response in that it has the potential to be 'constrained' by local maxima (Vanderplaats 2007). If, however, a potential area of optimum could be identified across a multi-modal response, SQP could be an effective solution.

Laskari et al. (2004), compare the use of PSO as a means of optimizing minimax problems to SQP. They conclude that for Black Box functions where gradient information is not available (as with EBBF's) that PSO may be a good alternative as an initial search tool with continued optimization performed by more efficient methods such as SQP.

With regard to the identification of such areas of potential in a multi-modal environment, Shan and Wang (2010) present a survey of strategies regarding optimization of EBBF functions. They conclude that two (2) methods are particularly promising; mapping and decomposition. Specifically, a mapping approach transforms the problem from an original higher-dimensional space to a new lower-dimensional one while preserving the optimum of the original function.

Decomposition refers to decomposition methods, decomposed models, adaptive sampling methods, modelling validation, etc.

Cai et al. (2017) propose a multi-point sampling method based on Kriging for efficient global optimization of expensive functions such as finite element analysis (FEA) and computational fluid dynamics (CFD). Kriging (Jones et al. 1998; Lophaven et al. 2002) is an interpolative Bayesian metamodeling technique that estimates an unknown response through a linear combination of a known function such as a polynomial trend plus an error term. Although more efficient than other mapping methods, Kriging relies on enough information about the response to create an adequately accurate map. As discussed by Cai et al. (2017) this is an efficient technique for computationally expensive functions. However, it is problematic for functions with high-modality and/or noise where many sampling points may be needed to capture, and assure accurate definition of, the modalities.

Tabatabaei et al. (2015) also provide a survey on methods to handle computationally expensive optimization problems. They focus on the use of surrogates and non-nature inspired methods. In general, surrogate methods are discussed within two (2) classifications; sequential and adaptive frameworks. Both involve sampling the problem to build the surrogate; the differences being based on when the surrogate is built. A stated challenge to either approach, however is the ability to handle noisy black-box functions.

The problem to be solved under this study is illustrative of a EBBF. Although the example is a relatively straightforward beam model, which can be solved quickly using commercial FEA software and modern computing hardware; the optimization technique is intended for extension to much larger problems where the cost of a single function evaluation can be quite significant. Further, extension of the problem to include a product with multiple family variants, each of which (potentially) has multiple natural frequencies within the operating range, adds complexity to the optimization effort. That is, the example problem illustrates a potential (likelihood) for high modality in the response. Therefore, the attraction of mapping and sampling methods (for example) of Shan and Wang (2010), Cai et al. (2017), and Tabatabaei et al. (2015) are significantly reduced given the required number of sampling points to accurately map such a response.

Laskari et al.'s (2004) conclusion, together with that of Fliege and Svaiter (2000) regarding use of Steepest Descent is the inspiration for this proposed method. That is, that the best overall method for a EBBF with potential for high modality may be to initially investigate the design space using a first-order method and then, from the region of most promising minimum response, continue the search using local SQP. A first order method, when limited to a few jumps and modified for use with constraints, is

theorized to be more efficient for the initial (global) search than direct methods. In addition, the use of a polynomial approximation during the steepest descent's 1-D search is theorized to be effective in identifying 'global' minima in a multi-modal environment.

2 Development and validation of proposed optimization method

The proposed optimization method is a Combined Optimization Algorithm; comprised of an initial survey of the entire design space using a Global Optimization tool followed by a more efficient Local Optimization tool to refine the potential solutions for a more accurate Global Optimum. The proposed method then first uses a derivative of the first-order method of SD (making it effective for constrained searches) for the global survey.

The derivative, termed Steepest Feasible Descent (SFD), includes consideration for both side, input and output constraints. It features a deterministic penalty system as well as programmatic considerations to assure feasibility of the result obtained during the embedded 1-D line search. In this way, feasibility of the line search across the multi-modal space is assured. Also, consideration is given to orientation of the search vector to assure that only feasible space is searched. Finally, weighting is given to the search vector with respect to differences in order of magnitude among the design variables to improve effectiveness of the search.

2.1 Steepest Feasible Descent as a constrained search tool

Multiple methods exist to apply penalties to an unconstrained search methodology and make it useful as a constrained tool. Chen and Chi (2010) for example utilize a penalty function to improve their particle swarm algorithm by applying a penalty to particles that are at the upper or lower bound of the design variable definition. Shahbazi (2005) explored an interior penalty (IP) method as a type of discontinuous Galerkin method for the spatial discretization of elliptic partial differential equations. As the author discusses however, a notable drawback of the IP method is that if the user-selected penalty parameter is not sufficiently large, the approximate solution is unstable.

In the development of the proposed SFD method, feasibility is considered during the execution of the 1-D line search in multiple ways. First, the length of the line search is limited by design variable constraint bounds (both side bounds and other). Secondly, as proposed by Vanderplaats (2007), an external penalty term is combined with the function value to form a

penalized function value to be used in the objective function. This is shown in (2) below.

$$f(x)_{pen} = f(x) + \alpha_p \sum_{j=1}^n \left(\max \left[0, g_j(x) \right] \right) \quad (2a)$$

$$f(x)_{pen} = f(x) + \alpha_p \sum_{j=1}^n \left(\max \left[0, g_j(x)^2 \right] \right) \quad (2b)$$

Two variations of (2) were considered during this work; both linear and second-order versions. Both provide a penalty (only) in the event of an unsatisfied constraint. However, if the square of the constraint is used ((2b)), the penalty value at the constraint bound has a slope of zero; ensuring a continuous slope of the penalized function value through this region. If only the linear form were used as in (2a), a discontinuity is possible at the constraint bounds adding risk of numerical ill-conditioning. For this reason, the penalty method of (2b) is selected for use in this work. Additionally, a penalty multiplier (α_p) is included to aid the 1-D line search by scaling the effect of the penalty to preclude minima from being identified within infeasible space. That is, a multiplier value that is too weak can limit the penalty value such that the penalized function value remains as infeasible. If too strong however, the minima could artificially be ‘pushed’ away from the constraint bound as illustrated in Fig. 3.

Although helpful in tailoring the penalty function, optimal selection of the penalty multiplier can be problem dependent; the risk of an improperly selected value being that the minima could either be within infeasible space or artificially ‘far’ from the constraint bound. Therefore, a programmatic element is incorporated to prevent a minimum (f_{pen}) from being identified within infeasible space during the line search. In this way, a penalty value can be selected conservatively small without risk of finding an infeasible result. It is recognized that the programmatic search could be avoided by incorporating a sub-problem to optimize the penalty multiplier such that the derivative of the penalized function value coincides with the constraint bound. However, this requires computation of the distance to the constraint bound. The combination of penalty multiplier and programmatic consideration then is theorized to improve the efficiency of the constraint-handling process.

In addition to considerations for constraints during the 1-D line search, feasibility is also considered in the determination of the descent vector by a programmatic implementation of the Method of Feasible Directions (MFD) (Vanderplaats 2007). One common implementation of MFD is to incorporate an offset or ‘push-off factor’ (Vanderplaats 2007) to the search vector to avoid a constraint bound. In the case of a nonlinear constraint bound however, an additional ‘optimization

exercise’ is needed within the larger optimization effort (Vanderplaats 2007) to avoid infeasible space.

Given consideration for use of this tool in cases where multiple, highly non-linear constraints may exist; a programmatic implementation of MFD is selected to avoid a potentially large subproblem. Figure 4 illustrates this process.

A minimum length for the 1-D search vector (S_n) is established (as a percentage of the bounded design space). If the distance from starting point of the search vector (X_0) to the nearest constraint bound (along the search vector) is measured to be below this limit, then the vector direction is programmatically modified by eliminating the coordinate term which points most directly to the nearby bound. The resulting search vector is then redirected to a trajectory ‘approximately parallel’ to the subject constraint bound. In this way, the new descent vector is guaranteed to provide at least a minimum search length within feasible space.

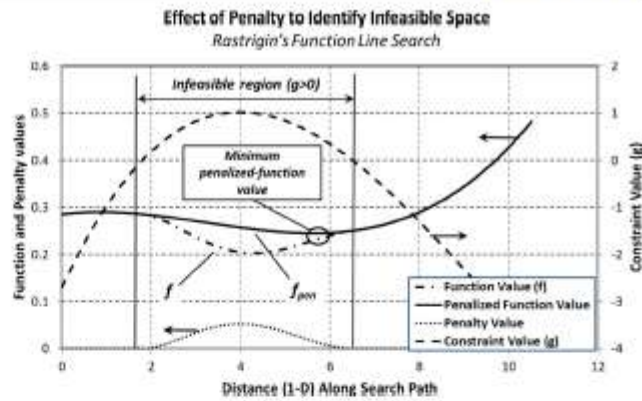
2.2 Sensitivity-based search vector

The gradient for the search vector is based on a finite difference approach. It is recognized that analytical methods, such as the Adjoint method (Maute et al. 2003, Hall et al. 1982 and Martins et al. 2005) and others offer significant computational efficiencies to the proposed finite difference technique. However, as with Othmer (2014), the problem to be solved involves the use of FEA as a Black Box function. Given an intended use for this optimization technique with commercial FEA programs, the source code is unavailable with which to incorporate an Adjoint method. Therefore, the finite difference approach is utilized with modifications for orientation to feasible space, etc as discussed elsewhere in this paper.

The parallel beam problem demonstrates a class of problems where the design variables may have significantly different orders of magnitude (length vs. spring stiffness vs. damping coefficient). This can potentially lead to sensitivity error in the search vector when a finite difference method is employed. That is, if a common step size were used for the finite difference calculation that is appropriate to the smaller variable, then it could be so small as to have an insignificant effect upon a larger variable’s effect. To mitigate this potential error, the finite difference step size (in the direction of each given design variable) is scaled to the magnitude of the given variable. In so doing, the likelihood is increased that the descent vector will be sensitive to the impact of each variable. (3) illustrates one method of determining such a scale effect upon the finite difference step size for a given design variable direction.

$$\Delta_x = \alpha_a \left(\frac{X_{Upper\ Bound} - X_{Lower\ Bound}}{2} \right), \quad \alpha_a = 0.5\% \quad (3)$$

Fig. 3 Identification of constraint boundaries



2.3 Confirmation of optimization method

It is proposed that a 'combined' search methodology of SFD followed by SQP is an efficient overall search tool by leveraging the strengths of each individual method. To challenge this theory and determine if the combined method is truly better than either of the methods used individually, a test was conducted using four (4) standard test functions (Molga and Smutnicki 2005), each of which is a closed form equation in (n) dimensions and for which theoretical global optimums are known. The test functions used in this study are 2-dimensional forms of De Jong,

Rosenbrock, Rastrigin and Schwefel; (Fig. 5). For each test function, the proposed 'combined' search methodology as well as the component methods were run from an array of 75 starting points across the design space. Starting points were determined using MATLAB's@ 'Haltonsef' quasi-random method in order to provide a balance between random selection and repeatability among the tests.

With consideration for EBBF's, a minimum Design Variable step size was established as a stopping criterion with magnitude selected to be meaningful with respect to practical design (e.g.; 0.001% of design variable magnitude).

For each test case, the coordinate location of the resulting global optimum, optimal function value and number of function evaluations was recorded. Key input values for the tests are given in Table 1. As noted, the SFD method was allowed a maximum of 30 jumps, but when used as part of the proposed Combined method the SFD portion was limited to only 2 jumps to identify the region of potential optimum. The SQP method was allowed to utilize 250 'jumps' as both individual and part of the Combined method. Results of these (unconstrained) tests are given in Table 2 below.

Overall, each method identified an 'optimal solution' near the theoretical optimum except for the SQP (individual) method on Schwefel. In this case, the identified solution is far from the known theoretical optimum. This is attributed to the selection of the Minimum Design Variable Step Size (0.001%) coupled with the extreme modality of the function. The proof of this conclusion is not presented here due to brevity. However, informal investigation with a reduced Step Size resulted in a result of similar accuracy to both SFD and Combined, but at the expense of significantly greater function evaluations. This illustrates a notable benefit of the proposed Combined method; that it is more tolerant of a coarse step size than the SQP used independently. This is particularly useful for EBBF models.

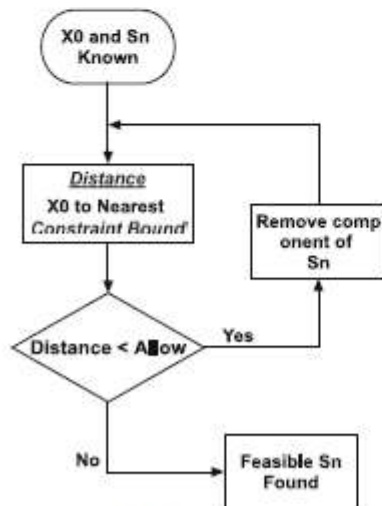
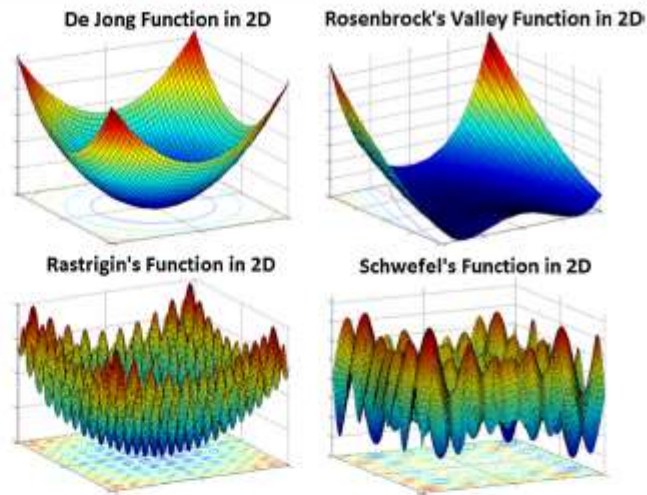


Fig. 4 Flowchart - feasible Sn selection

Fig. 5 Test functions in 2D



For Rastrigin, the proposed Combined method identified an optimum of approximately the same accuracy as SQP (individually) but with slightly more function evaluations (6.2%). Both methods were significantly more accurate and had fewer function evaluations than SFD (individual).

All methods identified an optimal solution for the unconstrained Rosenbrock's Valley of approximately the same accuracy. However, the SQP (individual) method resulted in approximately 188.6% more function evaluations than SFD (individual) and 307.3% more than the proposed Combined method.

No practical benefit is demonstrated for De Jong's unimodal function among any of the methods evaluated. Each found an optimum of approximately the same accuracy with similar numbers of function evaluations.

These results confirm that the proposed Combined method leverages the 'best' qualities of either of the individual methods for some multi-modal responses (with consideration for use with EBBF's), without significant consequence to the other functions.

Constrained response of the proposed method was evaluated in a similar method and used the same test functions (Molga and Smutnicki 2005). For each, a circular region of

infeasibility was created, centred at the location of theoretical global optimum. (4) provides the constraint equation used where (x_{ps}, y_{ps}) represents the coordinate location of the point being evaluated and (x_{center}, y_{center}) , $R_{constraint}$ are the center and radius of the cylindrical constraint region.

$$R_{constraint} \leq \sqrt{(x_{ps} - x_{center})^2 + (y_{ps} - y_{center})^2} \quad (4)$$

For each constrained test, the location of the 75 start points and other parameters (Table 1) remained the same as those used for the previous unconstrained tests. Constraint region parameters are depicted in Table 3 for each test case together with the results.

Modifications incorporated to the SFD approach for constraint handling successfully prevent solutions from being identified in the infeasible region. That is, all Search Path Endpoints (for SFD searches where the penalty method is employed) result in potential solutions that are exterior to the constraint region's radius. Table 3 documents this in that the minimum distance from any Search Path's Endpoint to the Constraint's Center (using SFD) is greater than (or equal to) the radius of the infeasible space. Figure 6 illustrates this graphically.

The results of Table 3 also indicate that constrained searches using the SQP method (individually) resulted in the identified optimum being located within infeasible space for both Rosenbrock Valley and Schwefel test functions. Practically speaking though, both are relatively small infractions. Although the same constraint function was used for all methods (Combined, SFD-only and SQP-only), it is possible that an accuracy setting for the SQP study (MATLAB function 'fmincon') was not set as appropriately as needed to prevent

Table 1 Key test parameters

Max Jumps – SFD (individual/ combined cases)	30 / 2
Max Jumps – SQP (both individual and combined cases)	250
Number of Start Points	75
Start Point Definition	Haltonset
Min Design Variable Step Size	0.001%
Penalty Multiplier Value (constrained test only per (2b))	0.250

Table 2 Unconstrained test results

	De Jong	Rosenbrock	Rastrigin	Schweffel
Coordinate Location of Overall Minimum				
Theoretical	(0,0)	(1,1)	(0,0)	(420.969,420.969)
SFD	(4.2e-4, -4.5e-4)	(1.0067, 1.0135)	(6.3e-3, -7.8e-3)	(420.86, 421.21)
SQP	(7.4e-6, 1.0e-3)	(0.9793, 0.9597)	(4.7e-5, 1.0e-3)	(-296.88, 438.27)
Combined	(3.9e-4, -1.4e-3)	(1.0065, 1.0135)	(6.3e-4, 7.7e-4)	(421.11, 419.46)
Function Value of Overall Minimum				
Theoretical	0	0	0	0
SFD	8.0e-9	1.51e-8	2.51e-4	5.8e-6
SQP	2.03e-8	1.55e-7	2.7e-6	0.107
Combined	4.3e-8	1.7e-8	2.5e-6	1.9e-4
Number of Function Evaluations				
SFD	1166	1685	3802	2477
SQP	1344	4863	2118	450
Combined	1137	1194	2250	1875

the infeasible results for Rosenbrock and Schweffel. Since the purpose of this study was primarily to validate the constraint performance of the SFD related searches, these SQP results were not further studied. Programmatic recognition and mitigation of such a result using the SQP method is an area for future work.

Table 3 illustrates that although the constraint region was co-located with the theoretical minimum for each of the test functions, each of the different optimization methods identified slightly different 'optimum' solutions. This is most pronounced for Schweffel where the SQP method (individually) found a significantly different result than either SFD

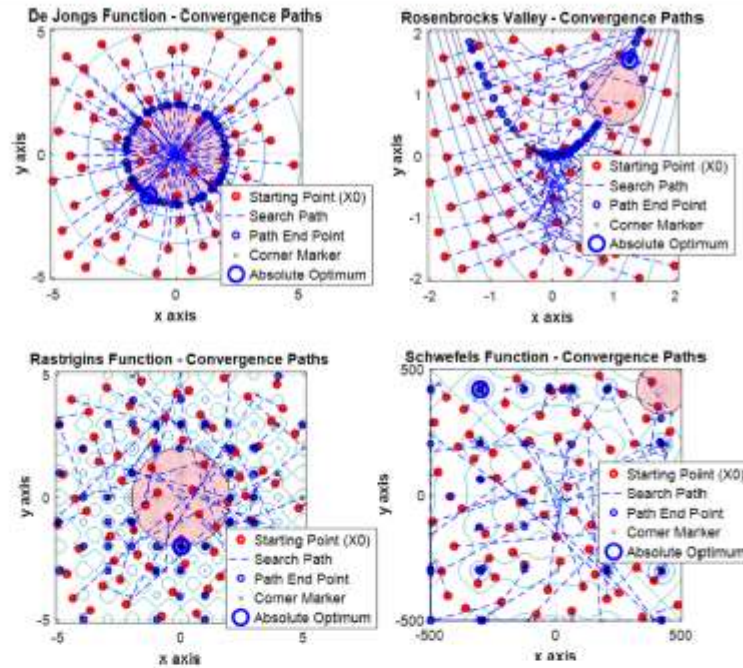
(individually) or the proposed Combined method. For Rastrigin, the SQP (individually) and Combined methods found identical solutions (to the reported precision), but SFD (individually) was slightly worse.

For the 'simplest' function, De Jong, the Combined method identified a solution (function value) approximately 7.8% higher (worse) than either of the individual solutions. Rosenbrock resulted in the identification of effectively identical function values by all methods, but in different locations. As noted in the literature, this is a particular challenge posed by the Rosenbrock function in that the gradient nears zero of a relatively large portion of the design space.

Table 3 Constrained test results

	De Jong	Rosenbrock	Rastrigin	Schweffel
Coordinate Location of Overall Minimum				
Theoretical	(0,0)	(1,1)	(0,0)	(420.969,420.969)
Constraint Center	(0,0)	(1,1)	(0,0)	(420.969,420.969)
Constraint Radius	2.0	0.5	2.0	100.0
Minimum Radial Distance of Each Search Path Endpoint from Constraint Center				
SFD	2.0009	0.5071	2.0038	116.6584
SQP	2.0000	0.4991	2.0000	99.9990
Combined	2.0008	0.6136	2.0000	723.1119
Function Value of Overall Minimum				
Theoretical	0	0	0	0
SFD	0.0742	0.0000	0.0504	0.0790
SQP	0.0742	0.0000	0.0500	0.1066
Combined	0.0800	0.0000	0.0500	0.0790
Number of Function Evaluations				
SFD	3549	2133	3715	2473
SQP	1038	4817	2061	456
Combined	2416	1324	2243	1802

Fig. 6 Convergence paths for constrained test cases using SFD method



A comparison of the number of function evaluations for the constrained searches (Table 3) shows that the proposed Combined method utilized the fewest function evaluations for Rosenbrock's Valley and fewer than the SFD (individual) method for Schwefel. It should be noted that SQP (individual) used by far the fewest function evaluations for Schwefel. However, the inaccuracy of the result overshadows this achievement. For Rastrigin, the SQP (individually) resulted in the fewest function evaluations, although the difference between SQP and the proposed Combined is only 8.1% for this multi-modal function. SQP (individually) is clearly the most efficient for the constrained De Jong compared to the other methods.

These constrained results support a similar conclusion to that of the previous unconstrained test; that for multi-modal functions the Combined method generally leverages the 'best' qualities of either of the individual methods; with function values identified of similar accuracy with similar or fewer function evaluations. The proposed Combined method is less effective with respect to the individual method for a unimodal function as indicated by De Jong's.

Given these test function results (both Constrained and Unconstrained), the proposed Combined method appears to be a good candidate for use with optimization of the parallel beam problem.

3 Parallel beam optimization

The parallel beam problem was solved with the proposed Combined method by first programmatically evaluating results from multiple global SFD start points to determine a single best result identifying a region of the design space as a potential solution. This single search endpoint was then used as the start point for the subsequent SQP search. As with the test functions, tests with both SFD and SQP methods (individually) were also conducted to challenge the effectiveness of the proposed Combined solution. All tests used the same set of 24 global start points, selected using MATLAB's @ Haltonset function.

A 'single' objective function was defined for multi-objective use as shown in (5).

$$\begin{aligned}
 f_{obj} &= f_{obj_a} + f_{obj_b} \\
 f_{obj_a} &= \sum_{i=1}^3 \left(\sum_{j_{i-min}}^{\max} \delta_{top-max} \right) \\
 f_{obj_b} &= \sum_{i=1}^3 (\delta_{top-max} - \delta_{top-min})
 \end{aligned} \tag{5}$$

where:

$i = 1$, top beam = family variant #1.

$i = 2$, top beam = family variant #2.
 $i = 3$, top beam = family variant #3.

In addition to side bound constraints, seven (7) input constraints are imposed on the parallel-beam model. These are given as (6). For this example, a minimum allowable space between support features is specified as 1.50".

An output constraint was also placed on the optimization to prevent a solution from being 'too flexible'. It is recognized that a theoretical solution to an optimal harmonic deformation problem allows the beam to become so flexible that its tip deformation can be ideally minimized. This has obvious practical implications however. So, the objective function includes an evaluation of tip deformation to a static load, with an output constraint set to limit the minimum allowable flexibility of the system. This output constraint is provided in (7) with a maximum static tip displacement of 2.0" allowed. As with the objective function, these output constraints apply to all family variants.

$$\begin{aligned}
 g_1 &= 1 - \frac{|L_1 - L_3|}{1.50} \\
 g_2 &= 1 - \frac{|L_1 - L_4|}{1.50} \\
 g_3 &= 1 - \frac{|L_2 - L_3|}{1.50} \\
 g_4 &= 1 - \frac{|L_2 - L_4|}{1.50} \\
 g_5 &= 1 - \frac{L_1}{1.50} \\
 g_6 &= \frac{L_2 - L_4}{1.50} + 1 \\
 g_7 &= \frac{L_1 - L_2}{1.50} + 1 \\
 g_{static} &= \frac{|deflection_{static}|}{2.0} - 1
 \end{aligned}
 \tag{6}$$

Table 4 Parallel beam optimization results

			Optimization Method		
			Combined	SFD	SQP
Design Variable Definition for Identified Optimum	Support Locations	L_1	29.248	27.892	65.750
		L_2	50.418	50.503	70.332
	Support Stiffnesses	K_1	44,060	34,556	14,551
		K_2	2520	26,765	48,351
		K_3	14,409	24,227	20,587
		K_4	4601	46,778	15,619
	Viscous Support Damping	C_1	0.413	0.200	0.500
		C_2	0.334	0.083	0.500
		C_3	0.306	0.404	0.500
		C_4	0.240	0.234	0.500
	Minimum Function Value	f_{obj}	1.4540	1.4515	1.4511
	Number of Function Evaluations		811	1492	1447

where:

$i = 1$, top beam = family variant #1.
 $i = 2$, top beam = family variant #2.
 $i = 3$, top beam = family variant #3.

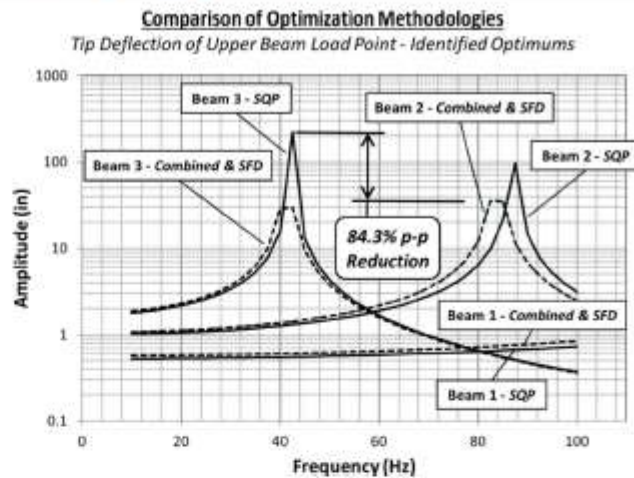
Numerical results of the optimizations for the Parallel Beam study are provided in Table 4. All resulted in Minimum Function Values that are approximately the same. SFD (individually) and SQP (individually) differ by only about 0.03% and the proposed Combined method's result is approximately 0.17% higher. However, each optimization method resulted in a different set of optimal input values.

The individual methods of SFD and SQP each utilized very nearly the same number of function evaluations, differing by only 3.1%. The proposed Combined method however used the fewest function evaluations; approximately 44.0% fewer than SQP and 45.6% fewer than SFD.

Figure 7 illustrates the Frequency Response Plots (FRP) of the identified optimal solutions for each of the methods. As shown, and as inferred by the identified Design Variable values of Table 4, the SFD (independently) and Combined methods resulted in beam performance that is practically identical. When compared to the optimum found by the independent use of SQP, the SFD and Combined methods resulted in a significant reduction in peak-to-peak values.

It is recognized that the improvement in physical response shown in this parallel beam comparison is influenced significantly by the coarseness of the frequency step used. That is, the frequency step used in this analysis allowed the curve to be shifted in frequency such that the peak was 'clipped'; whereas if a finer frequency step had been used then the amplitude at the new resonance would be identified more accurately. This is illustrated by comparing the 'Beam 2-SQP' and 'Beam 2-Combined & SFD' curves of Fig. 7. However, for the purposes of this discussion, this physical detail is mute. The

Fig. 7 Parallel beam results – comparison of optimal solutions



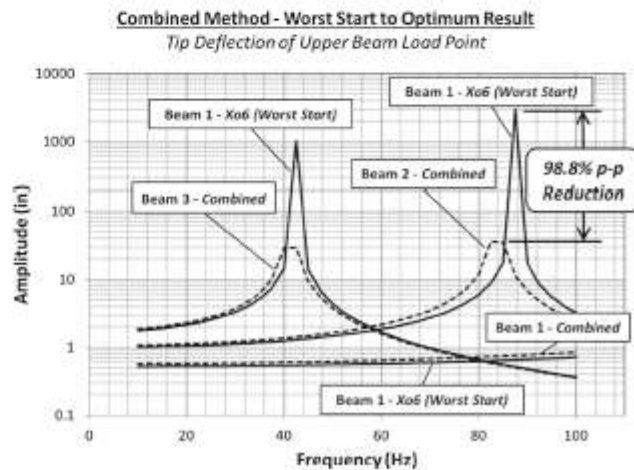
comparison of interest is the ability of the different optimization methods to identify a result and the efficiency with which it does so. From that perspective, the fact that a peak-to-peak improvement of 84.3% by the Combined and SFD (individual) responses as compared to the individual SQP (Fig. 7) is significant.

Figure 8 illustrates the improvement obtained by the proposed Combined method as compared to the worst starting point. For each method, the same group of 24 (Haltonset) starting points was used to seed the attempts. Starting point 'Xo6' proved to have the worst (highest) function evaluation value, the FRP being illustrated in Fig. 8. As shown, the

Combined method resulted in a peak-to-peak reduction in tip amplitude of 98.8%.

The results of Figs. 7 and 8 illustrate another issue sometimes experienced in practical design; that due to design constraints, a system (platform-style or other) cannot always be designed to fully operate below the fundamental natural frequency. In this example, even though improvements were made through optimization, natural frequencies remain within the range of interest for two (2) of the family variants (Beam 2 and Beam 3). However, the resonant responses were significantly modified as predicted by Den Hartog's (1985) explanation of the DDVA in Fig. 2. Given further understanding of

Fig. 8 Parallel beam results – improvement of combined method from worst start point



details of the design, output constraints might be added to further 'tune' the system for acceptability.

The optimal solution is also shown to be a 'compromise' in that, although significant reductions were made in the resonant responses, the third (stiffest) family variant (Beam 1) worsened slightly in the process as illustrated by both Figs. 7 and 8. This highlights an important aspect of platform-style design, that 'compromise' solutions must be considered and managed in the optimization process.

4 Conclusions

A proposed Combined optimization method utilizing the method of Steepest Feasible Descent as an initial search tool, followed by a use of the more efficient SQP method for 'local' refinement was demonstrated to be effective on both classical test functions and a parallel beam harmonic response problem. Key conclusions are:

- The proposed Combined method is shown to leverage the 'best' of the component methods for an improved result on some multi-modal responses, without significant consequence to other test surfaces used.
- Tests of the proposed method using classical test functions resulted in a difference in the number of function evaluations from 6.2% greater (worse) to 75.4% fewer (better) for the proposed method vs the alternatives on multi-modal responses for unconstrained optimizations.
- Constrained searches using the same classical test functions resulted in function evaluations for the proposed method ranging from 8.8% greater (worse) to 72.5% fewer (better) for the proposed as compared to the alternatives with multi-modal responses.
- The proposed method is much less productive for unimodal responses with function evaluations ranging from 2.5% fewer to 15.4% fewer on unconstrained searches and from 132.8% more to 31.9% fewer on constrained searches.
- When tested against the component methods using the parallel beam problem, the proposed method identified an optimum with function value within 0.17% of the component methods but utilized more than 44% fewer function evaluations in the process. This demonstrates a significant advantage to the proposed Combined method when used with EBBF models.
- The proposed SFD method, whether used individually or as part of the proposed Combined method, is shown to be effective as a constrained search tool, incorporating both deterministic and programmatic feasibility elements as well as a sensitivity-based search vector.
- The proposed method is shown to be more tolerant of a coarse design variable stepsize as a stopping criterion than the SQP method implemented individually. This is illustrated with the Schwefel test function and is an important benefit with respect to use with EBBF's.
- The platform-style parallel beam structure was successfully optimized for harmonic loading, with significant improvements to peak response amplitudes, even though natural frequencies remained in the frequency range of interest due to design constraints of the system.

Compliance with Ethical Standards

Conflict of Interest The authors declare that they have no conflict of interest.

References

- Alcasson B, O'hoff N (1988) Minimum stiffness of optimally located supports for maximum value of beam eigenfrequencies. *J Sound Vib* 120(3):457–463
- Banks A, Vincent J, Aryakoba C (2007) A review of particle swarm optimization. Part I: background and development. *Natural Computing* 6(4):467–484
- Cai X, Qiu H, Gao L, Yang P, Shao X (2017) A multi-point sampling method based on kriging for global optimization. *Struct Multidiscip Optim* 56(1):1–18
- Chen T, Chi T (2010) On the improvements of the particle swarm optimization algorithm. *Adv Eng Softw* 41(2):229–239
- Den Hartog JP (1985) *Mechanical vibrations*. Courier Corporation
- Fliege J, Svaiter B (2000) Steepest descent methods for multicriteria optimization. *Math Meth Oper Res* 51(3):479–494
- Hajela P (1990) Genetic Search – An Approach to the Nonconvex Optimization Problem. *AIAA J* 28(7):1205–1210
- Hall MC, Cacuci DG, Schlesinger ME (1982) Sensitivity analysis of a radiative-convective model by the adjoint method. *J Atmos Sci* 39(9):2038–2050
- Hao K, Mei L, Ripin Z (2011) Tuned vibration absorber for suppression of hand-arm vibration in electric grass trimmer. *Volucella* 41:494–508
- Jones D, Schonlau M, Welch W (1998) Efficient global optimization of expensive black-box functions. *J Glob Optim* 13(4):455–492
- Kolda T, Lewis R, Torczon V (2003) Optimization by direct search: New perspectives on some classical and modern methods. *Society for Industrial and Applied Mathematics* 45(3):385–482
- Laskari E, Panopoulou K, Vrahatis M (2004) Particle swarm optimization for minmax problems. *Evolutionary Computing CEC* 2:1980–1987
- Lophaven S, Nielsen H, Sondergaard J (2002) *Amatlab Kriging Toolbox*. Technical University of Denmark, Kongens Lyngby, Technical Report No. IMM-TR-2002-12
- Martins JR, Alonso JJ, Reuther JJ (2005) A coupled-adjoint sensitivity analysis method for high-fidelity aero-structural design. *Optim Eng* 6(1):33–62
- Maute K, Nikbay M, Farhat C (2003) Sensitivity analysis and design optimization of three-dimensional non-linear aeroelastic systems by the adjoint method. *Int J Numer Methods Eng* 56(6):911–933
- Molga M, Smutnicki C (2005) *Test Functions for Optimization Needs*
- Othmer C (2014) Adjoint methods for car aerodynamics. *J Math Ind* 4(1):6
- Ozguven H, Candir B (1986) Suppressing the first and second resonances of beams by dynamic vibration absorbers. *J Sound Vib* 111(3):377–390

- Piemon H (2012) Tunable dynamic support for resonance avoidance in bar feeders, Dissertation presented in partial fulfillment of the requirements for the degree of Doctor of Philosophy in the Graduate School of the Ohio State University, Industrial and Systems Engineering
- Russell D (2006) Bending modes, Damping and the sensation of sting in baseball bats, Engineering of Sport 6, 6th International Sports Engineering Conference, ISEA
- Shahbazi K (2005) An explicit expression for the penalty parameter of the interior penalty method. *J Comput Phys* 205(2):401–407
- Shan S, Wang G (2010) Survey of modeling and optimization strategies to solve high-dimensional design problems with computationally-expensive black-box functions. *Struct Multidiscip Optim* 41(2): 219–241
- Tabarabaei M, Hakanen J, Hartikainen M, Miettinen K, Sindhya K (2015) A survey on handling computationally expensive multiobjective optimization problems using surrogates: non-nature inspired methods. *Struct Multidiscip Optim* 52(1):1–25
- Vanderplaats GN (2007) *Multidiscipline design optimization*, 1st edn. Vanderplaats Research and Development, Incorporated, Colorado Springs
- Venter G, Sobieszcwanski-Sobieski J (2003) Particle Swarm Optimization. *AIAA J* 41(8):1583–1589
- Vesterström J, Thomsen R (2004) A comparative study of differential evolution, particle swarm optimization, and evolutionary algorithms on numerical benchmark problems. *Evolutionary Computation, CEC2004, Volacella 2*:1980–1987
- Wang B, Chen J (1996) Application of genetic algorithm for the support location optimization of beams. *Comput Struct* 58(4):797–800
- Wang D (2004) Optimization of support positions to minimize the maximal deflection of structures. *Int J Solids Struct* 41(26):7445–7458
- Wang D, Jiang J, Zhang W (2004) Optimization of support positions to maximize the fundamental frequency of structures. *Int J Numer Methods Eng* 61(10):1584–1602
- Wang D (2006) Optimal design of structural support positions for minimizing maximal bending moment. *Finite Elem Anal Des* 43(2):95–102
- Wang D, Friwell M, Lei Y (2006) Maximizing the natural frequency of a beam with an intermediate elastic support. *J Sound Vib* 291(3–5): 1229–1238
- Yang C, Li D, Cheng L (2011) Dynamic vibration absorbers for vibration control with in a frequency band. *J Sound Vib* 330(8):1582–1598
- Zhu J, Zhang W (2006) Maximization of structural natural frequency with optimal support layout. *Struct Multidiscip Optim* 31(6):462–469
- Zoutendijk G (1960) *Methods of feasible directions*. Elsevier, Amsterdam

Appendix B

Technical Paper – Hauser, Wang, *Structural and Multidisciplinary Optimization*, 2019



Design optimization of a rotordynamic beam system with elastic supports to minimize flexural responses using a combined optimization algorithm

Bret R. Hauser¹ · Bo P. Wang¹

Received: 7 July 2019 / Revised: 3 November 2019 / Accepted: 12 November 2019
© Springer-Verlag GmbH Germany, part of Springer Nature 2020

Abstract

Modern rotating machines are often required to operate with increasingly limited physical footprints and/or overall weights, necessitating that they utilize wide-ranging shaft speed to accomplish needed power levels. It is not uncommon then that the resulting speed envelope crosses or encompasses multiple critical speeds with the requirement that flexural vibrations be limited to safe and acceptable levels. Design optimization of this class of problem can be particularly difficult in that responses can exhibit high modality adding significant complexity and time to the optimization effort. This paper presents a design optimization methodology appropriate to an economic solution for this class of problem. A simplified rotordynamic example is used to challenge the proposed optimization method against other more “conventional” techniques with results of the proposed method extensible to more complicated, practical rotordynamic problems.

Keywords Rotordynamic optimization · Parallel beam · Elastic supports

1 Introduction

Designers of complex machinery sometimes face the challenge to optimize high-modality responses within the constraints of limited temporal or financial budgets.

Common design mitigations for rotordynamic systems address critical speed avoidance through a variety of means including “placement” of the resonance frequency with respect to the operating speed band, incorporation of damped vibration absorbers, and the like. Often though, these design mitigations are tuned, with effective results limited to a relatively narrow band of operational speeds. As such, they may be insufficient if the required operating speed band is wide and encompasses multiple critical speeds. Therefore, a different design mitigation technique is required for this class of

problem that serves to minimize the response(s) throughout the full (wide) speed range.

The presence of high modality limits the effectiveness of some conventional optimization methodologies due to the challenge of “crossing” local maxima in search of the optimal solution. Other challenges may exist for rotordynamic systems in that the analyses often include tools such as commercial Finite Element Analysis (FEA) codes which serve as “black-box” function generators. That is, only output responses are available from these programs further limiting efficiency of some conventional optimization tools. Also, if a given function evaluation is sufficiently expensive, it may fit the classification for an expensive black-box function (EBBF). In problems where these factors are combined, as with many rotordynamic systems, efficiency of the optimization method becomes particularly important.

A hybrid optimization methodology is proposed for improved efficiency on rotordynamic problems. The presented design optimization method leverages efficiencies of “simpler” techniques as a more efficient solution for EBBF problems with high-modality response than other, more popular techniques. A simplified academic example consisting of a parallel beam with rotating inner shaft, stationary outer shaft, and mass-eccentricity loading is used to illustrate optimization challenges. The simplified example shares core elements

Responsible Editor: Emilio Carlos Nelli Silva

✉ Bret R. Hauser
bret.hauser@tx.ti.com

Bo P. Wang
bpwang@uts.edu

¹ University of Texas at Arlington, Arlington, TX, USA

Published online: 03 January 2020

Springer

common to a variety of more complex, practical rotordynamic industry applications, making it a useful platform to efficiently evaluate the proposed optimization method.

2 Motivation and example problem

Figure 1 illustrates a simplification of the problem under study, a rotating shaft supported within a non-rotating outer housing by two radial bearings. Figure 2 provides a schematic view of the system where elastic supports (Mount 1 and 2) connect the non-rotating outer housing to ground and elastic bearings (Bearing 1 and 2) and connect the rotating shaft to the outer shaft. A mass eccentricity exists within the rotating shaft's end-mounted disk as the sole source of loading to the system. Design variables as input to the optimization problem are limited for this simplified example to the axial locations of the two elastic Mounts between the non-rotating housing and ground. The goal of this study then is to minimize the magnitudes of both flexural deflection of the end-mounted disk and reaction force of Bearing 2.

Although simple in its academic form, this problem illustrates a class of design problems typical of many rotordynamic designs whereby an optimal solution is needed in consideration of a high-modality response. Analysis of the design through Finite Element Analysis adds the complexity of a black-box function (BBF) in that only direct outputs (deformations, forces, etc.) are available from the function solver but without access to hessian or other data commonly used to improve the effectiveness of optimization. As discussed later, the FEA code used in this study is self-generated by the first author and could potentially be modified to output hessian and other information useful in enhancing an optimization process. For purposes of this study, however, the code is used as an example of commercial FEA codes that are limited in their use to that of a BBF generator and unable to output such information. Results of this study then are extensible to more



Fig. 1 Example rotordynamic system

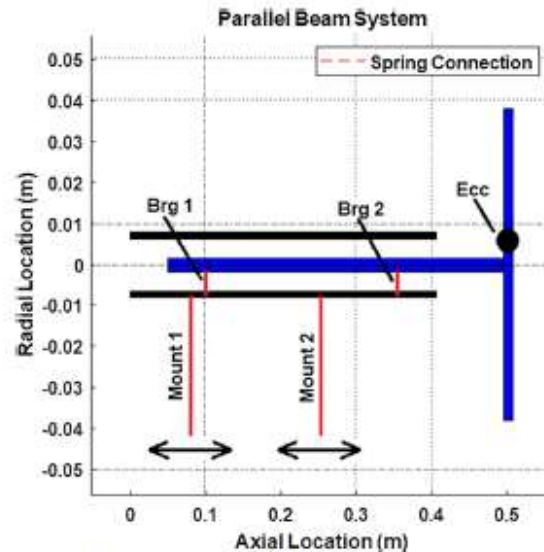


Fig. 2 Elastically supported parallel beam structure

complicated rotordynamic problems that might commonly be solved with these commercial FEA codes.

Similarly, the FEA code used in this study utilizes beam elements for computational efficiency. Although not explicitly an expensive black-box function (EBBF), this beam element code serves as a computationally efficient example with which to exercise the proposed optimization method with respect to rotordynamic analyses in general. The findings (quantity and accuracy of function evaluations, etc.) are extensible to more complex analyses where, for example, commercial FEA codes are used to solve large models using three-dimensional meshes where the high expense (temporal or financial) of a single design solution is truly so great as to be considered an expensive black-box function (EBBF).

The example problem assumes that the system is required to operate through a range of shaft speeds that encompasses multiple critical speeds as illustrated in Fig. 3. The design optimization problem then seeks to minimize the magnitude of the responses throughout the speed range by minimizing the area under the curve for each response and thereby reducing the overall vibratory responses throughout the defined speed range.

The example problem is multi-objective in that both tip deformation and bearing reaction force are to be minimized. The authors recognize that methodologies and commercial tools exist with which to conduct multi-objective optimization (MOO) and with application to rotordynamic systems. For example, Longxi et al. (2017) utilized the commercial FEA program "ANSYS" and the commercial optimization software ISight to optimize a two-disk flexible rotor with multiple design objectives. Bettebghor et al. (2013) conducted a two-

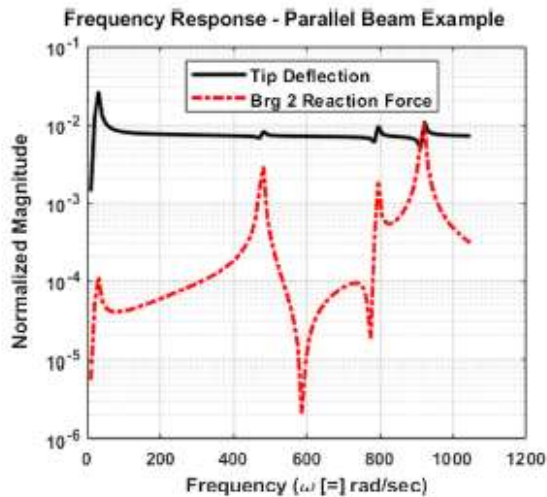


Fig. 3 Frequency response plot (example)

objective design optimization of an aircraft structural optimization with rotordynamic effects using Pareto optimality. A challenge to use of Pareto optimality (Vanderplaats 2007) is that the technique is best used if the various objective functions are of the same general type and order of magnitude. This is not the case for the current example problem or of the anticipated extensions toward rotordynamic problems in general. Therefore, an alternative means of optimizing multiple responses are investigated.

Rather than Pareto optimality, the proposed method utilizes a technique often incorporated within that and other MOO methods that of weighted sums (Marler and Arora 2010). Here, a single objective function (OF) is formed as a combination of multiple singular objectives with weighting factors serving to address both variances in orders of magnitude as well as objective priorities (presented and discussed in Section 7.1). The use of weighted sums is selected in consideration for the potentially high-modality response of the rotordynamic system (as experienced in this example) and the potential for both quantity and cost of function evaluations. The specifics of the OF used in this example are described in Section 7.1, but the multimodal nature of the response is illustrated in Fig. 4 here as a function of variation in the two design variables.

Figures 2 and 3 illustrate a significant challenge to optimization methods offered by high-modality responses. That is, the need to “cross” local maxima in search of a global or even an acceptable local minimum is of key importance in rotordynamic design and can be challenging for some optimization methodologies. The proposed method is anticipated to perform well on this class of problem and is challenged for both effectiveness and efficiency against other common methodologies by this academic example.

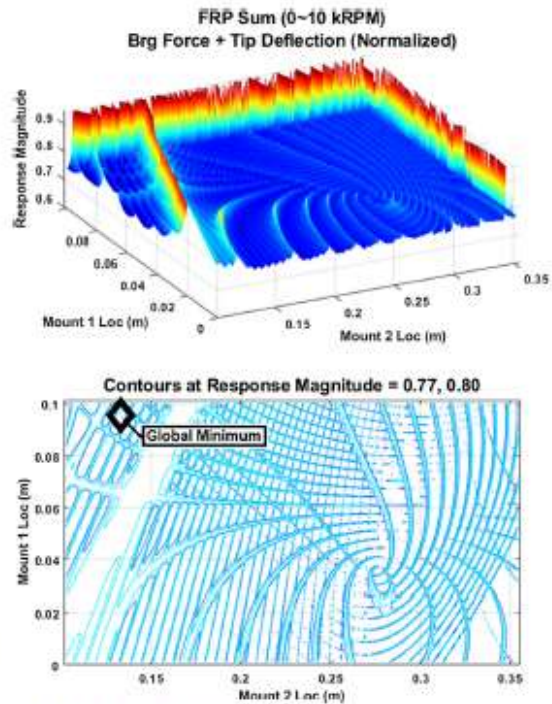


Fig. 4 Objective function response

3 Vibration suppression in rotordynamic systems

A variety of methods have been studied as means of mitigation to vibrations experienced by rotordynamic machines. Perhaps the earliest and most traditional method is to design the system such that the fundamental critical speed frequency is “placed” above the operating speed. (Gunter Jr 1966). Since the early 1900s, however, supercritical operation of machinery has been a preferred practice to achieve increasing power levels with minimal system weight or footprint. (Vance et al. 2010; Stocki et al. 2012; Bonfitto et al. 2017). As a result, machine designers are faced with the challenge of minimizing flexural vibrations, particularly at the crossing of these critical speeds.

Direct damping is too often difficult to implement explicitly into rotordynamic systems in practice. Therefore, alternate methods to minimize rotordynamic vibrations have been researched. For example, geometry variation of the rotating shaft is explored as another passive mitigation alternative (Strauß et al. 2007) for a rotordynamic shaft where neither bearing location nor added damping are considered. Active magnetic bearings (AMBs) offer another alternative toward limiting amplitude at resonance and have been explored with application to vibration suppression in rotordynamic systems (Srinivas et al. 2018, Bonfitto et al. 2017; Srinivasan et al. 1997; Yoon et al. 2012).

Optimal placement of bearing location is a method commonly used to influence critical speeds (Lund 1980; Rajan et al. 1987; Huang et al. 2002; Liu and Yang 2018; Shiau and Chang 1991) and was also recently explored using a genetic algorithm (GA) optimization method to maximize a first mode natural frequency for a motorized spindle-bearing system (Lin et al. 2007).

Some researchers have explored the use of robust- and reliability-based design optimization (RBDO) techniques as means to effectively use simpler passive mitigation methods for rotor systems with consideration for variation inherent to design variables (Stocki et al. 2012; Hong et al. 2011; Lian and Kim 2006). Although beneficial at identifying the robustness of the solution, these optimization methods are often computationally intensive and therefore challenging to implement for EBBF functions.

This paper is focused on an optimal solution for rotordynamic vibrations across a wide operating speed range. Therefore, a method useful to an EBBF function with high-modality response is needed.

4 Optimization methodologies appropriate to rotordynamic systems

Optimization of rotordynamic systems includes not only application to the direct physics of the problem but also consideration for the modality of response. A review of literature with respect to both aspects is presented in this section.

4.1 Optimization of rotordynamic equipment

Various optimization methodologies have been reported by researchers with direct application to rotordynamic systems. Rotating structures are unique in the field of structural dynamics in that the gyroscopic and circulatory matrices are asymmetric due to the cross-coupling stiffness effects. As such, they are non-self-adjoint systems (Zu 1994; Lee et al. 1988; Lee 1991; Ouisse and Foltête 2011). Because of this, optimization methods appropriate to non-rotating structural dynamic applications may not be successful (Jha et al. 2016).

One common area of focus in the design of these systems is the optimization of rotating imbalance to address physical, field-based systems. The influence coefficient (IC) balancing method is reported as an “easily implemented” method for field balancing when used with least square (LS) methods (Untarouï et al. 2008). Although the IC method assumes a linear correlation between lateral vibrations and mass unbalance, the authors explain that given the nonlinear nature of some constraints, the optimization problem can become nonlinear. As a result, the semi-definite programming (SDP) technique, Convex Min-max methodology, is proposed using a linear matrix inequality (LMI).

A real-coded genetic algorithm (GA) for use with mixed integer optimization is applied as part of a proposed virtual bearing method of optimization for rotordynamic systems (Liu and Yang 2018). There, a method is proposed which allows the placement of critical speeds for a rotordynamic system based on both optimal bearing quantity and location with bearing stiffness as a digital parameter. The mixed integer optimization technique (Deep et al. 2009) then works in conjunction with other “variables data” to identify the optimal solution.

A hybrid of GA together with the Nelder-Mead (NM) method is investigated by multiple researchers to leverage GA as a global search tool followed by Nelder-Mead as a more efficient local search method (Chelouah and Siarry 2003). GA is reported as an efficient tool for identification of promising “valleys” within the design space but is also reported to suffer from slow convergence. Nelder-Mead (NM) is then used as a classical “hill-climbing” algorithm, to investigate the “promising” regions for the global optimum. Although NM is reported as “extremely flexible and suitable for exploring difficult terrains” (Fan et al. 2006), it is an unconstrained optimization technique. A hybrid of particle swarm optimization (PSO) and NM is also researched (Fan et al. 2006) to leverage the benefits of an evolutionary algorithm with a local search tool. Although not explicitly applied to a rotordynamic system, the hybrid GA-NM and PSO-NM methods are reported as being effective and efficient for nonlinear responses with multiple minimums.

Another evolutionary hybrid approach used for multimodal response is a combination of GA and PSO (Kao and Zahara 2008). The resulting hybrid (GA-PSO) integrates the concept of evolving individuals (GA) with the self-improvement of PSO. Data from this study supports that although the proposed GA-PSO method may find a better optimum, it sometimes requires significantly more evaluations to do so.

Various gradient-based optimization methodologies have been reported in literature. For example, a nonlinear rotordynamic system was successfully addressed as a linear optimization problem through use of sequential linear programming (SLP) to minimize system weight in consideration for eigenvalue constraints (Chen and Wang 1992). SLP is also used for the placement of critical speeds (Strauß et al. 2007) in conjunction with the method of moving asymptotes (MMA) (Svanberg 1987). It was observed that use of MMA increased the likelihood that feasible results would be identified and therefore was preferred to the linear SLP method alone.

Two gradient-based methods, gradient projection method (GPM) and sequential quadratic programming (SQP), were compared for a rotordynamic system with stress, frequency, and harmonic response constraints (Pugachev 2013). Although GPM was more flexible and computationally advantageous than SQP, it suffered on the non-self-adjoint rotordynamic application and was not always stable. The

SQP method, although more sophisticated, sometimes got “stuck” in a non-optimal solution due to the multimodal response.

SQP was also coupled with hybrid analytical and numerical sensitivity analysis (Pugachev et al. 2015). The authors used an internal FEA code to export sensitivity information of the modal equation. While beneficial in terms of convergence and stability, the overall time required suffered since a numerical analysis was necessary. Among the reasons cited for using the numerical method were that the skew-symmetric gyroscopic matrix for the rotordynamic system makes the generalized eigenvalue problem asymmetric, violating the assumption necessary for standard sensitivity analysis of linear eigenvalue problems.

A procedure for eigenvalue reanalysis is proposed (Palazzolo et al. 1983) for application with rotordynamic systems with usefulness in improving the computational efficiency of iterative optimization schemes. It is based on use of a receptance formula (Palazzolo et al. 1982) useful to predict damped natural frequencies of the system, increasing efficiencies for repeated analyses during optimizations and improving convergence characteristics when only an incomplete set of modes is available.

4.2 Optimization methodologies applied to high-dimensional problems with high-modality responses

In practice, the many input considerations common to rotordynamic designs serve to augment their categorization as EBBF functions to include high dimensionality as well. It is reported that this area of high-dimensional, computationally expensive black box (HEB) problems (Shan and Wang 2010) is an area that is less well researched than optimization strategies for “low dimensionality” problems.

The success of hybrid techniques, both in terms of HEB functions and as applied to optimization of rotordynamic systems in general, is an inspiration toward the proposed combined optimization methodology discussed here. Rather than reducing dimensionality or employing surrogates to directly address HEB systems as with Shan and Wang (2010), a hybrid of optimization strategies is employed given the singular functional model; first to generally scan the design space for regions of potential optimum and then to follow with a more efficient local search tool.

Although not always used in conjunction with systems of high modality, “first-order” methods including the method of steep descent (SD) (Vanderplaats 2007) may be useful for the problem at hand. These gradient-based methods are known to be initially productive but become inefficient as the solution approaches the optimal result. They are typically useful for single objective and unconstrained searches neither of which applies to the example problem at hand. However, a proposed

approach using the method of SD for multicriteria optimization (Fliege and Svaiter 2000) together with the method of feasible directions (Zoutendijk 1960) for use in constrained cases has potential. Given that it is a first-order method, the authors recommend that it should be considered only as a “first step” toward efficiency rather than an efficient method unto itself.

An attribute shared by many of the “natural computing” paradigms such as described previously is the ability to deal with noisy or incomplete data (Banks et al. 2007). They cite that PSO can find solutions near optima faster than GA but is more prone to premature convergence than evolutionary algorithms (EA). In another work, the effectiveness of EA, PSO, and differential evolution (DE) was compared (Vesterström and Thomsen 2004), and it was concluded that, in general, the DE algorithm outperforms both PSO and EA in terms of consistent speed of convergence and ability to find the optimum. However, the authors note that PSO was particularly problematic with noisy functions.

Separately, PSO is compared as a means of optimizing minimax problems to SQP (Laskari et al. 2004). The authors conclude that for black-box functions where gradient information is not available (as with HEB’s) that PSO may be a good alternative as an initial search tool with continued optimization performed by more efficient methods such as SQP.

All direct methods, including GA, PSO, and SQP, are applicable to constrained functions and are also known to potentially require a high number of function evaluations, especially for high-modality responses (Vanderplaats 2007). This makes them undesirable as “stand-alone” optimization tools for EBBF’s.

The proposed optimization methodology is inspired by the previous observation regarding potential for SQP as an effective follow-on to an initial global search (Laskari et al. 2004), together with potential for use of steepest descent as an initial search tool (Fliege and Svaiter 2000). That is, an efficient overall method for a HEB or EBBF with high-modality response may be to initially investigate the design space using a “simple” first-order method and then, from the region of most promising minimum response, continue the search using local SQP. The present authors considered this theory in a previous work (Hauser and Wang 2018) for a non-rotating system and explore its use for rotating systems here.

5 Rotordynamic model description

As described previously, the prediction of two key results from the rotordynamic system are sought:

- Flexural tip deformations
- Reaction force of bearing support #2

An appropriately featured and correct definition of the equation of motion (EOM) is key to developing a rotordynamic model capable of supporting the needs of this study. Since this analysis includes a rotating shaft within a non-rotating housing, a fixed reference frame is required (Kumar 2016). Other key considerations included in the EOM used in this study are:

- Rotatory effects on system stiffness
- Gyroscopic effects of the rotating elements including lumped mass and disk parameters
- Consistent mass, stiffness, and damping matrices
- Timoshenko shear effects
- Bearing stiffness and damping effects
- Consideration for both stepped and linearly varying (conic) hollow and solid shaft elements
- Multi-body connectivity of the rotating shaft to the exterior housing

The resulting EOM is given as Eq. (1) below.

$$([M_T] + [M_R])\{q\} + ([C] + \Omega[G])\{\dot{q}\} + ([K] + [K_B] + [K_S])\{q\} = \{F\}$$

where:

- M_T = Translational Mass
- M_R = Rotatory Mass
- C = External damping
- G = Gyroscopic effect
- K = External stiffness
- K_B = Bending stiffness
- K_S = Shear stiffness effects
- F = External Loads
- Ω = Rotating speed
- q = element nodal displacements

Assumptions designed to reduce the computational burden used in the model of this study include the following:

- Axial force effects are neglected.
- Torsional effects are neglected.
- Internal material damping effects are neglected.

Beam elements in three-dimensional (3D) space are utilized, also to reduce computational burden for this illustrative study. The simplification is possible since the example problem is axisymmetric in nature. As with the above assumptions, however, the use of beam elements in this example does not preclude the findings of this study from being applicable to more complicated and computationally expensive models such as those using 3D mesh to address non-axisymmetric geometries (thereby meeting the requirements of a HEB model). This is because the rotordynamic response of the systems, in general, is similar regardless of the element methodology

used (beam vs 3D or other) or other assumptions. Rather, the simplified beam model used here allows for a more efficient study of the optimization method with respect to the non-self-adjoint rotordynamic physics.

The example problem of Fig. 1 above is evaluated in three-dimensional space but, for clarity, shown schematically in two dimensions in Fig. 5. As illustrated later, the axial dimension is defined as “x” with lateral dimensions in “y” and “z”.

In general, shape functions are derived with consideration for Timoshenko shear effects and used as input to a Lagrangian derivation for the EOM. Consideration for the various aspects of the model (rotatory, gyroscopic, etc.) is defined as part of the kinetic and potential energy functions (Nelson and McVaugh 1976; Zorzi and Nelson 1977; Nelson 1980). A two-node element model was incorporated for this work and, although some references utilized a 6-DOF model (by separating nodal rotations due to bending and shear effects) (Greenhill et al. 1985), a 4-DOF model (combining rotational effects) was selected for this work. In so doing, computational efficiency is improved while retaining the needed functionality of 2 translational and 2 rotational DOF per node. The nodal deformations then are illustrated in Fig. 6 with definitions provided as Eq. (2). In the illustration, total nodal rotation ($\hat{\theta}_x$) is the sum of bending effects (θ_x) and shear effects (γ_{xy}).

$$\{q\} = \begin{Bmatrix} v \\ w \\ \theta_y \\ \theta_z \end{Bmatrix} = \begin{Bmatrix} \text{Translation-UY} \\ \text{Translation-UZ} \\ \text{Rotation about y-axis} \\ \text{Rotation about z-axis} \end{Bmatrix} \quad (2)$$

Shape function development is made for a 3D beam element with inclusion of Timoshenko shear effects (Bazoune et al. 2003). Equation (3) identifies the functions as being built upon a third-order translational displacement equation to support interelement continuity of slope (C^1 element) (Cook 2007).

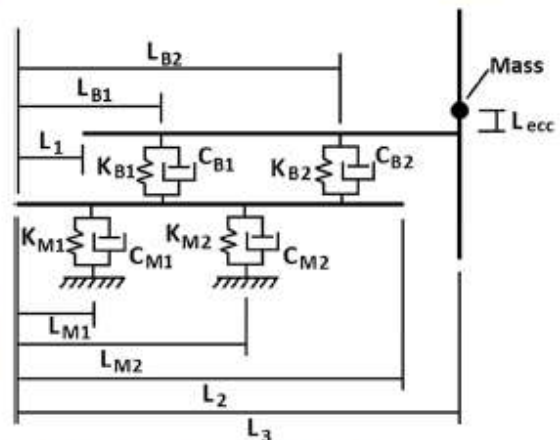


Fig. 5 Schematic of rotordynamic example problem

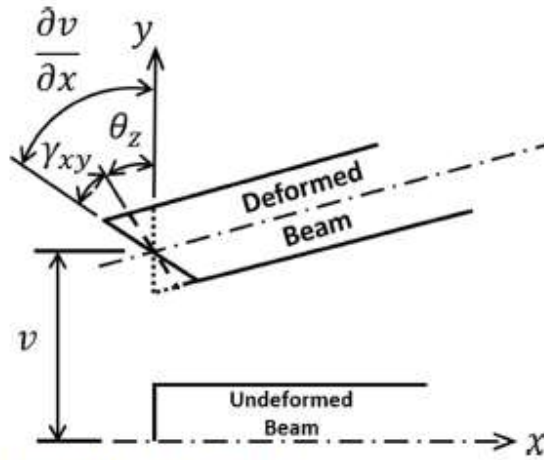


Fig. 6 Nodal DOF (XY plane only)

$$v(x) = a_0 + a_1x + a_2x^2 + a_3x^3 \tag{3}$$

The rotordynamic OM of Eq. (1) can be solved as an eigenvalue problem to identify key results including critical speed, stability, and direction of whirl (Childs and Childs 1993; Vance et al. 2010). Although optimization of critical speeds is a common method used for rotordynamic systems (Chen and Wang 1992; Strauß et al. 2007; Liu and Yang 2018), the sample problem of this study instead requires optimization of flexural response across multiple frequencies spanning (potentially) multiple critical frequencies. Therefore, a different solution to the EOM is required.

A computationally expensive time-based solution of the EOM can be used to evaluate the flexural response of the system. However, a more efficient method used here is to convert the EOM to a steady-state component analysis equation (in sin and cos) and solve the determinant for both eigenvalue and eigenvector complex results (Childs and Childs 1993). The general solution for a n-DOF problem is developed and shown as Eq. (4).

$$\begin{Bmatrix} X_{1s} \\ \vdots \\ X_{Nr} \\ X_{1c} \\ \vdots \\ X_{Nc} \end{Bmatrix} = INV \begin{bmatrix} [-\omega^2[M] + [K]]_{NN} & -\omega[C]_{NwN} \\ \omega[C]_{NwN} & [-\omega^2[M] + [K]]_{NN} \end{bmatrix} \begin{Bmatrix} F_{1s} \\ \vdots \\ F_{Nr} \\ F_{1c} \\ \vdots \\ F_{Nc} \end{Bmatrix}$$

where:

$$\begin{aligned} s &= \text{sin components} \\ c &= \text{cosine components} \end{aligned} \tag{4}$$

The rotordynamic EOM then is solved for purposes of this study via a special purpose FEA code written by the first author using the method of steady-state component analysis

where resulting flexural deformations ($X_{1s} \dots X_{Nc}$) per Eq. (4) are utilized to derive the tip deflections and bearing reaction forces as a function of frequency (ω). The static tip deformation (used in the output constraint of Section 7.2) is computed from the EOM by applying rotational speeds (Ω) and accelerations (q) of “0.”

A mesh discretization exercise was performed to identify an appropriate mesh density for this study. Section 7.1 describes the objective function for the optimization study as comprised of the sum of result values for both bearing reaction force and the vector sum of lateral tip deflection across the studied frequencies per Eq. (8). Similarly, Section 7.2 describes the tip deflection under static load as a constraint equation per Eq. (10). The mesh discretization study was conducted by evaluating these results as a function of increasing node count toward the goal of identifying that mesh density resulting in less than $\pm 5\%$ stepwise change in results compared to the neighboring coarse mesh result.

As shown in Fig. 7, the static tip deformation per Eq. (10) is effectively unchanged for all nodal densities studied. The tip displacement sums across frequencies (UY and UZ) per Eq. (8) are identical to each other and below $\pm 5\%$ for all node densities studied, with most consistent behavior above approximately 100 total nodes. This is expected given that the bearings are modelled with isotropic properties for this study.

The summation of Bearing 2’s reaction force results across frequencies per Eq. (8) yielded the most significant variation with nodal density among the results. As can be seen in the figure, coarse nodal densities resulting in less than approximately 75 total nodes saw stepwise changes of more than $\pm 25\%$. Successful convergence to the $\pm 5\%$ threshold was achieved for total node counts of 130 and greater.

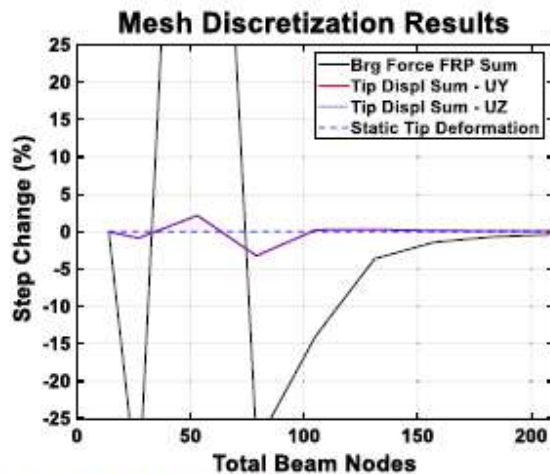


Fig. 7 Mesh discretization results

6 Description of proposed optimization method

The proposed optimization method is a combined algorithm comprised of an initial survey of the entire design space using a global optimization tool followed by a more efficient local optimization tool to refine the potential solutions for a more accurate solution. Intended use of the method surveys the design space from numerous discrete starting points with limited iterations of the global tool to identify an area of potential, followed by the local tool from that location to an identified optimum.

The global tool is a derivative of the well-known first-order method of SD, made useful for this purpose by specifically addressing the issue of high-modality response (typical of rotordynamic problems such as this example) and the influence of various constraints. As with the method of SD, the high-level program flow of the global tool is as follows:

1. Select search vector direction from start point.
2. Perform 1D line search across the design space to identify optimum of this iteration.
3. Repeat the process from the “new” start point as a subsequent iteration, continuing until convergence or iteration count limits are achieved.

Two (2) significant challenges exist to the effective implementation of this modified first-order approach; termed steepest feasible descent (SFD):

- Selection of the search direction given consideration for:
 - Black box function generators
 - Constraint bounds
 - Sensitivity to input variables with significant variations in magnitude
- 1-D line search appropriate to multimodal response and constraint effects (both input and result variables)

The discussions of this section present solutions to these challenges implemented within SFD to make it a useful first-order method for this class of problem. In addition, a discussion of the use of SQP as the follow-on direct search method is included.

6.1 Search vector direction – finite difference and magnitude sensitivity

The gradient for the search vector definition is based on a finite difference (FD) approach because of the use of FEA as a BB function generator. It is recognized that analytical methods such as the adjoint method (Maute et al. 2003; Hall et al. 1982; Martins et al. 2005) and others offer significant

computational efficiencies to the proposed FD technique. However, as with Othmer (2014), the problem to be solved involves the use of FEA as a black-box function generator. It is recognized by the authors that the special purpose FEA tool of this example could be modified; otherwise, the methodology is intended to be representative of (and useful with) a commercial FEA program. For commercial FEA programs, the source code is commonly unavailable to the optimization routine precluding effective use of the adjoint method. Therefore, the FD approach is utilized with modifications for orientation to feasible space, etc. as discussed in this section.

A challenge to the FD method is that the rotordynamic problem under study demonstrates a class of problems where the design variables may have significantly different orders of magnitude (length vs. spring stiffness and potentially other dimensions). This can lead to sensitivity error in the search vector when this method is employed. That is, if a common step size was computed as appropriate to a variable with smaller magnitude, and subsequently applied to all design variables, then the step size could be so small as to have an insignificant effect upon a variable of larger magnitude.

An option (to the common step size) explored here is to define the step size for each design variable individually based upon the magnitude of the variable at its lower and upper (side) bounds. In this way, the step sizes used in the FD evaluation of the search vector would be more numerically appropriate to each variable. This is given in Eq. (5) below and provides the benefit a “generalized” nondimensionalization technique within the code for user convenience.

$$\Delta_x = \alpha_a \left(\frac{x_{Upper\ Bound} - x_{Lower\ Bound}}{2} \right)$$

where:

$$\alpha_a = \text{percentage of average} \quad (5)$$

A value of 0.5% is selected for the sensitivity factor α_a to balance the need for a large enough step to be meaningful while remaining small enough to consider only “local” effects around the starting point (XO). This becomes particularly important when the response has high modality as with this example.

A simple test was used to confirm the theory that the method of Eq. (5) may be more useful than a common step size with respect to search vector sensitivity. Specifically, the test seeks to (1) support that a common step size is or is not a “problem” to search vector sensitivity and (2) whether the method of Eq. (5) addresses it effectively. For simplicity, a function generator is defined as the classical closed-form equation for frequency response function (or “magnification factor”) of a single degree of freedom (SDOF) system with damping (Craig and Kurdila 2006). This is shown as Eq. (6),

and parameters stiffness, damping, and mass (k , c , m) are considered. For simplicity, only a single value of frequency (Ω) is considered here.

$$\frac{U(r)}{U_o} = \frac{1}{\sqrt{(1-r^2)^2 + (2\zeta r)^2}}$$

where:

$$\begin{aligned} r &= \frac{\Omega}{\omega_n} \\ \zeta &= \frac{c}{c_{cr}} \\ \omega_n &= \sqrt{\frac{k}{m}} \\ c_{cr} &= 2\sqrt{km} \end{aligned} \tag{6}$$

The test is conducted by use of a standard SD optimization problem, modified to compute the finite difference-based search vector using either a “common” step size among the variables (k , c , and m) or the method of Eq. (5). Rather than continuing to an optimal solution, this test seeks only to output the search vector components from a given start point (XO) for the different methods. A comparison of the search vector components is made to derive conclusions regarding sensitivity.

Two (2) cases are considered in this test of the step-size method: (1) design variables with minimal difference in magnitude and (2) significant difference in magnitude. Side-bound constraints (only) are considered for the input variables so as not to otherwise influence the sensitivity evaluation. Three runs are considered:

1. Min difference data set – “common” step size
2. Larger difference data set – “common” step size
3. Larger difference data set – Eq. (5)

For purposes of this study, the “common” step size was defined as the square root of the sum of the squares (RSS) of distance across the design space for each variable, that is, the RSS of the distance (max vs min) for each input variable. Alternatively, the method of Eq. (5) identified the step size (Δ_x) in each dimension by the use of that equation. Table 1 provides the input data for the dimensions of the study and Table 2 for the results.

“Run 1” utilized a common step size (RSS) among the variables in the “Min” data set and resulted in variations in

Table 1 Input data – search vector sensitivity test

	Min set	Larger set
Mass	1–10 kg	10–100 kg
Stiffness	10–50 N/m	100–50,000 N/m
Damping ratio	0.10–0.50	0.01–0.50

Table 2 Resulting search vector components

		m	k	c
1	Common – min set	0.973	-0.229	0
2	Common – larger set	0	0	0
3	Eq. (5) – larger set	0.117	0	0.993

magnitude among the search vector components (for each of the design variables). This indicates that for the variation of this data set, at least some sensitivity to the design variables exists in the search vector although the value of “0” for the damping dimension (smallest magnitude among the variables) indicates that limitations exist with the RSS approach.

“Run 2” also utilized a common (RSS) step approach but as applied to the “larger” data set. As shown, all search vector components returned a value of “0” supporting that a common step size per RSS methodology is inappropriate (insensitive) where larger variations in magnitude exist.

“Run 3” utilizes the step size method of Eq. (5) applied to the “larger” data set (as compared to the “common” step size method applied to this same data set as in “run 2”). As shown, the search vector components of “run 3” indicate improved sensitivity for this data with larger variations in magnitude with the method of Eq. (5) as opposed to a complete lack of sensitivity to this larger variation data set using the common (RSS) step size. As with “run 1” previously, the component sensitivity to one dimension for “run 3” (stiffness in this case) is not preserved indicating that step sensitivity is not optimal using Eq. (5) but is improved over the “common” step size method.

The difference in search vector direction between runs 1 and 3 is attributed to the relative starting points and inconsequential to the results of this study. Rather, the important aspect is confirmation that a sensitivity problem can exist if a common step size is used with finite difference methods on data sets with larger differences in magnitude and also that the method of Eq. (5) is a method of mitigation.

As supported by the results of this test, the finite difference method of search vector determination in concert with sensitivity considerations per Eq. (5) is incorporated to the proposed SFD method to address both the challenges of black-box function generators where design variables can have significant differences in their respective magnitudes.

6.2 Search vector direction – constraint handling

In addition to finite difference and design variable magnitude considerations in development of the optimal descent search vector, consideration is also given to the influence of constraints for both design and results variables.

A common method of constraint handling in this context is termed the method of feasible directions (MFD) where, in one

implementation, (Vanderplaats 2007) an offset or “push-off factor” is applied to the search vector to avoid a constraint bound. In the case of a nonlinear constraint bound(s), however, an additional “optimization exercise” is needed within the larger optimization effort (Vanderplaats 2007) to avoid infeasible space.

The proposed method of SFD is intended to be used in optimization circumstances where multiple nonlinearities exist, including the influence of high-modality responses and other effects. Therefore, the proposed SFD method incorporates a programmatic implementation of MFD to avoid a potentially large subproblem for a more conventional implementation of MFD. The pseudo-code of Fig. 8 illustrates this process. Figure 9 illustrates the process in a conventional flowchart format.

For a given start point ($X0$) and search vector (S_n), a length across the design space (to the nearest constraint bound) is established for the intended 1-D line search. It is desired that this 1-D search length be as long as possible in order to prevent multiple (and inefficient) short line searches near a constraint bound (as might be experienced where S_n “points” directly into a nearby bound from a given $X0$).

If the distance from the given $X0$ to the nearest constraint bound (along S_n) is measured to be below a predetermined percentage of the distance across the design space, then the vector direction is programmatically modified to redirect away from the offending constraint bound by eliminating that coordinate term (of S_n) which points most directly to the concerning bound. The process is repeated until the resulting search vector has a trajectory that is “sufficiently parallel” to the subject constraint bound(s) in that the distance from $X0$ along the vector to the bound is acceptably large as compared to the overall design space. In this way, the new search vector is created to provide at least a minimum search length within feasible space with minimal computational effort. Note that in the case that a “corner”

- a) Identify start point ‘ $X0$ ’
- b) Establish search vector ‘ S_n ’
- c) Compute distance along S_n from $X0$ to nearest constraint bound
- d) Compare distance to minimum allowable
- e) If distance < min allowable, identify S_n vector component point most directly to constraint bound and convert that component of S_n vector to ‘0’
- f) Compare distance along new S_n to nearest bound against minimum allowable
- g) If distance < min allowable, repeat (e)
- h) If distance > min allowable, use S_n for line search

Fig. 8 Pseudo-code – feasible S_n selection

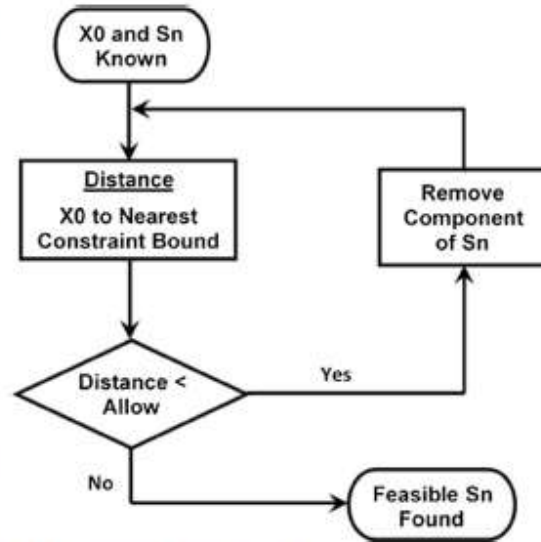


Fig. 9 Flowchart – feasible S_n selection

constraint exists and sufficient length cannot be established, then the proposed SFD method establishes the $X0$ as a locally optimal point which can then be used by the more efficient direct search method discussed later in this section.

6.3 Line search – multimodal and constraint considerations

As with conventional SD methods, the proposed SFD method uses a 1-D line search along a given S_n vector to identify a given iteration’s optimum. Various methods for such searches have been developed over the years but given consideration for use with high-modality responses a polynomial search is implemented in the proposed SFD method.

Conceptually, the polynomial 1-D search is computed based on an initial sampling of points along the length of the S_n vector, from which a regression coefficient is computed and compared to a predetermined acceptance criterion. If unacceptable, additional points are programmatically selected near the anticipated minima, and the order of the polynomial increased (up to a user-defined maximum) to improve the curve fit. For responses of low or moderate modality, acceptance by this method can generally be achieved relatively quickly. However, for high-modality responses, convergence can be challenging. In this event, a subsequent numerical strategy is implemented.

For high-modality responses where a maximum point density has been reached without acceptable fit quality, the strategy shifts from that of adding points near the anticipated minima to that of eliminating points far from the observed minimum (along the 1-D search). In this way, the quality of the curve fit can (potentially) be improved near the observed minimum.

The maximum number of points used in the resulting 1-D search is a compromise between increased solution times and accuracy of the polynomial fit. In practice, the authors have identified this as a problem-dependent consideration, with acceptable results achieved in most cases (including the high-modality example here) with a maximum of no more than 15–20 function evaluations along a given S_n vector.

As with determination of the descent vector S_n , constraints (both input- and results-based) must be considered in the line search algorithm. Multiple methods exist to apply penalties to an unconstrained search methodology and make it useful as a constrained tool. Chen and Chi (2010), for example, utilize a penalty function to improve their particle swarm algorithm by applying a penalty to particles that are at the upper or lower bound of the design variable definition. Shahbazi (2005) explored an interior penalty (IP) method as a type of discontinuous Galerkin method for the spatial discretization of elliptic partial differential equations. As discussed, however, a notable drawback of the IP method is that if the user-selected penalty parameter is not sufficiently large, the approximate solution is unstable.

$$f(x)_{pen} = f(x) + \alpha_p \sum_{j=1}^n \left(\max[0, g_j(x)] \right) \tag{7a}$$

$$f(x)_{pen} = f(x) + \alpha_p \sum_{j=1}^n \left(\max[0, g_j(x)]^2 \right) \tag{7b}$$

In the development of the proposed SFD method, feasibility with respect to constraint(s) is considered during the execution of the line search in multiple ways. First, the length of the line search is limited by design variable constraint bounds (both side bounds and other, discussed previously). Second, as proposed by Vanderplaats (2007), an external penalty term is combined with the function value $f(x)$ (of Eq. (8) in Section 7.1) to form a penalized function value $f(x)_{pen}$ to be used as the objective function. This is shown as Eq. (7).

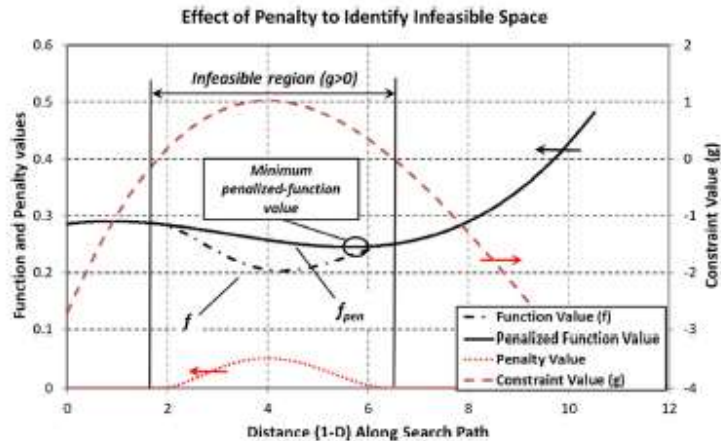
Two variations of Eq. (7) are considered during this work, a linear and second-order version. Both provide a penalty only in the event of an unsatisfied constraint. However, if the square of the constraint is used as in Eq. (7b), the penalty value at the constraint bound has a slope of zero ensuring a continuous slope of the penalized function value through this region. If only the linear form was used as in Eq. (7a), a discontinuity is possible at the constraint bounds adding risk of numerical ill-conditioning. For this reason, the penalty method of Eq. (7b) is selected for use in this work. Additionally, a penalty multiplier (α_p) is included to aid the 1-D line search by scaling the effect of the penalty to preclude minima from being identified within infeasible space. That is, a multiplier value that is too weak can limit the penalty value such that the penalized function value remains as infeasible. If too strong, however, the minima could artificially be “pushed” away from the constraint bound. Figure 10 illustrates these concepts.

Although helpful in tailoring the penalty function, optimal selection of the penalty multiplier can be problem dependent; the risk of an improperly selected value being that the resulting minima could either remain within infeasible space (Fig. 10) or be pushed artificially “far” from the constraint bound.

Therefore, a programmatic element is incorporated to the SFD method in the event that the penalized minimum (f_{pen}) is identified as being infeasible. In this case, the function values at the bounding constraints are evaluated, and the appropriate minimum is identified (such as the right-most constraint bound of Fig. 10). In this way, a minimum (f_{pen}) is precluded from being identified within infeasible space during the line search allowing that a penalty value can be selected conservatively small while avoiding excessive “pushout” without risk of finding an infeasible result.

It is recognized that this programmatic search could be avoided by incorporating a subproblem to optimize the penalty multiplier such that the “0” of the penalized function value’s derivative coincides with the constraint bound. However, this

Fig. 10 Use of penalty function to identify infeasible space



requires computations potentially adding significant encumbrance to the overall problem. The proposed combination of penalty multiplier and programmatic consideration then is theorized to achieve the desired constraint-handling effects acceptably with improved computational efficiency.

6.4 SQP as a follow-on direct search

As discussed previously, direct search methods such as SQP are well-known to be more efficient than first-order methods and are effective as constrained search tools. However, they are also known to be more limited by local minima and maxima than other methods, including first-order methods. Therefore, the proposed method incorporates SQP as a local search tool to be implemented from the most promising result following the SFD's global search.

It should be noted that in the proposed method, the penalty function applied per Eq. (7b) is applied as part of the objective function and therefore common to both SFD and SQP processes.

7 Numerical example

The rotor dynamic problem used in this study is a simplified example of a class of problem that is commonly experienced in industry.

As illustrated in Figs. 1 and 4, both "fixed" and "variable" model parameters are included in the global model with values identified in the tables below. By limiting the dimensionality to this simplified example (two design variables only), the practicality of direct mapping allows for a baseline global optimum to be achieved (Fig. 4). The addition of dimensionality to this example precludes such a study due to its increased scope, detracting from key results made in the current study. Observations regarding the performance of the optimization methods however remain exemplary of a HEB model with high-modality results. Fixed model parameters for this study are given in Table 3 and variable parameters in Table 4.

7.1 Objective function

The example problem consists of the need to minimize both lateral deformation of the rotating beam's end-mounted disk and the reaction force of bearing "B2" each across multiple frequencies. Therefore, a "single" objective function is defined for multi-objective use as shown in Eq. (8).

$$f_{obj} = f_{obj_a} + f_{obj_b}$$

Table 3 Fixed model parameters (ref. Fig. 5)

L_1	0.0508	m
L_2	0.4064	
L_3	0.5080	
L_{B1}	0.1016	
L_{B2}	0.3556	
L_{axc}	1.27×10^{-4}	
K_{B1}	2.627×10^6	N/m
K_{B2}		
K_{M1}	2.627×10^4	
K_{M2}		
C_{B1}	1.751	N-s/m
C_{B2}		
C_{M1}		
C_{M2}		
Mass	0.454	Kg

where:

$$f_{obj_a} = \sum_{f=1}^{max} \frac{F_{Bearing\ B2\ Reaction}}{10^4}$$

$$f_{obj_b} = \sum_{f=1}^{max} \sqrt{(\delta_{UY})^2 + (\delta_{UZ})^2}$$
(8)

Note that the portion of the objective function focused on the bearing reaction force (f_{obj_a}) is reduced by a factor of 10^4 to create similar scale between the two objective function components (f_{obj_a} and f_{obj_b}). Otherwise, the influence of tip deflection on the objective function (f_{obj_b}) would be minimized.

7.2 Constraint function

The optimization problem of this study then is to minimize the objective function of Eq. (8) given the fixed and variable model parameters of Tables 3 and 4, subject to both input- and results-based constraints. These constraints are discussed in this section.

Both input and output constraints are placed on the example problem. Input constraints include the side-bound limitation that the axial location for the non-rotating mounts "L_{M1}" and "L_{M2}" lie within the bounds of neighboring features (ref. Fig. 5). That is, mount "M1" is allowed to move from the left end of the external tube to the axial location of bearing "B1." Similarly, mount "M2" can range only between bearings "B1" and "B2." In addition, a minimum space of 0.0127 m is defined between support features to represent the physical width of the mounts and an assumption that they may not be superimposed for this example. These input constraints are provided in Eq. (9) below.

Table 4 Variable model parameters (ref. Fig. 5)

L_{M1}	0–0.1016	m
L_{M2}	0.1016–0.3556	

$$\begin{aligned}
 g_1 &= 1 - \frac{L_{M1}}{0.0127} \\
 g_2 &= \frac{L_{M1}}{(L_{B1} - 0.0127)} - 1 \\
 g_3 &= 1 - \frac{L_{M2}}{(L_{B1} + 0.0127)} \\
 g_4 &= \frac{L_{M2}}{(L_{B2} - 0.0127)} - 1
 \end{aligned}
 \tag{9}$$

An output constraint is also considered to mitigate the potential for a solution being “too flexible.” It is recognized that a theoretical solution to flexural vibrations might result in an optimum where the beam stiffness is insufficient for practical use. Therefore, this output constraint function includes an evaluation of tip deformation to a static load as a means of assuring some minimum acceptable stiffness to the system. This output constraint is provided in Eq. (10) where a maximum static tip displacement of 0.0762 m is allowed.

$$g_{\text{result}} = \frac{\sqrt{(\delta_{UY-st})^2 + (\delta_{UZ-st})^2}}{0.0762} - 1
 \tag{10}$$

The example problem was solved with the proposed combined method and compared with its component methods individually (SFD and SQP) as well as GA and PSO methods to support a comparison of both efficiency and effectiveness. The proposed combined, SFD (only), and SQP (only) algorithms utilize discrete starting points to seed the routines; therefore, the design space is evenly divided into 9 regions to facilitate survey of the design space. The approximate center of each start region is then used as the (9) discrete starting points (identified in Table 5). The starting points and their regions are illustrated in Fig. 11.

MATLAB’s “GA” function was used as the constrained genetic algorithm routine. Instead of using discrete starting points, GA relies on identified ranges to bind the initial population(s). To compare methods as directly as possible, the geometric bounds of the nine starting regions were used as input regions to the GA routine, each being defined with an initial population size of 9 points. These starting ranges are

Table 5 Starting points (combined, SFD, and SQP)

Start point	L_{M1} (m)	L_{M2} (m)
1	0.0170	0.1440
2	0.0170	0.2287
3	0.0170	0.3133
4	0.0509	0.1440
5	0.0509	0.2287
6	0.0509	0.3133
7	0.0847	0.1440
8	0.0847	0.2287
9	0.0847	0.3133

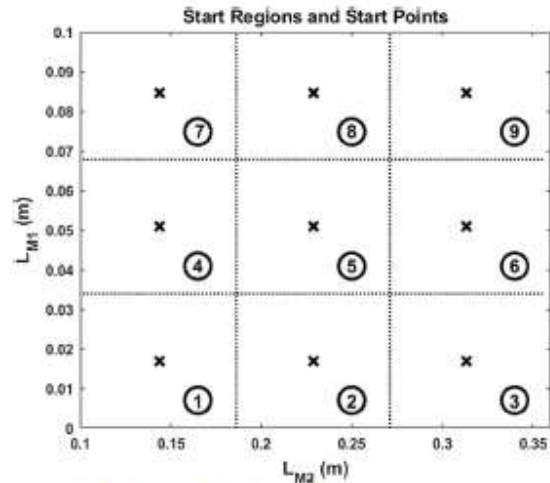


Fig. 11 Start locations for optimizations

identified in Table 6. In this way, the (previously unstated) assumption that results of an optimization are to some degree influenced by the start point location is equally challenged for all methods.

MATLAB’s “particle swarm” function unfortunately does not allow for constrained optimization at the time of this study. Therefore, an alternative PSO routine (Chen – 2016) was used which allows for nonlinear constraints. In this way, the constraints of Eqs. (9) and (10) are incorporated directly for the PSO routine. As with the genetic algorithm, particle swarm utilizes starting regions rather than discrete points. Therefore, the regions identified for GA (Table 6) are also used along with an initial swarm size of 9 (for each region) for PSO.

For GA and PSO alike, this start region strategy results in an effective starting population across the entire design space of 81 points (9 regions each with 9 points) compared with only 9 discrete starting points for the combined, SFD, and SQP methods. In order that this variation does not inadvertently skew the study (either toward excessive function evaluations for the GA/PSO or reduced probability of success for the

Table 6 Starting regions (GA and PSO)

Start region	L_{M1} (m)	L_{M2} (m)
1	0.0–0.0339	0.1016–0.1863
2	0.0–0.0339	0.1863–0.2710
3	0.0–0.0339	0.2710–0.3556
4	0.0339–0.0678	0.1016–0.1863
5	0.0339–0.0678	0.1863–0.2710
6	0.0339–0.0678	0.2710–0.3556
7	0.0678–0.1016	0.1016–0.1863
8	0.0678–0.1016	0.1863–0.2710
9	0.0678–0.1016	0.2710–0.3556

others), an additional run with both GA and PSO is conducted with an initial population (swarm) size of 9 points across a single region spanning the entire design space.

As discussed previously, Fig. 4 illustrates results of a direct mapping of the objective function of Eq. (8) across the design space. To achieve an acceptable level of smoothness of the function's local minima, each design variable (L_{M1} and L_{M2}) was studied in increments of 2.54×10^{-4} m. The value of this discretization size was based on physical examination of the mapping results in consideration for balance between the ability to identify the global minimum and computational efficiency. Details of this selection are not presented further for purposes of brevity.

Given the mapping discretization step size, a minimum design variable step of 2.54×10^{-6} m is established as a stopping threshold for all optimization studies. This is determined to be appropriate since it is 2 orders of magnitude below the mapping survey's selected discretization step size.

8 Results

Numerical results for optimizations of the rotordynamic model are provided in Table 7 for each of the optimization methodologies including both "9 region" and "single region" studies for GA and PSO. Table 8 provides a comparison among the results.

The mapping study of Fig. 4 was conducted with a step size (2.54×10^{-4} m) that was determined as a compromise between being small enough to be practically useful in identifying a global minimum and large enough to reduce computational burden. This resulted in approximately 387,500 points across the 2D design space and, with an average function evaluation of approximately 2.2 sec, consumed approximately 3840 CPU-h. The absolute minimum function value identified from the mapping exercise is 0.722320 at the location (L_{M1} , L_{M2}) = (0.0955, 0.1333). This global optimum is plotted for reference on Fig. 4 and is used as a baseline for comparison among the optimization results (Tables 7 and 8).

The results of Table 7 illustrate that all methodologies which completed successfully identified a function value within approximately 2.9% of each other. However, the location of the optimal value (L_{M1} and L_{M2}) differed among the solutions. A subjective inspection of the mapped results (Fig. 4) supports that several locations across the design space have similar f_{obj} values with respect to the various local maxima of the system. It is not surprising then that the numerical optimizations would identify multiple locations with similar minimal function values.

A comparison of results from Table 7 identifies that the lowest function value (f_{obj}) was produced by the GA process using 9 starting regions each with 9 start points per region (total 81 start points). Here, the function value was approximately 0.7301, or 1.08% above the mapped result (0.7223). The GA method using a starting population of 9 across a single region (full design space) failed to identify feasible options from which to continue and therefore failed in-process. It is recognized that an initial starting population of 9 (single or multi-region) is lower than considered "normal" for GA but is comparable to the 9 start points used with the SFD, SQP, and proposed combination methods studied here.

The worst results were obtained with the SFD and SQP methods applied independently with errors of 2.51% and 3.95% to the mapped optimum, respectively. The two PSO methods (9 regions and 1 region) and the proposed combined method were similar in their objective function accuracy with errors of 1.64%, 1.93%, and 1.88%, respectively.

Efficiencies of the methods in terms of the number of function evaluations required provide the greatest variability among the results. For this metric, all methods are compared against the proposed combined method which required 358 function evaluations.

Although the GA method found the most accurate function value (+ 1.08% above mapped global), it required significantly more function evaluation than the proposed combination method (+ 1247%). Both PSO methods also required significantly greater function evaluations than the combination method at 863% and 86%, respectively, for a 9-region and single-region start strategy. These data support statements

Table 7 Optimization results

(Mapping result – Fig. 4) $f_{obj, min} = 0.722320$ (L_{M1} , L_{M2}) $= (0.0955, 0.1333)$		Optimization method										
		Combined			SFD	SQP	GA	PSO				
	Start method	9 pts	9 pts	9 pts	9 regions total	81 pts	1 region	9 pts total	9 regions total	81 pts total	1 region	9 pts total
Design variable	L_{M1} (m)	0.0783	0.0776	0.0889	0.0835		No feasible result found		0.0481			0.0859
	L_{M2} (m)	0.2041	0.2038	0.3127	0.1260				0.1961			0.1947
Min function value	f_{obj}	0.735935	0.740436	0.750859	0.730086				0.734185			0.736278
Total function evaluations		358	304	484	4824				3446			666

Table 8 Comparisons of results

Baseline for comparison: (mapping result – Fig. 4) $f_{obj_min} = 0.722320$ (L_{M1}, L_{M2}) = (0.0955, 0.1333)		Optimization method						
		Combined	SFD	SQP	GA		PSO	
					9 regions 81 pts	1 region 9 pts	9 regions 81 pts	1 region 9 pts
Min function value	f_{obj}	+ 1.88%	+ 2.51%	+ 3.95%	+ 1.08 %	No feasible result found	+ 1.64%	+ 1.93%
Total function evaluations		Baseline	- 15.1%	+ 35.2%	+ 1247%		+ 863%	+ 86.0%

made in literature (Vanderplaats 2007; Vesterstrøm and Thomsen 2004; Banks et al. 2007) that methods like GA, PSO, and others can require a high number of function evaluations, causing challenges when applied to multimodal responses.

When used individually, the SQP solution identified an optimum with approximately 4% error to the mapped optimum but required approximately 35% more function evaluations than the proposed combined method.

The SFD method when used individually found an optimum a little closer to the mapped optimum (+ 2.51%) and used the fewest function evaluations of any tested method (- 15.1% compared to the proposed combination method). Another interesting comparison from Table 7 is that the proposed combined and the SFD (alone) found an optimum with location very close to each other as opposed to the SQP (alone) that identified an optimum more distant.

These results support that the use of SQP is more effective as a local search tool (as with the combined method including SFD + SQP) as compared to SQP used alone, that is, as a global search tool where both efficiency and effectiveness were less successful.

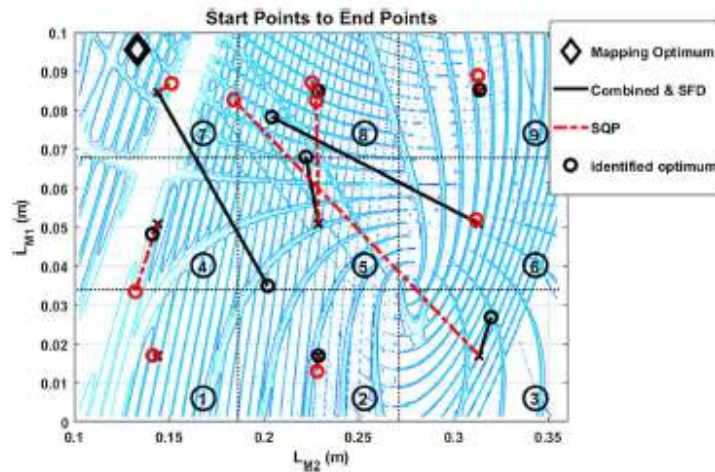
The SFD routine when used individually found an optimum that differs by only 0.6% from the proposed combined

solution yet improved efficiency by 15.1% by omitting the “follow-on” SQP local search. This supports that the SFD routine as an individual technique has merits when compared with SQP, GA, and PSO for use on BB functions where evaluations are expensive, and response modality is high.

Figures 10 and 11 provide a graphical illustration of the behavior of each of the methods with respect to ability to travel across a design space with high-modality response. For clarity of these figures, only the starting and ending points are shown for each study. That is, for each starting point (plotted as an “X”), the resulting end point (plotted as an “O”) is plotted along with a straight line connecting the two. In this way, the ability of the optimization method to move across the design space is illustrated without the added visual complexity of the detailed path used in the process.

Figure 12 illustrates the results of the proposed combined method as well as SFD and SQP methods applied individually. Given that the combined method and SFD are identical except for the addition of a single SQP optimization at the end of the SFD, both combined and SFD results are plotted together. (As shown in Table 7, the resulting optimum location from combined and SFD is slightly different but close enough for common illustration in Fig. 12.) This data shows that the combined/SFD process from start points in regions 5 and 6 travelled the

Fig 12 Start vs end locations – SFD and SQP methods



furthest across the design space. Importantly, the SFD/combined method with a start point in region 5 is observed to “jump” the major local ridge to identify an optimum near the mapped optimum in region 7 (reference Fig. 4 for visual illustration of the major ridge). SQP on the other hand had the greatest travel from start points in regions 3 and 5 but failed to “jump” the major local ridge near the mapped optimum of region 7.

Figure 13 illustrates the same information for both GA and PSO searches. For the GA method, only 2 of the 9 starting regions concluded with a successful search starting in regions 1 and 2. The other starting regions (including the single-region study) failed in that feasible solutions were not identified by the GA method.

Of these two GA searches (starting in regions 1 and 2), both concluded with optimums in region 5, indicating significant travel across the design space. However, neither crossed the major local ridge near the mapped optimum (region 7).

The 9-region PSO method resulted in 7 of the 9 starting regions reaching a feasible optimum and 2 of failing to find feasible solutions. Of the 7 PSO reaching conclusion, all moved significantly across the design space and 1 starting in region 3 moved across the full extent of the design space including “jumping” the major local ridge to identify an optimum near the mapped optimum of region 7.

The PSO search starting from 9 points across the entire design space (1 region) identified an optimum in region 8 like other PSO (9 region) conclusions but is not illustrated in Fig. 13 for clarity.

These comparisons suggest that all methods tested can cross local maxima to at least some degree. The proposed combined, SFD (alone), and PSO were the only methods that successfully “jumped” the major ridge near the mapped optimum of region 7. However, given the data of Table 7, each method does so with significantly different efficiencies, PSO requiring significantly more function evaluations than the combined or SFD (alone) approaches.

Design robustness is also important to the rotordynamic designer. Of the 6 optimum solutions identified through these methods, no information exists to inform the designer with respect to output variation due to design tolerance (input) variation. As evidenced by this example, robustness of the various solutions could be an important consideration in favoring one solution over another.

The coupling of rotordynamic mechanisms as an EBBF function together with the field of reliability-based design optimization is an opportunity for further research that would be meaningful to the rotordynamic practitioner.

Given these data, the proposed combination method is identified as the preferred optimization methodology (among those tested) for the practicing rotordynamic engineer or scientist because of the combination of accuracy and function evaluations. The data supports also that the developed method of SFD may be an acceptable method if efficiency is preferred at the risk of a slightly “less optimal” result.

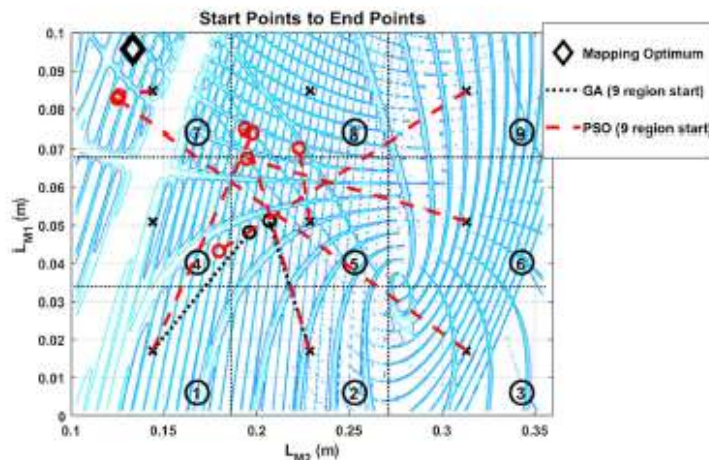
9 Conclusions

A proposed combined optimization method, utilizing the method of steepest feasible descent as an initial search tool followed by a use of the more efficient SQP method for “local” refinement, was evaluated against other common optimization methods using a simplified 2-DOF rotordynamic system illustrative of an EBBF (and potentially HEB) problems with high-modality responses.

Key conclusions are:

- The authors’ proposed combination method (SFD followed by SQP) is shown by this study to be an effective tool for optimization of rotordynamic systems. The data supports that this method is potentially more useful to the machine designer than other

Fig 13 Start vs end locations – GA and PSO methods



methods described in literature when faced with the combined challenges of optimizing a non-self-adjoint system with high-modality response and use of an HEB solver (such as FEA) to evaluate the system.

- Of the 7 optimization methods tested, difference in the function value of the identified optimums varied by approximately 2.9%, but the number of function evaluations used varied by more than 1200%.
- Of the optimization methods tested, only GA with a single starting region failed to identify a feasible solution. This indicates that a limited starting population may be problematic for successful use of GA, an important factor for an EBBF problem with high-modality results without a priori knowledge of the likely location of the solution.
- The multi-region GA method (9 start regions, 81 total start points) identified the lowest function value (+ 1.08% compared to the mapped optimum) but required more than + 1200% more function evaluations than the combined method. This supports that GA may not be an effective solution where function evaluations are expensive with high-modality responses.
- Both PSO methods (single and multi-start regions) identified solutions within approximately $\pm 0.20\%$ that of the combined method but required between + 86 and + 863% more function evaluations for single-region and 9-region start strategies, respectively; supporting that PSO methods may also be challenging to implement for high-modality systems and particularly where each function evaluation is expensive.
- SQP (applied independently) identified the worst optimal result of the methods studied and required approximately + 35% more function evaluations than the combined method. These results support literature conclusions that SQP is less effective as a global search tool given limitations in ability to traverse local maxima.
- The developed method of SFD (applied independently) identified an optimum function value at approximately + 0.6% greater than that of the combined method with 54 fewer (- 15.1%) function evaluations. Given this, the SFD method (applied independently) may be an effective and efficient choice as a global search tool for systems where the cost of each function value is high (such as EBBF functions) and where response modality is high.
- Comparison of starting point locations vs identified optimums supports that all methods can cross local maxima but with differing effectiveness and efficiencies. The proposed combined, SFD (independently), and PSO methods demonstrated the ability to cross a major "ridge" in the response map, whereas the SQP (independently) and GA did not.
- The seven tested optimization methods all lack the ability to provide feedback regarding robustness of the solution to input variance. This is particularly important for a

EBBF problem such as this rotordynamic example (and by extension HEB problems) and is an area that would benefit from further study.

- The proposed combination method (SFD followed by SQP) is identified as a preferred method among those tested with respect to the ability to identify the "best" optimum within a limited number of function evaluations.
- The developed SFD method (applied individually) is identified as a potential candidate method for EBBF functions with high-modality responses where the cost of function evaluations is particularly high such that efficiency is highly valued against the risk of a slightly less optimal result.

Compliance with ethical standards

Conflict of interest The authors declare that they have no conflict of interest.

Replication of results Algorithmic concepts, methodologies, equations, pseudo-code, and data necessary to replicate the results found in this work are presented in the previous sections.

References

- Banks A, Vincent J, Anyakoha C (2007) A review of particle swarm optimization. Part I: background and development. *Nat Comput* 6(4):467–484
- Bazoune A, Khulief YA, Stephen NG (2003) Shape functions of three-dimensional Timoshenko beam element. *J Sound Vib* 259(2):473–480
- Bettebghor D, Blondeau C, Toal D, Eres H (2013) Bi-objective optimization of pylon-engine-nacelle assembly: weight vs. tip clearance criterion. *Struct Multidiscip Optim* 48(3):637–652
- Bonfitto A, Tonoli A, Silvagni M (2017) Sensorless active magnetic dampers for the control of rotors. *Mechatronics* 47:195–207
- Chelouah R, Siarry P (2003) Genetic and Nelder–Mead algorithms hybridized for a more accurate global optimization of continuous multimodal functions. *Eur J Oper Res* 148(2):335–348
- Chen SS (2016) Constrained particle swarm optimization, v1.31.4, BSD License Copyright ©. <https://www.mathworks.com/matlabcentral/fileexchange/25986-constrained-particle-swarm-optimization>
- Chen TY, Chi TM (2010) On the improvements of the particle swarm optimization algorithm. *Adv Eng Softw* 41(2):229–239
- Chen TY, Wang BP (1992) Optimum design of rotor-bearing systems with eigenvalue constraints. In ASME 1992 International Gas Turbine and Aeroengine Congress and Exposition (pp. V005T14A034–V005T14A034). American Society of Mechanical Engineers
- Childs D, Childs DW (1993) Turbomachinery rotordynamics: phenomena, modeling, and analysis. John Wiley & Sons
- Cook RD (2007) Concepts and applications of finite element analysis. John Wiley & Sons
- Craig RR, Kurdila AJ (2006) Fundamentals of structural dynamics. John Wiley & Sons
- Deep K, Singh KP, Kansal ML, Mohan C (2009) A real coded genetic algorithm for solving integer and mixed integer optimization problems. *Appl Math Comput* 212(2):505–518

- Fan SKS, Liang YC, Zahara E (2006) A genetic algorithm and a particle swarm optimizer hybridized with Nelder–Mead simplex search. *Comput Ind Eng* 50(4):401–425
- Fliege J, Svaiter BF (2000) Steepest descent methods for multicriteria optimization. *Math Meth Oper Res* 51(3):479–494
- Greenhill LM, Bickford WB, Nelson HD (1985) A conical beam finite element for rotor dynamics analysis. *J Vib Acoust Stress Reliab Des* 107(4):421–430
- Gunter Jr EJ (1966) Dynamic stability of rotor-bearing systems
- Hall MC, Cacuci DG, Schlesinger ME (1982) Sensitivity analysis of a radiative-convective model by the adjoint method. *J Atmos Sci* 39(9):2038–2050
- Hauser BR, Wang BP (2018) Optimal design of a parallel beam system with elastic supports to minimize flexural response to harmonic loading using a combined optimization algorithm. *Struct Multidiscip Optim* 58(4):1453–1465
- Hong S, Lee S, Jun S, Lee DH, Kang H, Kang YS, Yang SS (2011) Reliability-based design optimization of axial compressor using uncertainty model for stall margin. *J Mech Sci Technol* 25(3):731–740
- Huang SC, Lin CA (2002) Sensitivity analysis and optimization of undamped rotor critical speeds to supports stiffness. *J Vib Acoust* 124(2):296–301
- Jha AK, Dewangan P, Sarangi M (2016) Model updating of rotor systems by using nonlinear least square optimization. *J Sound Vib* 373:251–262
- Kao YT, Zahara E (2008) A hybrid genetic algorithm and particle swarm optimization for multimodal functions. *Appl Soft Comput* 8(2):849–857
- Kumar D (2016) Rotordynamic analysis using 3d elements in fixed and rotating reference frame. ASME 2016 International Mechanical Engineering Congress and Exposition. American Society of Mechanical Engineers. pp. V001T03A017–V001T03A017
- Laskari E, Parsopoulos K, Vrahatis M (2004) Particle swarm optimization for minimax problems. *Evolutionary Computing CEC2002, Vol. 2, 1980–1987*
- Lee CW (1991) A complex modal testing theory for rotating machinery. *Mech Syst Signal Process* 5(2):119–137
- Lee CW, Katz R, Ubooy AG, Scott RA (1988) Modal analysis of a distributed parameter rotating shaft. *J Sound Vib* 122(1):119–130
- Lian Y, Kim NH (2006) Reliability-based design optimization of a transonic compressor. *AIAA J* 44(2):368–375
- Lin CW, Tu JF (2007) Model-based design of motorized spindle systems to improve dynamic performance at high speeds. *J Manuf Process* 9(2):94–108
- Liu S, Yang B (2018) Optimal vibration reduction of flexible rotor systems by the virtual bearing method. *J Vib Acoust* 140(2):021008
- Longxi Z, Shengxi J, Jingjing H (2017) Numerical and experimental study on the multiobjective optimization of a two-disk flexible rotor system. *International Journal of Rotating Machinery*, 2017
- Lund JW (1980) Sensitivity of the critical speeds of a rotor to changes in the design. *J Mech Des* 102(1):115–121
- Marler RT, Arora JS (2010) The weighted sum method for multi-objective optimization: new insights. *Struct Multidiscip Optim* 41(6):853–862
- Martins JR, Alonso JJ, Reuther JJ (2005) A coupled-adjoint sensitivity analysis method for high-fidelity aero-structural design. *Optim Eng* 6(1):33–62
- Maute K, Nikbay M, Farhat C (2003) Sensitivity analysis and design optimization of three-dimensional non-linear aeroelastic systems by the adjoint method. *Int J Numer Methods Eng* 56(6):911–933
- Nelson HD (1980) A finite rotating shaft element using Timoshenko beam theory. *J Mech Des* 102(4):793–803
- Nelson HD, McVaugh JM (1976) The dynamics of rotor-bearing systems using finite elements. *J Eng Ind, ASME* 98(2):593–600
- Othmer C (2014) Adjoint methods for car aerodynamics. *J Math Ind* 4(1): 6
- Ouisse M, Foltête E (2011) Experimental modal analysis of non-self adjoint systems: inverse problem regularization. In: *Structural Dynamics, Volume 3*. Springer, New York, pp 1251–1260
- Palazzo AB, Wang BP, Pilkey WD (1982) A receptance formula for general second-degree square lambda matrices. *Int J Numer Methods Eng* 18(6):829–843
- Palazzo AB, Wang BP, Pilkey WD (1983) Eigensolution reanalysis of rotor dynamic systems by the generalized receptance method. *J Eng P, ASME* 105(3):543–550
- Pugachev AO (2013) Application of gradient-based optimization methods for a rotor system with static stress, natural frequency, and harmonic response constraints. *Struct Multidiscip Optim* 47(6):951–962
- Pugachev AO, Sheremetyev AV, Tykhomirov VV, Shpilenko OI (2015) Structural dynamics optimization of rotor systems for a small-size turboprop engine. *J Propuls Power* 31(4):1083–1093
- Rajan M, Rajan SD, Nelson HD, Chen WJ (1987) Optimal placement of critical speeds in rotor-bearing systems. *J Vib Acoust Stress Reliab Des* 109(2):152–157
- Shahbazi K (2005) An explicit expression for the penalty parameter of the interior penalty method. *J Comput Phys* 205(2):401–407
- Shan S, Wang GG (2010) Survey of modeling and optimization strategies to solve high-dimensional design problems with computationally-expensive black-box functions. *Struct Multidiscip Optim* 41(2): 219–241
- Shiau TN, Chang JR (1991) Multiobjective optimization of rotor-bearing system with critical speeds constraints. In *ASME 1991 International Gas Turbine and Aeroengine Congress and Exposition* (pp. V005T14A010–V005T14A010). American Society of Mechanical Engineers
- Srinivas RS, Tiwari R, Kannababu C (2018) Application of active magnetic bearings in flexible rotordynamic systems – a state-of-the-art review. *Mech Syst Signal Process* 106:537–572
- Srinivasan S, Maslen EH, Barrett LE (1997) Optimization of bearing locations for rotor systems with magnetic bearings. *J Eng Gas Turbines Power* 119(2):464–468
- Stocki R, Szolc T, Tuzowski P, Knabel J (2012) Robust design optimization of the vibrating rotor-shaft system subjected to selected dynamic constraints. *Mech Syst Signal Process* 29:34–44
- Strauß F, Inagaki M, Starke J (2007) Reduction of vibration level in rotordynamics by design optimization. *Struct Multidiscip Optim* 34(2):139–149
- Svanberg K (1987) The method of moving asymptotes—a new method for structural optimization. *Int J Numer Methods Eng* 24(2):359–373
- Untaroiu CD, Allaire PE, Foiles WC (2008) Balancing of flexible rotors using convex optimization techniques: optimum min-max LMI influence coefficient balancing. *J Vib Acoust* 130(2):021006
- Vance JM, Zeidan FY, Murphy BG (2010) *Machinery vibration and rotordynamics*. John Wiley & Sons
- Vanderplaats GN (2007) *Multidiscipline design optimization*. Vanderplaats Research & Development, Incorporated
- Vesterstrom J, Thomsen R (2004) A comparative study of differential evolution, particle swarm optimization, and evolutionary algorithms on numerical benchmark problems. In *Proceedings of the 2004*

- Congress on Evolutionary Computation (IEEE Cat. No. 04TH8753) (Vol. 2, pp. 1980-1987). IEEE
- Yoon SY, Lin Z, Allaire PE (2012) Control of surge in centrifugal compressors by active magnetic bearings: theory and implementation. Springer Science & Business Media
- Zorzi ES, Nelson HD (1977) Finite element simulation of rotor-bearing systems with internal damping. *J Eng P, ASME* 99(1):71-76
- Zoutendijk G (1960) *Methods of feasible directions: a study in linear and non-linear programming*. Elsevier
- Zu JW (1994) Self-adjoint and non self-adjoint spinning Timoshenko beam systems
- Publisher's note** Springer Nature remains neutral with regard to jurisdictional claims in published maps and institutional affiliations.

Appendix C

EOM Development and Steady-State Solution for Jeffcott Rotor System

(25) / (42) IN MATRIX FORM

$$\begin{bmatrix} 1 & 0 \\ 0 & \delta \end{bmatrix} \begin{Bmatrix} \ddot{s} \\ \ddot{\phi} \end{Bmatrix} + \begin{bmatrix} \frac{c}{m} & 0 \\ 0 & \frac{c}{m}\delta + z\dot{\delta} \end{bmatrix} \begin{Bmatrix} \dot{s} \\ \dot{\phi} \end{Bmatrix} + \begin{bmatrix} \omega_{cr}^2 - \dot{\phi}^2 & 0 \\ 0 & 0 \end{bmatrix} \begin{Bmatrix} s \\ \phi \end{Bmatrix} = \begin{bmatrix} \dot{\phi}\omega_{cr}\cos\beta - g\sin\phi \\ e\omega_{cr}^2\sin\beta - g\cos\phi \end{bmatrix} \quad (48)$$

ASSUME SYNCHRONOUS WHIRL $\rightarrow \dot{\phi} = \omega$ (49)

$$\begin{bmatrix} 1 & 0 \\ 0 & \delta \end{bmatrix} \begin{Bmatrix} \ddot{s} \\ \ddot{\phi} \end{Bmatrix} + \begin{bmatrix} \frac{c}{m} & 0 \\ 0 & \frac{c}{m}\delta + z\dot{\delta} \end{bmatrix} \begin{Bmatrix} \dot{s} \\ \dot{\phi} \end{Bmatrix} + \begin{bmatrix} \omega_{cr}^2 - \omega^2 & 0 \\ 0 & 0 \end{bmatrix} \begin{Bmatrix} s \\ \phi \end{Bmatrix} = \begin{bmatrix} \omega^2 e \cos\beta - g \sin\phi \\ \omega^2 e \sin\beta - g \cos\phi \end{bmatrix}$$

BY THE FBD (PAGE 3 OR NOTES) $\beta = \omega t - \phi$ (50)

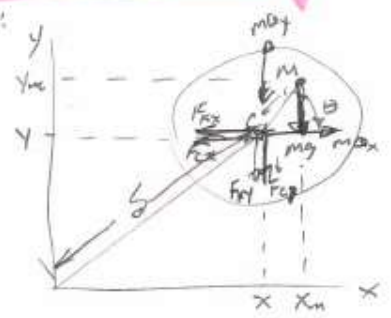
(50) INTO (49)

$$\begin{bmatrix} 1 & 0 \\ 0 & \delta \end{bmatrix} \begin{Bmatrix} \ddot{s} \\ \ddot{\phi} \end{Bmatrix} + \begin{bmatrix} \frac{c}{m} & 0 \\ 0 & \frac{c}{m}\delta + z\dot{\delta} \end{bmatrix} \begin{Bmatrix} \dot{s} \\ \dot{\phi} \end{Bmatrix} + \begin{bmatrix} \omega_{cr}^2 - \omega^2 & 0 \\ 0 & 0 \end{bmatrix} \begin{Bmatrix} s \\ \phi \end{Bmatrix} = e\omega^2 \begin{bmatrix} \cos(\omega t - \phi) \\ \sin(\omega t - \phi) \end{bmatrix}$$

EOM development and Steady-State solution for Jeffcott rotor begins here

BY NEWTON (REF (2))

FBD:



LET:

- K_x, K_y = LATERAL STIFFNESS OF SHAFT & EXT. SHAFT SUPPORTS.
- C_x, C_y = EXTERNAL DAMPING DUE TO AERODYNAMICS & OTHER SUPPORT STRUCTURE (BARS, ETC.)
- θ = ANGULAR DIM OF SHAFT ROTATION
- $\theta = \omega t$ (ω = SPIN RATE OF SHAFT)
- E = DIST. OF MASS FR. ROTOR & (C)

3DOF SYSTEM!
(x, y, θ)

$$\begin{aligned} x_m &= x + E \cos\theta \\ y_m &= y + E \sin\theta \\ F_{Kx} &= (K_x)x & F_{Ky} &= (K_y)y \\ F_{Cx} &= (C_x)\dot{x} & F_{Cy} &= (C_y)\dot{y} \\ a_x &= \frac{d^2}{dt^2}(x_m) & a_y &= \frac{d^2}{dt^2}(y_m) \end{aligned}$$

$$\begin{aligned} \sum F_x &= m a_x = -F_{Kx} - F_{Cx} = m a_x \\ -K_x x - C_x \dot{x} &= m \frac{d^2}{dt^2}(x + E \cos\theta) \\ \text{BY } \theta &= \omega t \\ -K_x x - C_x \dot{x} &= m \frac{d^2}{dt^2}(x + E \cos(\omega t)) \\ -K_x x - C_x \dot{x} &= m [\ddot{x} - E \omega^2 \cos(\omega t)] \end{aligned}$$

$$\therefore \ddot{x} + \frac{C_x}{m} \dot{x} + \frac{K_x}{m} x = E \omega^2 \cos(\omega t) \quad (52)$$

$$\begin{aligned} \sum F_y = m a_y &\Rightarrow -K_y Y - C_y \dot{Y} = m \frac{d^2}{dt^2} (Y + E \sin \theta) \\ &\text{by } \theta = \omega t \\ -K_y Y - C_y \dot{Y} &= m \{ \ddot{Y} - E \omega^2 \sin \omega t \} \\ \therefore m \ddot{Y} + C_y \dot{Y} + K_y Y &= m E \omega^2 \sin \omega t \\ \ddot{Y} + \frac{C_y}{m} \dot{Y} + \frac{K_y}{m} Y &= E \omega^2 \sin \omega t \quad (53) \end{aligned}$$

$$\sum M = I \ddot{\theta} \Rightarrow -m g E \cos \theta = I \ddot{\theta} \quad (54)$$

ASSUMPTIONS:

1) $\omega = \dot{\theta} = \text{CONSTANT}$

2) REFERENCE COORD. SYSTEM = STATIC EQUILIBRIUM $\therefore g$ NEGLECTED

3) SYMMETRIC SYSTEM (IE: $K_x = K_y, C_x = C_y$)

BY ASSUMPTIONS (1) & (2), EQ (54) IS OMITTED.

BY ASSUMPTION (3), EDM (52) & (53) REWRITTEN:

$$\ddot{X} + \frac{C_x}{m} \dot{X} + \frac{K_x}{m} X = E \omega^2 \cos \omega t \quad (55)$$

$$\ddot{Y} + \frac{C_y}{m} \dot{Y} + \frac{K_y}{m} Y = E \omega^2 \sin \omega t \quad (56)$$

$$\text{EDM} \quad \begin{bmatrix} 1 & 0 \\ 0 & 1 \end{bmatrix} \begin{Bmatrix} \ddot{X} \\ \ddot{Y} \end{Bmatrix} + \begin{bmatrix} \frac{C_x}{m} & 0 \\ 0 & \frac{C_y}{m} \end{bmatrix} \begin{Bmatrix} \dot{X} \\ \dot{Y} \end{Bmatrix} + \begin{bmatrix} \frac{K_x}{m} & 0 \\ 0 & \frac{K_y}{m} \end{bmatrix} \begin{Bmatrix} X \\ Y \end{Bmatrix} = E \omega^2 \begin{Bmatrix} \cos \omega t \\ \sin \omega t \end{Bmatrix} \quad (57)$$

DEFINE $S = X + iY$ = WHIRL RADIUS IN COMPLEX NOTATION. (58)

\therefore MULTIPLYING (56) BY i AND ADDING TO (55) FOR EDM IN COMPLEX NOMENCLATURE

$$(\ddot{X} + \frac{C_x}{m} \dot{X} + \frac{K_x}{m} X) + i(\ddot{Y} + \frac{C_y}{m} \dot{Y} + \frac{K_y}{m} Y) = E \omega^2 (\cos \omega t + i \sin \omega t)$$

$$(\ddot{X} + i \ddot{Y}) + \frac{C_x}{m} (\dot{X} + i \dot{Y}) + \frac{K_x}{m} (X + i Y) = E \omega^2 (\cos \omega t + i \sin \omega t)$$

BY (58) & EULER'S ($\cos \theta \pm i \sin \theta = e^{\pm i \theta}$)

$$\text{EDM} \quad \boxed{\ddot{S} + \frac{C}{m} \dot{S} + \frac{K}{m} S = E \omega^2 e^{i \omega t}} \quad (58)$$

$$\text{WHERE } e^{i \omega t} = \cos \omega t + i \sin \omega t$$

$$\text{SOLUTION } S = S_{\text{HOMO}} + S_{\text{PART}} \quad (59)$$

HOMOGENEOUS SOLUTION (TRANSIENT)

$$(58) \text{ BECOMES } \ddot{\delta} + \frac{c}{m} \dot{\delta} + \frac{k}{m} \delta = 0$$

$$\text{CHARACT. EQN} \Rightarrow A s^2 + B s + C = 0$$

$$s = \frac{-B \pm \sqrt{B^2 - 4AC}}{2A} \quad A=1, B=\frac{c}{m}, C=\frac{k}{m}$$

$$\sqrt{B^2 - 4AC} = \sqrt{\left(\frac{c}{m}\right)^2 - 4(1)\left(\frac{k}{m}\right)}$$

(60)

GIVEN c & k ARE 'LATERAL CHARACTERISTICS';

$$\left(\frac{k}{m}\right) = \omega_n^2$$

$$\left(\frac{c}{m}\right) = 2\zeta\omega_n$$

WHERE ζ = DAMPING RATIO
 $= \frac{c}{c_{cr}}$

AND $0 \leq \zeta \leq 1$

$$\therefore \sqrt{B^2 - 4AC} = \sqrt{(2\zeta\omega_n)^2 - 4\omega_n^2}$$

$$= \sqrt{4\omega_n^2(\zeta^2 - 1)}$$

$$\text{GIVEN } 0 \leq \zeta \leq 1, (\zeta^2 - 1) \leq 0$$

$$\therefore \sqrt{B^2 - 4AC} < 0 \Rightarrow \delta_h = e^{-\alpha t} (C_1 \cos \beta_1 t + C_2 \sin \beta_1 t) \quad (59)$$

(NOTE: β_1 USED HERE TO DIFFERENTIATE FROM ANGLE β USED ELSEWHERE)

$$\alpha = \frac{B}{2A}, \beta_1 = \frac{\sqrt{4AC - B^2}}{2A}$$

$$\therefore \alpha = \frac{c}{2m} = \frac{c}{2M} \quad (60)$$

$$\beta_1 = \frac{\sqrt{4\omega_n^2 - 4\omega_n^2\zeta^2}}{2} = \frac{2\omega_n\sqrt{1-\zeta^2}}{2}$$

$$\beta_1 = \omega_n\sqrt{1-\zeta^2} \quad (61)$$

WHERE ω_n = 'LATERAL NATURAL FREQ' = $\sqrt{\frac{k}{m}}$

(60)(61) INTO (59)

$$\delta_h = e^{-\frac{c}{2m}t} (C_1 \cos(\omega_n\sqrt{1-\zeta^2}t) + C_2 \sin(\omega_n\sqrt{1-\zeta^2}t)) \quad (59A)$$

INITIAL CONDITIONS:

$$s(u) = 0, \dot{s}(u) = 0$$

$$\delta_h(0) = e^{-\frac{c}{2m}(0)} (C_1 \cos((\omega_n\sqrt{1-\zeta^2})(0)) + C_2 \sin((\omega_n\sqrt{1-\zeta^2})(0))) = 0$$

$$\dot{\delta}_h(0) = e^{-\frac{c}{2m}(0)} (-\omega_n\sqrt{1-\zeta^2} C_1 \sin((\omega_n\sqrt{1-\zeta^2})(0)) + \omega_n\sqrt{1-\zeta^2} C_2 \cos((\omega_n\sqrt{1-\zeta^2})(0))) = 0$$

$$\therefore \delta_h = 0 \quad (61)$$

NOT CORRECT
 - DOES NOT CONSIDER
 STEADY STATE SOLUTION

PARTICULAR SOLUTION (STEADY STATE)

ASSUME OF SAME FORM AS FORCING FUNCTION FROM (58)

ALSO, SINCE DAMPING PRESENT IN (58), ASSUME STEADY STATE RESPONSE IS OUT OF PHASE WITH EXCITATION BY SOME AMOUNT (CRAIG, P 87)

LET PHASE DIFFERENCE = ϕ

$$c. \quad \dot{s}_p = D e^{i(\omega t - \phi)} \quad (62)$$

$$\dot{\dot{s}}_p = i\omega D e^{i(\omega t - \phi)} \quad (63)$$

$$\dot{\dot{\dot{s}}}_p = -\omega^2 D e^{i(\omega t - \phi)} \quad (64)$$

Sub (63) (64) INTO (58)

$$-\omega^2 D e^{i(\omega t - \phi)} + \frac{c}{m} i\omega D e^{i(\omega t - \phi)} + \frac{k}{m} D e^{i(\omega t - \phi)} = E \omega^2 e^{i\omega t}$$

$$\left[\left(\frac{k}{m} - \omega^2 \right) D + \frac{c}{m} \omega D i \right] e^{i(\omega t - \phi)} = E \omega^2 e^{i\omega t}$$

$$\left[\left(\frac{k}{m} - \omega^2 \right) D + \frac{c}{m} \omega D i \right] e^{-i\phi} = E \omega^2$$

BY EULERS:

$$\left[\left(\frac{k}{m} - \omega^2 \right) D + \frac{c}{m} \omega D i \right] (\cos \phi - i \sin \phi) = E \omega^2 \quad (65)$$

REAL PART: $\left(\frac{k}{m} - \omega^2 \right) D \cos \phi + \frac{c}{m} \omega D \sin \phi = E \omega^2 \quad (66)$

IMAG. PART: $-\left(\frac{k}{m} - \omega^2 \right) D \sin \phi + \frac{c}{m} \omega D \cos \phi = 0 \quad (67)$

BY (67) $-(k - m\omega^2) D \sin \phi + c\omega D \cos \phi = 0$

$$c\omega \cos \phi = (k - m\omega^2) \sin \phi$$

$$\frac{\sin \phi}{\cos \phi} = \tan \phi = \frac{c\omega}{(k - m\omega^2)}$$

$$\tan \phi = \frac{\frac{c}{m} \omega}{\left(\frac{k}{m} - \omega^2 \right)}$$

BY (60) $\frac{c}{m} = 2\zeta \omega_n$, $\frac{k}{m} = \omega_n^2$

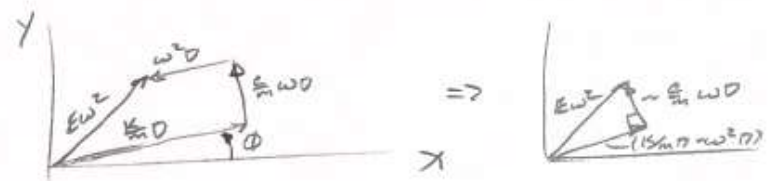
$$\tan \phi = \frac{2\zeta \omega \omega_n \left(\frac{1}{\omega_n^2} \right)}{\left(\omega_n^2 - \omega^2 \right) \left(\frac{1}{\omega_n^2} \right)} \Rightarrow \tan \phi = \frac{2\zeta \frac{\omega}{\omega_n}}{\left(1 - \frac{\omega^2}{\omega_n^2} \right)}$$

LET $R = \frac{\omega}{\omega_n}$ = FREQUENCY RATIO $\therefore \tan \phi = \frac{2\zeta R}{(1 - R^2)} \quad (68)$

ASSUMES STEADY STATE ONLY
SEE PG. 28

PHASE ANGLE

PLOTTING (66) AS A FORCE VECTOR POLYGON:



BY PYTHAGOREAN THM:

$$\left(\frac{k}{m}D - \omega^2 D\right)^2 + \left(\frac{c}{m}D\omega\right)^2 = (E\omega^2)^2$$

$$D^2 \left[\left(\frac{k}{m} - \omega^2\right)^2 + \left(\frac{c}{m}\omega\right)^2 \right] = (E\omega^2)^2$$

$$D = \frac{E\omega^2}{\sqrt{\left(\frac{k}{m} - \omega^2\right)^2 + \left(\frac{c}{m}\omega\right)^2}} \quad (67a)$$

BY (60) WHERE $\frac{k}{m} = \omega_n^2$, $\frac{c}{m} = 2\zeta\omega_n$

$$D = \frac{E\omega^2 \left(\frac{1}{\omega_n^2}\right)}{\sqrt{\left(\omega_n^2 - \omega^2\right)^2 + \left(2\zeta\omega_n\omega\right)^2} \left(\frac{1}{\omega_n^2}\right)}$$

$$= \frac{E \frac{\omega^2}{\omega_n^2}}{\sqrt{\left(\frac{\omega_n^2 - \omega^2}{\omega_n^2}\right)^2 + \left(2\zeta\frac{\omega}{\omega_n}\right)^2}}$$

← ASSUMES STEADY STATE ONLY →
∴ ζ BEYOND PT. WHERE TRANSIENT DIES OUT. SEE PG 28

BY $R = \frac{\omega}{\omega_n}$ (68):

$$D = \frac{ER^2}{\sqrt{(1-R^2)^2 + (2\zeta R)^2}} = \text{AMPLITUDE OF WHIRL RADIUS}$$

NONDIMENSIONAL FORM OF WHIRL RADIUS AMPLITUDE:

$$\frac{D}{E} = \frac{R^2}{\sqrt{(1-R^2)^2 + (2\zeta R)^2}} \quad (69)$$

NOTE THAT WHIRL RADIUS AMPLITUDE (69) AND PHASE ANGLE (68) FOR A JEFFCOTT ROTOR WITH CENTERED DISK IS 'SAME' AS RESPONSE FOR A SDOF SYSTEM WITH DAMPING (CRAIG PG 38)

KEY DIFFERENCE IS THAT ABOVE IS FOR 'WHIRL' CHARACTERISTICS AS OPPOSED TO SDOF IN CRAIG IS LINEAR DISPLACEMENT. φ OF ABOVE IS PHASE ANGLE OF IMBALANCE VECTOR WITH RESPECT TO SHAFT RESTORING FORCE VECTOR.

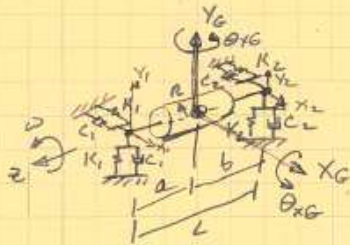
- $0 \leq \phi < \frac{\pi}{2}$ - FORCES IN 'PHASE' ∴ ADDITIVE
- $\phi = \frac{\pi}{2}$ - WHIRL RADIUS BOUNDED ONLY BY DAMPING (3) ($R = \omega/\omega_n = 1$)
- $\frac{\pi}{2} < \phi$ - FORCES 'OPPOSE' ∴ ALLOW F/MIN RESPONSE

Appendix D

EOM Development for Modified Jeffcott Rotor System

ROTOR GYROSCOPIC EFFECTS - JEFFCOYT - STIFF SHAFT / ELASTIC BRGS -

(FOLLOWING YOON)



m = MASS OF ROTOR / SHAFT

ASSUMPTIONS:

- ROTOR SHAFTS HAVE NEGLIGIBLE MASS W.R.T. REST OF SYSTEM
- ROTOR / SHAFT STIFFNESS \gg K BRGS.
- EACH BRG SYMMETRIC IN X & Y
- ROTOR / SHAFT = AXISYMMETRIC

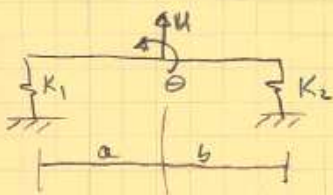
ROTOR INERTIA TERMS:

POLAR = $I_{ZZ} = J_P = \frac{mR^2}{2}$

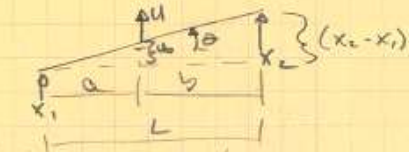
TRANSVERSE = $I_{XX} = I_{YY} = J_T = \frac{m}{4} (R^2 + \frac{1}{3}L^2)$

DEFINE RATIO OF POLAR TO TRANSVERSE M.O.I. = P

$$P = \frac{J_P}{J_T} = \frac{\frac{mR^2}{2}}{\frac{m}{4} (R^2 + \frac{1}{3}L^2)} = \frac{2R^2}{(R^2 + \frac{1}{3}L^2)} = \frac{2}{1 + \frac{L^2}{3R^2}} = P$$



$F = F_1 + F_2$
 $F = K_1 X_1 + K_2 X_2 + C_1 \dot{X}_1 + C_2 \dot{X}_2$



$\frac{L}{X_2 - X_1} = \frac{a}{u}$ $\left\{ \begin{array}{l} X_2 = X_1 + L \sin \theta \\ \sin \theta = \frac{X_2 - X_1}{L} \end{array} \right.$
 $\therefore u = \frac{a(X_2 - X_1)}{L}$

$u = u_0 + X_1$
 $= X_1 + \frac{a(X_2 - X_1)}{L} = \frac{L-a}{L} X_1 + \frac{a}{L} X_2$
 $= X_1 \frac{(L-a)}{L} + \frac{a}{L} X_2$

$u = \frac{X_1 b + X_2 a}{L}$

\Rightarrow BY SAME PROCESS IN 'X' & 'Y' DIRECTIONS

FOR SMALL θ , $\sin \theta \approx \theta$

$X_G = \frac{1}{L} (b X_1 + a X_2)$ (86)
 $Y_G = \frac{1}{L} (b Y_1 + a Y_2)$

$\therefore \sin \theta = \theta \frac{X_2 - X_1}{L} \Rightarrow$ BY SAME PROCESS FOR θ_{XG} & θ_{YG} :

$\theta_{XG} = \frac{1}{L} (Y_2 - Y_1)$ (87)
 $\theta_{YG} = \frac{1}{L} (X_2 - X_1)$

- TRANSLATION -

$$\sum F = 0 = F - K_1 X_1 - K_2 X_2 - C_1 \dot{X}_1 - C_2 \dot{X}_2 \quad (87a)$$

$$u = X_1 + a \sin \theta \quad X_2 = X_1 + L \sin \theta$$

$$\therefore X_1 = u - a \sin \theta \quad = (u - a \sin \theta) + L \sin \theta$$

- BY SMALL θ -

$$X_1 = u - a\theta \quad X_2 = (u - a\theta + L\theta) = u + (L - a)\theta$$

$$\dot{X}_1 = \dot{u} - a\dot{\theta} \quad \dot{X}_2 = \dot{u} + b\dot{\theta}$$

SUB X_G & Y_G FOR u TO YIELD EQNS IN SPECIFIC DIRECTIONS!

$$\left. \begin{aligned} X_1 &= X_G - a\theta_{yG} & X_2 &= X_G + b\theta_{yG} \\ \dot{X}_1 &= \dot{X}_G - a\dot{\theta}_{yG} & \dot{X}_2 &= \dot{X}_G + b\dot{\theta}_{yG} \\ Y_1 &= Y_G - a\theta_{xG} & Y_2 &= Y_G + b\theta_{xG} \\ \dot{Y}_1 &= \dot{Y}_G - a\dot{\theta}_{xG} & \dot{Y}_2 &= \dot{Y}_G + b\dot{\theta}_{xG} \end{aligned} \right\} (88)$$

$$\sum F = ma = m\ddot{u}$$

$$m\ddot{u} + K_1 X_1 + K_2 X_2 + C_1 \dot{X}_1 + C_2 \dot{X}_2 = F$$

- SUBSTITUTING (88) & REPLACING \ddot{u} WITH \ddot{X}_G & \dot{Y}_G :

$$m\ddot{X}_G + K_1(X_G - a\theta_{yG}) + K_2(X_G + b\theta_{yG}) + C_1(\dot{X}_G - a\dot{\theta}_{yG}) + C_2(\dot{X}_G + b\dot{\theta}_{yG}) = F_x$$

$$m\ddot{X}_G + X_G(K_1 + K_2) + \theta_{yG}(-K_1 a + K_2 b) + \dot{X}_G(C_1 + C_2) + \dot{\theta}_{yG}(-aC_1 + bC_2) = F_x \quad (89)$$

SIMILARLY

$$m\ddot{Y}_G + Y_G(K_1 + K_2) + \theta_{xG}(-K_1 a + K_2 b) + \dot{Y}_G(C_1 + C_2) + \dot{\theta}_{xG}(-aC_1 + bC_2) = F_y$$

- ROTATION -

$$\sum M = 0 = \sum (\text{SPRING REACTIONS} + \text{GYROSCOPIC MOMENT})$$

- BY REFERENCE (13), GYROSCOPIC MOMENT IS DERIVED AS:

$$T_{\text{GYRO}} = J_p (\text{ROT. SPD}) (\text{PRECESSION SPD})$$

- BY FIG ON NOTES PG 21, PRECESSION $\dot{\theta} = \dot{\theta}$ \therefore PRECESSION SPD = $\dot{\theta}$ PREVIOUSLY, SHAFT ROT SPD = ω

$$\therefore T_{\text{GYRO}} = J_p \omega \dot{\theta} \quad (90)$$

$$\therefore \sum M = 0 = M - K_2 X_2 b + K_1 X_1 a - J_p \omega \dot{\theta} = 0$$

- SUBSTITUTE (88) & $T_{\text{GYRO}} = \dot{\theta}$ FOR DOT ABOUT θ_{yG} AS SHOWN ON PG 21 THESE NOTES
 $T_{\text{GYRO}} = \dot{\theta}$ FOR θ_{xG}

$$\therefore M_x + K_1 X_1 a - K_2 Y_2 b - J_p \omega \dot{\theta}_{yG} + C_1 \dot{Y}_1 a - C_2 \dot{Y}_2 b = 0$$

$$M_y + K_1 X_1 a - K_2 X_2 b + J_p \omega \dot{\theta}_{xG} + C_1 \dot{X}_1 a - C_2 \dot{X}_2 b = 0$$

$$\sum M = I \alpha = I \ddot{\theta}$$

$$\begin{aligned} \therefore I \ddot{\theta}_G - K_1 a (\dot{y}_G - a \dot{\theta}_G) + K_2 b (\dot{y}_G + b \dot{\theta}_G) + J_p \omega \dot{\theta}_G \\ - c_1 a (\dot{y}_G - a \dot{\theta}_G) + c_2 b (\dot{y}_G + b \dot{\theta}_G) = M_x \end{aligned}$$

$$I \ddot{\theta}_G + \dot{y}_G (-K_1 a + K_2 b) + \theta_G (K_1 a^2 + K_2 b^2) + \dot{y}_G (-c_1 a + c_2 b) + \dot{\theta}_G (c_1 a^2 + c_2 b^2) + (J_p \omega) \dot{\theta}_G = M_x$$

- SIMILARLY -

$$I \ddot{\theta}_G + \dot{x}_G (-K_1 a + K_2 b) + \theta_G (K_1 a^2 + K_2 b^2) + \dot{x}_G (-c_1 a + c_2 b) + \dot{\theta}_G (c_1 a^2 + c_2 b^2) - (J_p \omega) \dot{\theta}_G = M_y \quad (91)$$

(89) (91) IN MATRIX FORMAT YIELD EOM WITH EXTERNAL LOADS F_x, F_y, M_x, M_y :

- SUB J_T FOR I IN (91) -

$$\begin{aligned} \begin{bmatrix} m & 0 & 0 & 0 \\ 0 & m & 0 & 0 \\ 0 & 0 & J_T & 0 \\ 0 & 0 & 0 & J_T \end{bmatrix} \begin{Bmatrix} \ddot{x}_G \\ \ddot{y}_G \\ \ddot{\theta}_G \\ \ddot{\theta}_G \end{Bmatrix} + \begin{bmatrix} (c_1 + c_2) & 0 & 0 & (-a c_1 + b c_2) \\ 0 & (c_1 + c_2) & (-a c_1 + b c_2) & 0 \\ 0 & (-a c_1 + b c_2) & (K_1 a^2 + K_2 b^2) & (J_p \omega) \\ (-a c_1 + b c_2) & 0 & (-J_p \omega) & (K_1 a^2 + K_2 b^2) \end{bmatrix} \begin{Bmatrix} \dot{x}_G \\ \dot{y}_G \\ \dot{\theta}_G \\ \dot{\theta}_G \end{Bmatrix} + \\ + \begin{bmatrix} (K_1 + K_2) & 0 & 0 & (-K_1 a + K_2 b) \\ 0 & (K_1 + K_2) & (-K_1 a + K_2 b) & 0 \\ 0 & (-a K_1 + b K_2) & (K_1 a^2 + K_2 b^2) & 0 \\ (-a K_1 + b K_2) & 0 & 0 & (K_1 a^2 + K_2 b^2) \end{bmatrix} \begin{Bmatrix} x_G \\ y_G \\ \theta_G \\ \theta_G \end{Bmatrix} = \begin{Bmatrix} F_x \\ F_y \\ M_x \\ M_y \end{Bmatrix} \quad (92) \end{aligned}$$

FOR SIMPLICITY, EQ (92) IS REWRITTEN : (EOM F/ DAMPED TEFSCOTT W/ STIFF ROTOR & ELASTIC/DAMPED SUPPORTS)

$$\begin{bmatrix} m & 0 & 0 & 0 \\ 0 & m & 0 & 0 \\ 0 & 0 & J_T & 0 \\ 0 & 0 & 0 & J_T \end{bmatrix} \begin{Bmatrix} \ddot{x}_G \\ \ddot{y}_G \\ \ddot{\theta}_G \\ \ddot{\theta}_G \end{Bmatrix} + \begin{bmatrix} \alpha_c & 0 & 0 & \gamma_c \\ 0 & \alpha_c & \gamma_c & 0 \\ 0 & \gamma_c & \delta_c & J_p \omega \\ \gamma_c & 0 & -J_p \omega & \delta_c \end{bmatrix} \begin{Bmatrix} \dot{x}_G \\ \dot{y}_G \\ \dot{\theta}_G \\ \dot{\theta}_G \end{Bmatrix} + \begin{bmatrix} \alpha_k & 0 & 0 & \gamma_k \\ 0 & \alpha_k & \gamma_k & 0 \\ 0 & \gamma_k & \delta_k & 0 \\ \gamma_k & 0 & 0 & \delta_k \end{bmatrix} \begin{Bmatrix} x_G \\ y_G \\ \theta_G \\ \theta_G \end{Bmatrix} = \begin{Bmatrix} F_x \\ F_y \\ M_x \\ M_y \end{Bmatrix} \quad (93)$$

WHERE :

$$\begin{aligned} \alpha_c &= c_1 + c_2 & \alpha_k &= K_1 + K_2 \\ \gamma_c &= -a c_1 + b c_2 & \gamma_k &= -a K_1 + b K_2 \\ \delta_c &= a^2 c_1 + b^2 c_2 & \delta_k &= a^2 K_1 + b^2 K_2 \end{aligned}$$

$\pm J_p \omega =$ GYROSCOPIC MOMENT TERMS.

Appendix E

EOM Development for Finite Element Program – MATLAB Source Code

```

% FILE = EOM_derivation_01Sep.m
clc; clearvars; close all hidden; close all force;
format long;
syms q vi wi thtayi thtazi vj wj thtajj thtajzj
syms qdot vidot widot thtayidot thtazidot vjdot wjdot thtajjdot thtajzdot
syms qddot viddot widdot thtayiddot thtaziddot vjddot wjddot thtajjddot thtajzddot
syms rho r A L s eta I Jt Jp G E omega etah etav k phi Lamz P %Qf Qc Qs eta
%% definition of variables
% coordinate system = x,y,z - x-axis = longitudinal axis of shaft
% v = translation in 'y' direction
% w = translation in 'z' direction
% i = node 1
% j = node 2
% rho = element density (mass/cu vol)
% r = element radius (sub with conical function in full program)
% A = element cross-section area (sub with conical function in full program)
% L = element length
% s = axial coordinate for purposes of integration, 's' ranges from '0' to 'L'
% eta = dimensionless axial coordinate, eta=s/L
% I = 2nd moment of area (stress calcs)
% Jt = Mass moment of Inertia (transverse about cg) - per unit length = rho*A*(r^2/4+L^2/12)
% Jp = Mass moment of Inertia (rotational/polar) - per unit length = rho*A*r^2/2
% G = Shear modulus
% E = Modulus of elasticity
% omega = rotating (spinning) speed of shaft
% etah = internal material hysteretic loss factor
% etav = internal material viscous damping factor
% k = shear correction factor (Timoshenko constant)
% phi = shear deformation parameter = ratio bending to shear stiffness
% Lamz = EI/(kGA)=phi*L^2/12
% P = applied axial force on element (for purposes of stiffening effects on lateral vibration only)

%% Header printout
disp(' ')
disp('##### Coordinate System #####')
disp(' x,y,z - x-axis=longitudinal axis of shaft')
disp(' (i,j)=(node1, node2)')
disp(' v = translation in y')
disp(' w = translation in w')
disp(' ')
disp(' ---- Nodal DOF Sequence ---- ')
disp(' q=[vi wi thtayi thtazi vj wj thtajj thtajz]')
disp(' ')
disp('##### EOM #####')
disp(' [M]*[qddot] + [C]*[qdot] + [K]*[q] = forcing function')
disp(' ')
disp(' [M] = [M_trans]+[M_rotatory]')
disp(' [C] = [ED]+[G]*omega')
disp(' [ED] = dissipation energy due to material internal viscous damping')
disp(' [G] = gyroscopic matrix')
disp(' [K] = [K_bend_incl_int_damping]+[K_axial]+[K_shear]')
disp(' ')
disp(' ----- Matrices and Confirmations to Reference Papers Follow -----')
disp(' ')

%% Define DOF vector & time derivatives

```

```

q=[vi;wi;thtayi;thtazi;vj;wj;thtayj;thtazj];
qdot=[vidot;widot;thtayidot;thtazidot;vjdot;wjdot;thtayjdot;thtazjdot];
qddot=[viddot;widot;thtayiddot;thtaziddot;vjddot;wjddot;thtayjddot;thtazjddot];

%% Create Shape Functions and Derivatives
% follow method of Bazoune and Khulief (2002) for Beam with Timoshenko Shear (see notes pgs 123-124)
% Lamz=E*It/(k*G*A); % Bazoune and Khulief (2002) Eq 23, Eq 163 of notes pg 124
% PHlz=12*Lamz/L^2; % Bazoune and Khulief (2002) Eq 35, pg 125 et al of notes
% PHlzbar=1/(1+PHlz); % Bazoune and Khulief (2002) Eq 34, pg 125 et al of notes
displ=[vi 0 0 0; % displacement values for 4 boundary conditions [vi thtai vj thtaj]
0 thtazi 0 0;
0 0 vj 0;
0 0 0 thtazj];close all hidden; close all force;
Coeffs=[1 0 0 0 ; % coeffs for simultaneous equations (Eq 168 of notes pg 124)
0 1 0 6*Lamz ;
1 L L^2 L^3 ;
0 1 2*L (3*L^2+6*Lamz)];
Coeffs_inv=inv(Coeffs);
a=Coeffs\displ; % (inverse of Coeffs)*dof
a0=a(1); a1=a(2); a2=a(3); a3=a(4); % correspond to notes eq 168, pg 124
% -----
% --- translational shape functions
v_temp=a0+a1*s+a2*s^2+a3*s^3; % put [a] coefficients in to equation for v(s) (eq 153, notes pg 123)
% separate terms of 'a' into matrix based on displacement [vi,thtai,vj,thtaj]
[vd,v]=coeffs(v_temp,[vi,thtazi,vj,thtazj]);
%{q}=[ vi; wi; thtayi; thtazi; vj; wj; thtayj; thtazj]
N_v= [ vd(1) 0 0 vd(2) vd(3) 0 0 vd(4)]; %XY plane (y, thtaz)
N_w= [ 0 vd(1) -vd(2) 0 0 vd(3) -vd(4) 0 ]; %XZ plane (w, thtay=-thtaz)
N_trans=[N_v;N_w]; % shape function for beam translation 'V' & 'W' per Nelson 1980, Eq(1)
% substitute variables into f(phi,eta) for visualization & comparison to papers
% N_trans=expand(subs(N_trans,[(12*Lamz) (-12*Lamz) (6*Lamz) (-6*Lamz)],[(phi*L^2) (-phi*L^2) (phi/2*L^2)...
% (-phi/2*L^2)]));
% N_trans=(subs(N_trans,[(L^3*phi+L^3) (L^2*phi+L^2) (L*phi+L)],[(L^3*(1+phi)) (L^2*(1+phi)) (L*(1+phi))]);
% N_trans=(subs(N_trans,[(s/L) s], [eta eta*L]));
% N_trans(1,:).' %matches Bazoune/Khulief Eq 38
% N_trans(2,:).' %matches Bazoune/Khulief Eq 44
% good to here. N_v matches Bazoune/Khulief for translational shape function (see notes pg 125-126)
% --- rotational shape functions
thta_temp=a1+2*a2*s+(3*s^2+6*Lamz)*a3; % put [a] coefficients in to equation for v(s) (eq 166, notes pg 124)
% separate terms of 'a' into matrix based on displacement [vi,thtai,vj,thtaj]
[vd,v]=coeffs(thta_temp,[vi,thtazi,vj,thtazj]);
%{q}=[ vi; wi; thtayi; thtazi; vj; wj; thtayj; thtazj]
% per Childs Eq 2.98
N_Beta=[ 0 -vd(1) vd(2) 0 0 -vd(3) vd(4) 0 ]; %XZ plane Thtay=-dw/ds (from N_trans)
N_Gamma=[vd(1) 0 0 vd(2) vd(3) 0 0 vd(4)]; %XY plane Thtaz= dv/ds (from N_trans)
N_rot=[N_Beta;N_Gamma]; % per Childs Eq 2.98

% substitute variables into f(phi,eta) for visualization & comparison to papers
% N_rot=expand(subs(N_rot,[(12*Lamz) (-12*Lamz) (6*Lamz) (-6*Lamz)],[(phi*L^2) (-phi*L^2) (phi/2*L^2)...
% (-phi/2*L^2)]));
% N_rot=(subs(N_rot,[(L^3*phi+L^3) (L^2*phi+L^2) (L*phi+L)],[(L^3*(1+phi)) (L^2*(1+phi)) (L*(1+phi))]);
% N_rot=(subs(N_rot,[(s/L) s], [eta eta*L]));
% N_rot(1,:).' %matches Bazoune/Khulief Eq 41
% N_rot(2,:).' %matches Bazoune/Khulief Eq 45
% good to here. N_v matches Bazoune/Khulief for rotational shape function (see notes pg 126-127)
% -----

```

```

% confirmed that shape functions and components (vd(1), etc) match references:
% - Childs Eq(2.79,2.97,2.98), Nelson(1980)Eq(1,2)&App, Nelson/McVaugh(1976)Eq(11,12,14),
% - Zorzi/Nelson(1977)Ea(2,5)&App, Bazoune/Khulief(2002)Eq(38,41,44,45), Greenhill/Nelson(1985) App,
% - Rouch/Kao(1978) Eq(5), Yokoyama(1987)
% - some typos exist in some references - by derivation & comparison confirmed that this code (above) is good.
% -----
% --- separate bending and shear components of N_trans & N_rot per Nelson (1980)
% --- split translational shape function
temp=subs(N_trans,[s Lamz],[eta*L phi*L^2/12]);
temp=simplify(temp*(1+phi)); % temporarily remove divisor of (1+phi) for easy comparison to papers
temp=expand(temp);
% N_trans=subs(N_trans,Lamz,phi*L^2/12); % convert to function of phi,L
% phi=shear deformation parameter=ratio bend to shear stiffnesses
% Bazoune/Khulief(2002)pg 477, Kosmatka(1994)pg 144, Yokoyama(1987)
N_trans_b_temp=subs(temp,phi,0); % phi=shear deformation parameter=0 means due to bending only
% N_trans_b_temp(1,:).' % confirmed per Nelson(1980), pg794 & Appendix - 'alpha' terms = bending
% N_trans_b_temp(2,:).' % confirmed per Nelson(1980), pg794 & Appendix - 'alpha' terms = bending
N_trans_s_temp=temp-N_trans_b_temp; %[N] due to bending (as function of eta=s/L) - less (1+phi) term
% N_trans_s_temp(1,:).' % confirmed per Nelson(1980), pg794 & Appendix - 'beta' terms = shear
% N_trans_s_temp(2,:).' % confirmed per Nelson(1980), pg794 & Appendix - 'beta' terms = shear
% --- translational shape functions - confirmed to Nelson (1980-pg794 & App) and notes pages 125-126
N_trans_b=subs(N_trans_b_temp,eta,s/L); % [N_trans(b)] due to bending (as function of s, phi)
N_trans_b=N_trans_b/(1+phi); % replace divisor of (1+phi) for full function
N_trans_b=subs(N_trans_b,phi,(12*E*I/(k*A*G*L^2))); %[N_trans(b)] (as function of s,E,I,k,A,G,L)
N_trans_s=subs(N_trans_s_temp,eta,s/L); % [N_trans(s)] due to shear (as function of s, phi)
N_trans_s=N_trans_s/(1+phi); % replace divisor of (1+phi) for full function
N_trans_s=subs(N_trans_s,phi,(12*E*I/(k*A*G*L^2))); %[N_trans(s)] (as function of s,E,I,k,A,G,L)
% --- split rotational shape function
temp=subs(N_rot,[s Lamz],[eta*L phi*L^2/12]);
temp=simplify(temp*(1+phi)); % temporarily remove divisor of (1+phi) for easy comparison to papers
temp=expand(temp); % ok per notes pg 126-127
% N_rot=subs(N_rot,Lamz,phi*L^2/12); % convert to function of phi,L
N_rot_b_temp=subs(temp,phi,0); % phi=shear deformation parameter=0 means due to bending only
N_rot_b=subs(N_rot_b_temp,eta,s/L)/(1+phi); % [N_rot] due to bending (fnctn of s/L, includes (1+phi) term)
N_Beta_b=N_rot_b(1,:);
N_Gamma_b=N_rot_b(2,:);
% N_rot_b_temp(1,:).' % confirmed per Nelson(1980), pg794 & Appendix - 'epsilon' terms = bending
% N_rot_b_temp(2,:).' % confirmed per Nelson(1980), pg794 & Appendix - 'epsilon' terms = bending
N_rot_s_temp=temp-N_rot_b_temp; %[N] due to shear (as function of eta=s/L) - less (1+phi) term
N_rot_s=subs(N_rot_s_temp,eta,s/L)/(1+phi); % [N_rot] due to shear (function of s/L, includes (1+phi) term)
% N_rot_s_temp(1,:).' % confirmed per Nelson(1980), pg794 & Appendix - 'delta' terms = shear
% N_rot_s_temp(2,:).' % confirmed per Nelson(1980), pg794 & Appendix - 'delta' terms = shear
% --- rotational shape functions - confirmed to Nelson (1980-pg794 & App) and notes pages 125-126
% -----

%% KE & PE Computations
% ----- KE = translational, rotational, gyroscopic, spin terms
% Per Nelson/McVaugh(1976), Nelson(1980), Childs, Greenhill/Nelson(1985)
mu=A*rho; % mu[=] element mass/length
% Jt=rho*(A*s)*(r^2/4+s^2/12); % diametral (transverse) MMOI of the unit
Mt=int(mu*(N_trans.*N_trans),s,0,L); % mass/lngh - Greenhill/Nelson(1985) Eq(15a), Childs Eq 2.101
Mr=int(Jt*(N_rot.*N_rot),s,0,L); % Greenhill/Nelson(1985) Eq(15b), Childs Eq 2.101
N=int(Jp*N_rot(1,:).*N_rot(2,:),s,0,L); % Greenhill/Nelson(1985) Eq(15c) w/ mod, Childs eq 2.101 mod to taper
Ketrans_rot=1/2*qdot.*(Mt+Mr)*qdot; % Greenhill/Nelson(1985) Eq 14, Childs Eq 2.101, Nelson(1980) Eq 8
KEgyro=omega*qdot.*N*q; % Nelson(1980) Eq 8, Childs Eq 2.101
KEspin=omega*int(2*rho*I,s,0,L)/2; % Nelson(1980) Eq 8, Childs Eq 2.101

```

```

% ----- sum for total
KE=KEtrans_rot+KEgyro+KEspin;           % Nelson(1980), Greenhill/Nelson, Childs Eq 2.101
% ----- PE = elastic bending, shear, axial load
% ----- Per Nelson/McVaugh(1976), Nelson(1980), Childs, Greenhill/Nelson(1985), Kosmatka(1994)
Bb=diff(N_rot,s);                       % Childs Eq 2.102
KPEb=int(E*I*(Bb.'*Bb),s,0,L);          % Childs Eq 2.102
eta1=(etah+1)/sqrt(1+etah^2);
eta2=etah/sqrt(1+etah^2)+omega*etav; % add with Kc skew-symmetric matrix directly to K_matrix later
PEB=int(E*I*eta1*Bb.'*Bb,s,0,L); % int damping assoc. w/ bending (add skew-symmetric Kc directly to K_matrix)
Bs=[N_rot(2,:)-N_rot(1,:)]-diff(N_trans,s); % solving for Gxy=Go (notes eq155,154,164, Choi (1992) Eq A1-A3)
KPEs=int(k*A*G*(Bs.'*Bs),s,0,L); % Nelson Eq 6b, Greenhill/Nelson Eq 12b (Timoshenko shear)
Ba=diff(N_trans,s);                     % Nelson(1980) Eq 6
KPEa=int(P*(Ba.'*Ba),s,0,L);           % Nelson Eq 6c, Greenhill/Nelson Eq 12c
% ----- Internal Damping = Bending Potential Energy & Dissipation Function
% Zorzi/Nelson(1977) & Greenhill/Nelson(1985) - w/ Internal Damping
% Nelson/McVaugh (1976) & Nelson (1980) - no Internal Damping
N1=[0 -1;1 0].';
Bc=diff(diff(N_trans_b,s),s);
Kc=int(E*I*((N1.'*Bb).'*Bb),s,0,L); % Zorzi/Nelson Eq13b, Greenhill/Nelson Eq18 - Int. Damping Circulation Mat.
ED=1/2*etav*qdot.*KPEb*qdot; % Greenhill/Nelson Eq 17b
% ----- sum for total PE
PE=1/2*q.*(KPEs+KPEa+PEB)*q;

%% LaGrangian EOM Derivation - d/dt[dKE/dXdotti-dPE/dXdotti]-dKE/dXi+dPE/dXi=0
% diff Ke/dXdotti
dKEdXdotti=[];
for ii=1:length(q)
    dKEdXdotti=[dKEdXdotti;diff(KE,qdot(ii))];
end
% diff Pe/dXdotti
dPEdXdotti=[];
for ii=1:length(q)
    dPEdXdotti=[dPEdXdotti;diff(PE,qdot(ii))];
end
% diff Ke/dXi
dKEdXi=[];
for ii=1:length(q)
    dKEdXi=[dKEdXi;diff(KE,q(ii))];
end
% diff Pe/dXi
dPEdXi=[];
for ii=1:length(q)
    dPEdXi=[dPEdXi;diff(PE,q(ii))];
end
% Lagrangian LHS - 'a-part' = time derivative terms
lhsa=dKEdXdotti-dPEdXdotti; %+dEDdXdotti;
% differentiate lhsa with respect to time
% separate 'qdot' and 'q' terms for time differentiation
lhsa_terms=[]; [row,col]=size(lhsa);
lhsa_terms=sym(zeros(1,length(qdot))+length(q));
for ii=1:row % separate qdot and q terms so can convert to qddot and qdot for time differentiation
    [vd,v]=coeffs(lhsa(ii),[qdot; q]);
    tempqdot=sym(zeros(1,length(qdot))); tempq=sym(zeros(1,length(q)));
    for jj=1:length(v)
        for kk=1:length(qdot)
            if v(jj)==qdot(kk)

```

```

        tempqdot(kk)=vd(jj);
    end
    if v(jj)==q(kk)
        tempq(kk)=vd(jj);
    end
end
end
lhsa_terms(ii,:)=[tempqdot tempq];
end
dlhsadt=[]; %'differentiate wrt time' by multiplying separated terms by qddot or qdot as appropriate
for ii=1:row
    ddotterms=0; dotterms=0;
    for jj=1:length(q)
        ddotterms=ddotterms+lhsa_terms(ii,jj)*qddot(jj);
        dotterms=dotterms+lhsa_terms(ii,jj+length(q))*qdot(jj);
    end
    dlhsadt=[dlhsadt; ddotterms dotterms];
end
M_matrix=[]; C_matrix_a=[]; % separate differentiated terms to M- (qddot) and C-matrix (qdot)
for ii=1:length(dlhsadt)
    M_matrix=[M_matrix;equationsToMatrix(dlhsadt(ii,1),qddot.')];
    C_matrix_a=[C_matrix_a;equationsToMatrix(dlhsadt(ii,2),qdot.')]; % C-matrix component from d/dt terms
end
% Second part of EOM per Lagrangian ('-dKE/dXi+dPE/dXi)
lhsb=(-dKEdX+dPEdX);
[rows,cols]=size(lhsb);
lhsb_terms=sym(zeros(1,length(qdot)+length(q)));
for ii=1:row % separate qdot and q terms
    [vd,v]=coeffs(lhsb(ii),[qdot; q]);
    tempqdot=sym(zeros(1,length(qdot))); tempq=sym(zeros(1,length(q)));
    for jj=1:length(v)
        for kk=1:length(qdot)
            if v(jj)==qdot(kk)
                tempqdot(kk)=vd(jj);
            end
            if v(jj)==q(kk)
                tempq(kk)=vd(jj);
            end
        end
    end
    lhsb_terms(ii,:)=[tempqdot tempq];
end
lhsb_eqtn=[];
for ii=1:row
    dotterms=0; qterms=0;
    for jj=1:length(q)
        dotterms=dotterms+lhsb_terms(ii,jj)*qdot(jj);
        qterms=qterms+lhsb_terms(ii,jj+length(q))*q(jj);
    end
    lhsb_eqtn=[lhsb_eqtn; dotterms qterms];
end
C_matrix_b=[]; K_matrix=[]; [rows,cols]=size(lhsb_eqtn);
for ii=1:rows
    C_matrix_b=[C_matrix_b;equationsToMatrix(lhsb_eqtn(ii,1),qdot.')];
    K_matrix=[K_matrix;equationsToMatrix(lhsb_eqtn(ii,2),q.')];
end
end

```



```

% Third part of EOM per Lagrangian: dED/dXdot is added term - adds to C_matrix since 'd/dXdot'
dEDdXdot=[];
for ii=1:length(q)
    dEDdXdot=[dEDdXdot;diff(ED,qdot(ii))];
end
ED_matrix=[]; [rows,cols]=size(dEDdXdot);
for ii=1:rows
    ED_matrix=[ED_matrix;equationsToMatrix(dEDdXdot(ii,:),qdot.')]; %Energy Diss Term per Greenhill/Nelson(1985)
end
% Add Internal Damping due to Damping Circulation Matrix (Kc)
% Note that Kc is skew-symmetric so adding as potential energy term (q.*Kc*q) 'zeros' the effect
% Therefore add Kc*eta2 directly to the K-matrix - results in matrices that match references per below

K_matrix=K_matrix+Kc*eta2;

%% Combine/print Matrices for Output
C_matrix=C_matrix_a+C_matrix_b+ED_matrix;
G_matrix=C_matrix_a+C_matrix_b;
% print matrices to screen
% disp('M_matrix = ')
% size(M_matrix)
M_matrix
% disp('ED_matrix = ')
% size(ED_matrix)
ED_matrix
% disp('G_matrix = ')
% size(G_matrix)
G_matrix
% disp('K_matrix = ')
% size(K_matrix)
K_matrix
% check ED_matrix=KPEb*etav per Greenhill/Nelson Eq 22
ED_matrix_check=ED_matrix/etav-KPEb % should be [zeros] if all correct
% check G_matrix=N-N.' per Childs eq 2.104 - initial check only - no Energy Dissipation Term
C_check=C_matrix/omega-ED_matrix/omega-(N-N.') % should be [zeros] if all correct - per Greenhill/Nelson Eq 22

%% Correctness Checks....
% Check K_matrix built via Lagrangian EOM method here against EOM in papers
% ---- K_matrix (total) per Greenhill/Nelson Eq 22
dmp_b=(1+etah)/sqrt(1+etah^2); % internal damping applied to bending stiffness term (KPEb)
dmp_c=(etav*omega+etah/sqrt(1+etah^2)); % internal damping applied to circulation matrix term (Kc)
K_EOM_GN=dmp_b*KPEb+KPEs+KPEa+dmp_c*Kc; % Greenhill/Nelson Eq 22 (includes correction for missing Ks term)

%% % ---- check for Euler Beam with no int damping (Nelson/McVaugh Eq 19 = EOM_GN less Timoshenko & int damping)
% turn off Timoshenko by Lamz=0
% turn off internal damping by etah=etav=0
% K_EOM_GN = K_matrix as stated in Greenhill Nelson Eq 22, K_matrix = as developed by above Lagrangian method
% --- Check K_matrix built via Lagrangian EOM method here against EOM in papers
disp('##### EULER-BERNOULLI BEAM WITHOUT INTERNAL DAMPING #####')
disp('--- turn shear and damping coefficients in derived EOM to "0"')
disp('--- compare derived EOM to EOM published in Nelson/McVaugh (should be [zeros] if ok)')
disp('----- compare derived M-matrix to M-matrix published in Nelson/McVaugh (should be [zeros] if ok)')
Mt_NM=[156 0 0 22*L 54 0 0 -13*L;
        0 156 -22*L 0 0 54 13*L 0;
        0 -22*L 4*L^2 0 0 -13*L -3*L^2 0;
        22*L 0 0 4*L^2 13*L 0 0 -3*L^2];

```

```

54 0 0 13*L 156 0 0 -22*L;
0 54 -13*L 0 0 156 22*L 0;
0 13*L -3*L^2 0 0 22*L 4*L^2 0;
-13*L 0 0 -3*L^2 -22*L 0 0 4*L^2];
Mt_NM=Mt_NM*(mu*L/420);
Mr_NM=[36 0 0 3*L -36 0 0 3*L;
0 36 -3*L 0 0 -36 -3*L 0;
0 -3*L 4*L^2 0 0 3*L -L^2 0;
3*L 0 0 4*L^2 -3*L 0 0 -L^2;
-36 0 0 -3*L 36 0 0 -3*L;
0 -36 3*L 0 0 36 3*L 0;
0 -3*L -L^2 0 0 3*L 4*L^2 0;
3*L 0 0 -L^2 -3*L 0 0 4*L^2];
Mr_NM=mu*r^2/(120*L)*Mr_NM;
Mr_NM=subs(Mr_NM,A*rho,mu);
M_matrix_NM=subs(M_matrix,[Lamz Jt],[0 mu*r^2/4]); %assumes Nelson/McVaugh use Jt=mu*r^2/4 'per length'
M_check_NM=M_matrix_NM-Mt_NM-Mr_NM % 'correct' Jt=mass*(r^2/4+L^2/12)
disp(' ----- compare derived G-matrix to G-matrix published in Nelson/McVaugh (should be [zeros] if ok)')
G_NM=[0 -36 3*L 0 0 36 3*L 0;
36 0 0 3*L -36 0 0 3*L;
-3*L 0 0 -4*L^2 3*L 0 0 L^2;
0 -3*L 4*L^2 0 0 3*L -L^2 0;
0 36 -3*L 0 0 -36 -3*L 0;
-36 0 0 -3*L 36 0 0 -3*L;
-3*L 0 0 L^2 3*L 0 0 -4*L^2;
0 -3*L -L^2 0 0 3*L 4*L^2 0];
G_NM=(-1)*G_NM*2*mu*r^2/(120*L); % inverse because Nelson/McVaugh EOM subtracts 'G', this code adds
C_matrix_NM=subs(C_matrix,[Lamz etav Jp],[0 0 mu*r^2/2]); %assumes Nel./McVaugh use Jp=mu*r^2/2 'per length'
C_matrix_NM=C_matrix_NM/omega; % comparison of matrices directly - omega factored out in paper G_NM
C_check_NM=C_matrix_NM-G_NM
disp(' ----- compare derived K-matrix to K-matrix published in Nelson/McVaugh (should be [zeros] if ok)')
K_EOM_GN_EBND=subs(K_EOM_GN,[etah etav Lamz],[0 0 0]);
K_matrix_EBND=subs(K_matrix,[etah etav Lamz (L^2*phi+L^2)^2],[0 0 0 (L^4*(1+phi)^2)]);
K_check_EBND=K_EOM_GN_EBND-K_matrix_EBND %- should be K_check=[zeros] if ok
% --- Check K_matrix components vs published matrices in paper
disp(' ----- compare derived K-matrix to K-matrix published in Nelson/McVaugh (should be [zeros] if ok)')
Kb_NM=[12 0 0 6*L -12 0 0 6*L;
0 12 -6*L 0 0 -12 -6*L 0;
0 -6*L 4*L^2 0 0 6*L 2*L^2 0;
6*L 0 0 4*L^2 -6*L 0 0 2*L^2;
-12 0 0 -6*L 12 0 0 -6*L;
0 -12 6*L 0 0 12 6*L 0;
0 -6*L 2*L^2 0 0 6*L 4*L^2 0;
6*L 0 0 2*L^2 -6*L 0 0 4*L^2];
Kb_NM=Kb_NM*(E*I/L^3);
Ka_NM=[36 0 0 3*L -36 0 0 3*L;
0 36 -3*L 0 0 -36 -3*L 0;
0 -3*L 4*L^2 0 0 3*L -L^2 0;
3*L 0 0 4*L^2 -3*L 0 0 -L^2;
-36 0 0 -3*L 36 0 0 -3*L;
0 -36 3*L 0 0 36 3*L 0;
0 -3*L -L^2 0 0 3*L 4*L^2 0;
3*L 0 0 -L^2 -3*L 0 0 4*L^2];
Ka_NM=Ka_NM*(P/(30*L));
K_matrix_b=K_matrix-KPEa;
K_matrix_b=subs(K_matrix_b,[etah etav],[0 0]);

```

```

K_matrix_b=subs(K_matrix_b,12*E*I/(k*G*A*L^2),phi);
K_matrix_b=subs(K_matrix_b,E*I/(k*G*A),Lamz);
K_matrix_b=subs(K_matrix_b,Lamz,0);
K_matrix_b=subs(K_matrix_b,phi,0);
Kb_NM_check=Kb_NM-simplify(K_matrix_b) %should be [zeros] if ok
Ka_NM_check=Ka_NM-sub(KPEa,[etah etav Lamz],[0 0 0]) %should be [zeros] if ok
% #####
% # K-matrix correct (30Dec2017) per Nelson/McVaugh for Euler Beam with No Internal Damping
% #####
% note Nelson/McVaugh Eq 19 shows Ka as 'neg' term - should be pos
% correctness of 'pos' confirmed here via derivation (LaGrangian) and vs Greenhill/Nelson Eq22

%% % ---- check for Euler Beam with int damping (Zorzi/Nelson Eq 15 = EOM_GN less Timoshenko)
% turn off Timoshenko by Lamz=0,phi=0
% turn on internal damping by leaving etah, etav as is
% K_EOM_GN = K_matrix as stated in Greenhill Nelson Eq 22, K_matrix = as developed by above Lagrangian method
% --- Check K_matrix built via Lagrangian EOM method here against EOM in papers
disp('##### EULER-BERNOULLI BEAM WITH INTERNAL DAMPING #####')
disp('--- turn shear coefficients in derived EOM to "0"')
disp('----- compare derived M-matrix to M-matrix published in Zorzi/Nelson (should be [zeros] if ok)')
Mt_ZN=[156 0 0 22*L 54 0 0 -13*L;
0 156 -22*L 0 0 54 13*L 0;
0 -22*L 4*L^2 0 0 -13*L -3*L^2 0;
22*L 0 0 4*L^2 13*L 0 0 -3*L^2;
54 0 0 13*L 156 0 0 -22*L;
0 54 -13*L 0 0 156 22*L 0;
0 13*L -3*L^2 0 0 22*L 4*L^2 0;
-13*L 0 0 -3*L^2 -22*L 0 0 4*L^2];
Mt_ZN=Mt_ZN*(mu*L/420);
Mr_ZN=[36 0 0 3*L -36 0 0 3*L;
0 36 -3*L 0 0 -36 -3*L 0;
0 -3*L 4*L^2 0 0 3*L -L^2 0;
3*L 0 0 4*L^2 -3*L 0 0 -L^2;
-36 0 0 -3*L 36 0 0 -3*L;
0 -36 3*L 0 0 36 3*L 0;
0 -3*L -L^2 0 0 3*L 4*L^2 0;
3*L 0 0 -L^2 -3*L 0 0 4*L^2];
Mr_ZN=mu*r^2/(120*L)*Mr_ZN;
Mr_ZN=subs(Mr_ZN,A*rho,mu);
M_matrix_ZN=subs(M_matrix,[Lamz Jt],[0 mu*r^2/4]); %assumes Nelson/McVaugh use Jt=mu*r^2/4 'per length'
M_check_ZN=M_matrix_ZN-Mt_ZN-Mr_ZN %'correct' Jt=mass*(r^2/4+L^2/12)
disp('----- compare derived G-matrix to G-matrix published in Zorzi/Nelson (should be [zeros] if ok)')
G_ZN=[0 -36 3*L 0 0 36 3*L 0;
36 0 0 3*L -36 0 0 3*L;
-3*L 0 0 -4*L^2 3*L 0 0 L^2;
0 -3*L 4*L^2 0 0 3*L -L^2 0;
0 36 -3*L 0 0 -36 -3*L 0;
-36 0 0 -3*L 36 0 0 -3*L;
-3*L 0 0 L^2 3*L 0 0 -4*L^2;
0 -3*L -L^2 0 0 3*L 4*L^2 0];
G_ZN=(-1)*G_ZN*2*mu*r^2/(120*L); % inverse because Nelson/McVaugh EOM subtracts 'G', this code adds
C_matrix_ZN=subs(C_matrix,[Lamz etav Jp],[0 0 mu*r^2/2]); %assumes Nel./McVaugh use Jp=mu*r^2/2 'per length'
C_matrix_ZN=C_matrix_ZN/omega; % omega factored out for matrix comparison in paper
C_check_ZN=C_matrix_ZN-G_ZN
disp('--- compare derived EOM to EOM published in Zorzi/Nelson (should be [zeros] if ok)')
% convert K_EOM_GN to function of Lamz

```

```

temp=subs(K_EOM_GN,(E*/(A*G*k)),Lamz);
temp=subs(temp,[Lamz phi],[0 0]); % no shear deformation for EB beam
K_EOM_GN_EBwithD=simplify(expand(temp)); %subs(temp,[Lamz phi],[0 0]);
% convert K_matrix to function of Lamz & phi
temp=subs(K_matrix,(E*/(A*G*k)),Lamz);
K_matrix_EBwithD=simplify(expand(subs(temp,[Lamz phi],[0 0])));
K_check_EBwithD=K_EOM_GN_EBwithD-K_matrix_EBwithD %- should be K_check=[zeros] if ok
% #####
% # K-matrix correct (01Jan2018) per Zorzi/Nelson for Euler Beam with Internal Damping
% NOTE: Kc*eta2 needs to be manually added to make this check (Euler with damping) be correct
% reason is not yet understood.
% #####
disp(' ----- compare derived K-matrix to K-matrix published in Zorzi/Nelson (should be [zeros] if ok)')
% --- Check K_matrix components vs published matrices in paper
Kb_ZN=[12 0 0 6*L -12 0 0 6*L;
0 12 -6*L 0 0 -12 -6*L 0;
0 -6*L 4*L^2 0 0 6*L 2*L^2 0;
6*L 0 0 4*L^2 -6*L 0 0 2*L^2;
-12 0 0 -6*L 12 0 0 -6*L;
0 -12 6*L 0 0 12 6*L 0;
0 -6*L 2*L^2 0 0 6*L 4*L^2 0;
6*L 0 0 2*L^2 -6*L 0 0 4*L^2];
Ka_ZN=[36 0 0 3*L -36 0 0 3*L;
0 36 -3*L 0 0 -36 -3*L 0;
0 -3*L 4*L^2 0 0 3*L -L^2 0;
3*L 0 0 4*L^2 -3*L 0 0 -L^2;
-36 0 0 -3*L 36 0 0 -3*L;
0 -36 3*L 0 0 36 3*L 0;
0 -3*L -L^2 0 0 3*L 4*L^2 0;
3*L 0 0 -L^2 -3*L 0 0 4*L^2];
Kc_ZN=[0 12 -6*L 0 0 -12 -6*L 0;
-12 0 0 -6*L 12 0 0 -6*L;
6*L 0 0 4*L^2 -6*L 0 0 2*L^2;
% 0 6*L -4*L^2 0 0 -6*L 2*L^2 0;
0 6*L -4*L^2 0 0 -6*L -2*L^2 0; % typo in Zorzi/Nelson, Kc(4,7)=-2L^2, not +2L^2
0 -12 6*L 0 0 12 6*L 0;
% 12 0 0 6*L -12 0 0 -6*L;
12 0 0 6*L -12 0 0 6*L; % typo in Zorzi/Nelson, Kc(6,8)=+6L, not -6L
% 6*L 0 0 -2*L^2 -6*L 0 0 4*L^2; % typo in Zorzi/Nelson, Kc(7,4)=+2L^2, not -2L^2
6*L 0 0 2*L^2 -6*L 0 0 4*L^2; % typo in Zorzi/Nelson, Kc(7,4)=+2L^2, not -2L^2
% 0 6*L -2*L^2 0 0 6*L -4*L^2 0];
0 6*L -2*L^2 0 0 -6*L -4*L^2 0]; % typo in Zorzi/Nelson, Kc(8,6)=-6L, not +6L
% convert KPEb to function of phi
KPEb_temp=subs(KPEb,(E*/(A*G*k)),Lamz);
KPEb_temp=subs(KPEb_temp,Lamz,0);
KPEa_temp=subs(KPEa,Lamz,0);
Kb_ZN_check=Kb_ZN-sub(KPEb_temp,Lamz,0)/(E*/L^3) %should be [zeros] if ok
Ka_ZN_check=Ka_ZN-sub(KPEa,Lamz,0)/(P/(30*L)) %should be [zeros] if ok
Kc_noshear=subs(Kc,E*/(k*G*A),Lamz);
Kc_noshear=subs(Kc_noshear,Lamz,0)/(E*/L^3);
Kc_ZN_check=Kc_ZN-Kc_noshear
% #####
% # K-matrix correct (01Jan2018) per Zorzi/Nelson for Euler Beam With Internal Damping - with apparant typos
% NOTE: sign of (7,4), (8,6) and symmetric appears to be reversed in Zorzi/Nelson paper
% correctness of all other terms vs derived matrix above supports this conclusion
% #####

```

```

%% % ---- check for Timoshenko Beam no int damping (Nelson-1980 Eq 11 = EOM_GN less int damping)
% turn on Timoshenko leaving Lamz as is
% turn off internal damping by etah=etav=0
% K_EOM_GN = K_matrix as stated in Greenhill Nelson Eq 22, K_matrix = as developed by above Lagrangian method
% --- Check K_matrix built via Lagrangian EOM method here against EOM in papers
disp('##### TIMOSHENKO BEAM WITHOUT INTERNAL DAMPING #####')
disp(' --- turn damping coefficients in derived EOM to "0"')
disp(' ----- compare derived M-matrix to M-matrix published in Nelson (1980) (should be [zeros] if ok)')
Mto_N=[156 0 0 22*L 54 0 0 -13*L;
0 156 -22*L 0 0 54 13*L 0;
0 -22*L 4*L^2 0 0 -13*L -3*L^2 0;
22*L 0 0 4*L^2 13*L 0 0 -3*L^2;
54 0 0 13*L 156 0 0 -22*L;
0 54 -13*L 0 0 156 22*L 0;
0 13*L -3*L^2 0 0 22*L 4*L^2 0;
-13*L 0 0 -3*L^2 -22*L 0 0 4*L^2];
Mto_N=Mto_N*(mu*L/(420*(1+phi)^2));
Mt1_N=[294 0 0 38.5*L 126 0 0 -31.5*L;
0 294 -38.5*L 0 0 126 31.5*L 0;
0 -38.5*L 7*L^2 0 0 -31.5*L -7*L^2 0;
38.5*L 0 0 7*L^2 31.5*L 0 0 -7*L^2;
126 0 0 31.5*L 294 0 0 -38.5*L;
0 126 -31.5*L 0 0 294 38.5*L 0;
0 31.5*L -7*L^2 0 0 38.5*L 7*L^2 0;
-31.5*L 0 0 -7*L^2 -38.5*L 0 0 7*L^2];
Mt1_N=Mt1_N*(mu*L/(420*(1+phi)^2));
Mt2_N=[140 0 0 17.5*L 70 0 0 -17.5*L;
0 140 -17.5*L 0 0 70 17.5*L 0;
0 -17.5*L 3.5*L^2 0 0 -17.5*L -3.5*L^2 0;
17.5*L 0 0 3.5*L^2 15.7*L 0 0 -3.5*L^2;
17.5*L 0 0 3.5*L^2 17.5*L 0 0 -3.5*L^2; %typo in Nelson(1980) Mt_2(4,5)=17.5*L,not 15.7*L
70 0 0 15.7*L 140 0 0 -17.5*L;
70 0 0 17.5*L 140 0 0 -17.5*L; %typo in Nelson(1980) Mt_2(5,4)=17.5*L,not 15.7*L
0 70 -17.5*L 0 0 140 17.5*L 0;
0 17.5*L -3.5*L^2 0 0 17.5*L 3.5*L^2 0;
-17.5*L 0 0 -3.5*L^2 -17.5*L 0 0 3.5*L^2];
Mt2_N=Mt2_N*(mu*L/(420*(1+phi)^2));
Mt_N=Mto_N+phi*Mt1_N+phi^2*Mt2_N;
Mro_N=[36 0 0 3*L -36 0 0 3*L;
0 36 -3*L 0 0 -36 -3*L 0;
0 -3*L 4*L^2 0 0 3*L -L^2 0;
3*L 0 0 4*L^2 -3*L 0 0 -L^2;
-36 0 0 -3*L 36 0 0 -3*L;
0 -36 3*L 0 0 36 3*L 0;
0 -3*L -L^2 0 0 3*L 4*L^2 0;
3*L 0 0 -L^2 -3*L 0 0 4*L^2];
Mro_N=Mro_N*(mu*r^2/(120*L*(1+phi)^2));
Mr1_N=[0 0 0 -15*L 0 0 0 -15*L;
0 0 15*L 0 0 0 15*L 0;
0 15*L 5*L^2 0 0 -15*L -5*L^2 0;
-15*L 0 0 5*L^2 15*L 0 0 -5*L^2;
0 0 0 15*L 0 0 5 15*L;
0 0 0 15*L 0 0 15*L; %typo in Nelson (1980), MR1_N(5,7)=0, not 5
0 0 -15*L 0 0 0 -15*L 0;
0 15*L -5*L^2 0 5 -15*L 5*L^2 0; %typo in Nelson (1980), MR1_N(7,5)=0, not 5

```

```

0 15*L -5*L^2 0 0 -15*L 5*L^2 0;
-15*L 0 0 -5*L^2 15*L 0 0 5*L^2];
Mr1_N=Mr1_N*(mu*r^2/(120*L*(1+phi)^2));
Mr2_N=[0 0 0 0 0 0 0;
0 0 0 0 0 0 0;
0 0 10*L^2 0 0 0 5*L^2 0;
0 0 0 10*L^2 0 0 0 5*L^2;
0 0 0 0 0 0 0;
0 0 0 0 0 0 0;
0 0 5*L^2 0 0 0 10*L^2 0;
0 0 0 5*L^2 0 0 0 10*L^2];
Mr2_N=Mr2_N*(mu*r^2/(120*L*(1+phi)^2));
Mr_N=Mro_N+phi*Mr1_N+phi^2*Mr2_N;
M_N=simplify(expand(Mt_N+Mr_N));
% Mr_N=subs(Mr_N,A*rho,mu);
M_matrix_N=subs(M_matrix,[Lamz Jt],[phi*L^2/12 mu*r^2/4]); %assumes ref use Jt=mu*r^2/4 'per length'
M_matrix_N=subs(M_matrix_N,(L^2*phi+L^2)^2,L^4*(1+phi)^2); %assumes ref use Jt=mu*r^2/4 'per length'
M_matrix_N=simplify(expand(M_matrix_N));
M_check_N=simplify(M_matrix_N-M_N) % 'correct' Jt=mass*(r^2/4+L^2/12)
disp(' ----- compare derived G-matrix to G-matrix published in Nelson (1980) (should be [zeros] if ok)')
Go_N=[0 -36 3*L 0 0 36 3*L 0;
36 0 0 3*L -36 0 0 3*L;
-3*L 0 0 -4*L^2 3*L 0 0 L^2;
0 -3*L 4*L^2 0 0 3*L -L^2 0;
0 36 -3*L 0 0 -36 -3*L 0;
-36 0 0 -3*L 36 0 0 -3*L;
-3*L 0 0 L^2 3*L 0 0 -4*L^2;
0 -3*L -L^2 0 0 3*L 4*L^2 0];
Go_N=Go_N*(2*mu*r^2/(120*L*(1+phi)^2)); %typo in Nelson (1980), Go_N should include (1+phi)^ in divisor...
G1_N=[0 0 -15*L 0 0 0 -15*L 0; % .... due to shape function
0 0 0 -15*L 0 0 0 -15*L;
15*L 0 0 -5*L^2 -15*L 0 0 5*L^2;
0 15*L 5*L^2 0 0 -15*L -5*L^2 0;
0 0 15*L 0 0 0 15*L 0;
0 0 0 15*L 0 0 0 15*L;
15*L 0 0 5*L^2 -15*L 0 0 -5*L^2;
0 15*L -5*L^2 0 0 -15*L 5*L^2 0];
G1_N=G1_N*(2*mu*r^2/(120*L*(1+phi)^2)); %typo in Nelson (1980), Go_N should include (1+phi)^ in divisor...
G2_N=[0 0 0 0 0 0 0; % .... due to shape function
0 0 0 0 0 0 0;
0 0 0 -10*L^2 0 0 0 -5*L^2;
0 0 10*L^2 0 0 0 5*L^2 0;
0 0 0 0 0 0 0;
0 0 0 0 0 0 0;
0 0 0 -5*L^2 0 0 0 -10*L^2;
0 0 5*L^2 0 0 0 10*L^2 0];
G2_N=G2_N*(2*mu*r^2/(120*L*(1+phi)^2)); %typo in Nelson (1980), Go_N should include (1+phi)^ in divisor...
G_N=Go_N+phi*G1_N+phi^2*G2_N; % .... due to shape function
G_N=(-1)*simplify(expand(G_N)); % inverse because Nelson/McVaugh EOM subtracts 'G', this code adds
C_matrix_N=subs(C_matrix,[Lamz etav Jp],[phi*L^2/12 0 mu*r^2/2]); %assumes ref use Jp=mu*r^2/2 'per length'
C_matrix_N=subs(C_matrix_N,(L^2+phi*L^2)^2,L^4*(1+phi)^2);
C_matrix_N=simplify(expand(C_matrix_N))/omega; % omega factored out for direct matrix comparison in paper
C_check_N=C_matrix_N-G_N
disp(' --- compare derived EOM to EOM published in Nelson (1980) (should be [zeros] if ok)')
K_EOM_GN_TimND=subs(K_EOM_GN,[etah etav],[0 0]);
temp=subs(K_EOM_GN_TimND,[12*Lamz A*G*L^2*k A*G*k],[phi*L^2 12*E*I/phi 12*E*I/(phi*L^2)]);

```

```

temp=subs(temp,[Lamz (L^2*phi+L^2)],[phi*L^2/12 L^2*(phi+1)]);
K_matrix_TimND=subs(K_matrix,[etah etav],[0 0]);
K_check_TimND=simplify(expand(K_EOM_GN_TimND-K_matrix_TimND)) %- should be K_check=[zeros] if ok
% #####
% # K-matrix correct (01Jan2018) per Nelson(1980) for Timoshenko Beam Without Internal Damping
% NOTE: sign of (7,4), (8,6) and symmetric appears to be reversed in Zorzi/Nelson paper
% correctness of all other terms vs derived matrix above supports this conclusion
% #####
% --- Check K_matrix components vs published matrices in paper
disp('----- compare derived K-matrix to K-matrix published in Nelson (1980) (should be [zeros] if ok)')
% Stiffness (K+A) per Nelson(1980) confirmed via Przemieniecki (includes typo correction noted below)
PHI=12*E*I/(k*A*G*L^2); % paper pg 794, Nomenclature definition of PHI
Coeff_k=E*I/(L^3*(1+PHI));
Ko_Nelson=[12 0 0 6*L -12 0 0 6*L;
            0 12 -6*L 0 0 -12 -6*L 0;
            0 -6*L 4*L^2 0 0 6*L 2*L^2 0;
            6*L 0 0 4*L^2 -6*L 0 0 2*L^2;
            -12 0 0 -6*L 12 0 0 -6*L;
            0 -12 6*L 0 0 12 6*L 0;
            0 -6*L 2*L^2 0 0 6*L 4*L^2 0;
            6*L 0 0 2*L^2 -6*L 0 0 4*L^2];
Ko_Nelson=Coeff_k*Ko_Nelson;
K1_Nelson=[0 0 0 0 0 0 0 0;
            0 0 0 0 0 0 0 0;
            0 0 L^2 0 0 0 -L^2 0;
            0 0 0 L^2 0 0 0 -L^2;
            0 0 0 0 0 0 0 0;
            0 0 0 0 0 0 0 0;
            0 0 -L^2 0 0 0 L^2 0;
            0 0 0 -L^2 0 0 0 L^2];
K1_Nelson=Coeff_k*K1_Nelson;
Coeff_a=P/(30*L*(1+PHI)^2);
% Ao_Nelson=[36 0 0 3 -36 0 0 3*L; % typo in Nelson(1980)
Ao_Nelson=[36 0 0 3*L -36 0 0 3*L; % typo correction - confirmed via Przemieniecki below
            0 36 -3*L 0 0 -36 -3*L 0;
            0 -3*L 4*L^2 0 0 3*L -L^2 0;
% 3 0 0 4*L^2 -3*L 0 0 -L^2; % typo in Nelson(1980)
            3*L 0 0 4*L^2 -3*L 0 0 -L^2; % typo correction - confirmed via Przemieniecki below
            -36 0 0 -3*L 36 0 0 -3*L;
            0 -36 3*L 0 0 36 3*L 0;
            0 -3*L -L^2 0 0 3*L 4*L^2 0;
            3*L 0 0 -L^2 -3*L 0 0 4*L^2];
Ao_Nelson=Coeff_a*Ao_Nelson;
A1_Nelson=[60 0 0 0 -60 0 0 0;
            0 60 0 0 0 -60 0 0;
            0 0 5*L^2 0 0 0 -5*L^2 0;
            0 0 0 5*L^2 0 0 0 -5*L^2;
            -60 0 0 0 60 0 0 0;
            0 -60 0 0 0 60 0 0;
            0 0 -5*L^2 0 0 0 5*L^2 0;
            0 0 0 -5*L^2 0 0 0 5*L^2];
A1_Nelson=Coeff_a*A1_Nelson;
A2_Nelson=[30 0 0 0 -30 0 0 0;
            0 30 0 0 0 -30 0 0;
            0 0 2.5*L^2 0 0 0 -2.5*L^2 0;
            0 0 0 2.5*L^2 0 0 0 -2.5*L^2];

```

```

-30 0 0 0 30 0 0 0;
0 -30 0 0 0 30 0 0;
0 0 -2.5*L^2 0 0 0 2.5*L^2 0;
0 0 0 -2.5*L^2 0 0 0 2.5*L^2);
A2_Nelson=Coeff_a*A2_Nelson;
%
#####
K_Nelson=Ko_Nelson+PHI*K1_Nelson; % paper Eq 12a, correlates to KPEb+KPEs above w/ etah=0
A_Nelson=Ao_Nelson+PHI*A1_Nelson+PHI^2*A2_Nelson; % paper Eq 12e, correlates to KPEa per above
K_Nelson=K_Nelson+A_Nelson; % all stiffness terms per EOM (paper, Eq 11, 12a, 12e)
% K_Nelson confirmed via Przemieniecki, Eq5.116, pg 79 - includes 'K' and 'A' parts !!
%
#####
% check Nelson(1980-corrected) to derived per Lagrangian without shear term or damping (sub-check)
disp(' ----- .... first without shear term (should be [zeros] if ok)')
K_Nelson_ns=Ko_Nelson/Coeff_k*(E*I/L^3)+Ao_Nelson/Coeff_a*(P/(30*L));
% convert K_matrix to function of phi
K_matrix_ns=subs(K_matrix,(12*E*I/(A*G*L^2*k)),phi);
K_matrix_ns=subs(K_matrix_ns,144*E^2*I^2/(A*G*L^5*k),phi*12*E*I/L^3);
K_matrix_ns=subs(K_matrix_ns,-144*E^2*I^2/(A*G*L^5*k),-phi*12*E*I/L^3);
K_matrix_ns=subs(K_matrix_ns,(-12*E^2*I^2/(A*G*L^3*k)),-phi*E*I/L);
K_matrix_ns=subs(K_matrix_ns,[Lamz phi etah],[0 0 0]);
K_Nelson_check_ns=K_Nelson_ns-K_matrix_ns % CHECKS WITHOUT SHEAR/DAMPING - 01Jan2018 5:04 PM
disp(' ----- .... second including shear term (should be [zeros] if ok)')
K_matrix_shear=subs(K_matrix,Lamz,(E*I/(k*G*A))); % subs per Bazoune/Khulief (2002),Eq 35
K_matrix_shear=subs(K_matrix_shear,[etah etah],[0 0]); % turn internal damping 'off' by etah=etah=0
% convert K_EOM_shear to function of phi
K_matrix_shear=subs(K_matrix_shear,(12*E*I/(A*G*k)),phi*L^2);
K_matrix_shear=subs(K_matrix_shear,144*E^2*I^2/(A*G*L^5*k),phi*12*E*I/L^3);
K_matrix_shear=subs(K_matrix_shear,A*G*L^2*k,12*E*I/phi);
K_matrix_shear=subs(K_matrix_shear,P,0);
K_matrix_shear=subs(K_matrix_shear,E*I/(A*G*k),Lamz);
K_matrix_shear=subs(K_matrix_shear,Lamz,phi*L^2/12);
K_matrix_shear=subs(K_matrix_shear,(L^2*phi+L^2),(L^2*(1+phi)));
K_matrix_shear=expand(simplify(K_matrix_shear));
% convert K_Nelson to function of phi
K_Nelson=subs(K_Nelson,P,0);
K_Nelson=subs(K_Nelson,(12*E*I/(A*G*L^2*k)),phi);
% compare K_matrix derived with shear to Nelson (1980) paper
Kb_N_check=K_matrix_shear-K_Nelson;
Kb_N_check=simplify(expand(Kb_N_check));
Kb_N_check=subs(Kb_N_check,A*G*L^2*k,(12*E*I/phi))
% check Axial Stiffness Nelson(1980-corrected) to derived per Lagrangian k)
disp(' ----- check K-axial including shear term (should be [zeros] if ok)')
K_matrix_axial=K_matrix-sub(K_matrix,P,0);
K_matrix_axial=subs(K_matrix_axial,Lamz,phi*L^2/12);
K_matrix_axial=simplify(expand(subs(K_matrix_axial,(L^2*phi+L^2),L^2*(1+phi))));
A_Nelson=simplify(expand(subs(A_Nelson,[A*G*L^2*k 2*A*G*L^2*k],[12*E*I/phi 2*12*E*I/phi]]));
A_Nelson=simplify(expand(subs(A_Nelson,A*G*L*k,12*E*I/(phi*L]]));
Ka_N_check=K_matrix_axial-A_Nelson

%%
disp('----- end -----')

```


Appendix F

EOM Matrix Integration, Linearly Varying Geometry – MATLAB Source Code

```

% Program 'Inertia_Calcs_Conic_Beam_27Feb.m'
clc;clearvars;close all;close hidden; close force
syms ri rj Ri Rj Le r R z dz M Rad Rout Rin rho
% References
% 1) Vector Mechanics for Engineers, Beer & Johnston, 3rd edition
% Mass and Polar MMOI
R=(Rj-Ri)/Le*z+Ri;
r=(rj-ri)/Le*z+ri;
% Area=int(2*pi*Rad,Rad,r,R);
Area=int(pi*Rad^2,Rad,r,R);
% Vol=int(Area,z,0,Le);
dV=pi*(R^2-r^2);
Vol=int(dV,z,0,Le);
Mass=Vol*rho;
dly=pi*rho/4*(R^4-r^4);
lp=int(2*dly,z,0,Le) % confirmed against closed form eqtns for solid pyramid
% It about lyy,lzz thru cg
% find lyy, lzz thru node i
dly_end=dly+z^2*rho*dV;
lt_end=int(dly_end,z,0,Le) % confirmed against closed form eqtns for solid pyramid
% find cg from node i
xbar=int(dV*z,z,0,Le)/Vol % confirmed against closed form eqtns for solid pyramid
% by parallel axis theorem, dlx=dlxcg+dm*z^2 therefore dlxcg=dlx-dm*z^2
lt=lt_end-Mass*xbar^2 % confirmed against closed form eqtns for solid pyramid
% numerically check the equations against Creo results
% input parameters
iiri=[0;0;.01;0;.01;.01;.01;.01];
iirj=[0;0;0;0.01;0.01;0.01;0;0.02];
iiRi=[0.052;0.025;0.025;0.025;0.025;0.052;0.052;0.052];
iiRj=[0.052;0.052;0.052;0.052;0.052;0.052;0.025;0.052];
% [ri rj Ri Rj] % for visualization
for ii=1:length(iiri)
my_mass(ii)=double(subs(Mass,[Le rho ri rj Ri Rj],[0.250 0.283 iiri(ii) iirj(ii) iiRi(ii) iiRj(ii)]));
my_lp(ii)=double(subs(lp,[Le rho ri rj Ri Rj],[0.250 0.283 iiri(ii) iirj(ii) iiRi(ii) iiRj(ii)]));
my_lt(ii)=double(subs(lt,[Le rho ri rj Ri Rj],[0.250 0.283 iiri(ii) iirj(ii) iiRi(ii) iiRj(ii)]));
end
output=[my_mass.' my_lp.' my_lt.'];

```

```

=====

% Program 'Matrix_Integration_27Feb2019.m'
clc;clearvars;close all; close force;close hidden;
syms Ri Rj ri rj Le s rho Ee k Ge Lamz etav etah omega P eta A I Vol Jp Jt
% *****
% Integrate Matrix input functions to account for tapered beam element.
% Matrix Cell components directly from 'EOM_derivation_01Sep.m'
% Integrated 'output' cell components are input to 'Rotor_FEA_Matrix_Fun_2018.m'
% *****
% --- Geometry Parameters - input
% % Greenhill (1985), replace 'rho' with 'delta' to separate from density
% delta=rj/ri; sigma=Rj/Ri;
% alpha1=2*(Ri^2*(sigma-1)-ri^2*(delta-1))/(Ri^2-ri^2);
% alpha2=(Ri^2*(sigma-1)^2-ri^2*(delta-1)^2)/(Ri^2-ri^2);
% delta1=4*(Ri^4*(sigma-1)-ri^4*(delta-1))/(Ri^4-ri^4);
% delta2=6*(Ri^4*(sigma-1)^2-ri^4*(delta-1)^2)/(Ri^4-ri^4);
% delta3=4*(Ri^4*(sigma-1)^3-ri^4*(delta-1)^3)/(Ri^4-ri^4);

```

```

% delta4=(Ri^4*(sigma-1)^4-ri^4*(delta-1)^4)/(Ri^4-ri^4);
% Ai=pi*(Ri^2-ri^2); li=pi*(Ri^4-ri^4)/4;
% dA=Ai*(1+alpha*eta+alpha^2*eta^2); dl=li*(1+delta*eta+delta^2*eta^2+delta^3*eta^3+delta^4*eta^4);
% A=int(dA,eta,0,1); l=int(dl,eta,0,1);
% Vol=(Le*pi*(Ri^2 + Ri*Rj + Rj^2 - ri^2 - ri*rj - rj^2))/3; %see Inertia_Calcs_27Feb.m for dev/confirm.
% Jp=-(Le*rho*pi*(- Ri^4 - Ri^3*Rj -... % MMOI-polar=f(varying radii) see Inertia_Calcs_27Feb.m for dev/confirm.
% Ri^2*Rj^2 - Ri*Rj^3 - Rj^4 + ri^4 + ri^3*rj + ri^2*rj^2 + ri*rj^3 + rj^4))/10;
% Jt=(pi*Le*Ri^4*rho)/20 + (pi*... % MMOI-transverse=f(varying radii) see Inertia_Calcs_27Feb.m for dev/confirm
% Le*Rj^4*rho)/20-(pi*Le*rho*ri^4)/20-(pi*Le*rho*rj^4)/20+(pi*Le^3*Ri^2*rho)/30+(pi*Le^3*Rj^2*rho)/5-(pi*...
% Le^3*rho*ri^2)/30-(pi*Le^3*rho*rj^2)/5-(pi*Le*rho*ri^2*rj^2)/20+(pi*Le*Ri*Rj^3*rho)/20+(pi*Le*Ri^3*Rj*...
% rho)/20+(pi*Le^3*Ri*Rj*rho)/10-(pi*Le*rho*ri*rj^3)/20-(pi*Le*rho*ri^3*rj)/20-(pi*Le^3*rho*ri*rj)/10-(Le^3*...
% rho*pi*(Ri^2 + 2*Ri*Rj+3*Rj^2-ri^2-2*ri*rj-3*rj^2)^2)/(48*(Ri^2+Ri*Rj+Rj^2-ri^2-ri*rj-rj^2))+pi*Le*Ri^2*...
% Rj^2*rho)/20;
% -----
% Above geometric properties (A,l,Jp,Jt) are correct as noted and should be input to the equations for M,C,K from
% 'EOM_Derivation' directly. However, the simplification of the equations (eg. K11 with Lamz^2, etc) seems to
% cause a problem with the accuracy of the MATLAB solver. Therefore, transfer the matrix equations below (M11,
% etc.) directly to the FEA_Matrix assembly routine and include numerical values for geometry props (A,l,Jp,Jt) per
% the equations above. Therefore, for equation derivation below, these equations are suppressed above and should be
% incorporated in the FEA_Matrix assembly routine.
% -----
% Mass Matrix
M11=(6*Jt*Le^3)/(5*(Le^2+12*Lamz)^2)+(Vol*rho*(13*Le^4+294*Le^2*Lamz+1680*Lamz^2))/(35*(Le^2+12*Lamz)^2);
M41=(Vol*Le*rho*(11*Le^4+231*Le^2*Lamz+1260*Lamz^2))/(210*(Le^2+12*Lamz)^2)-(Jt*Le^2*(-Le^2+60*Lamz))/(10*...
(Le^2+12*Lamz)^2);
M51=(3*Vol*rho*(3*Le^4+84*Le^2*Lamz+560*Lamz^2))/(70*(Le^2+12*Lamz)^2)-(6*Jt*Le^3)/(5*(Le^2+12*Lamz)^2);
M81=-(Jt*Le^2*(-Le^2+60*Lamz))/(10*(Le^2+12*Lamz)^2)-(Vol*Le*rho*(13*Le^4+378*Le^2*Lamz+2520*Lamz^2))/(420*...
(Le^2+12*Lamz)^2);
M32=+(Jt*Le^2*(-Le^2+60*Lamz))/(10*(Le^2+12*Lamz)^2)-(Vol*Le*rho*(11*Le^4+231*Le^2*Lamz+1260*Lamz^2))/(210*...
(Le^2+12*Lamz)^2);
M33=(Vol*Le^2*rho)/120+(2*Jt*Le*(Le^4+15*Le^2*Lamz+360*Lamz^2))/(15*(Le^2+12*Lamz)^2)+(Vol*Le^6*rho)/(840*...
(Le^2+12*Lamz)^2);
M73=(Vol*Le^6*rho)/(840*(Le^2+12*Lamz)^2)-(Jt*Le*(Le^4+60*Le^2*Lamz-720*Lamz^2))/(30*(Le^2+12*Lamz)^2)-(Vol*...
Le^2*rho)/120;
% 'EOM_derivation_01Sep.m' created with assumption that Jt & Jp are 'per unit length' therefore need
% to modify here so that 'Jt' is 'per full length' rather than unit length for use in the actual code since it
% calculates Jt & Jp 'per full length'.
M11=simplify(subs(M11,Jt,Jt/Le))
M41=simplify(subs(M41,Jt,Jt/Le))
M51=simplify(subs(M51,Jt,Jt/Le))
M81=simplify(subs(M81,Jt,Jt/Le))
M32=simplify(subs(M32,Jt,Jt/Le))
M33=simplify(subs(M33,Jt,Jt/Le))
M73=simplify(subs(M73,Jt,Jt/Le))
% -----
% Dissipation Energy Matrix
ED11=(12*Ee*I*Le*etav)/(Le^2+12*Lamz)^2
ED18=(6*Ee*I*Le^2*etav)/(Le^2 + 12*Lamz)^2
ED33=etav*((Ee*I)/Le+(3*Ee*I*Le^3)/(Le^2+12*Lamz)^2)
% -----
% Rotatory Matrix
G61= (6*Jp*Le^3)/(5*(Le^2+12*Lamz)^2)
G13= (Jp*Le^2*(-Le^2+60*Lamz))/(10*(Le^2+12*Lamz)^2)
G83= (Jp*Le*(Le^4+60*Le^2*Lamz-720*Lamz^2))/(30*(Le^2+12*Lamz)^2)
G34= (2*Jp*Le*(Le^4+15*Le^2*Lamz+360*Lamz^2))/(15*(Le^2+12*Lamz)^2)
% -----

```

```

% Stiffness Matrix
K11=P/Le+(Le^3*P)/(5*(Le^2+12*Lamz)^2)+(12*Ee*I*Le*(etah+1))/((etah^2+1)^(1/2)*(Le^2+12*Lamz)^2)+(144*(Vol/Le)*...
Ge*Lamz^2*k)/(Le*(Le^2+12*Lamz)^2)
K33=(Le*P)/12+(Le^5*P)/(20*(Le^2+12*Lamz)^2)+(36*Vol*Ge*Lamz^2*k)/(Le^2+12*Lamz)^2+(4*Ee*I*(etah+1)*(Le^4+6*...
Le^2*Lamz+36*Lamz^2))/(Le*(etah^2+1)^(1/2)*(Le^2+12*Lamz)^2)

K41=(Le^4*P)/(10*(Le^2+12*Lamz)^2)+(Le^2*(6*Ee*I+6*Ee*I*etah))/((etah^2+1)^(1/2)*(Le^4+24*Le^2*Lamz+144*Lamz^2))..
.
+(72*(Vol/Le)*Ge*Lamz^2*k)/(Le^2+12*Lamz)^2
K73=(Le^5*P)/(20*(Le^2+12*Lamz)^2)-(Le*P)/12-(144*Ee*I*Lamz^2-2*Ee*I*Le^4+24*Ee*I*Le^2*Lamz-
2*Ee*I*Le^4*etah+...

144*Ee*I*Lamz^2*etah+24*Ee*I*Le^2*Lamz*etah)/((etah^2+1)^(1/2)*(Le^5+24*Le^3*Lamz+144*Le*Lamz^2)))+(36*Vol*...
Ge*Lamz^2*k)/(Le^2+12*Lamz)^2
K61ttl=(12*Ee*I*Le*(etav*omega+etah/(etah^2+1)^(1/2)))/(Le^2+12*Lamz)^2;
K31ttl=(6*Ee*I*Le^2*(etav*omega + etah/(etah^2 + 1)^(1/2)))/(Le^2 + 12*Lamz)^2;
K83ttl=((Ee*I)/Le-(3*Ee*I*Le^3)/(Le^2+12*Lamz)^2)*(etav*omega+etah/(etah^2+1)^(1/2));
K34ttl=((Ee*I)/Le+(3*Ee*I*Le^3)/(Le^2+12*Lamz)^2)*(etav*omega+etah/(etah^2+1)^(1/2)) ;
% -----
% separate following into terms involving omega and those not (K=Ksub+Kc*omega, Kc=int damping circ matrix, Kc
% also included in Ksub but without reference to omega) - Greenhill Eq 22 et al.
C=coeffs(K61ttl,omega);
K61=simplify(C(1))
K61_dcm=simplify(C(2)) % K61 adds to K-matrix, K61_dcm adds to K_dcm(*omega)
C=coeffs(K31ttl,omega);
K31=simplify(C(1))
K31_dcm=simplify(C(2)) % K31 adds to K-matrix, K31_dcm adds to K_dcm(*omega)
C=coeffs(K83ttl,omega);
K83=simplify(C(1))
K83_dcm=simplify(C(2)) % K83 adds to K-matrix, K83_dcm adds to K_dcm(*omega)
C=coeffs(K34ttl,omega);
K34=simplify(C(1))
K34_dcm=simplify(C(2)) % K34 adds to K-matrix, K34_dcm adds to K_dcm(*omega)
disp('----- end -----')

```

Appendix G
Shape Functions and EOM Matrices

Shape Functions

$$\begin{pmatrix} v(s) \\ w(s) \\ \beta(s) \\ \Gamma(s) \end{pmatrix} = \begin{pmatrix} \psi_{d1} & 0 & 0 & \psi_{d2} & \psi_{d3} & 0 & 0 & \psi_{d4} \\ 0 & \psi_{d1} & -\psi_{d2} & 0 & 0 & \psi_{d31} & -\psi_{d4} & 0 \\ 0 & -\psi_{r1} & \psi_{r2} & 0 & 0 & -\psi_{r3} & \psi_{r4} & 0 \\ \psi_{r1} & 0 & 0 & \psi_{r2} & \psi_{r3} & 0 & 0 & \psi_{r4} \end{pmatrix}$$

where:

$$\psi_{d1} = \bar{\Phi}[-3\varepsilon^2 + 2\varepsilon^3 + 1 + \Phi(1 - \varepsilon)]$$

$$\psi_{d2} = L\bar{\Phi}\left[\varepsilon - 2\varepsilon^2 + \varepsilon^3 + \frac{\Phi}{2}(\varepsilon - \varepsilon^2)\right]$$

$$\psi_{d3} = \bar{\Phi}[3\varepsilon^2 - 2\varepsilon^3 + \Phi\varepsilon]$$

$$\psi_{d4} = L\bar{\Phi}\left[-\varepsilon^2 + \varepsilon^3 + \frac{\Phi}{2}(\varepsilon^2 - \varepsilon)\right]$$

$$\psi_{r1} = \frac{6}{L}\bar{\Phi}[-\varepsilon + \varepsilon^2]$$

$$\psi_{r2} = \bar{\Phi}[3\varepsilon^2 - 4\varepsilon + 1 + \Phi(1 - \varepsilon)]$$

$$\psi_{r3} = \frac{6}{L}\bar{\Phi}[\varepsilon - \varepsilon^2]$$

$$\psi_{r4} = \bar{\Phi}[3\varepsilon^2 - 2\varepsilon + \Phi\varepsilon]$$

$$\Phi = \frac{12\Lambda}{L^2} \quad \text{and} \quad \bar{\Phi} = \frac{1}{1 + \Phi}$$

EOM Matrices

$$M = \begin{bmatrix} M11 & 0 & 0 & M41 & M51 & 0 & 0 & M81 \\ 0 & M11 & M32 & 0 & 0 & M51 & -M81 & 0 \\ 0 & M32 & M33 & 0 & 0 & M81 & M73 & 0 \\ M41 & 0 & 0 & M33 & -M81 & 0 & 0 & M73 \\ M51 & 0 & 0 & -M81 & M11 & 0 & 0 & M32 \\ 0 & M51 & M81 & 0 & 0 & M11 & M11 & 0 \\ 0 & -M81 & M73 & 0 & 0 & M41 & M33 & 0 \\ M81 & 0 & 0 & M73 & M32 & 0 & 0 & M33 \end{bmatrix}$$

$$M11=(6*Jt*Le^2)/(5*(Le^2+12*Lamz)^2)+(Vol*rho*(1680*Lamz^2+294*Lamz*Le^2+13*Le^4))/(35*(Le^2+12*Lamz)^2);$$

$$M41=(Le*Vol*rho*(1260*Lamz^2+231*Lamz*Le^2+11*Le^4))/(210*(Le^2+12*Lamz)^2)-(Jt*Le*(-Le^2+60*Lamz))/(10*(Le^2+12*Lamz)^2);$$

$$M51=(3*Vol*rho*(560*Lamz^2+84*Lamz*Le^2+3*Le^4))/(70*(Le^2+12*Lamz)^2)-(6*Jt*Le^2)/(5*(Le^2+12*Lamz)^2);$$

$$M81=-((Jt*Le*(-Le^2+60*Lamz))/(10*(Le^2+12*Lamz)^2)-(Le*Vol*rho*(2520*Lamz^2+378*Lamz*Le^2+13*Le^4))/(420*(Le^2+12*Lamz)^2));$$

$$M32=(Jt*Le*(-Le^2+60*Lamz))/(10*(Le^2+12*Lamz)^2)-(Le*Vol*rho*(1260*Lamz^2+231*Lamz*Le^2+11*Le^4))/(210*(Le^2+12*Lamz)^2);$$

$$M33=(2*Jt*(360*Lamz^2+15*Lamz*Le^2+Le^4))/(15*(Le^2+12*Lamz)^2)+(Le^2*Vol*rho)/120+(Le^6*Vol*rho)/(840*(Le^2+12*Lamz)^2);$$

$$M73=(Le^6*Vol*rho)/(840*(Le^2+12*Lamz)^2)-(Le^2*Vol*rho)/120-(Jt*(-720*Lamz^2+60*Lamz*Le^2+Le^4))/(30*(Le^2+12*Lamz)^2);$$

$$A=(pi*(Ri^2 + Ri*Rj + Rj^2 - ri^2 - ri*rj - rj^2))/3;$$

$$I=(-(pi*(-Ri^4 - Ri^3*Rj - Ri^2*Rj^2 - Ri*Rj^3 - Rj^4 + ri^4 + ri^3*rj + ri^2*rj^2 + ri*rj^3 + rj^4))/20);$$

$$Lamz=Ee*I/(k*Ge*A);$$

$$Vol=(pi*(-3*Ri^2+3*Rj*Ri+3*ri^2-3*rj*ri))/3+(pi*Le*(3*Ri^2-3*ri^2))/3-(pi*(-Ri^2+2*Ri*Rj-Rj^2+ri^2-2*ri*rj+rj^2))/(3*Le);$$

$$Jp=Le^3*((Ri^2*rho*pi*(Ri-Rj)^2)/Le^4-(rho*ri^2*pi*(ri-rj)^2)/Le^4)+Le^2*((rho*ri^3*pi*(ri-rj))/Le^2-(Ri^3*rho*pi*(Ri-Rj))/Le^2)+Le^4*((rho*ri*pi*(ri-rj)^3)/(2*Le^6)-(Ri*rho*pi*(Ri-Rj)^3)/(2*Le^6))+Le^5*((rho*pi*(Ri-Rj)^4)/(10*Le^8)-(rho*pi*(ri-rj)^4)/(10*Le^8))+Le*((rho*pi*Ri^4)/2-(rho*ri^4*pi)/2);$$

$$Jt=(Le^3*((Ri^2*rho*pi*(Ri-Rj)^2)/Le^4-(rho*ri^2*pi*(ri-rj)^2)/Le^4))/2+(Le^2*((rho*ri^3*pi*(ri-rj))/Le^2-(Ri^3*rho*pi*(Ri-Rj))/Le^2))/2+(Le^4*((rho*ri*pi*(ri-rj)^3)/(2*Le^6)-(Ri*rho*pi*(Ri-Rj)^3)/(2*Le^6))/2+(Le^5*((rho*pi*(Ri-Rj)^4)/(10*Le^8)-(rho*pi*(ri-rj)^4)/(10*Le^8)))/2+(Le*((rho*pi*Ri^4)/2-(rho*ri^4*pi)/2))/2-(Le*rho*pi*(60*Le^4*Ri^4-120*Le^4*Ri^2*ri^2+60*Le^4*ri^4-120*Le^3*Ri^4+120*Le^3*Ri^3*Rj+240*Le^3*Ri^2*ri^2-120*Le^3*Ri^2*ri*rj-120*Le^3*Ri*Rj*ri^2-120*Le^3*ri^4+120*Le^3*ri^3*rj+84*Le^2*Ri^4-168*Le^2*Ri^3*Rj+84*Le^2*Ri^2*Rj^2-168*Le^2*Ri^2*ri^2+168*Le^2*Ri^2*ri*rj-44*Le^2*Ri^2*rj^2+168*Le^2*Ri*Rj*ri^2-80*Le^2*Ri*Rj*ri*rj-44*Le^2*Rj^2*ri^2+84*Le^2*ri^4-168*Le^2*ri^3*rj+84*Le^2*ri^2*rj^2-24*Le*Ri^4+72*Le*Ri^3*Rj-72*Le*Ri^2*Rj^2+48*Le*Ri^2*ri^2-72*Le*Ri^2*ri*rj+24*Le*Ri^2*rj^2+24*Le*Ri*Rj^3-72*Le*Ri*Rj*ri^2+96*Le*Ri*Rj*ri*rj-24*Le*Ri*Rj*rj^2+24*Le*Rj^2*ri^2-24*Le*Rj^2*ri*rj-24*Le*ri^4+72*Le*ri^3*rj-72*Le*ri^2*rj^2+24*Le*ri*rj^3+3*Ri^4-12*Ri^3*Rj+18*Ri^2*Rj^2-6*Ri^2*ri^2+12*Ri^2*ri*rj-6*Ri^2*rj^2-12*Ri*Rj^3+12*Ri*Rj*ri^2-24*Ri*Rj*ri*rj+12*Ri*Rj*rj^2+3*Rj^4-6*Rj^2*ri^2+12*Rj^2*ri*rj-6*Rj^2*rj^2+3*ri^4-12*ri^3*rj+18*ri^2*rj^2-12*ri*rj^3+3*rj^4))/(240*(-3*Le^2*Ri^2+3*Le^2*ri^2+3*Le*Ri^2-3*Le*Ri*Rj-3*Le*ri^2+3*Le*ri*rj-Ri^2+2*Ri*Rj-Rj^2+ri^2-2*ri*rj+rj^2));$$

$$ybar=(-(6*Le^3+8*Le^2-3*Le)*Ri^2+(6*Le-8*Le^2)*Ri*Rj-3*Le*Rj^2+(6*Le^3-8*Le^2+3*Le)*ri^2+(8*Le^2-6*Le)*ri*rj+3*Le*rj^2)/((-12*Le^2+12*Le-4)*Ri^2+(8-12*Le)*Ri*Rj-4*Rj^2+(12*Le^2-12*Le+4)*ri^2+(12*Le-8)*ri*rj+4*rj^2);$$

$$m_props(end,4:end)=[Vol Vol*rho ybar Jt Jp];$$

$$C = [ED] + \Omega[G]$$

$$ED = \begin{bmatrix} ED11 & 0 & 0 & ED18 & -ED11 & 0 & 0 & ED18 \\ 0 & ED11 & -ED18 & 0 & 0 & -ED11 & -ED18 & 0 \\ 0 & -ED18 & ED33 & 0 & 0 & ED18 & -ED33 & 0 \\ ED18 & 0 & 0 & ED33 & -ED18 & 0 & 0 & -ED33 \\ -ED11 & 0 & 0 & -ED18 & ED11 & 0 & 0 & -ED18 \\ 0 & -ED11 & ED18 & 0 & 0 & ED11 & ED18 & 0 \\ 0 & -ED18 & -ED33 & 0 & 0 & ED18 & ED33 & 0 \\ ED18 & 0 & 0 & -ED33 & -ED18 & 0 & 0 & ED33 \end{bmatrix}$$

$$\begin{aligned} ED11 &= (12 * Ee * I * Le * etav) / (Le^2 + 12 * Lamz)^2; \\ ED18 &= (6 * Ee * I * Le^2 * etav) / (Le^2 + 12 * Lamz)^2; \\ ED33 &= etav * ((Ee * I) / Le + (3 * Ee * I * Le^3) / (Le^2 + 12 * Lamz)^2); \end{aligned}$$

$$M = \begin{bmatrix} 0 & G61 & G13 & 0 & 0 & -G61 & G13 & 0 \\ -G61 & 0 & 0 & G13 & G61 & 0 & 0 & G13 \\ -G13 & 0 & 0 & G34 & G13 & 0 & 0 & -G83 \\ 0 & -G13 & -G34 & 0 & 0 & G13 & G83 & 0 \\ 0 & -G61 & -G13 & 0 & 0 & G61 & -G13 & 0 \\ G61 & 0 & 0 & -G13 & -G61 & 0 & 0 & -G13 \\ -G13 & 0 & 0 & -G83 & G13 & 0 & 0 & G34 \\ 0 & -G13 & G83 & 0 & 0 & G13 & -G34 & 0 \end{bmatrix}$$

$$\begin{aligned} G61 &= (6 * Jp * Le^2) / (5 * (Le^2 + 12 * Lamz)^2); \\ G13 &= (Jp * Le * (-Le^2 + 60 * Lamz)) / (10 * (Le^2 + 12 * Lamz)^2); \\ G83 &= (Jp * (-720 * Lamz^2 + 60 * Lamz * Le^2 + Le^4)) / (30 * (Le^2 + 12 * Lamz)^2); \\ G34 &= (2 * Jp * (360 * Lamz^2 + 15 * Lamz * Le^2 + Le^4)) / (15 * (Le^2 + 12 * Lamz)^2); \end{aligned}$$

$$K = [K_{base}] + \Omega[K_{dcmv}]$$

$$K_{base} = \begin{bmatrix} K11 & K61 & -K31 & K41 & -K11 & -K61 & -K31 & K41 \\ -K61 & K11 & -K41 & -K31 & K61 & -K11 & -K41 & -K31 \\ K31 & -K41 & K33 & K34 & -K31 & K41 & K73 & -K83 \\ K41 & K31 & -K34 & K33 & -K41 & -K31 & K83 & K73 \\ -K11 & -K61 & K31 & -K41 & K11 & K61 & K31 & -K41 \\ K61 & -K11 & K41 & K31 & -K61 & K11 & K41 & K31 \\ K31 & -K41 & K73 & -K83 & -K31 & K41 & K33 & K34 \\ K41 & K31 & K83 & K73 & -K41 & -K31 & -K34 & K33 \end{bmatrix}$$

$$\begin{aligned} K11 &= P / Le + (Le^3 * P) / (5 * (Le^2 + 12 * Lamz)^2) + (12 * Ee * I * Le * (etah + 1)) / ((etah^2 + 1)^{1/2} * (Le^2 + 12 * Lamz)^2) + \dots \\ &\quad (144 * Ge * Lamz^2 * Vol * k) / (Le^2 * (Le^2 + 12 * Lamz)^2); \\ K33 &= (Le * P) / 12 + (Le^5 * P) / (20 * (Le^2 + 12 * Lamz)^2) + (36 * Ge * Lamz^2 * Vol * k) / (Le^2 + 12 * Lamz)^2 + (4 * Ee * I * (etah + 1) * \dots \\ &\quad (36 * Lamz^2 + 6 * Lamz * Le^2 + Le^4)) / (Le * (etah^2 + 1)^{1/2} * (Le^2 + 12 * Lamz)^2); \\ K41 &= (Le^4 * P) / (10 * (Le^2 + 12 * Lamz)^2) + (Le^2 * (6 * Ee * I + 6 * Ee * I * etah)) / ((etah^2 + 1)^{1/2} * (144 * Lamz^2 + 24 * Lamz * \dots \\ &\quad Le^2 + Le^4)) + (72 * Ge * Lamz^2 * Vol * k) / (Le * (Le^2 + 12 * Lamz)^2); \\ K73 &= (Le^5 * P) / (20 * (Le^2 + 12 * Lamz)^2) - (Le * P) / 12 - (144 * Ee * I * Lamz^2 - 2 * Ee * I * Le^4 + 24 * Ee * I * Lamz * Le^2 + 144 * Ee * \dots \\ &\quad I * Lamz^2 * etah - 2 * Ee * I * Le^4 * etah + 24 * Ee * I * Lamz * Le^2 * etah) / ((etah^2 + 1)^{1/2} * (144 * Lamz^2 * Le + 24 * Lamz * Le^3 + \dots \\ &\quad Le^5)) + (36 * Ge * Lamz^2 * Vol * k) / (Le^2 + 12 * Lamz)^2); \\ K61 &= (12 * Ee * I * Le * etah) / ((etah^2 + 1)^{1/2} * (Le^2 + 12 * Lamz)^2); \\ K31 &= (6 * Ee * I * Le^2 * etah) / ((etah^2 + 1)^{1/2} * (Le^2 + 12 * Lamz)^2); \\ K83 &= (etah * ((Ee * I) / Le - (3 * Ee * I * Le^3) / (Le^2 + 12 * Lamz)^2)) / (etah^2 + 1)^{1/2}; \\ K34 &= (etah * ((Ee * I) / Le + (3 * Ee * I * Le^3) / (Le^2 + 12 * Lamz)^2)) / (etah^2 + 1)^{1/2}; \end{aligned}$$

$$K_{dcmv} = \begin{bmatrix} 0 & K61_dcm & -K31_dcm & 0 & 0 & -K61_dcm & -K31_dcm & 0 \\ -K61_dcm & 0 & 0 & -K31_dcm & K61_dcm & 0 & 0 & -K31_dcm \\ K31_dcm & 0 & 0 & K34_dcm & -K31_dcm & 0 & 0 & -K83_dcm \\ 0 & K31_dcm & -K34_dcm & 0 & 0 & -K31_dcm & K83_dcm & 0 \\ 0 & -K61_dcm & K31_dcm & 0 & 0 & K61_dcm & K31_dcm & 0 \\ K61_dcm & 0 & 0 & K31_dcm & -K61_dcm & 0 & 0 & K31_dcm \\ K31_dcm & 0 & 0 & -K83_dcm & -K31_dcm & 0 & 0 & K34_dcm \\ 0 & K31_dcm & K83_dcm & 0 & 0 & -K31_dcm & -K34_dcm & 0 \end{bmatrix}$$

$$K61_dcm = (12 * Ee * I * Le * etav) / (Le^2 + 12 * Lamz)^2;$$

$$K31_dcm = (6 * Ee * I * Le^2 * etav) / (Le^2 + 12 * Lamz)^2;$$

$$K83_dcm = etav * ((Ee * I) / Le - (3 * Ee * I * Le^3) / (Le^2 + 12 * Lamz)^2);$$

$$K34_dcm = etav * ((Ee * I) / Le + (3 * Ee * I * Le^3) / (Le^2 + 12 * Lamz)^2);$$

Appendix H

Robustness Evaluation – MATLAB Source Code (Toy Problem)

```

function main
% file = Robustness_Code_Rastrigin_Toy_Pblm.m, 12Jan2020
clc; clear variables; close all; fclose all;
delete(gcf('nocreate')); % stop local the parallel pool
% =====
% Written by Bret Hauser - Dec 2019
% Adviser Bo P. Wang, PhD
% =====
%% ----- Comments for Use -----
% - This code computes a response-equation fit to existing data points based on design space center point and +/-
%   tolerances of each DOF so that min/max of design space in addition to the value at the proposed optimum location
%   can be computed to support a robustness statement against response limits.
% - Method is based on multinomial expansion of sinusoidal response in sin and cos of multi DOF and selected order
%    $y = \sum([\cos(x_1) + \sin(x_1)]^n + [\cos(x_2) + \sin(x_2)]^n + \dots + [\cos(x_m) + \sin(x_m)]^n)$  for 'm' DOF and 'nth' order
%   Matlab does not have a built in function to fit data to more than 2 independent variables per Mathworks
%   respnse. Multinomial theorem used for expansion - ref 'mathonweb.com/help_ebook/html/expressions_8.htm',
%   'The Binomial and Multinomial Theorems' ... and others. Process yields polynomial that is 'complete' in terms
%   of multinomial expansion (ie; includes all potential terms as with Pascal's pyramid, etc.).
% - Coefficients assigned to each resulting term are optimized via fminunc or other to yield equation that best fits
%   the existing (actual) data. Routine searches for allowable NRMSE as function of polynomial order (for loops)
%   with stopping point either NRMSE_allowable or all defined orders searched. Optimization based on minimizing
%   objective function based on least squares method (minimize sum of residuals^2) with no constraints.
% - Intended use is to non-convex response with high modality - Rastrigins chosen as good example 'toy problem'
% - Rotordynamic responses are generally sinusoidal and assumed that functions are continuous and differentiable.
% - Taylor series considered but based on fit of equation in 'small' neighborhood around assumed point with increased
%   accuracy closest to the assumed point and reduced accuracy with increasing distance from it. Goal of this
%   routine is to have acceptable accuracy across selected design space (mean +/- tol each DOF) as evenly as possible.
%   In this sense, need 'global' solution whereas Taylor series is 'local' solution. Either Taylor series or
%   multinomial expansion is possible with enough terms, but decision to go with multinomial expansion made and
%   shown to be acceptable thru the 'toy problem' here. Direct comparisons of both techniques not made and later
%   optimization of process may result in change from multinomial expansion to Taylor series due to efficiency.
% -----
% - Key matrices used in this routine are:
%   exp = [exponent combinations (terms), columns=DOF] to create multinomial expansion equation
%   coef = [coefficients for terms] has same length as exp
%   X0 = same as coef - renamed 'X0' for input to optimization code, converted to 'coef' for easy read of
%   calculations in subroutines
%   inp_data = [rows=values, cols=DOF] data points of Actual data. Generated by 'x' number of points between
%   tolerance bounds of each DOF to create grid with which to fit polynomial. Actual data generated by
%   function solve of each defined point. This toy problem data generated by function solve of
%   Rastrigins equation in selected number of DOF.
% ---
%% ----- User Input -----
tic; tstart=tic; %start timer
% define input variables
xopt=[0 0 0 0]; %0 0]; %0.5 .5]; %0.25 0.25]; % potential optimum from optimization study (cntr of design space)
tol=[-0.5 0.5; % tols for each DOF=[rows=DOF, cols = lower tol, upper tol]
    -0.5 0.5; % TOLS IN SYMMETRIC FORMAT ONLY
    -0.5 0.5;
    -0.5 0.5];
polyordervec=[2 3 4 5 6 7 8 9 10 11 12 13 14 15]; % define polynomial order (loop until NRMSE < allow)
NRMSE_allow=0.1; % [%] threshold for acceptance - can abort search loop if below this value
runtime_allow=15.0; % [mins] prevents 'runaway' optimization - will queue to abort search loop at this value
discretpts=1; % number of discretization points greater than polyorder for response fit (min = 1)
optroutine=2; % 1=fminunc, 2=fmincon - opt routine for polynomial coefficients -
%% ----- Main Optimization Loop on polynomial order to derive potential equations -----

```

```

result=[]; mycoefs=zeros(length(polyordervec),max(polyordervec)); % initialize
polyDOF=length(xopt); % # of DOF (variables) derived from size of input data xopt location
for iiorder=1:length(polyordervec)
    polyorder=polyordervec(iiorder);
    discret=polyorder+discretpts; % number of points per DOF for robustness polynomial calculations
% -----
dofcount=length(xopt);
for ii=1:dofcount
    dofbounds(ii,:)=[xopt(ii)+tol(ii,1) xopt(ii)+tol(ii,2)]; % dofbounds=[rows=DOF, col1=LB, col2=UB]
end
% programmatic creation of input matrix 'inp_data' based on center points 'xopt' with tolerance bounds 'tol'
[inp_data_temp]=make_input_data(polyDOF,discret,xopt,tol);
inp_data=inp_data_temp;
% develop response data for inp_data matrix of values
for ii=1:length(inp_data(:,1))
    resp_data(ii)=10*polyDOF;
    for pointii=1:polyDOF
        resp_data(ii)=resp_data(ii)+(inp_data(ii,pointii).^2-10*cos(2*pi*inp_data(ii,pointii)));
    end
    % in actual use, these points would be evaluated thru function generator
end
% -----
% programmatic multinomial expansion of (x+y+...polyDOF)^polyorder
% (this section works to produce matrix 'exp' and is confirmed
% exp = matrix of order values for the variables for the various terms such that exp=[rows=terms, cols=variables]
% example-(x+y)^2=x^2+2xy+y^2 - exp=[2 0;1 1;0 2]
% ---
% expansion of (x+y+...polyDOF)^polyorder
row=1; temprows=(polyorder+1)^polyDOF;
temp=zeros(polyorder+1,polyDOF); exp=[];
for ii=1:(polyorder+1)^(polyDOF-1)
    temp(:,1)=linspace(0,polyorder,polyorder+1);
    exp=[exp;temp];
    flag=0;
    temp(:,2)=temp(:,2)+1;
    if temp(1,2)>polyorder
        for jj=2:polyDOF
            if temp(1,jj)>polyorder && jj<polyDOF
                temp(:,jj)=0; temp(:,jj+1)=temp(:,jj+1)+1;
            else
                break
            end
        end
    end
end
exp(sum(exp,2)~=polyorder,:)= []; % eliminate all rows where sum of exponents among terms do not = polyorder
% -----
% optimize on polynomial - use parallel processing all avail cores if DOF high enough
if polyDOF<=2
    optionsunc=optimoptions('fminunc','MaxFunctionEvaluations',60000,'maxiterations',2000,'display','none'); %'iter'
    optionscon=optimoptions('fmincon','algorithm','sqp','MaxFunctionEvaluations',60000,'maxiterations',2000,...
        'display','none'); %'iter' , 'StepTolerance',1e-8
else
    optionsunc=optimoptions('fminunc','MaxFunctionEvaluations',60000,'maxiterations',2000,'UseParallel',true,...
        'display','none'); %,'HessUpdate','bfgs'); %'iter'
    % per https://www.mathworks.com/help/optim/ug/fminunc.html#butpb7p-options

```

```

optionscon=optimoptions('fmincon','algorithm','sqp','MaxFunctionEvaluations',60000,'maxiterations',2000,...
    'UseParallel',true,'display','none'); %'iter'
end
terms=length(exp(:,1));
X0=ones(terms,1); % assume poly = 2nd order with cross-terms and constant, 6 terms for 2DOF space
f=@(x)rosenbrockwithgrad(x,inp_data,exp,resp_data);
con=@confun; % value artificially set to '0' - no real constraints this problem
A=[];B=[];Aeq=[];Beq=[];
for ii=1:dofcount
    dofbounds(ii,:)=[xopt(ii)+tol(ii,1) xopt(ii)+tol(ii,2)]; % dofbounds=[rows=DOF, col1=LB, col2=UB]
end
LB=[]; UB=[]; % coef determination = unconstrained
% --- choose optimization routine ---
warning 'off'; % suppress warning messages output during fmincon (matix is singular to working precision)
% note all are unconstrained optimizations LB=UB=A=B==[], g==0
if optroutine==1; [x,feval,exitflag,output]=fminunc(f,X0,optionsunc); end
if optroutine==2; [x,feval,exitflag,output]=fmincon(f,X0,A,B,Aeq,Beq,LB,UB,con,optionscon); end
if optroutine==3; [x,feval,exitflag,output,Population,Scores]=ga(f,length(X0),[],[],[],LB,UB,[],[],optionsga); end
% ---
if optroutine<=2; function_evals=output.funcCount; end % output.funcCount capitalized for fminunc, fmincon
if optroutine==3; function_evals=output.funccount; end % output.funccount not capitalized for ga
mycoefs(iiorder,1:length(x))=[x.];
warning 'on';
% -----
% compute resulting fit per optimized X0 coefficients and NRMSE
coef=x;
for ii=1:length(inp_data(:,1)) % loop thru all the data points
    temp_resp_trial=0; %initial value for response this trial X0
    for jj=1:length(exp(:,1)) % loop thru the terms of the equation (exp, inp_data & X0)
        this_term=0; % initialize this term
        for kk=1:length(inp_data(1,:))
            this_term=this_term+((cos(inp_data(ii,kk)).^exp(jj,kk)).*(sin(inp_data(ii,kk)).^exp(jj,kk)).*coef(jj));
        end
        temp_resp_trial=temp_resp_trial+this_term;
    end
    resp_result(iiorder,ii)=temp_resp_trial;
end
resid=(resp_result- resp_data); % residual between actual data and computed data with optimized X0 coefficients
[~,c]=size(resid);
RMSE=sqrt(sum(resid(iiorder,:).^2)/(1*c)); % only use row from current iiorder (this polynomial order run)
NRMSE_pcmt=RMSE/mean(resp_data)*100; % NRMSE=[]'%
result=[result; polyorder discret function_evals NRMSE_pcmt];
if NRMSE_pcmt<NRMSE_allow % stop search on polyorder if meet error tolerance
    break
end
if toc(tstart)/60>runtime_allow % stop search on polyorder if solution greater than allowable time [mins]
    break
end
end
opttime_min=toc(tstart)/60;
%% ----- print optimization results to the screen -----
% trim cols from mycoefs where coefs='0' all poly-order runs (ie, none of the equations have these terms - too long)
[~,c]=find(sum(abs(mycoefs))~=0); mycoefs=mycoefs(:,c);
% print results
result
% mycoefs

```

```

[r,~]=find(result(:,4)==min(result(:,4))); % select based on minimum NRMSE
ttl_func_evals=sum(result(:,3)) %sum over all order surveys
myOrder=result(r,1)
myPoints=result(r,2)
myFuncEvals=result(r,3)
myNRMSE=result(r,4)
mycoefs=mycoefs(r,:) % selected 'X0' coefficients from chosen order ('r')
%% ----- search calculated results for min/max -----
% --- use optimization toolbox to identify minima/maxima using CALCULATED equation within design space
for ii=1:dofcount
    dofbounds(ii,:)=[xopt(ii)+tol(ii,1) xopt(ii)+tol(ii,2)]; % dofbounds=[rows=DOF, col1=LB, col2=UB]
end
for optii=1:2
    maxminflag=optii; % [1]=search for maxima, [2]=search for minima
    f=@(x)SurveyCalc(x,exp,maxminflag,coef);
    con=@confun; % value artificially set to '0' - no real constraints this problem
    A=[];B=[];Aeq=[];Beq=[];
    LB=dofbounds(:,1).'; UB=dofbounds(:,2).'; % X0 bounds based on tolerances and design space mean
    X0=(UB+LB)/2;
    % --- choose optimization routine ---
    warning 'off'; % suppress warning messages output during fmincon (matix is singular to working precision)
    % note all are unconstrained optimizations LB=UB=A=B==[], g==0
    if optroutine==1 || optroutine==2; [x,feval,exitflag,output]=fmincon(f,X0,A,B,Aeq,Beq,LB,UB,con,optionscon); end
    % ---
    if optroutine<=2; function_evals=output.funcCount; end % output.funcCount capitalized for fminunc, fmincon
    if optii==1; maximaloc=x; maximavalue=-feval; end
    if optii==2; minimaloc=x; minimavalue=feval; end
    warning 'on';
end
maximaloc
maximavalue
minimaloc
minimavalue
calcroutineend=toc(tstart);
calculated_robustness_time_min=calcroutineend/60-opttime_min;
%% ----- calculate ACTUAL surface with high discret for plotting & subjective comparison (only if 2DOF)
% --- use optimization toolbox to identify minima/maxima using CALCULATED equation within design space
for ii=1:dofcount
    dofbounds(ii,:)=[xopt(ii)+tol(ii,1) xopt(ii)+tol(ii,2)]; % dofbounds=[rows=DOF, col1=LB, col2=UB]
end
% find maxima/minima starting from each design bound corner & centerpoint
for optii=1:2
    maxminflag=optii; % [1]=search for maxima, [2]=search for minima
    f=@(x)SurveyExact(x,maxminflag,polyDOF);
    con=@confun; % value artificially set to '0' - no real constraints this problem
    A=[];B=[];Aeq=[];Beq=[];
    LB=dofbounds(:,1).'; UB=dofbounds(:,2).'; % X0 bounds based on tolerances and design space mean
    X0=(UB+LB)/2;
    % --- choose optimization routine ---
    warning 'off'; % suppress warning messages output during fmincon (matix is singular to working precision)
    % note all are unconstrained optimizations LB=UB=A=B==[], g==0
    if optroutine==1 || optroutine==2; [x,feval,exitflag,output]=fmincon(f,X0,A,B,Aeq,Beq,LB,UB,con,optionscon); end
    % ---
    if optroutine<=2; function_evals=output.funcCount; end % output.funcCount capitalized for fminunc, fmincon
    if optii==1; exactmaximaloc=x; exactmaximavalue=-feval; end
    if optii==2; exactminimaloc=x; exactminimavalue=feval; end

```

```

% mycoefs(iiorder,1:length(x))=[x.'];
warning 'on';
end
% print results of robustness on exact equation
exactmaximaloc
exactmaximavalue
exactminimaloc
exactminimavalue
actroutineend=toc(tstart);
%% --- plot NRMSE convergence against polynomial order for all DOF systems (not just 2DOF)
% --- plot for visualization if 2DOF
if length(inp_data(1,:))<=2 % only plot for 2DOF
% --- plot min/max vs actual data for subjective (qualitative) comparison (2DOF only)
[x_data,y_data]=meshgrid(unique(inp_data(:,2)),unique(inp_data(:,2)));
% create response for dense mesh
for ii=1:length(x_data(1,:))
for jj=1:length(y_data(:,1))
z_data(ii,jj)=10*2+(x_data(ii,jj)^2-10*cos(2*pi*x_data(ii,jj)))+(y_data(ii,jj)^2-10*cos(2*pi*...
y_data(ii,jj))); %Rastrigins in 2D
end
end
z_datasize=size(z_data);
% ---
figure;
subplot(2,1,1);
surf(x_data,y_data,z_data); hold on; grid on; % exact results as surface plot
plot3(maximaloc(1),maximaloc(2),maximavalue,'r','markersize',20); % maxima
plot3(minimaloc(1),minimaloc(2),minimavalue,'r','markersize',20); % minima
xlabel('DOF 1','fontweight','bold','fontsize',12);
ylabel('DOF 2','fontweight','bold','fontsize',12);
zlabel('Response','fontweight','bold','fontsize',12);
title({'Robustness Code Challenge Results';...
'Rastrigin Surface {\it (Exact)} vs Identified Minima/Maxima {\it (Calculated)}'},...
'fontweight','bold','fontsize',14);
subplot(2,1,2);
plot(result(:,1),result(:,4)); grid on; %NRMSE convergence
title('NRMSE Convergence','fontweight','bold','fontsize',14);
xlabel('Equation Order','fontweight','bold','fontsize',12);
ylabel('NRMSE (%)','fontweight','bold','fontsize',12);
set(gcf,'color','w','Position',[5 5 700 900]);
else
figure; plot(result(:,1),result(:,4)); grid on; %NRMSE convergence
title('NRMSE Convergence','fontweight','bold','fontsize',14);
xlabel('Equation Order','fontweight','bold','fontsize',12);
ylabel('NRMSE (%)','fontweight','bold','fontsize',12);
set(gcf,'color','w','Position',[5 5 700 400]);
end
% ---
%% --- solution time result and release parallel pool if used above
calculated_robustness_time_min=calcroutineend/60-opttime_min;
actual_robustness_time_min=actroutineend/60-calculated_robustness_time_min-opttime_min;
% ---
opttime_min
calculated_robustness_time_min
actual_robustness_time_min
tend=toc; grad_iter_time_mins=toc(tstart)/60-opttime_min

```

```

delete(gcf('nocreate')); % stop local the parallel pool
%% ----- End - Main Function -----

function [inp_data_temp]=make_input_data(polyDOF,discret,xopt,tol)
% programmatic creation of input matrix 'inp_data' based on center points 'xopt' with tolerance bounds 'tol'
row=1; temprows=(discret)^polyDOF;
temp=zeros(discret,polyDOF); inp_data_temp=[];
for ii=2:polyDOF
    temp(:,ii)=xopt(ii)+tol(ii,1);
end
delta=(tol(:,2)-tol(:,1))/(discret-1);
for ii=1:(discret)^(polyDOF-1)
    temp(:,1)=linspace(xopt(1)+tol(1,1),xopt(1)+tol(1,2),discret);
    inp_data_temp=[inp_data_temp;temp];
    flag=0;
    temp(:,2)=temp(:,2)+delta(2); %temp(:,2)+(tol(ii,2)-tol(ii,1))/discret; %+1;
    if temp(1,2)>(xopt(2)+tol(2,2))
        for jj=2:polyDOF
            if temp(1,jj)>xopt(jj)+tol(jj,2) && jj<polyDOF
                temp(:,jj)=xopt(jj)+tol(jj,1); temp(:,jj+1)=temp(:,jj+1)+delta(jj+1);
            else
                break
            end
        end
    end
end
end
end

function [f]=rosenbrockwithgrad(x,inp_data,exp,resp_data) %Optimizations Objective Function
% minimize f as unconstrained optimization
coef=x;
temp_resp_trial=0; this_grad_term=ones(length(exp(:,1)),1); % initialize values
parfor jj=1:length(exp(:,1)) % loop thru the terms of the equation (exp, inp_data & X0)
    this_term=0; %ones(length(inp_data(:,1)),1); % initialize this term
    this_term=sum(((cos(inp_data(:,:)).^exp(jj,:)).*(sin(inp_data(:,:)).^exp(jj,:)).*coef(jj)),2);
    temp_resp_trial=temp_resp_trial+this_term;
end
resp_trial=temp_resp_trial.';
resid=(resp_trial- resp_data); % residual between actual data and computed data with this X0 coefficients
[r,c]=size(resid);
RMSE=sqrt(sum(sum(resid.^2))/(r*c));
f=sum(resid.^2); % least squares method

function [g,heq]=confun(x)
g=0; % dummy constraint if using fmincon or ga for opt of coefficients (unconstrained problem)
heq=[];

function [f]=SurveyCalc(x,exp,maxminflag,coef) %Objective Function to find maxima/minima of calculated response
temp_resp_trial=0; resp_trial=0; % initialize values
for jj=1:length(exp(:,1)) % loop thru the terms of the equation (exp, inp_data & X0)
    this_term=0; %ones(length(inp_data(:,1)),1); % initialize this term
    for kk=1:length(x) %length(inp_data(1,:)) % loop thru variables
        this_term=this_term+((cos(x(kk)).^exp(jj,kk)).*(sin(x(kk)).^exp(jj,kk)).*coef(jj));
    end
    resp_trial=resp_trial+this_term;
end
% ---

```



```

% modify 'f' for maxima/minima search
if maxminflag==1 % search for local maxima
    f=min((resp_trial)*(-1));
elseif maxminflag==2 % search for local minima
    f=min(resp_trial);
end

function [f]=SurveyExact(x,maxminflag,polyDOF) %Objective Function to find maxima/minima of exact response
temp_resp_trial=0; resp_trial=0; % initialize values
this_term=0; %initial value for response this trial X0
for jj=1:length(x) % loop thru the DOF (columns) for each X0 data point
    this_term=this_term+(x(jj).^2-10*cos(2*pi*x(jj))); %Rastrigins in nD
end
exact_result=this_term+10*polyDOF; %completes Rastrigins in nD
% ---
% modify 'f' for maxima/minima search
if maxminflag==1 % search for local maxima
    f=min((exact_result)*(-1));
elseif maxminflag==2 % search for local minima
    f=min(exact_result);
end

```

Appendix I

System Data File – Parallel Beam Example Problem

```

% Program 'System_Data_Flex_Rotordynamics_v1_4.m'
%% =====
% ---- System Data -----
% Supports Flexible_Rotordynamics_v1_4
% =====
%% INPUT SECTION - Rotor system definition
% Title of System
    TIT='Parallel Beam System';
% -----
% Constants used in this script - update as appropriate
    g=32.2*12; % accel due to gravity [=] in/s^2 (32.2ft/s^2*12in/ft)
    k=0.9; % Timoshenko shear factor (default = 0.90)
    polyfitorder=3; % order for polynomial fit of Critical Speeds (by mode) (default = 3)
    FRPpoints=100; % number of freq points for FRP generation (default = 100)
    modepts=50; % number of geometric points to plot for mode shape (default = 50)
    staticmodes=16; % number of non-rotating modes to evaluate (default = 16)
    min_eig_factor=0; % only identify static eigenvalues above (this factor*'maxW') this frequency (def=0)
    max_eig_factor=5.0; % only identify static eigenvalues below (this factor*'maxW') this frequency (def=5)
    text_output=1; % '1' = text output, '0' = no text output (DOE or Optimization runs)
    output_file='run_output.txt'; % output file for textual output (required, but only used if text_output=1 above)
    create_plots=1; % '1' = create plots, '0' = do not create plots
    animate=1; % '1'=show animation of 3D mode shape plots, '0'=no animation
% -----
% System Model Data
% *****
% NOTE: Units to be entered as Lbf, Lbm, in, sec, RPM, deg (angle)
% *****
% Beam Rotational Speed Range for study
    ShaftRPM=[0 10000 10]; % [min_RPM max_RPM number_of_points]
% -----
% Snode = Super Node Definition of System *** important - SNID numbers must be sequential in order of position
% Super Nodes define bounding ends of each Super Element
% Axial location (only) defined here
% -----
% |SNode| Axial |
% | No | Location|
Snode=[ 1 0.0000;
        2 3.0000;
        3 4.0000;
        4 10.0000;
        5 14.0000;
        6 16.0000;
        7 2.0000;
        8 4.0000;
        9 14.0000;
        10 19.5000;
        11 20.0000];
% -----
% Selemdef = Super Element Definition of System *** important - SEID numbers must be sequential in order of position
% SNode 'i' and SNode 'j' define ends of Super Element
% SNode 'i' of one Selem and SNode 'j' of another must be coincident to form continuous beam
% Elements may be solid, hollow, cylindrical or conical
% (MID=Material ID number) / (element Rotate = 0=no , 1=yes) / Mass Ecc [=] lbm-in (applicable to w^2)
% Note - element eccentric mass distributed as forces on bounding nodes, distributed by mass
% -----
% |Beam| - Nodes - | No | | Beam | Mass |

```

```

% | No | SNi ri Ri SNj rj Rj | Elems | MID | Rotates | Ecc |
Selemdf=[ 1 1 0.2500 0.3125 2 0.2500 0.3125 4 2 0 0.000;
1 2 0.2500 0.3125 3 0.2500 0.3125 4 2 0 0.000;
1 3 0.2500 0.3125 4 0.2500 0.3125 4 2 0 0.000;
1 4 0.2500 0.3125 5 0.2500 0.3125 4 2 0 0.000;
1 5 0.2500 0.3125 6 0.2500 0.3125 4 2 0 0.000;
2 7 0.0000 0.0625 8 0.0000 0.0625 4 1 1 0.000;
2 8 0.0000 0.0625 9 0.0000 0.0625 4 1 1 0.000;
2 9 0.0000 0.0625 10 0.0000 0.0625 4 1 1 0.000;
2 10 0.0000 1.5000 11 0.0000 1.5000 2 1 1 0.005];

% -----
% Material Table
% [MID E Rho-m eta-v eta-h nu] E=Modulus of Elasticity (psi=Lbf/in^2)
MTableinp=[ 1 2.9e7 0.283 0 0 0.30; % Rho-m=Mass density (Lbm/in^3)3.0in
2 1.0e7 0.0975 0 0 0.33]; % eta-v=int visc damping[=]lbf*sec/in
% % eta-h=int hysteretic loss factor (unitless) = damping ratio * 2
% % nu=Poisson's Ratio

% -----
% Bearing Support Stiffness/Damping properties (include very stiff springs to model 'constrained' nodes)
% KDef=[SNIDi SNIDj Ky Kz Kthy Kthz Cy Cz Cthy Cthz] Ky,Kz[=]lbf/in Kthy,Kthz[=]in*lbf/rad
% Cy,Cz[=]lbf*sec/in Cthy,Cthz[=]in*lbf*sec/rad
KDef=[ 2 0 1.5e2 1.5e2 0 0 0 0 0 0; % SNIDj=0 means tied to ground
4 0 1.5e2 1.5e2 0 0 0 0 0 0;
3 8 1.5e4 1.5e4 0 0 0 0 0 0;
5 9 1.5e4 1.5e4 0 0 0 0 0 0];

% -----
% Boundary Conditions Applied to Nodes
% BCSN=[SNID BCy BCz BChy BCthz] (0='free', 1='fixed')
BCSN=[ 1 0 0 0 0
7 0 0 0 0];
% Constrain all nodes against planar motion in this plane
% BCPlane=[ XY XZ] '0' = Free, '1'=Constrained
BCPlane=[ 0 0];

% -----
% Discrete (lumped) Disk Properties
% DiskSN=[SNID OD thk Rho-m CG_rad_eccentricity] Rho=Mass density (Lbm/in^3)
DiskSN=[ ];%1 0 0 0 0]; % radial eccentricity of disk CG from shaft centerline [=] in

% -----
% Discrete (lumped) Mass Properties
% MImpSN=[SNID Mass ltrans lpolar rad_ecc] Weight[=]lbm,ltrans=ixx=lyy[=]bm*in^2,lpolar=lzz[=]lbm*in^2
% radial eccentricity of mass from shaft centerline [=] in
MImpSN=[ ];%1 0 0 0 0;
%2 0 0 0 0];

% -----
% External Load Properties - HARMONIC (use to provide external harmonic loads to ROTORDYNAMIC analyses)
% LoadDef=[SNID Fx_axial Fy Fz Myy Mzz] - Harmonic external load magnitudes
LoadDef=[ 1 0 0.0 0 0 0
2 0 0.0 0 0 0];

% -----
% External Load Properties - STATIC (use to provide external harmonic loads to STATIC analyses)
% LoadDef_static=[SNID Fy Fz Myy Mzz] - Constant external load magnitudes (note lateral only)
LoadDef_static=[ 11 1 1 0 0];

% ----- end of data input section -----
%% pack input data - DO NOT CHANGE THIS SECTION
warning 'off'
MYDATA.animate=animate;

```

```

MYDATA.BCPlane=BCPlane;
MYDATA.BCSN=BCSN;
MYDATA.text_output=text_output;
MYDATA.output_file=output_file;
MYDATA.create_plots=create_plots;
MYDATA.DiskSN=DiskSN;
MYDATA.FRPpoints=FRPpoints;
MYDATA.g=g;
MYDATA.k=k;
MYDATA.KDef=KDef;
MYDATA.LoadDef=LoadDef;
MYDATA.LoadDef_static=LoadDef_static;
MYDATA.max_eig_factor=max_eig_factor;
MYDATA.min_eig_factor=min_eig_factor;
MYDATA.MImpSN=MImpSN;
MYDATA.modepts=modepts;
MYDATA.MTableinp=MTableinp;
MYDATA.polyfitorder=polyfitorder;
MYDATA.Snode=Snode;
MYDATA.Selemdef=Selemdef;
MYDATA.ShaftRPM=ShaftRPM;
MYDATA.staticmodes=staticmodes;
MYDATA.TIT=TIT;
%% Assumptions
% all nodes lie along x-axis (y=0, z=0)
% added 'lumped' disks assumed to be rigid
% external axial force 'P' used for shear calcs only (Greenhill) - no actual 'axial' DOF included
% analysis does not include axial DOF, therefore assumes '1 node' is constrained axially and all other nodes are
% free to float axially due to elastic behavior (ie; no stiffness effects due to axial constraints on nodes)
% mass eccentricities can be either applied to Super Element definition or as lumped mass or lumped disk definition.
% if applied to Super Element, the distributed to bounding nodes by mass balance (evenly for cylinder, scaled for
% conical, etc). If applied as lumped mass/disk then applied directly to assigned Super Node.
% SIMPLIFYING ASSUMPTION that no externally applied axial torque on the system, externally applied axial force only
% influences element stiffness but no axial deformation results
% SIMPLIFYING ASSUMPTION that all eccentric masses are in phase
% SIMPLIFYING ASSUMPTION that lateral forces = sinusoidal & only tied to vibratory response, not static deflections
% Units:
% Input units defined here = [Lbf, Lbm, in, sec, RPM, deg (angle), Lbm/in^3] = 'BIN'
% Model units automatically converted to = [Lbf, slinch, in, sec, RPM, deg (angle), slinch/in^3]
% = Consistent Units (slinch=Lbf-s^2/in)
% key data out of this file includes:
% Title of System
% Snode=[SNID x r R ] Super Node Locations
% Selemdef=[beam SNi SNj Elems MID Rot Ecc] Super Element Definition of System
% SEkey=[SEID SNiDi SNiDj NiDi NIDj xloci xlocj ri Ri rj Rj] key relating super nodes to model nodes
% MTable=[MID E rho-m etav etah nu] Mat Table (converted to mass density)
% BCK=[NID Ky Kz Kthz Kthz] Brg Support Stiff/Damping properties
% BC=[NID BCy BCz BCthy BCthz] Nodal Constraint (0='free', 1='fixed')
% Lump=[NID Mass Itrans Ipolar rad_eccentricity] Discrete (lumped) node mass Properties
% Load=[NID Fx_axial Fy Fz Myy Mzz] External 'Constant' Load Properties
% ElemData=[Element-ID Nodei Nodej MID ri Ri rj Rj lngth] Element Data
% XData=[NID XLoc] node location matrix (assume y=z=0)
% k Timoshenko Shear Factor
% NOTE: No 'Section Table' since elements are not cylindrical, instead ri,Ri,rj,Rj defined per element data

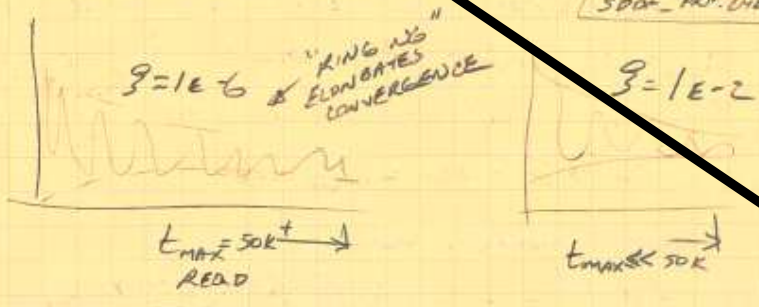
```

Appendix J

Equation Development – Solution of EOM via Steady-State Component Analysis

72

CHANGES TO TIME SOLTN METHOD OF DEVELOPING FRP
 (PAGES 11 ETAL THIS NOTEBOOK) SUCCESSFULLY REDUCE ERROR
 TO ACCEPTABLE VALUES BUT AT COST OF SOLTN TIME.
 FREQ SWEEP $\omega = 1 \sim 50$ IN STEP = 1 W/ ODE45 M ODE113
 WITH $T_{MAX} = 500$ & $T_{STEPS} = 50 \sim 500K$ RESULT IN ERROR
 ACCEPTABLE FOR $\zeta = 1E-6 \sim 1E-4$, BUT TIME = ± 8 HRS / SWEEP.
 - NOTE: HIGH VALUES OF ζ (STILL UNDERDAMPED) DO NOT
 REQUIRE NEAR THE LNGETH (T_{MAX}, T_{STEPS}) TO ACHIEVE LOW ERROR
 SINCE CONVERGENCE HAPPENS QUICKLY



3DOF_FRP_CHECKS_ODE113.M
 3DOF_FRP_CHECK_ODE45.M

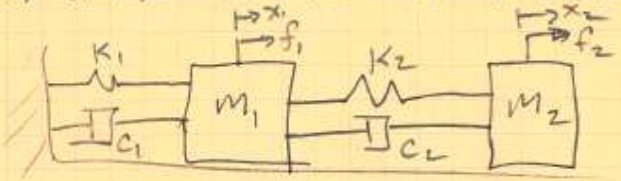
Steady State Component Analysis begins here

BETTER METHOD =

- 1.) ODE45/113 TO SOLVE ODE FOR SPECIFIC VALUES
- 2.) STEADY STATE SOLUTION OF ODE FOR FRP PLOTS, ω_n ID, ETC

HARIHARA & CHILDS 'SOLVING PROBLEMS IN DYNAMICS & VIBRATION USING MATLAB' DISCUSS THIS METHOD ON 2DOF MODEL (PG 56+)

THEIR METHOD (EXPANDED BELOW) SEEMS USEFUL TO GENERATE THE FRP (AND PHASE PLOT) IN ACCEPTABLE TIME PERIOD.



EDM:

$$\begin{bmatrix} m_1 & 0 \\ 0 & m_2 \end{bmatrix} \begin{Bmatrix} \ddot{x}_1 \\ \ddot{x}_2 \end{Bmatrix} + \begin{bmatrix} c_1 + c_2 & -c_2 \\ -c_2 & c_2 \end{bmatrix} \begin{Bmatrix} \dot{x}_1 \\ \dot{x}_2 \end{Bmatrix} + \begin{bmatrix} k_1 + k_2 & -k_2 \\ -k_2 & k_2 \end{bmatrix} \begin{Bmatrix} x_1 \\ x_2 \end{Bmatrix} = \begin{Bmatrix} f_1(t) \\ f_2(t) \end{Bmatrix}$$

CONSIDERING A 1-DOF VERSION:

$$[M] \ddot{x}_1 + [C] \dot{x}_1 + [K] x_1 = f_1(t) \quad (134)$$

FULL SOLUTION (PG 68 & 34 THESE NOTES)

$$x_{TOT} = x_{TRANSIENT} + x_{STEADY STATE}$$

FOR PURPOSES OF FRF DEVELOPMENT, ONLY INTERESTED IN STEADY STATE SOLUTION WHERE TRANSIENT HAS DIED OUT (LONG 't')
- THUS PBLM DISCUSSED PG. 72 THESE NOTES.

ASSUME x_{ss} = COMBINATION OF BOTH SIN & COS ELEMENTS

$$\begin{aligned} x_{1,ss} &= x_{1,s} \sin(\omega t) + x_{1,c} \cos(\omega t) \\ \dot{x}_{1,ss} &= \omega x_{1,s} \cos(\omega t) - \omega x_{1,c} \sin(\omega t) \\ \ddot{x}_{1,ss} &= -\omega^2 x_{1,s} \sin(\omega t) - \omega^2 x_{1,c} \cos(\omega t) \end{aligned} \quad \left. \begin{array}{l} \text{(DOF 1)} \\ (\omega = \text{APPLIED FREQ.}) \end{array} \right\} (135)$$

(135) INTO (134) IN MATRIX FORM

$$[M] \begin{Bmatrix} -\omega^2 x_{1,s} \sin(\omega t) \\ -\omega^2 x_{1,c} \cos(\omega t) \end{Bmatrix} + [C] \begin{Bmatrix} \omega x_{1,s} \cos(\omega t) \\ -\omega x_{1,c} \sin(\omega t) \end{Bmatrix} + [K] \begin{Bmatrix} x_{1,s} \sin(\omega t) \\ x_{1,c} \cos(\omega t) \end{Bmatrix} = \begin{Bmatrix} f_{1,s} \sin(\omega t) \\ f_{1,c} \cos(\omega t) \end{Bmatrix} \quad (136)$$

WHERE $f_{1,s}$ & $f_{1,c}$ ARE AMPLITUDE OF SIN / COS COMPONENTS OF FORCING FUNCTION

$$-\omega^2 M \begin{Bmatrix} x_{1,s} \\ x_{1,c} \end{Bmatrix} + \omega C \begin{Bmatrix} -x_{1,c} \\ x_{1,s} \end{Bmatrix} + K \begin{Bmatrix} x_{1,s} \\ x_{1,c} \end{Bmatrix} = \begin{Bmatrix} f_{1,s} \\ f_{1,c} \end{Bmatrix} \quad (137)$$

$$\begin{bmatrix} -\omega^2 M + K & -\omega C \\ +\omega C & -\omega^2 M + K \end{bmatrix} \begin{Bmatrix} x_{1,s} \\ x_{1,c} \end{Bmatrix} = \begin{Bmatrix} f_{1,s} \\ f_{1,c} \end{Bmatrix} \quad (138) \quad \text{1-DOF}$$

STEADY STATE SOLUTION TO EOM (134)

FOR FRF PLOTTING:

$$\text{AMPLITUDE}_{ss} = X_1 = \sqrt{x_{1,s}^2 + x_{1,c}^2} \quad (139)$$

$$\text{PHASE} = \phi_1 = \tan^{-1} \left(\frac{x_{1,s}}{x_{1,c}} \right)$$



STEADY-STATE COMPONENT ANALYSIS

(2-DOF)
 MEOP COROLLARY TO EOTN'S) 134-139 : (PER FIG PG (72))
 THESE WORDS

ASSUME X_{2SS} , ETC PER EQ 135

STDY STATE SOLUTION (PER 136) BECOMES:

DOF1

$$M_1(-\omega^2 X_{1s} \sin(\omega t) - \omega^2 X_{1c} \cos(\omega t)) + (C_1 + C_2)[\omega X_{1s} \cos(\omega t) - \omega X_{1c} \sin(\omega t)] + (-C_2)[\omega X_{2s} \cos(\omega t) - \omega X_{2c} \sin(\omega t)] + (K_1 + K_2)[X_{1s} \sin(\omega t) + X_{1c} \cos(\omega t)] + (-K_2)[X_{2s} \sin(\omega t) + X_{2c} \cos(\omega t)] = \begin{cases} f_{1s}(t) \\ f_{1c}(t) \end{cases} \quad (140)$$

DOF2

$$M_2(-\omega^2 X_{2s} \sin(\omega t) - \omega^2 X_{2c} \cos(\omega t)) + (-C_2)[\omega X_{1s} \cos(\omega t) - \omega X_{1c} \sin(\omega t)] + (C_2)[\omega X_{2s} \cos(\omega t) - \omega X_{2c} \sin(\omega t)] + (-K_2)[X_{1s} \sin(\omega t) + X_{1c} \cos(\omega t)] + (K_2)[X_{2s} \sin(\omega t) + X_{2c} \cos(\omega t)] = \begin{cases} f_{2s}(t) \\ f_{2c}(t) \end{cases}$$

(140) IN MATRIX FORM (2)

$$M_1 \begin{Bmatrix} -\omega^2 X_{1s} \sin(\omega t) \\ -\omega^2 X_{1c} \cos(\omega t) \end{Bmatrix} + (C_1 + C_2) \begin{Bmatrix} -\omega X_{1c} \sin(\omega t) \\ \omega X_{1s} \cos(\omega t) \end{Bmatrix} + (-C_2) \begin{Bmatrix} -\omega X_{2c} \sin(\omega t) \\ \omega X_{2s} \cos(\omega t) \end{Bmatrix} + (K_1 + K_2) \begin{Bmatrix} X_{1s} \sin(\omega t) \\ X_{1c} \cos(\omega t) \end{Bmatrix} + (-K_2) \begin{Bmatrix} X_{2s} \sin(\omega t) \\ X_{2c} \cos(\omega t) \end{Bmatrix} = \begin{cases} f_{1s} \sin(\omega t) \\ f_{1c} \cos(\omega t) \end{cases}$$

$$M_2 \begin{Bmatrix} -\omega^2 X_{2s} \sin(\omega t) \\ -\omega^2 X_{2c} \cos(\omega t) \end{Bmatrix} + (-C_2) \begin{Bmatrix} -\omega X_{1c} \sin(\omega t) \\ \omega X_{1s} \cos(\omega t) \end{Bmatrix} + (C_2) \begin{Bmatrix} -\omega X_{2c} \sin(\omega t) \\ \omega X_{2s} \cos(\omega t) \end{Bmatrix} + (-K_2) \begin{Bmatrix} X_{1s} \sin(\omega t) \\ X_{1c} \cos(\omega t) \end{Bmatrix} + (K_2) \begin{Bmatrix} X_{2s} \sin(\omega t) \\ X_{2c} \cos(\omega t) \end{Bmatrix} = \begin{cases} f_{2s} \sin(\omega t) \\ f_{2c} \cos(\omega t) \end{cases} \quad (141)$$

$$\begin{aligned} M_1(-\omega^2 X_{1s}) + (C_1 + C_2)(-\omega X_{1c}) + (-C_2)(-\omega X_{2c}) + (K_1 + K_2)(X_{1s}) + (-K_2)(X_{2s}) &= f_{1s} \\ M_1(-\omega^2 X_{1c}) + (C_1 + C_2)(\omega X_{1s}) + (-C_2)(\omega X_{2s}) + (K_1 + K_2)(X_{1c}) + (-K_2)(X_{2c}) &= f_{1c} \\ M_2(-\omega^2 X_{2s}) + (-C_2)(-\omega X_{1c}) + (C_2)(-\omega X_{2c}) + (-K_2)(X_{1s}) + (K_2)(X_{2s}) &= f_{2s} \\ M_2(-\omega^2 X_{2c}) + (-C_2)(\omega X_{1s}) + (C_2)(\omega X_{2s}) + (-K_2)(X_{1c}) + (K_2)(X_{2c}) &= f_{2c} \end{aligned}$$

(141) IN MATRIX FORM

$$\begin{bmatrix} M_1 & 0 & 0 & 0 \\ 0 & M_1 & 0 & 0 \\ 0 & 0 & M_2 & 0 \\ 0 & 0 & 0 & M_2 \end{bmatrix} \begin{Bmatrix} -\omega^2 X_{1s} \\ -\omega^2 X_{1c} \\ -\omega^2 X_{2s} \\ -\omega^2 X_{2c} \end{Bmatrix} + \begin{bmatrix} (C_1 + C_2) & 0 & -C_2 & 0 \\ 0 & (C_1 + C_2) & 0 & -C_2 \\ -C_2 & 0 & C_2 & 0 \\ 0 & -C_2 & 0 & C_2 \end{bmatrix} \begin{Bmatrix} -\omega X_{1c} \\ \omega X_{1s} \\ -\omega X_{2c} \\ \omega X_{2s} \end{Bmatrix} + \begin{bmatrix} (K_1 + K_2) & 0 & -K_2 & 0 \\ 0 & (K_1 + K_2) & 0 & -K_2 \\ -K_2 & 0 & K_2 & 0 \\ 0 & -K_2 & 0 & K_2 \end{bmatrix} \begin{Bmatrix} X_{1s} \\ X_{1c} \\ X_{2s} \\ X_{2c} \end{Bmatrix} = \begin{Bmatrix} f_{1s} \\ f_{1c} \\ f_{2s} \\ f_{2c} \end{Bmatrix} \quad (142)$$

2 MATRICES NOT 'CLEAN' IN TERMS OF $M_1 \begin{pmatrix} m_1 & 0 \\ 0 & m_2 \end{pmatrix}$ ETC.

COMBINE 'M' & 'K' TERMS SINCE $\begin{Bmatrix} x_{1s} \\ x_{2s} \\ x_{1c} \\ x_{2c} \end{Bmatrix}$ SAME & REORDER

$$\begin{bmatrix} \omega^2 m_1 & 0 & 0 & 0 \\ 0 & -\omega^2 m_2 & 0 & 0 \\ 0 & 0 & -\omega^2 m_1 & 0 \\ 0 & 0 & 0 & -\omega^2 m_2 \end{bmatrix} \begin{Bmatrix} x_{1s} \\ x_{2s} \\ x_{1c} \\ x_{2c} \end{Bmatrix} + \begin{bmatrix} 0 & 0 & -\omega(c_1+c_2) & -\omega(-c_2) \\ 0 & 0 & -\omega(-c_2) & -\omega(c_1) \\ \omega(c_1+c_2) & \omega(-c_2) & 0 & 0 \\ \omega(-c_2) & \omega(c_1) & 0 & 0 \end{bmatrix} \begin{Bmatrix} x_{1s} \\ x_{2s} \\ x_{1c} \\ x_{2c} \end{Bmatrix} + \begin{bmatrix} (K_1+K_2) & -K_2 & 0 & 0 \\ -K_2 & K_2 & 0 & 0 \\ 0 & 0 & -(K_1+K_2) & -K_2 \\ 0 & 0 & -K_2 & K_2 \end{bmatrix} \begin{Bmatrix} x_{1s} \\ x_{2s} \\ x_{1c} \\ x_{2c} \end{Bmatrix} = \begin{Bmatrix} f_{1s} \\ f_{2s} \\ f_{1c} \\ f_{2c} \end{Bmatrix}$$

$$\begin{bmatrix} -\omega^2 m_1 + (K_1+K_2) & -K_2 & 0 & 0 \\ -K_2 & -\omega^2 m_2 + K_2 & 0 & 0 \\ 0 & 0 & -\omega^2 m_1 + (K_1+K_2) & -K_2 \\ 0 & 0 & -K_2 & -\omega^2 m_2 + K_2 \end{bmatrix} \begin{Bmatrix} x_{1s} \\ x_{2s} \\ x_{1c} \\ x_{2c} \end{Bmatrix} + \begin{Bmatrix} 0 & 0 & -\omega(c_1+c_2) & -\omega(-c_2) \\ 0 & 0 & -\omega(-c_2) & -\omega(c_1) \\ \omega(c_1+c_2) & \omega(-c_2) & 0 & 0 \\ \omega(-c_2) & \omega(c_1) & 0 & 0 \end{Bmatrix} \begin{Bmatrix} x_{1s} \\ x_{2s} \\ x_{1c} \\ x_{2c} \end{Bmatrix} = \begin{Bmatrix} f_{1s} \\ f_{2s} \\ f_{1c} \\ f_{2c} \end{Bmatrix} \quad (143)$$

(143) SIMPLIFIES TO:

$$\begin{bmatrix} [-\omega^2[M] + [K]] & -\omega[C] \\ \omega[C] & [-\omega^2[M] + [K]] \end{bmatrix} \begin{Bmatrix} x_{1s} \\ x_{2s} \\ x_{1c} \\ x_{2c} \end{Bmatrix} = \begin{Bmatrix} f_{1s} \\ f_{2s} \\ f_{1c} \\ f_{2c} \end{Bmatrix}$$

GENERALIZED FOR N-DOF BSLM:

$$\begin{bmatrix} [-\omega^2[M] + [K]]_{N \times N} & -\omega[C]_{N \times N} \\ \omega[C]_{N \times N} & [-\omega^2[M] + [K]]_{N \times N} \end{bmatrix} \begin{Bmatrix} x_{1s} \\ x_{2s} \\ x_{1c} \\ x_{2c} \\ \vdots \\ x_{1c} \\ x_{2c} \\ \vdots \end{Bmatrix} = \begin{Bmatrix} f_{1s} \\ f_{2s} \\ f_{1c} \\ f_{2c} \\ \vdots \\ f_{1c} \\ f_{2c} \\ \vdots \end{Bmatrix} \quad (144)$$

→ STEADY STATE SOLTN TO MDOF EOM
(COMPARE TO (138) ON PG. 73 THESE NOTES)

$$\left. \begin{aligned} \text{AMPLITUDE}(\omega) &= X_i = \sqrt{(X_{is})^2 + (X_{ic})^2} \\ \text{PHASE}(\omega) &= \phi_i = \tan^{-1}\left(\frac{X_{is}}{X_{ic}}\right) \end{aligned} \right\} \begin{aligned} &\text{SAME AS (139)} \\ &\text{PULL VALUES FOR} \\ &\text{EACH DOF (i) OUT} \\ &\text{OF EQ (144) (145)} \end{aligned}$$

DOF SOLTN TO 144

$$\begin{Bmatrix} X_{is} \\ \vdots \\ X_{is} \\ X_{ic} \\ \vdots \\ X_{ic} \end{Bmatrix} = \text{INV} \begin{bmatrix} [-\omega^2 m_1 + k_1]_{N \times N} & -\omega^2 [c_1]_{N \times N} \\ \omega^2 [c_1]_{N \times N} & [-\omega^2 m_2 + k_2]_{N \times N} \end{bmatrix} \begin{Bmatrix} f_{1s} \\ \vdots \\ f_{1s} \\ f_{1c} \\ \vdots \\ f_{1c} \end{Bmatrix} \quad (145)$$

*

Appendix K
FEM Confirmation Test Results – Static Loading

Response to Static Load - Boundary Conditions = S-S

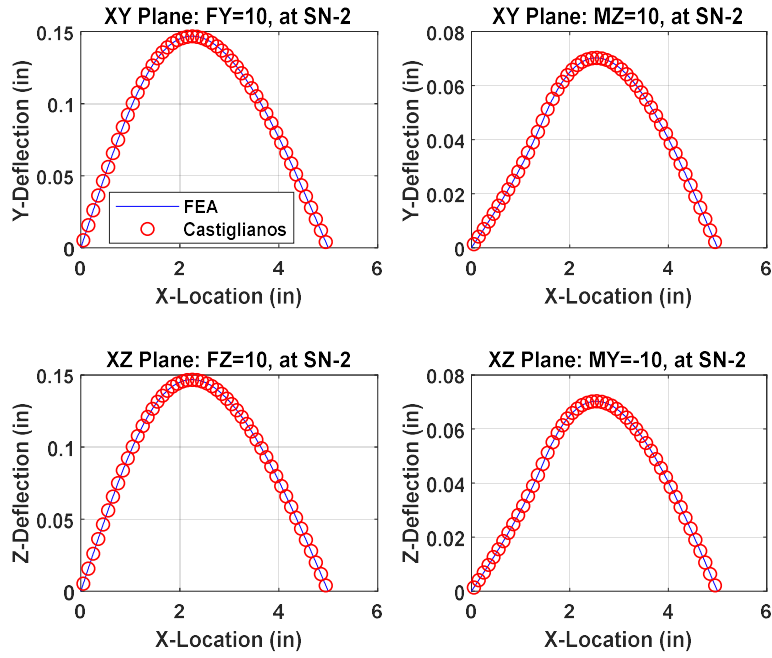


Figure App-K-1 Static load FEM confirmation response – SS end conditions

Response to Static Load - Boundary Conditions = C-S

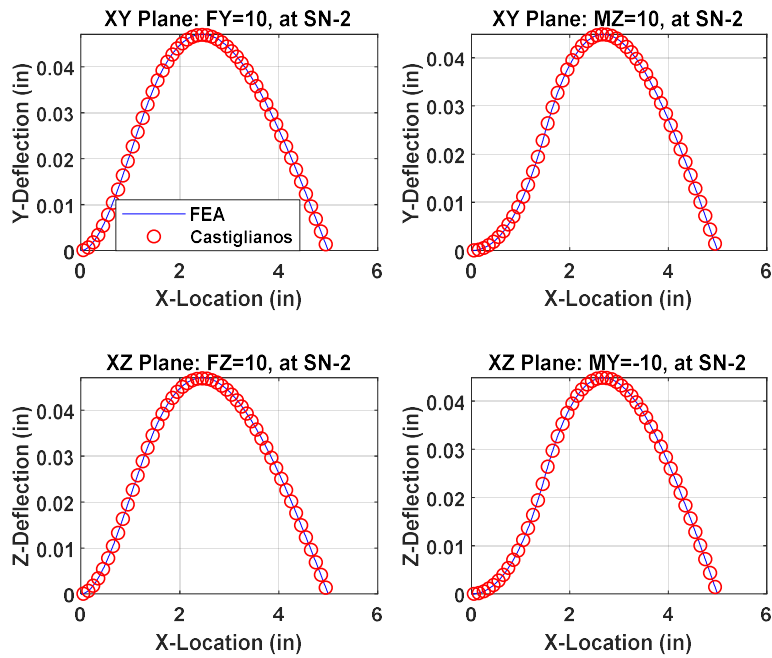


Figure App-K-2 Static load FEM confirmation response – CS end conditions

Response to Static Load - Boundary Conditions = C-C

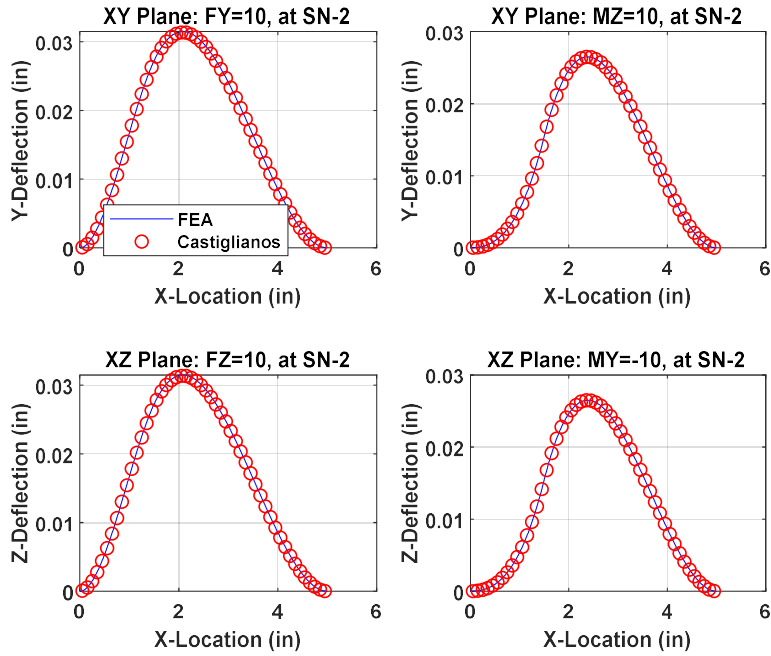


Figure App-K-3 Static load FEM confirmation response – CC end conditions

Response to Static Load - Boundary Conditions = C-F

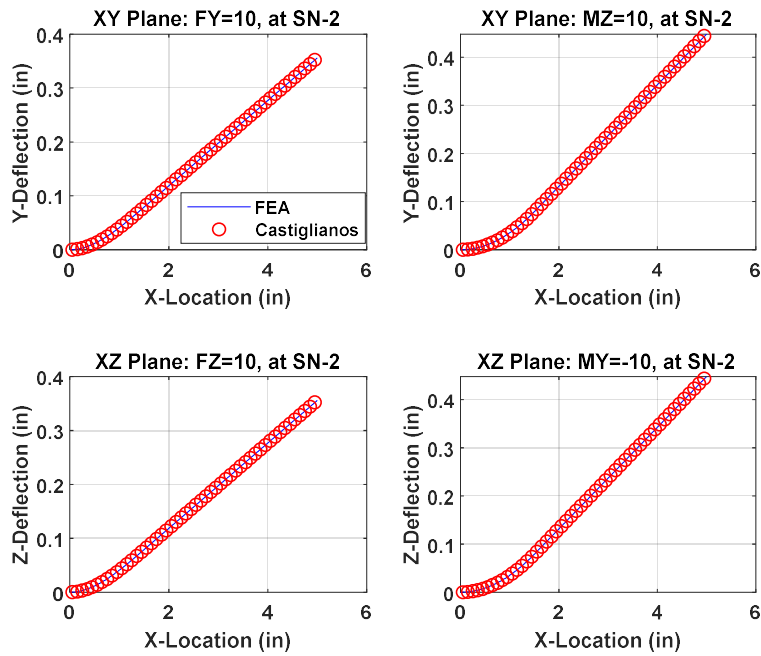


Figure App-K-4 Static load FEM confirmation response – CF end conditions

Appendix L

FEM Confirmation Test Results – Non-rotating vibration

Non-Rotating Beam Natural Frequency Calculations Clamped - Clamped End Conditions

Ref. = Blevins, Formulas for Natural Frequency and Mode Shape, pg 108

$$L_{\text{bar}} := 5\text{in} \quad r_o := .05\text{in} \quad r_i := 0\text{in} \quad E := 29.0 \cdot 10^6 \text{psi} \quad \rho := .2836 \frac{\text{lb}}{\text{in}^3}$$

$$\lambda_1 := 4.73004074 \quad \lambda_2 := 7.85320462 \quad \lambda_3 := 10.9956079 \quad \lambda_4 := 14.1371655 \quad \lambda_5 := 17.2787597$$

$$x := 0\text{in}, 0.005\text{in}..L_{\text{bar}} \quad I := \frac{\pi(r_o^4 - r_i^4)}{4} \quad A_{\text{bar}} := \pi(r_o^2 - r_i^2) \quad \text{mass}_{\text{perL}} := A_{\text{bar}} \cdot \rho$$

$$V_{\text{bar}} := A_{\text{bar}} \cdot L_{\text{bar}} \quad m_{\text{bar}} := A_{\text{bar}} \cdot L_{\text{bar}} \cdot \rho$$

$$A_{\text{bar}} = 0.00785 \cdot \text{in}^2 \quad I = 4.90874 \times 10^{-6} \cdot \text{in}^4$$

$$V_{\text{bar}} = 0.03927 \cdot \text{in}^3 \quad E \cdot I = 142.35342 \cdot \text{lbf} \cdot \text{in}^2$$

$$m_{\text{bar}} = 0.01114 \cdot \text{lb}$$

Cantilevered Bar:

$$\omega_1 := \left(\frac{\lambda_1^2}{L_{\text{bar}}^2} \right) \cdot \sqrt{\frac{E \cdot I}{\text{mass}_{\text{perL}}}} = 4445.48478 \frac{1}{\text{s}} \quad \omega_2 := \left(\frac{\lambda_2^2}{L_{\text{bar}}^2} \right) \cdot \sqrt{\frac{E \cdot I}{\text{mass}_{\text{perL}}}} = 12254.15 \frac{1}{\text{s}}$$

$$\omega_3 := \left(\frac{\lambda_3^2}{L_{\text{bar}}^2} \right) \cdot \sqrt{\frac{E \cdot I}{\text{mass}_{\text{perL}}}} = 24023.03392 \frac{1}{\text{s}} \quad \omega_4 := \left(\frac{\lambda_4^2}{L_{\text{bar}}^2} \right) \cdot \sqrt{\frac{E \cdot I}{\text{mass}_{\text{perL}}}} = 39711.29498 \frac{1}{\text{s}}$$

$$f_1 := \frac{\omega_1}{2 \cdot \pi} = 707.52088 \cdot \text{Hz}$$

$$f_2 := \frac{\omega_2}{2 \cdot \pi} = 1950.30855 \cdot \text{Hz}$$

$$f_3 := \frac{\omega_3}{2 \cdot \pi} = 3823.3846 \cdot \text{Hz}$$

$$f_4 := \frac{\omega_4}{2 \cdot \pi} = 6320.24889 \cdot \text{Hz}$$

Non-Rotating Beam Natural Frequency Calculations Clamped - Simply Supported End Conditions

Ref. = Blevins, Formulas for Natural Frequency and Mode Shape, pg 108

$$L_{\text{bar}} := 5\text{in} \quad r_o := .05\text{in} \quad r_i := 0\text{in} \quad E := 29.0 \cdot 10^6 \text{psi} \quad \rho := .2836 \frac{\text{lb}}{\text{in}^3}$$

$$\lambda_1 := 3.92660231 \quad \lambda_2 := 7.06858275 \quad \lambda_3 := 10.21017612 \quad \lambda_4 := 13.35176878 \quad \lambda_5 := 16.49336143$$

$$x := 0\text{in}, 0.005\text{in}..L_{\text{bar}} \quad I := \frac{\pi(r_o^4 - r_i^4)}{4} \quad A_{\text{bar}} := \pi(r_o^2 - r_i^2) \quad \text{mass}_{\text{perL}} := A_{\text{bar}} \cdot \rho$$

$$V_{\text{bar}} := A_{\text{bar}} \cdot L_{\text{bar}} \quad m_{\text{bar}} := A_{\text{bar}} \cdot L_{\text{bar}} \cdot \rho$$

$$A_{\text{bar}} = 0.00785 \cdot \text{in}^2 \quad I = 4.90874 \times 10^{-6} \cdot \text{in}^4$$

$$V_{\text{bar}} = 0.03927 \cdot \text{in}^3 \quad E \cdot I = 142.35342 \cdot \text{lbf} \cdot \text{in}^2$$

$$m_{\text{bar}} = 0.01114 \cdot \text{lb}$$

Cantilevered Bar:

$$\omega_1 := \left(\frac{\lambda_1^2}{L_{\text{bar}}^2} \right) \cdot \sqrt{\frac{E \cdot I}{\text{mass}_{\text{perL}}}} = 3063.5375 \frac{1}{\text{s}} \quad \omega_2 := \left(\frac{\lambda_2^2}{L_{\text{bar}}^2} \right) \cdot \sqrt{\frac{E \cdot I}{\text{mass}_{\text{perL}}}} = 9927.82374 \frac{1}{\text{s}}$$

$$\omega_3 := \left(\frac{\lambda_3^2}{L_{\text{bar}}^2} \right) \cdot \sqrt{\frac{E \cdot I}{\text{mass}_{\text{perL}}}} = 20713.61177 \frac{1}{\text{s}} \quad \omega_4 := \left(\frac{\lambda_4^2}{L_{\text{bar}}^2} \right) \cdot \sqrt{\frac{E \cdot I}{\text{mass}_{\text{perL}}}} = 35421.50183 \frac{1}{\text{s}}$$

$$f_1 := \frac{\omega_1}{2 \cdot \pi} = 487.57714 \cdot \text{Hz}$$

$$f_2 := \frac{\omega_2}{2 \cdot \pi} = 1580.06222 \cdot \text{Hz}$$

$$f_3 := \frac{\omega_3}{2 \cdot \pi} = 3296.6737 \cdot \text{Hz}$$

$$f_4 := \frac{\omega_4}{2 \cdot \pi} = 5637.50711 \cdot \text{Hz}$$

Non-Rotating Beam Natural Frequency Calculations *Clamped - Free End Conditions*

Ref. = Blevins, Formulas for Natural Frequency and Mode Shape, pg 108

$$L_{\text{bar}} := 5\text{in}$$

$$r_o := 0.05\text{in}$$

$$r_i := 0\text{in}$$

$$E := 29.0 \cdot 10^6 \text{ psi}$$

$$\rho := .2836 \frac{\text{lb}}{\text{in}^3}$$

$$\lambda_1 := 1.87510407$$

$$\lambda_2 := 4.69409113$$

$$\lambda_3 := 7.85475744$$

$$\lambda_4 := 10.99554073$$

$$\lambda_5 := 14.13716839$$

$$x := 0\text{in}, 0.005\text{in}..L_{\text{bar}} \quad I := \frac{\pi(r_o^4 - r_i^4)}{4} \quad A_{\text{bar}} := \pi(r_o^2 - r_i^2) \quad \text{mass}_{\text{perL}} := A_{\text{bar}} \cdot \rho$$

$$V_{\text{bar}} := A_{\text{bar}} \cdot L_{\text{bar}} \quad m_{\text{bar}} := A_{\text{bar}} \cdot L_{\text{bar}} \cdot \rho$$

$$A_{\text{bar}} = 0.00785 \cdot \text{in}^2 \quad I = 4.90874 \times 10^{-6} \cdot \text{in}^4$$

$$V_{\text{bar}} = 0.03927 \cdot \text{in}^3 \quad E \cdot I = 142.35342 \cdot \text{lbf} \cdot \text{in}^2$$

$$m_{\text{bar}} = 0.01114 \cdot \text{lb}$$

Cantilevered Bar:

$$\omega_1 := \left(\frac{\lambda_1^2}{L_{\text{bar}}^2} \right) \cdot \sqrt{\frac{E \cdot I}{\text{mass}_{\text{perL}}}} = 698.61856 \frac{1}{\text{s}} \quad \omega_2 := \left(\frac{\lambda_2^2}{L_{\text{bar}}^2} \right) \cdot \sqrt{\frac{E \cdot I}{\text{mass}_{\text{perL}}}} = 4378.16776 \frac{1}{\text{s}}$$

$$\omega_3 := \left(\frac{\lambda_3^2}{L_{\text{bar}}^2} \right) \cdot \sqrt{\frac{E \cdot I}{\text{mass}_{\text{perL}}}} = 12258.99652 \frac{1}{\text{s}} \quad \omega_4 := \left(\frac{\lambda_4^2}{L_{\text{bar}}^2} \right) \cdot \sqrt{\frac{E \cdot I}{\text{mass}_{\text{perL}}}} = 24022.74041 \frac{1}{\text{s}}$$

$$f_1 := \frac{\omega_1}{2 \cdot \pi} = 111.1886 \cdot \text{Hz}$$

$$f_2 := \frac{\omega_2}{2 \cdot \pi} = 696.80704 \cdot \text{Hz}$$

$$f_3 := \frac{\omega_3}{2 \cdot \pi} = 1951.07989 \cdot \text{Hz}$$

$$f_4 := \frac{\omega_4}{2 \cdot \pi} = 3823.33788 \cdot \text{Hz}$$

Table App-L-1 Non-Rotating FEM confirmation response – CC end conditions

Single Beam - Clamped-Clamped

Beam Length	5.00	4.00	3.00	2.00	1.00	0.50		
Beam Outer Radius	0.05	0.05	0.05	0.05	0.05	0.05		
Beam Inner Radius	0	0	0	0	0	0		
Beam Density	0.2836	0.2836	0.2836	0.2836	0.2836	0.2836		
Beam Modulus	2.90E+07	2.90E+07	2.90E+07	2.90E+07	2.90E+07	2.90E+07		
Beam Aspect Ratio	50.0	40.0	30.0	20.0	10.0	5.0		
	No. Elements	Timoshenko Coef.						
Blevins Results (Hz): (Blevins = Euler-Bernoulli Beam Theory)								
Mode 1	N/A	707.5	1105.5	1965.3	4422.0	17688.0	70752.1	
Mode 2		1950.3	3047.4	5417.5	12189.4	48757.7	195031.0	
Mode 3		3823.4	5974.0	10620.5	23896.2	95584.6	382338.0	
Mode 4		6320.2	9875.4	17556.2	39501.6	158006.0	632025.0	
FEM Code Results (Hz)								
Mode 1	128	1.00	706.5	1102.9	1956.5	4375.8	16966.7	60990.6
Mode 2			1942.9	3028.8	5358.3	11892.1	44466.0	145591.0
Mode 3			3796.4	5908.1	10413.9	22886.9	82132.3	248798.4
Mode 4			6249.5	9704.8	17029.6	36994.6	127192.1	361639.8
Mode 1	128	0.95	706.5	1102.7	1956.1	4373.5	16933.9	60613.6
Mode 2			1942.5	3028.0	5355.6	11879.0	44296.4	144126.3
Mode 3			3795.2	5905.2	10405.0	22845.5	81664.5	245676.5
Mode 4			6246.6	9697.7	17008.2	36897.9	126243.1	356488.8
Mode 1	128	0.90	706.4	1102.6	1955.6	4371.0	16897.7	60202.6
Mode 2			1942.1	3027.0	5352.6	11864.5	44110.2	142548.0
Mode 3			3793.9	5902.0	10395.2	22799.7	81153.7	242342.0
Mode 4			6243.3	9689.9	16984.5	36791.5	125212.5	351017.6
Mode 1	128	0.85	706.3	1102.4	1955.0	4368.2	16857.4	59752.5
Mode 2			1941.7	3025.9	5349.2	11848.3	43904.7	140842.3
Mode 3			3792.4	5898.5	10384.3	22748.9	80593.7	238772.1
Mode 4			6239.6	9681.1	16958.1	36673.5	124089.3	345193.8

Error (Code-Blevins/Blevins)

	Timoshenko Coef.	Beam Aspect Ratio					
		50.0	40.0	30.0	20.0	10.0	5.0
Mode 1	1.00	-0.14%	-0.24%	-0.45%	-1.04%	-4.08%	-13.80%
	0.95	-0.15%	-0.25%	-0.47%	-1.10%	-4.26%	-14.33%
	0.90	-0.16%	-0.26%	-0.50%	-1.15%	-4.47%	-14.91%
	0.85	-0.17%	-0.28%	-0.53%	-1.22%	-4.70%	-15.55%
Mode 2	1.00	-0.38%	-0.61%	-1.09%	-2.44%	-8.80%	-25.35%
	0.95	-0.40%	-0.64%	-1.14%	-2.55%	-9.15%	-26.10%
	0.90	-0.42%	-0.67%	-1.20%	-2.67%	-9.53%	-26.91%
	0.85	-0.44%	-0.70%	-1.26%	-2.80%	-9.95%	-27.78%
Mode 3	1.00	-0.71%	-1.10%	-1.95%	-4.22%	-14.07%	-34.93%
	0.95	-0.74%	-1.15%	-2.03%	-4.40%	-14.56%	-35.74%
	0.90	-0.77%	-1.21%	-2.12%	-4.59%	-15.10%	-36.62%
	0.85	-0.81%	-1.27%	-2.22%	-4.80%	-15.68%	-37.55%
Mode 4	1.00	-1.12%	-1.73%	-3.00%	-6.35%	-19.50%	-42.78%
	0.95	-1.17%	-1.80%	-3.12%	-6.59%	-20.10%	-43.60%
	0.90	-1.22%	-1.88%	-3.26%	-6.86%	-20.75%	-44.46%
	0.85	-1.28%	-1.97%	-3.41%	-7.16%	-21.47%	-45.38%

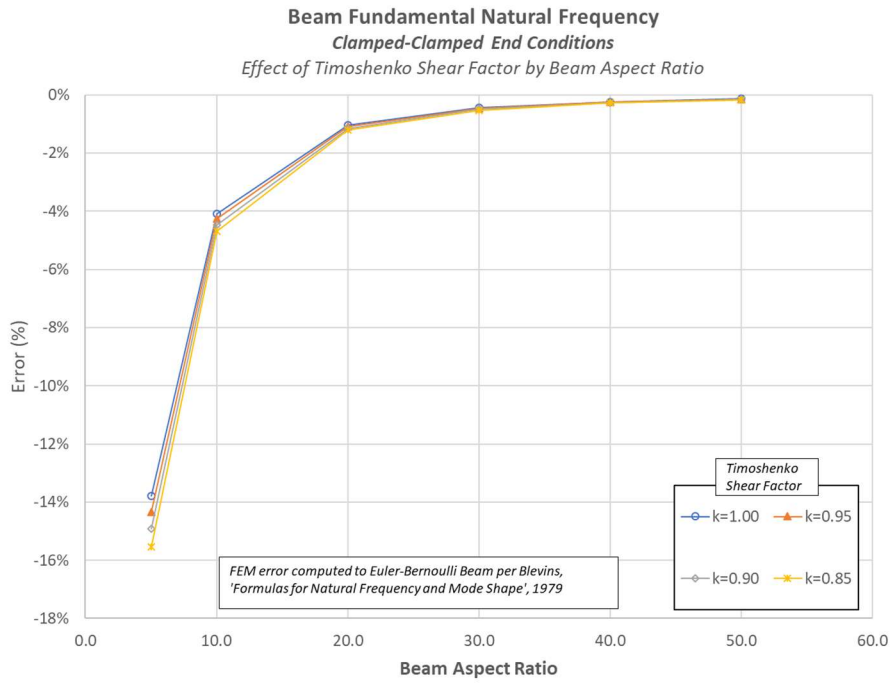


Figure App-L-1 Non-Rotating FEM confirmation response – CC end conditions, mode 1

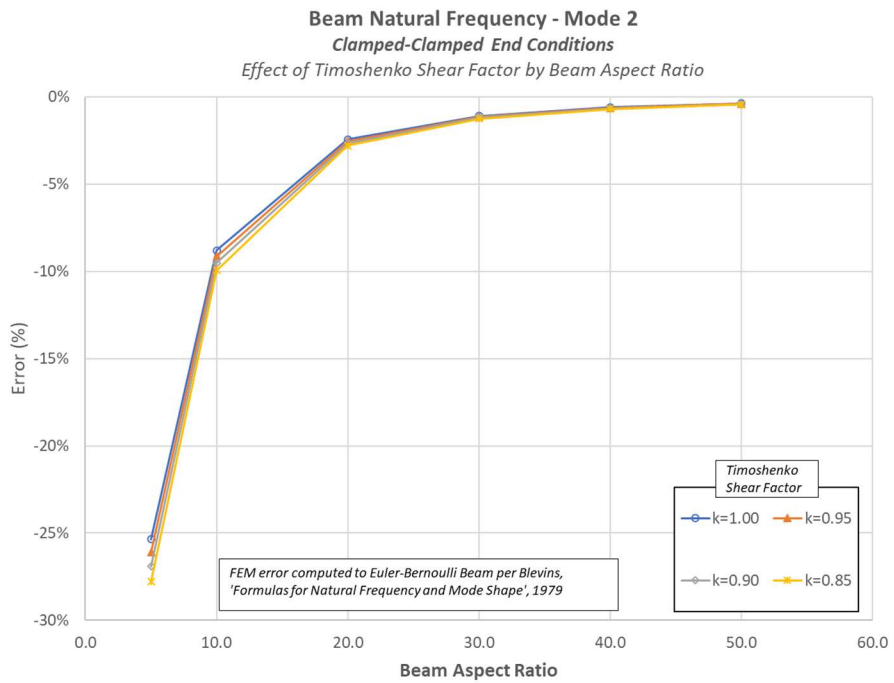


Figure App-L-2 Non-Rotating FEM confirmation response – CC end conditions, mode 2

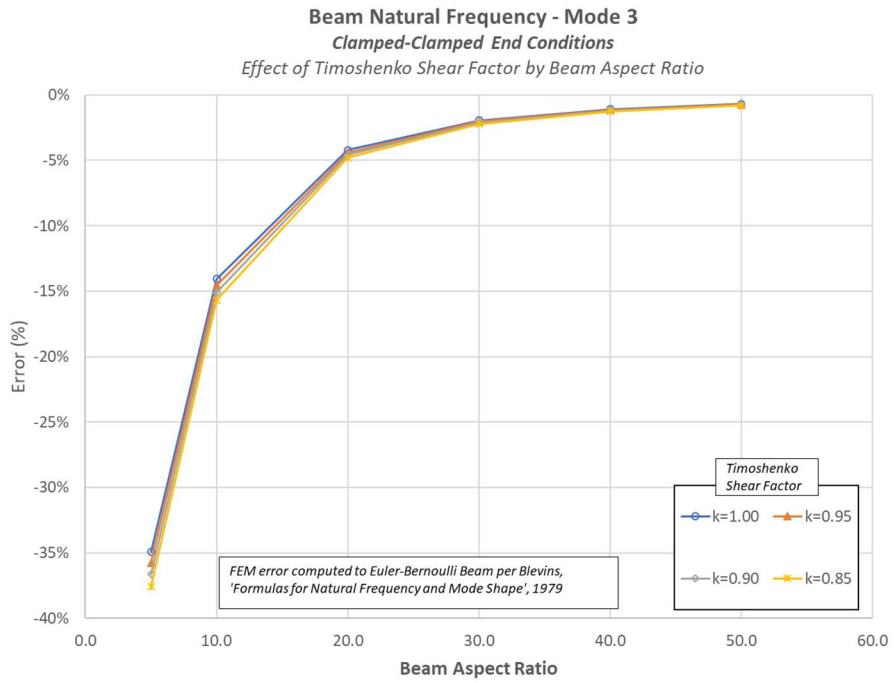


Figure App-L-3 Non-Rotating FEM confirmation response – CC end conditions, mode 3

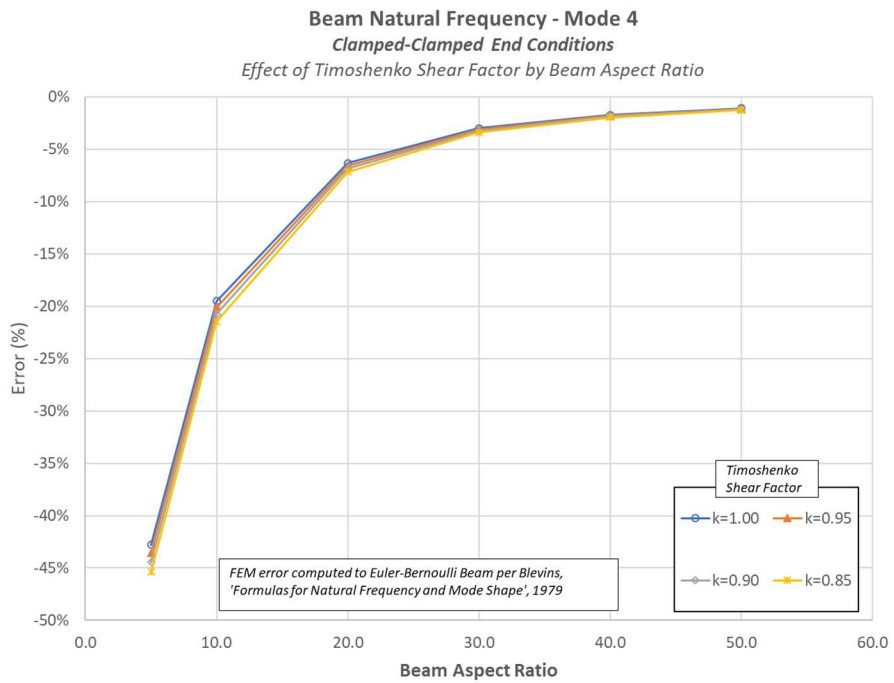


Figure App-L-4 Non-Rotating FEM confirmation response – CC end conditions, mode 4

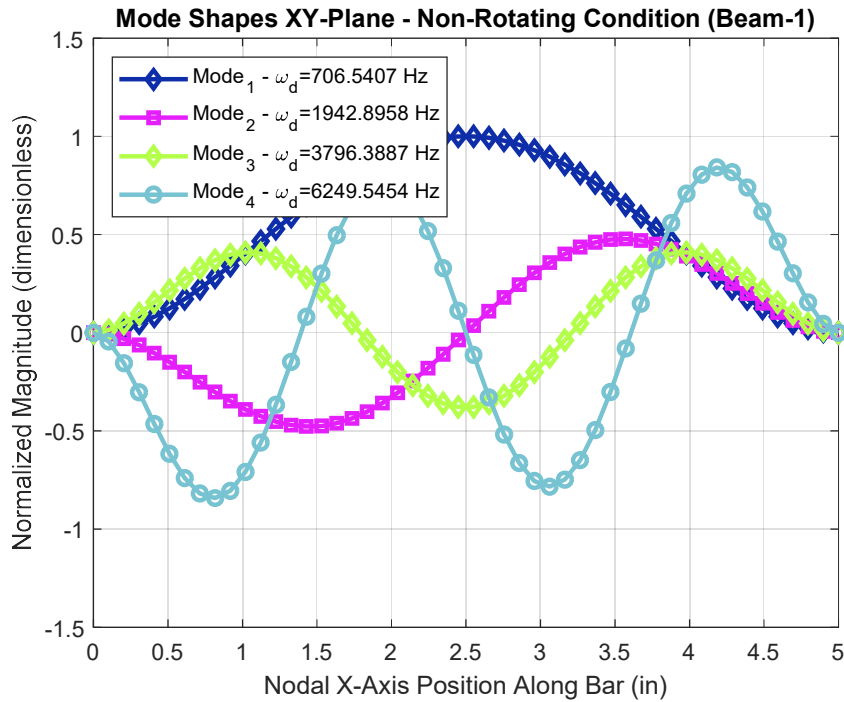


Figure App-L-5 Non-Rotating FEM confirmation response – CC end conditions, XY mode shapes

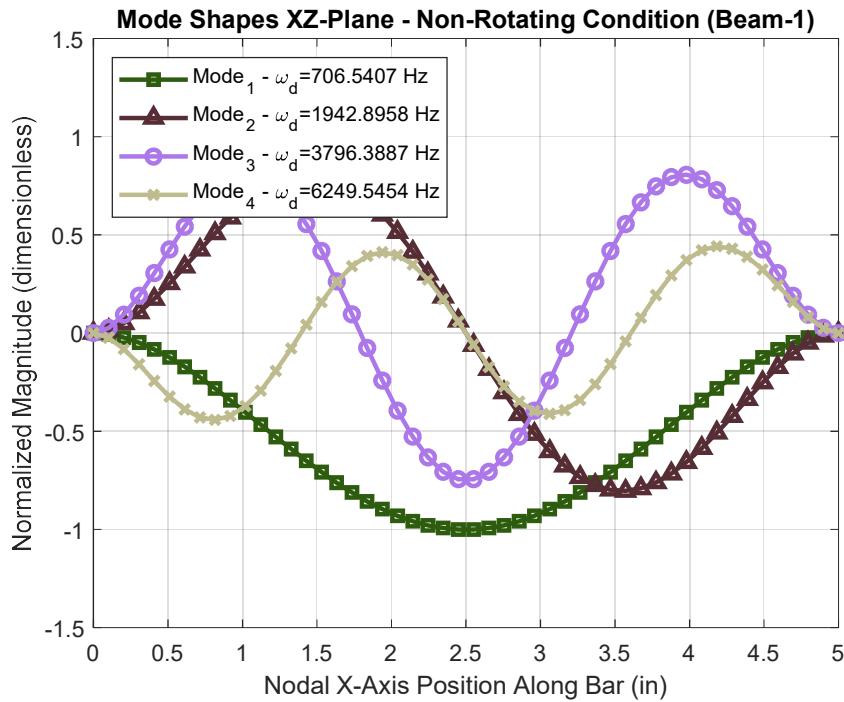


Figure App-L-6 Non-Rotating FEM confirmation response – CC end conditions, XZ mode shapes

Table App-L-2 Non-Rotating FEM confirmation response – CS end conditions

Single Beam - Clamped-Simply Supported

Beam Length	5.00	4.00	3.00	2.00	1.00	0.50		
Beam Outer Radius	0.05	0.05	0.05	0.05	0.05	0.05		
Beam Inner Radius	0	0	0	0	0	0		
Beam Density	0.2836	0.2836	0.2836	0.2836	0.2836	0.2836		
Beam Modulus	2.90E+07	2.90E+07	2.90E+07	2.90E+07	2.90E+07	2.90E+07		
Beam Aspect Ratio	50.0	40.0	30.0	20.0	10.0	5.0		
	No. Elements	Timoshenko Coef.						
Blevins Results (Hz): (Blevins = Euler-Bernoulli Beam Theory)								
Mode 1	N/A	487.6	761.8	1354.4	3047.4	12189.4	48757.7	
Mode 2		1580.1	2468.8	4389.1	9875.4	39501.6	158006.0	
Mode 3		3296.7	5151.1	9157.4	20604.2	82416.8	329667.0	
Mode 4		5637.5	8808.6	15659.7	35234.4	140938.0	563751.0	
FEM Code Results (Hz)								
Mode 1	128	1.00	487.3	760.9	1351.0	3029.1	11893.0	44468.4
Mode 2			1576.0	2458.7	4356.1	9707.7	37003.3	127203.2
Mode 3			3279.1	5107.9	9021.4	19933.5	73172.6	231933.0
Mode 4			5586.7	8685.8	15279.2	33405.7	117674.3	348211.6
Mode 1	128	0.95	487.2	760.8	1350.9	3028.2	11879.9	44298.8
Mode 2			1575.9	2458.2	4354.6	9700.6	36906.5	126253.2
Mode 3			3278.3	5106.1	9015.8	19907.0	72853.6	229522.9
Mode 4			5584.7	8680.9	15264.3	33337.3	116955.8	343837.0
Mode 1	128	0.90	487.2	760.8	1350.7	3027.3	11865.4	44112.5
Mode 2			1575.6	2457.7	4353.0	9692.8	36799.9	125221.6
Mode 3			3277.5	5104.1	9009.7	19877.6	72503.8	226929.0
Mode 4			5582.4	8675.5	15247.8	33261.7	116172.2	339157.4
Mode 1	128	0.85	487.2	760.7	1350.5	3026.2	11849.3	43906.5
Mode 2			1575.4	2457.1	4351.3	9684.0	36681.8	124097.4
Mode 3			3276.6	5101.8	9002.8	19845.0	72118.6	224129.5
Mode 4			5579.9	8669.5	15229.4	33177.9	115314.1	334139.1

Error (Code-Blevins/Blevins)

	Timoshenko Coef.	Beam Aspect Ratio					
		50.0	40.0	30.0	20.0	10.0	5.0
Mode 1	1.00	-0.07%	-0.12%	-0.25%	-0.60%	-2.43%	-8.80%
	0.95	-0.07%	-0.13%	-0.26%	-0.63%	-2.54%	-9.14%
	0.90	-0.08%	-0.14%	-0.27%	-0.66%	-2.66%	-9.53%
	0.85	-0.08%	-0.15%	-0.29%	-0.69%	-2.79%	-9.95%
Mode 2	1.00	-0.25%	-0.41%	-0.75%	-1.70%	-6.32%	-19.49%
	0.95	-0.27%	-0.43%	-0.78%	-1.77%	-6.57%	-20.10%
	0.90	-0.28%	-0.45%	-0.82%	-1.85%	-6.84%	-20.75%
	0.85	-0.29%	-0.48%	-0.86%	-1.94%	-7.14%	-21.46%
Mode 3	1.00	-0.53%	-0.84%	-1.49%	-3.26%	-11.22%	-29.65%
	0.95	-0.56%	-0.87%	-1.55%	-3.38%	-11.60%	-30.38%
	0.90	-0.58%	-0.91%	-1.61%	-3.53%	-12.03%	-31.16%
	0.85	-0.61%	-0.96%	-1.69%	-3.68%	-12.50%	-32.01%
Mode 4	1.00	-0.90%	-1.39%	-2.43%	-5.19%	-16.51%	-38.23%
	0.95	-0.94%	-1.45%	-2.53%	-5.38%	-17.02%	-39.01%
	0.90	-0.98%	-1.51%	-2.63%	-5.60%	-17.57%	-39.84%
	0.85	-1.02%	-1.58%	-2.75%	-5.84%	-18.18%	-40.73%

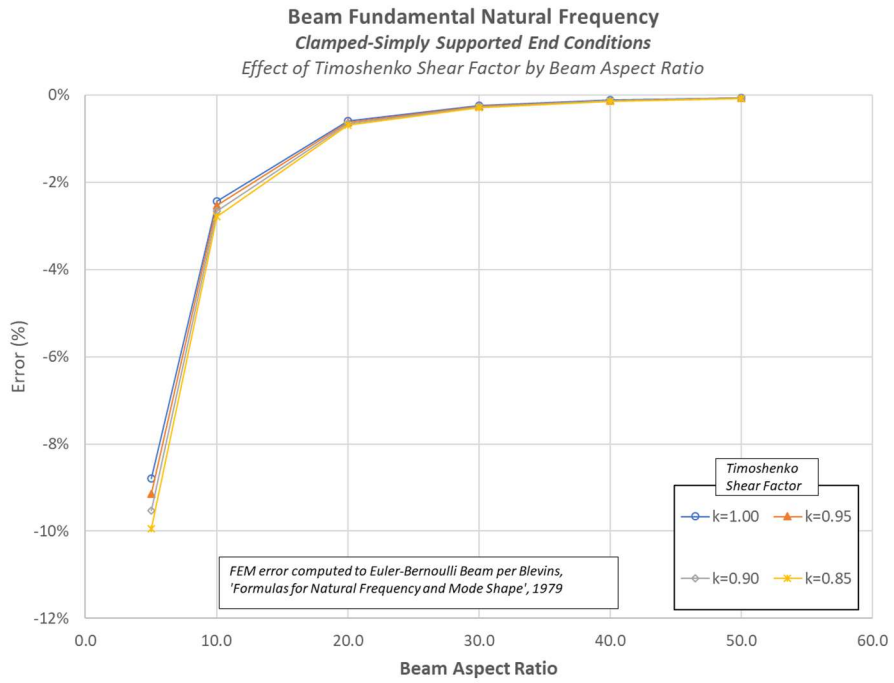


Figure App-L-7 Non-Rotating FEM confirmation response – CS end conditions, mode 1

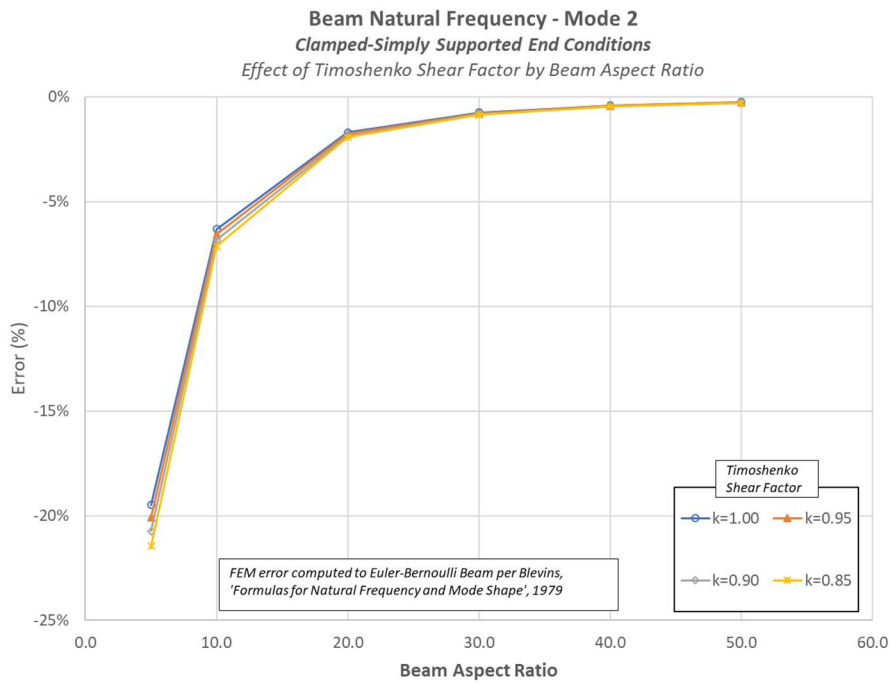


Figure App-L-8 Non-Rotating FEM confirmation response – CS end conditions, mode 2

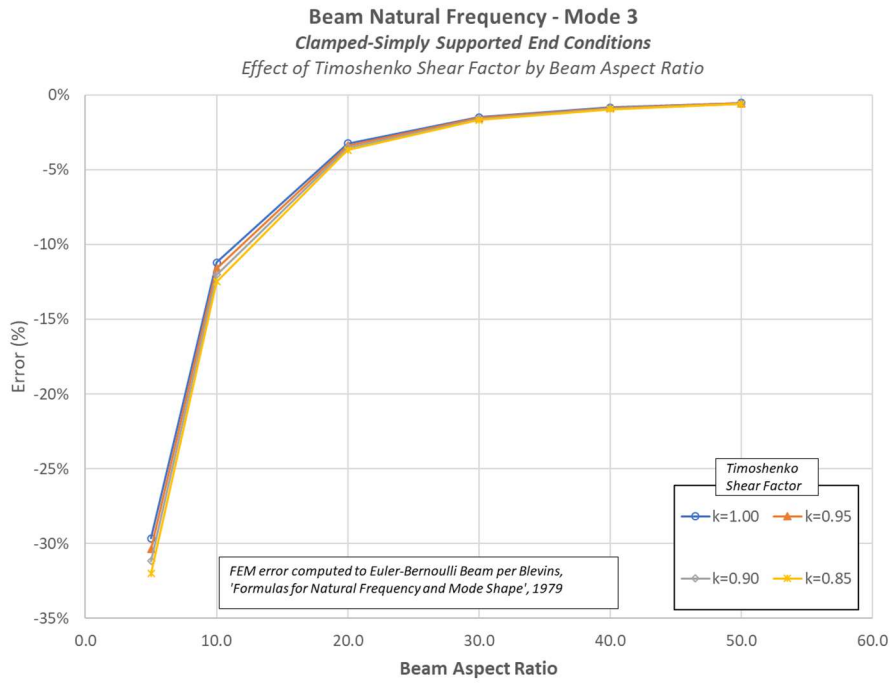


Figure App-L-9 Non-Rotating FEM confirmation response – CS end conditions, mode 3

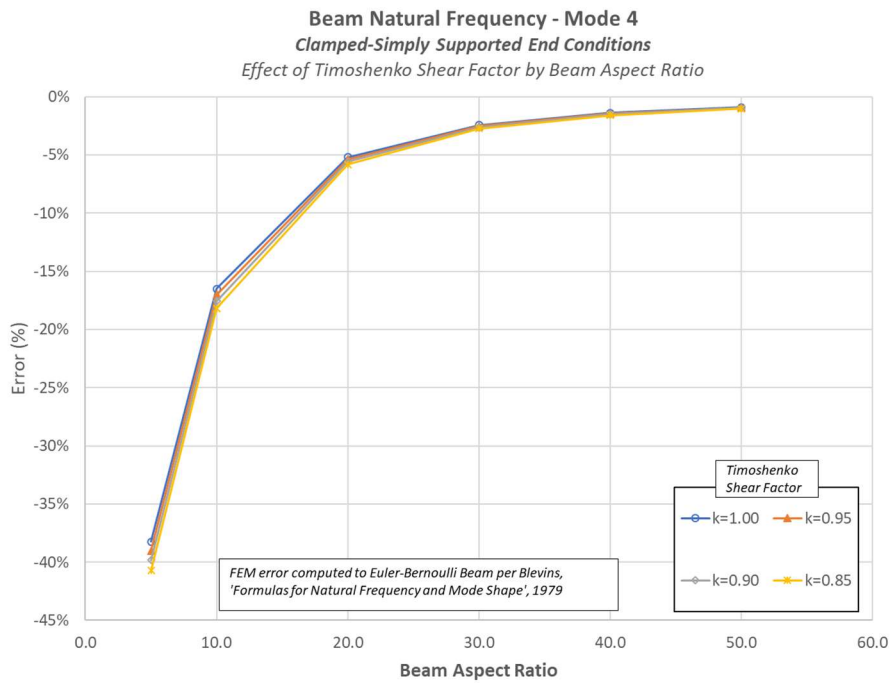


Figure App-L-10 Non-Rotating FEM confirmation response – CS end conditions, mode 4

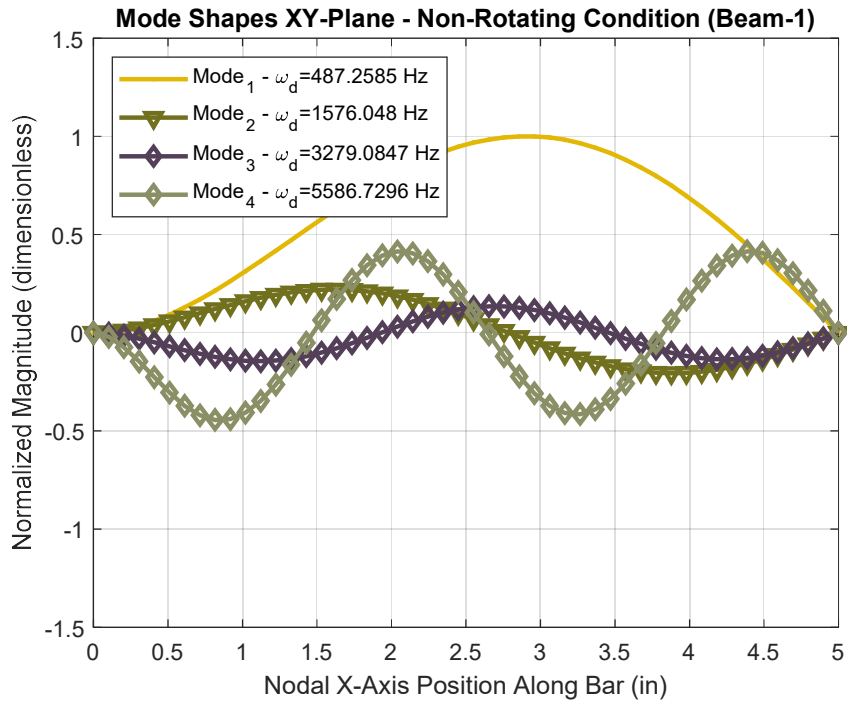


Figure App-L-11 Non-Rotating FEM confirmation response – CS end conditions, XY mode shapes

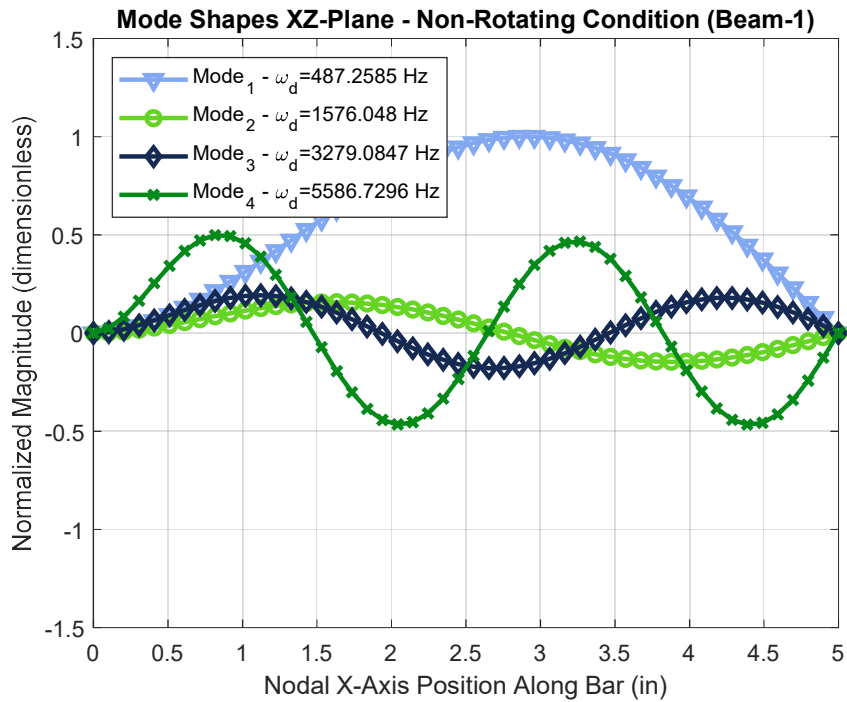


Figure App-L-12 Non-Rotating FEM confirmation response – CS end conditions, XZ mode shapes

Table App-L-3 Non-Rotating FEM confirmation response – CF end conditions

Single Beam - Clamped-Free

Beam Length	5.00	4.00	3.00	2.00	1.00	0.50		
Beam Outer Radius	0.05	0.05	0.05	0.05	0.05	0.05		
Beam Inner Radius	0	0	0	0	0	0		
Beam Density	0.2836	0.2836	0.2836	0.2836	0.2836	0.2836		
Beam Modulus	2.90E+07	2.90E+07	2.90E+07	2.90E+07	2.90E+07	2.90E+07		
Beam Aspect Ratio	50.0	40.0	30.0	20.0	10.0	5.0		
	No. Elements	Timoshenko Coef.						
Blevins Results (Hz): (Blevins = Euler-Bernoulli Beam Theory)								
Mode 1	N/A	111.2	173.7	308.9	694.9	2779.7	11118.9	
Mode 2		696.8	1088.8	1935.6	4355.0	17420.2	69680.7	
Mode 3		1951.1	3048.6	5419.7	12194.2	48777.0	195108.0	
Mode 4		3823.3	5974.0	10620.4	23895.9	95583.4	382334.0	
FEM Code Results (Hz)								
Mode 1	128	1.00	111.2	173.7	308.8	694.6	2766.4	10899.1
Mode 2			696.0	1086.6	1928.4	4317.3	16825.3	61406.9
Mode 3			1944.7	3032.8	5369.3	11941.4	45092.9	151551.4
Mode 4			3799.2	5915.3	10437.2	23000.8	83515.8	259131.2
Mode 1	128	0.95	111.2	173.7	308.8	694.3	2765.9	10890.8
Mode 2			696.0	1086.5	1928.1	4315.8	16803.7	61146.4
Mode 3			1944.5	3032.2	5367.4	11932.1	44969.2	150432.3
Mode 4			3798.3	5913.1	10430.4	22968.8	83145.4	256522.8
Mode 1	128	0.90	111.2	173.7	308.8	694.2	2765.3	10881.7
Mode 2			695.9	1086.4	1927.8	4314.2	16779.8	60860.6
Mode 3			1944.2	3031.5	5365.3	11921.7	44832.9	149217.6
Mode 4			3797.3	5910.7	10422.9	22933.5	82739.5	253714.2
Mode 1	128	0.85	111.2	173.7	308.8	694.2	2764.6	10871.5
Mode 2			695.9	1086.3	1927.4	4312.4	16753.1	60545.7
Mode 3			1943.9	3030.7	5362.9	11910.1	44682.0	147894.6
Mode 4			3796.2	5907.9	10414.5	22894.1	82292.6	250681.1

Error (Code-Blevins/Blevins)

	Timoshenko Coef.	Beam Aspect Ratio					
		50.0	40.0	30.0	20.0	10.0	5.0
Mode 1	1.00	0.02%	0.01%	-0.02%	-0.05%	-0.48%	-1.98%
	0.95	0.02%	0.01%	-0.02%	-0.10%	-0.50%	-2.05%
	0.90	0.02%	0.00%	-0.02%	-0.10%	-0.52%	-2.13%
	0.85	0.02%	0.00%	-0.03%	-0.11%	-0.54%	-2.23%
Mode 2	1.00	-0.11%	-0.20%	-0.37%	-0.87%	-3.41%	-11.87%
	0.95	-0.12%	-0.20%	-0.39%	-0.90%	-3.54%	-12.25%
	0.90	-0.13%	-0.21%	-0.40%	-0.94%	-3.68%	-12.66%
	0.85	-0.13%	-0.22%	-0.42%	-0.98%	-3.83%	-13.11%
Mode 3	1.00	-0.32%	-0.52%	-0.93%	-2.07%	-7.55%	-22.32%
	0.95	-0.34%	-0.54%	-0.96%	-2.15%	-7.81%	-22.90%
	0.90	-0.35%	-0.56%	-1.00%	-2.24%	-8.09%	-23.52%
	0.85	-0.37%	-0.59%	-1.05%	-2.33%	-8.40%	-24.20%
Mode 4	1.00	-0.63%	-0.98%	-1.73%	-3.75%	-12.63%	-32.22%
	0.95	-0.65%	-1.02%	-1.79%	-3.88%	-13.01%	-32.91%
	0.90	-0.68%	-1.06%	-1.86%	-4.03%	-13.44%	-33.64%
	0.85	-0.71%	-1.11%	-1.94%	-4.19%	-13.90%	-34.43%

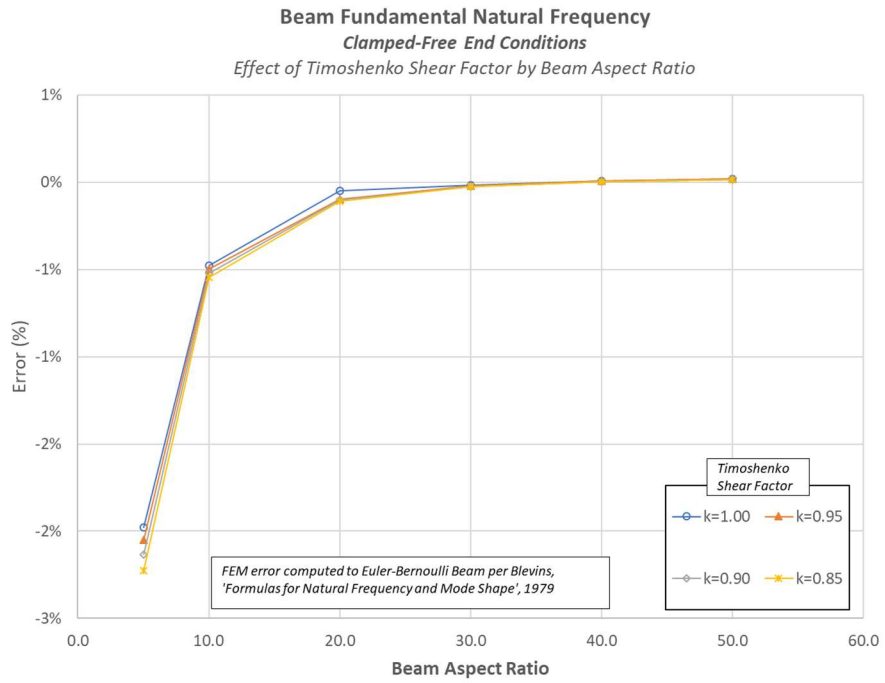


Figure App-L-13 Non-Rotating FEM confirmation response – CF end conditions, mode 1

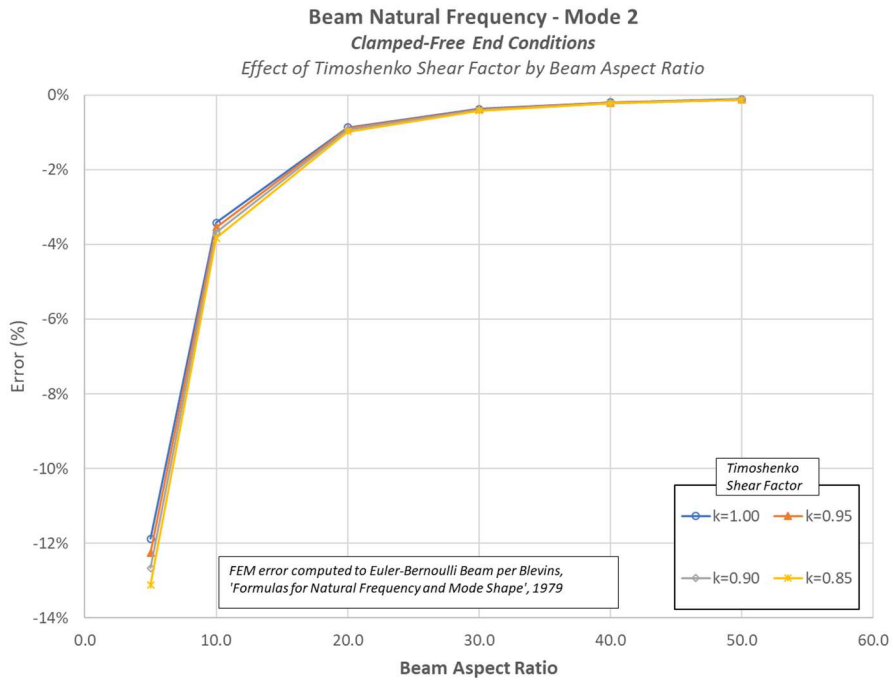


Figure App-L-14 Non-Rotating FEM confirmation response – CF end conditions, mode 2

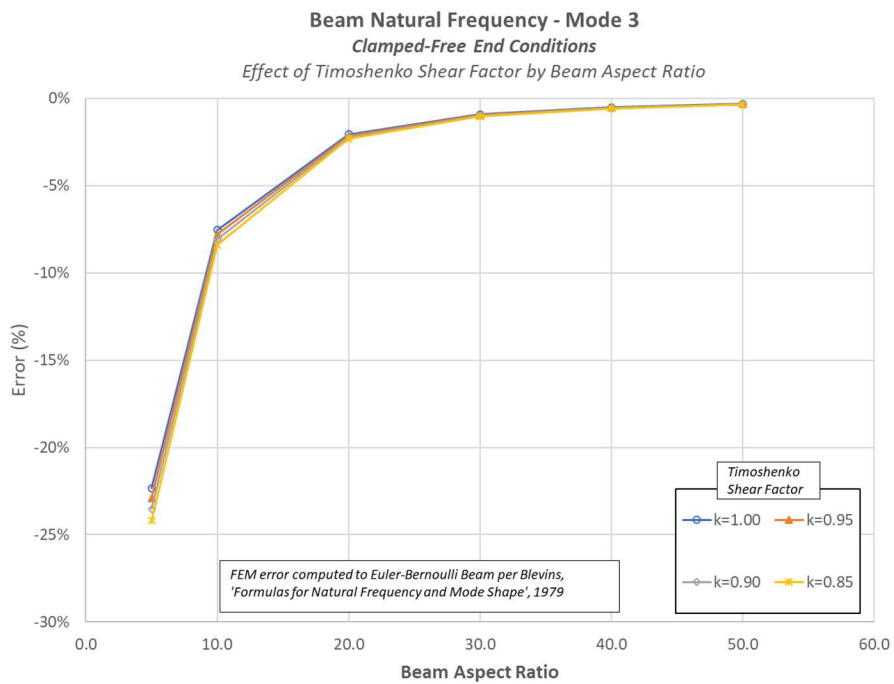


Figure App-L-15 Non-Rotating FEM confirmation response – CF end conditions, mode 3

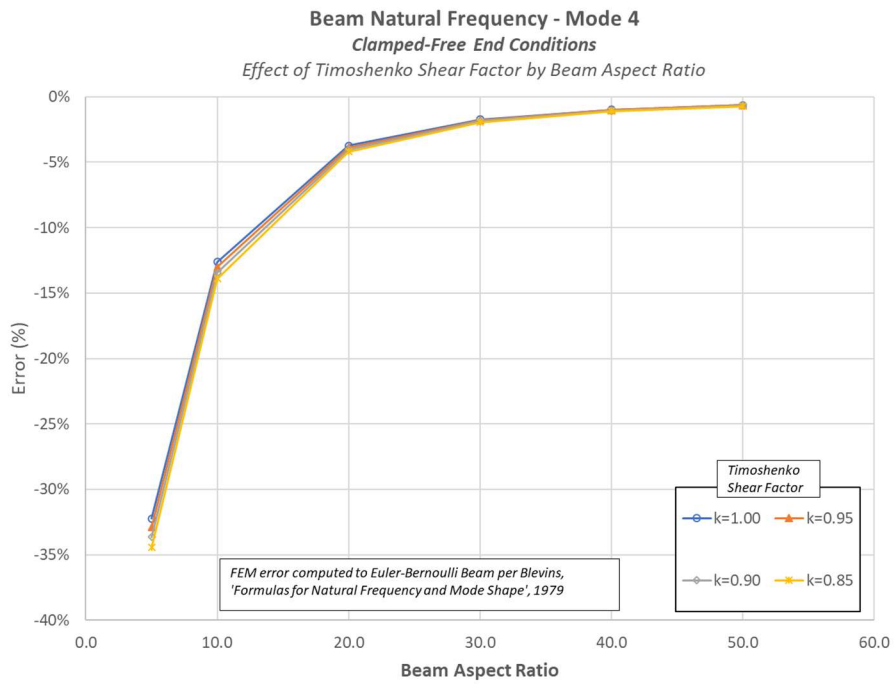


Figure App-L-16 Non-Rotating FEM confirmation response – CF end conditions, mode 4

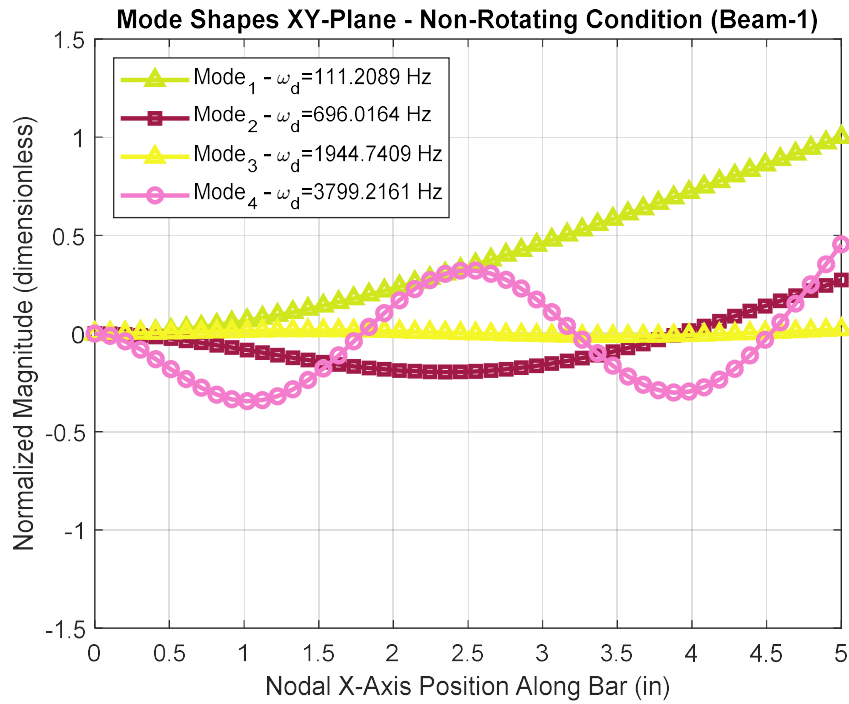


Figure App-L-17 Non-Rotating FEM confirmation response – CF end conditions, XY mode shapes

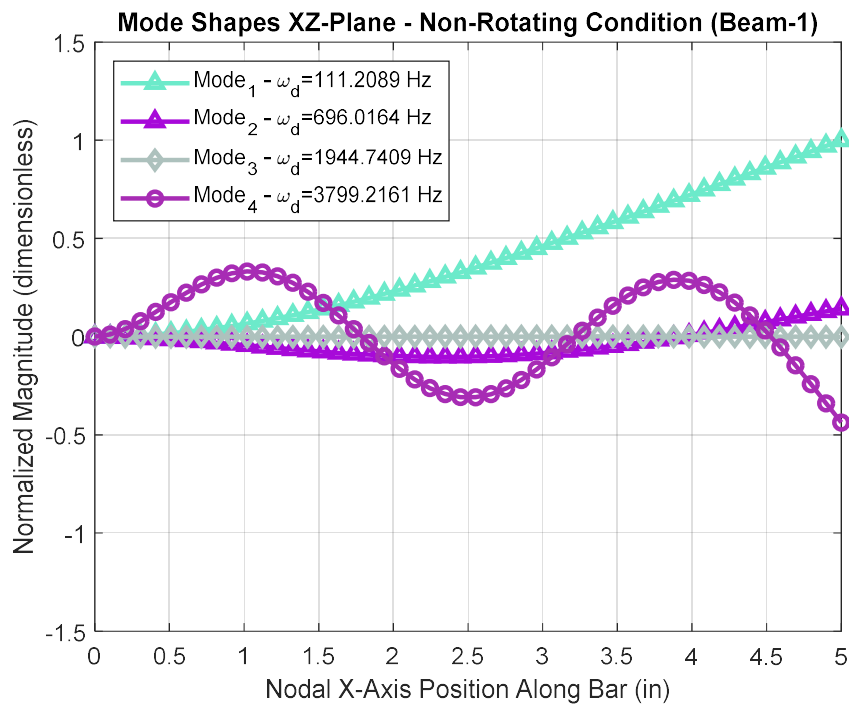


Figure App-L-18 Non-Rotating FEM confirmation response – CF end conditions, XZ mode shapes

Appendix M

FEM Confirmation Test Results – Rotordynamic Code Comparison Output Plots

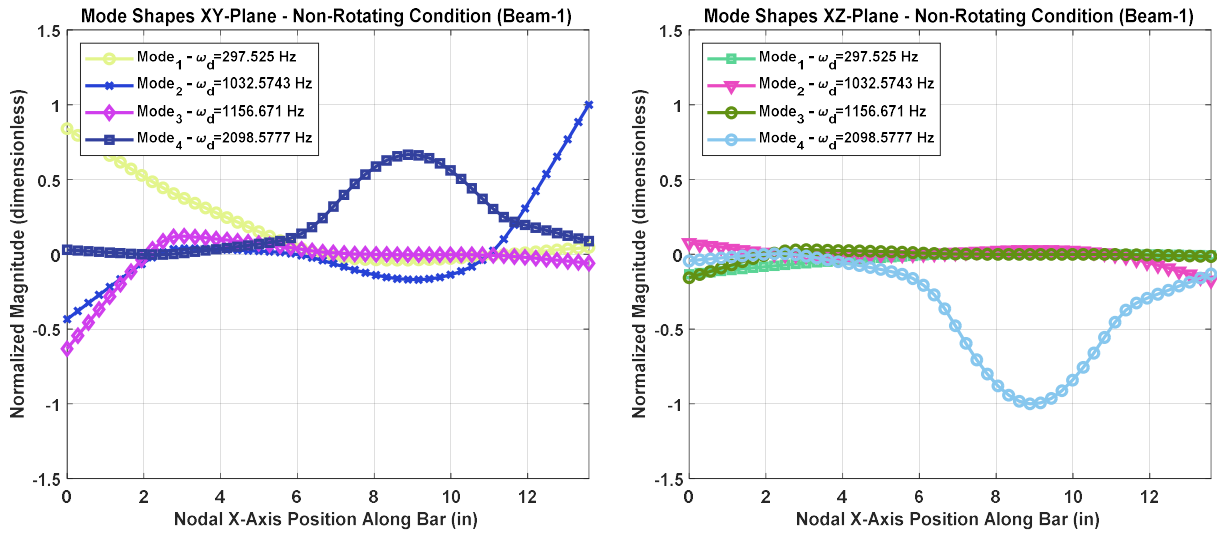


Figure App-M-1 Zorzi/Nelson - Non-Rotating Mode Shapes – Undamped Case

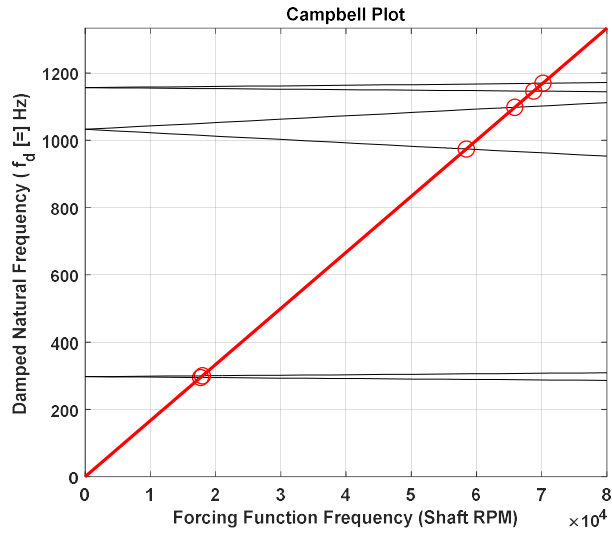


Figure App-M-2 Zorzi/Nelson – Campbell Plot – Undamped Case

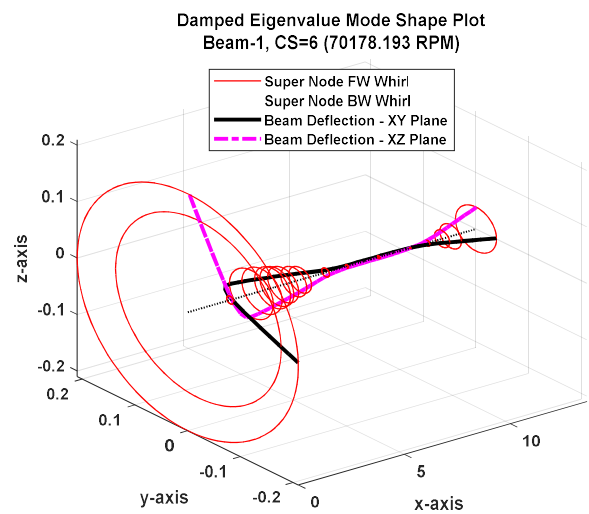
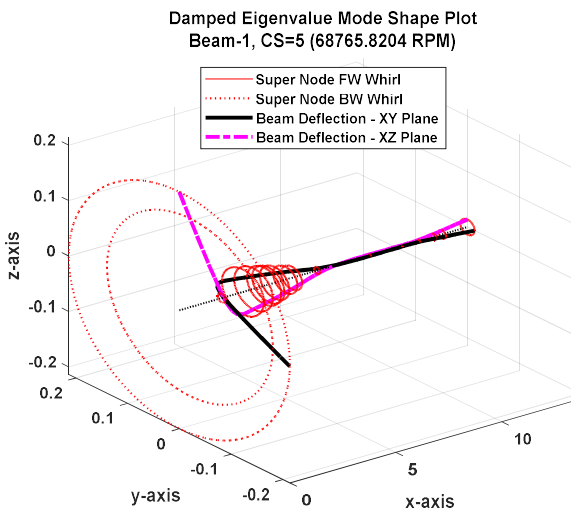
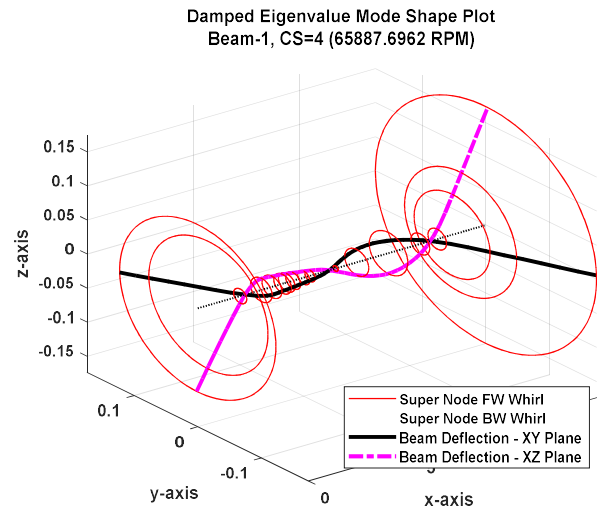
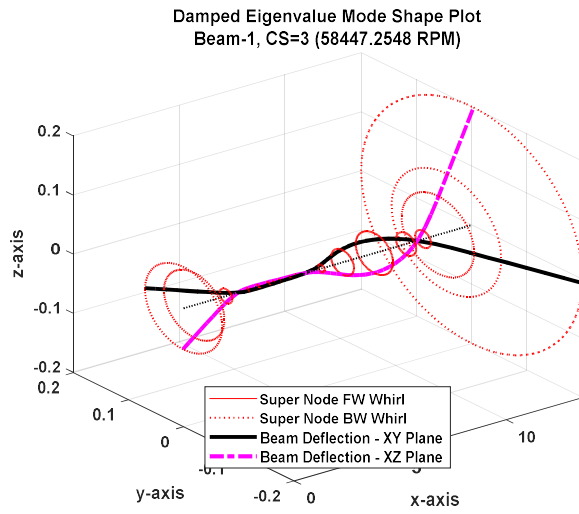
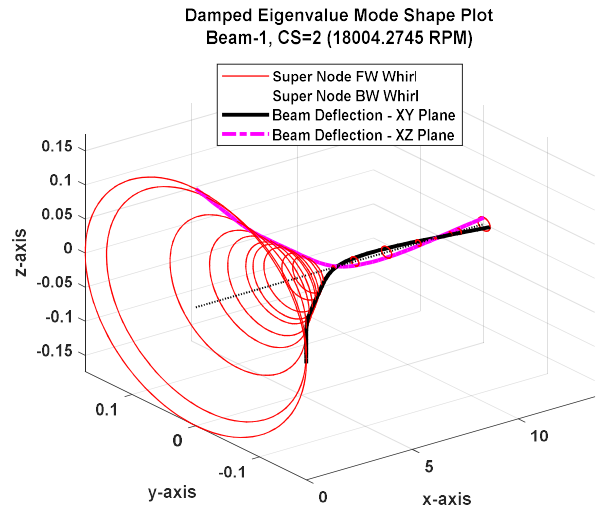
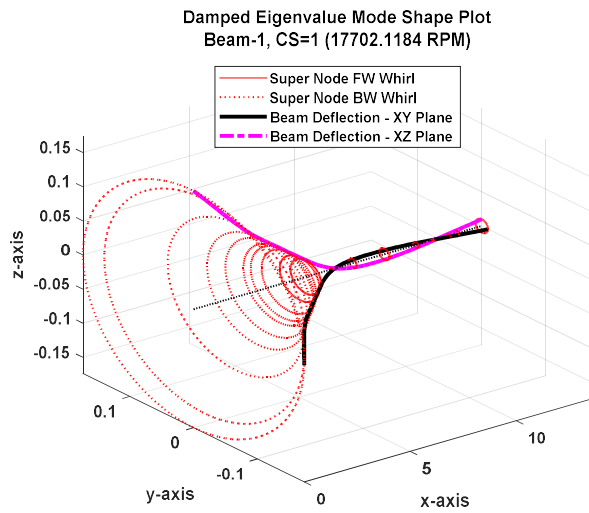


Figure App-M-3 Zorzi/Nelson – Damped Eigenvalue Mode Shape Plots – Undamped Case

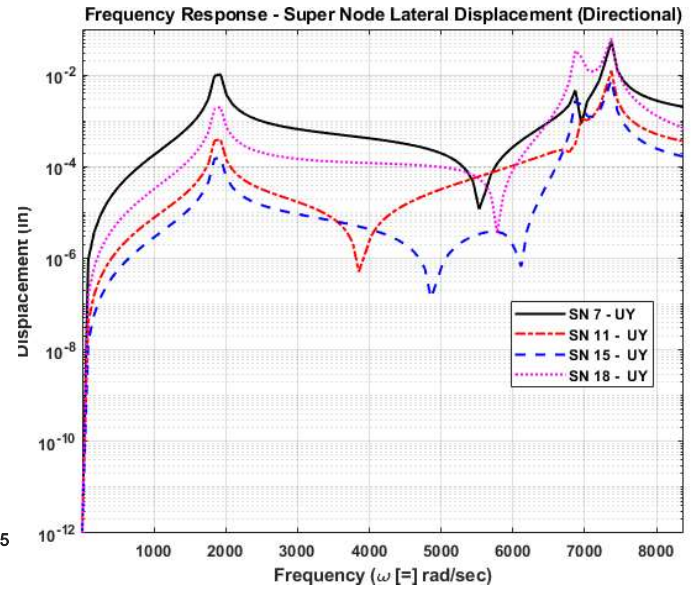
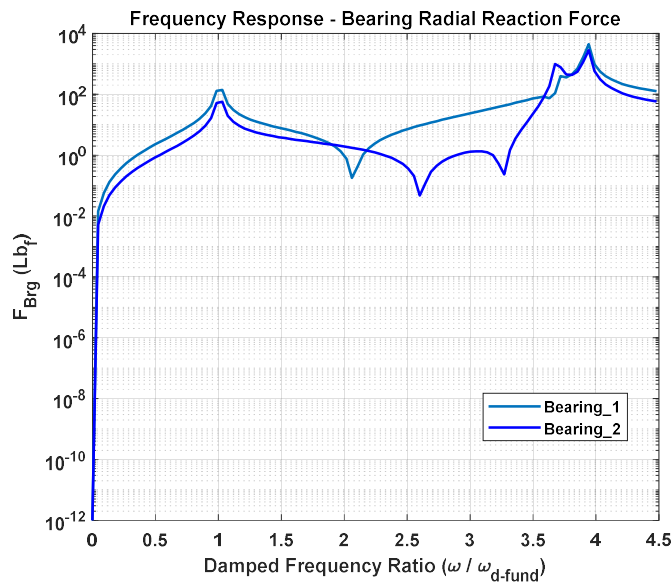


Figure App-M-4 Zorzi/Nelson – Frequency Response Plots – Undamped Case

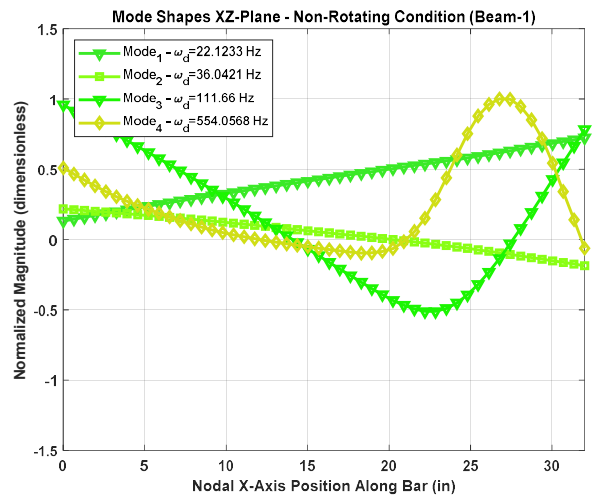
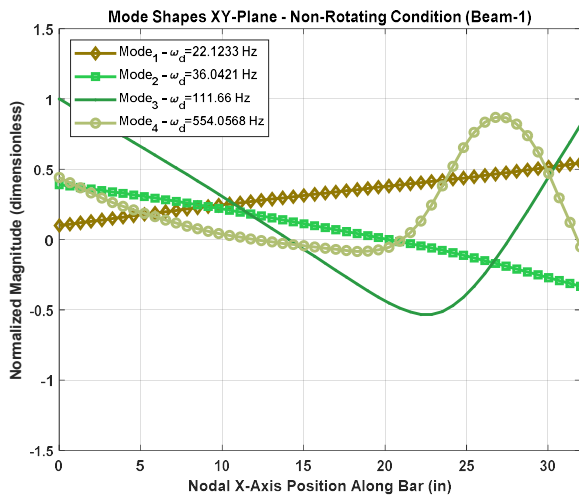


Figure App-M-5 Vance - Non-Rotating Mode Shapes – $k=1.751e6$ N/m

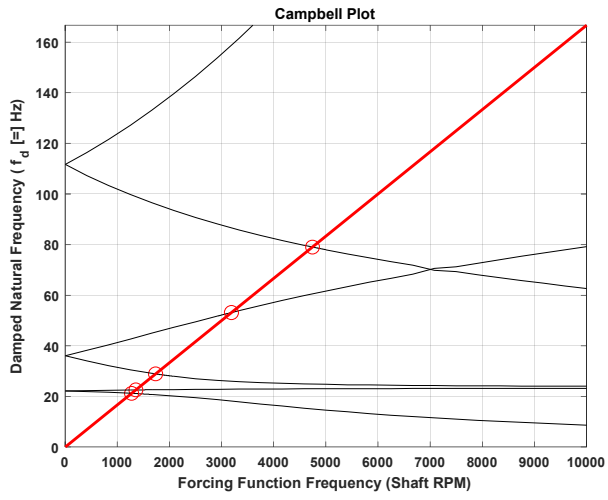


Figure App-M-6 Vance – Campbell Plot - $k=1.751e6$ N/m

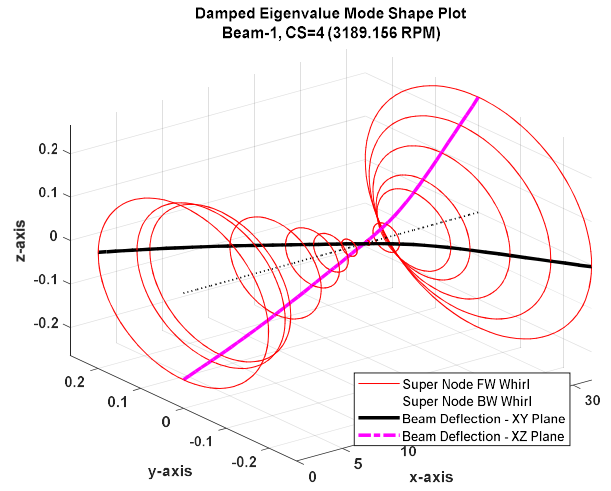
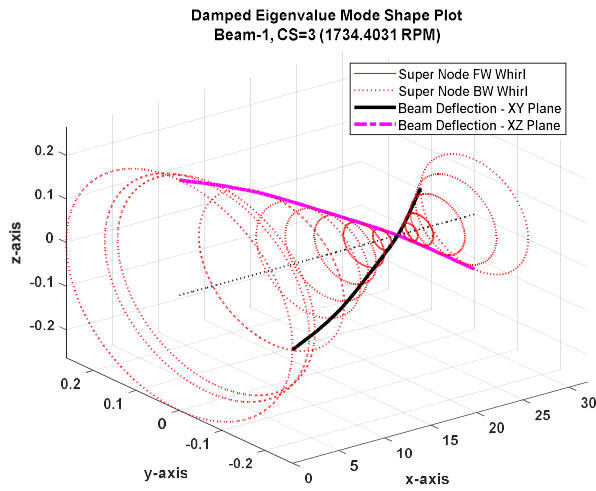
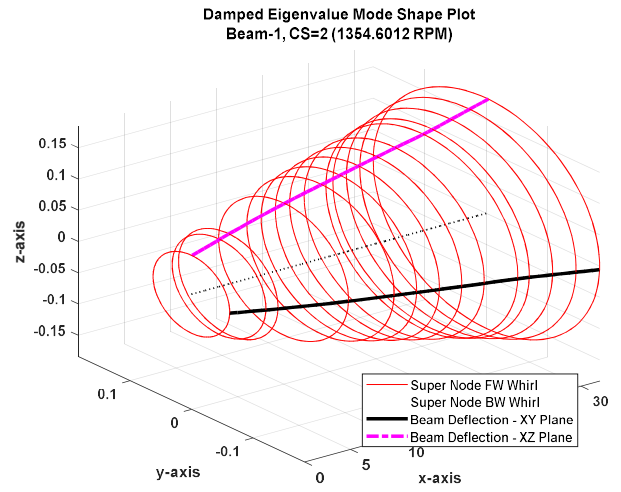
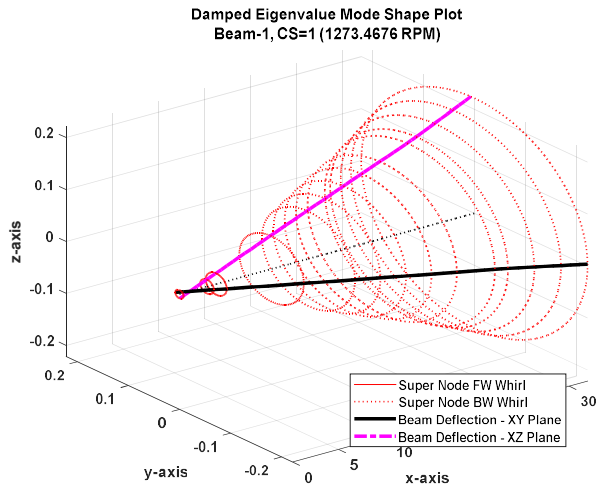


Figure App-M-7 Vance – Damped Eigenvalue Mode Shape Plots – $k=1.751e6$ N/m

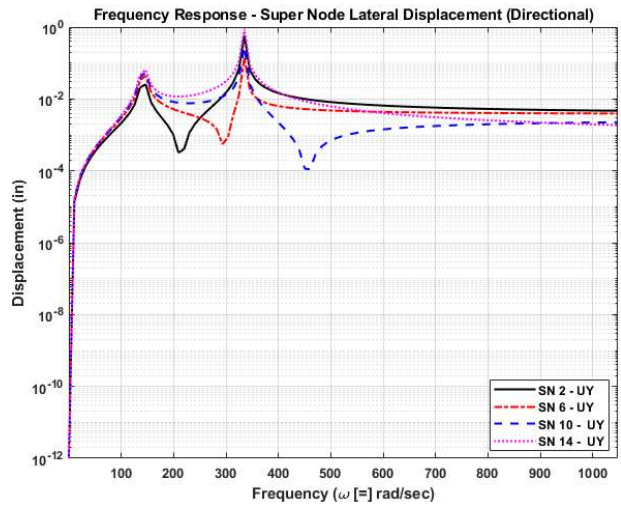
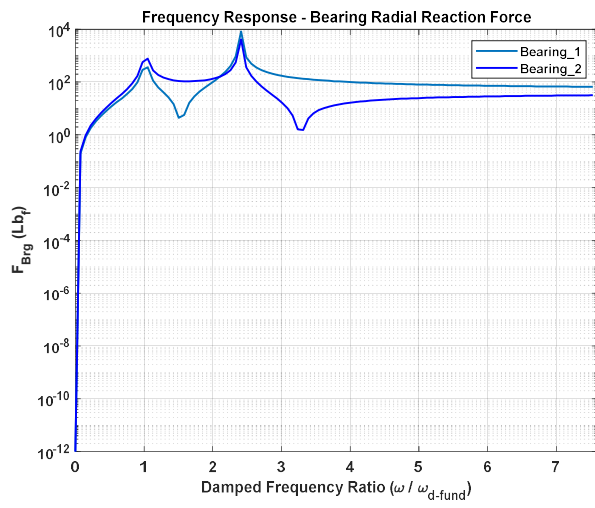


Figure App-M-8 Vance – Frequency Response Plots – $k=1.751e6$ N/m

Appendix N

Mode Shape Plots – Non-Isotropic Supports with Internal Material Damping

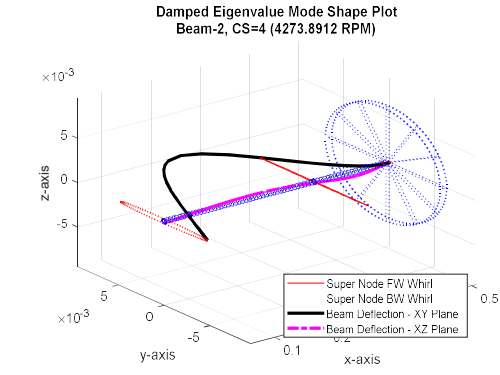
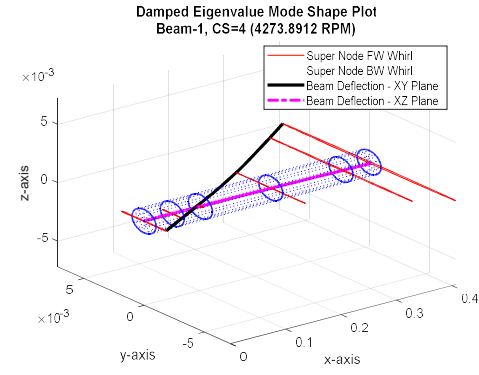
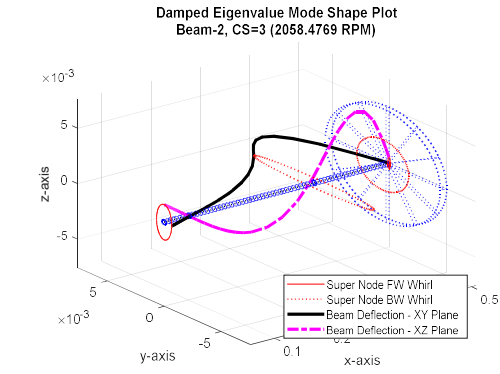
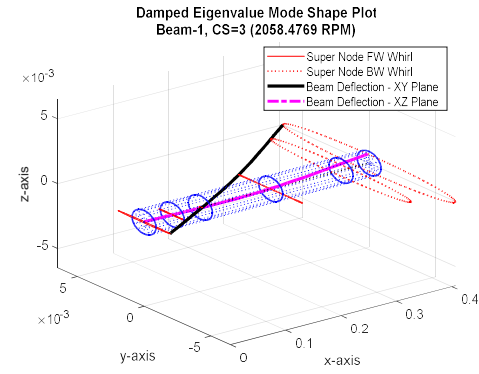
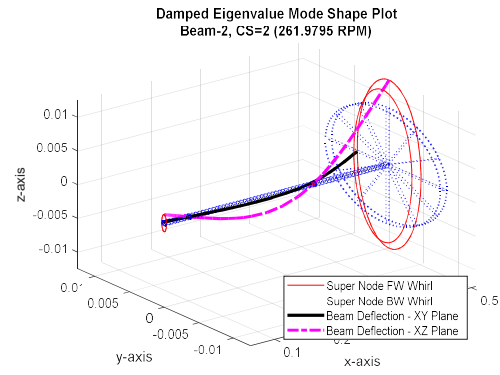
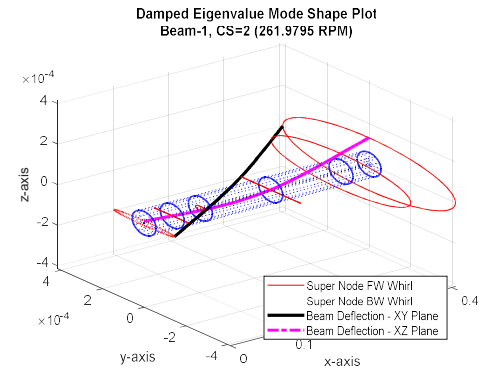
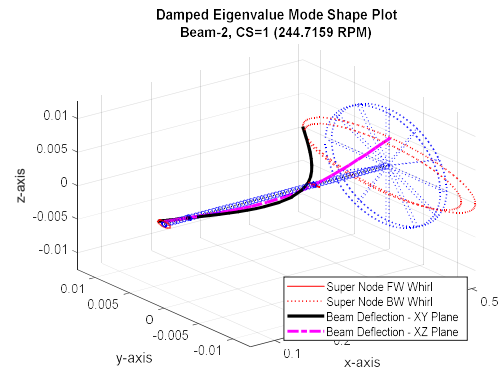
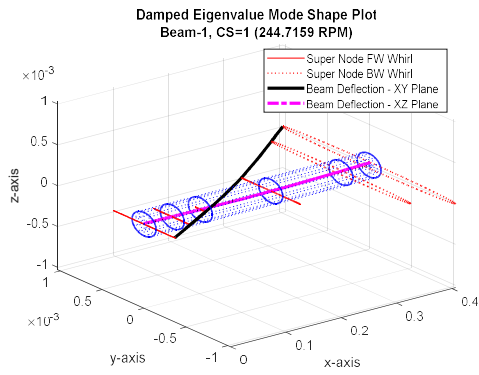


Figure App-N-1 Demonstration Mode Shape Plot – Starting Point 5

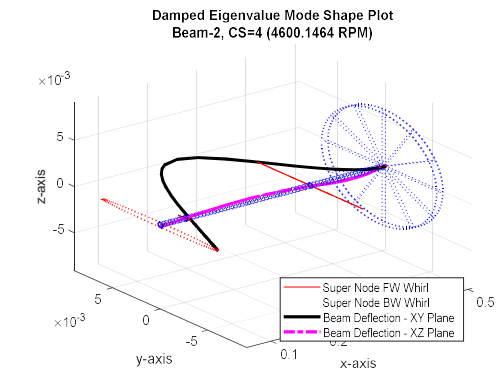
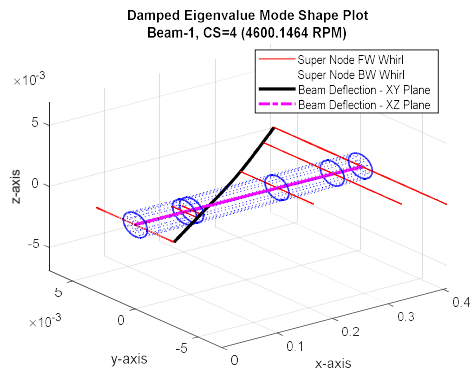
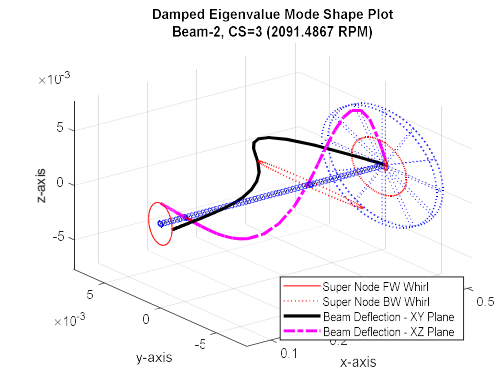
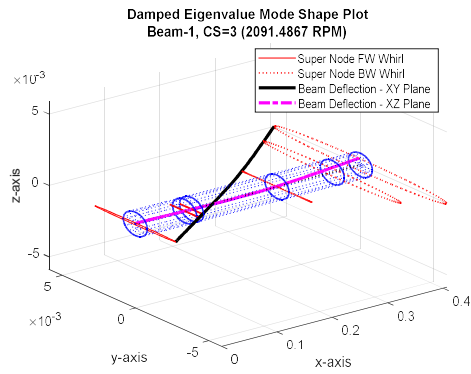
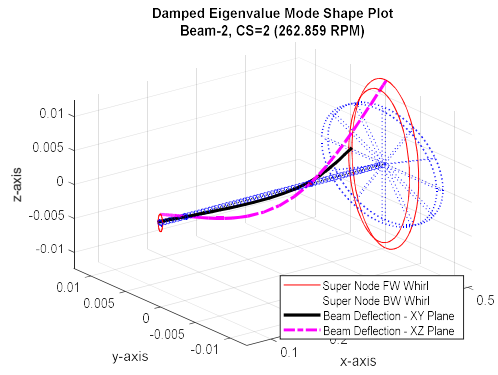
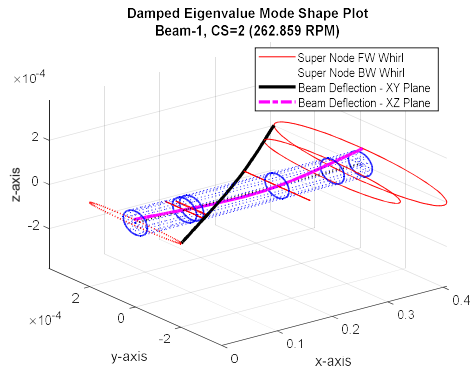
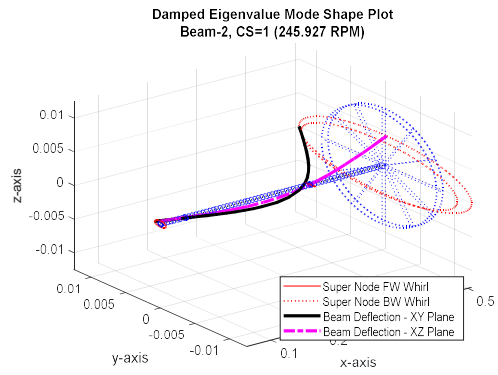
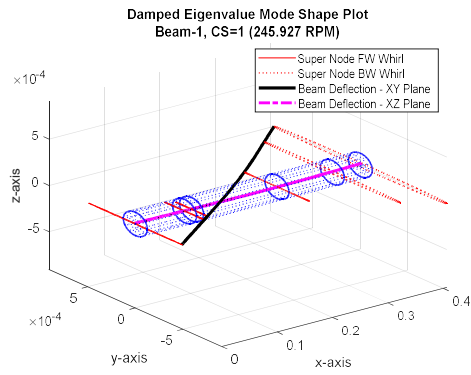


Figure App-N-2 Demonstration Mode Shape Plot – SFD Optimum

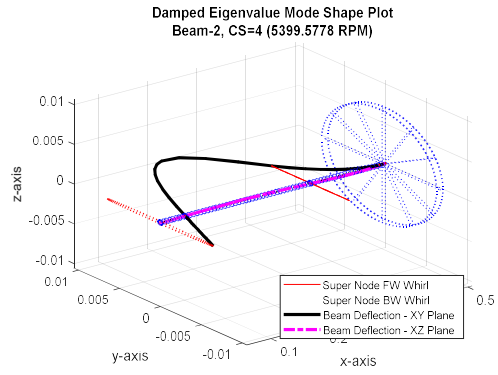
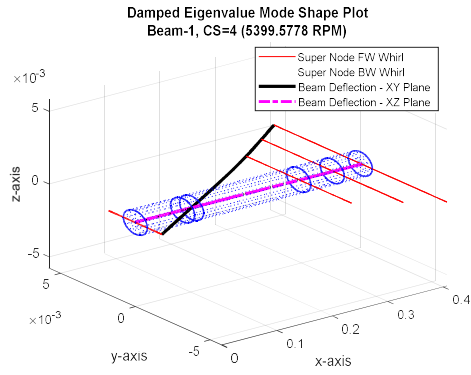
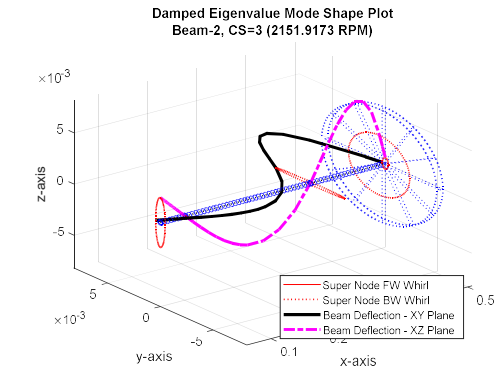
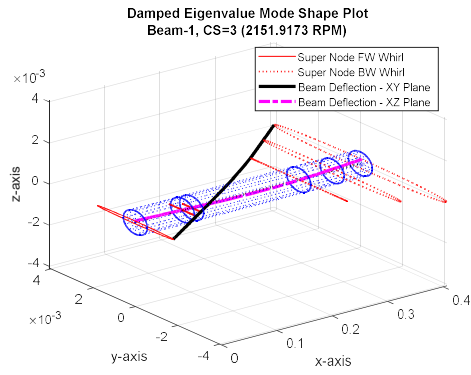
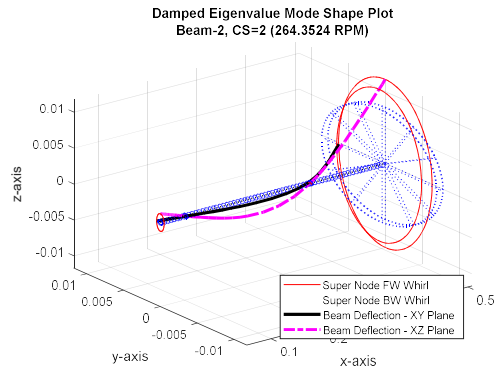
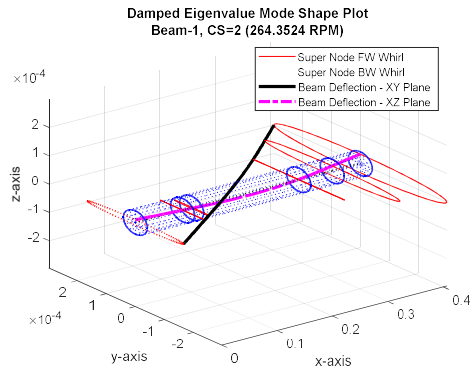
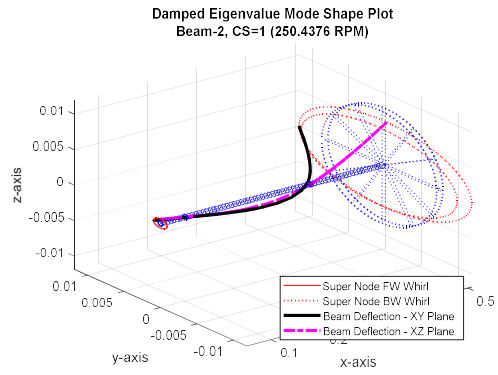
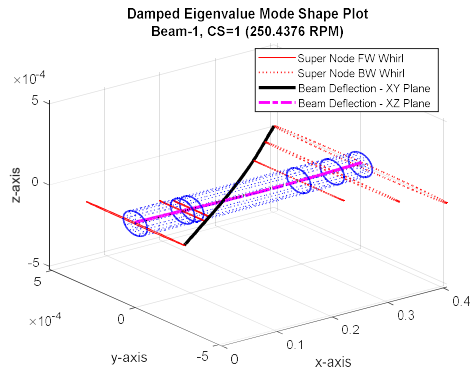


Figure App-N-3 Demonstration Mode Shape Plot – SQP Optimum

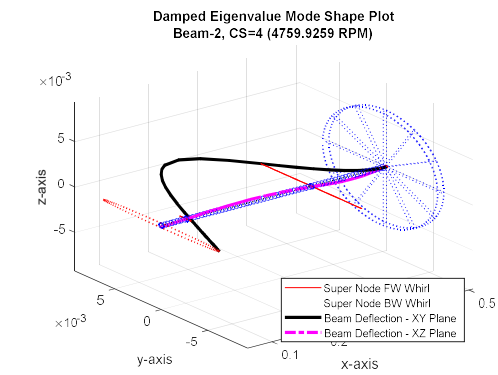
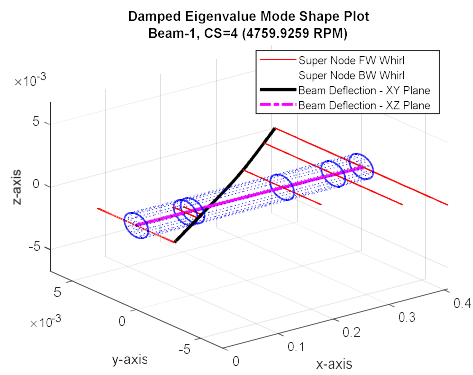
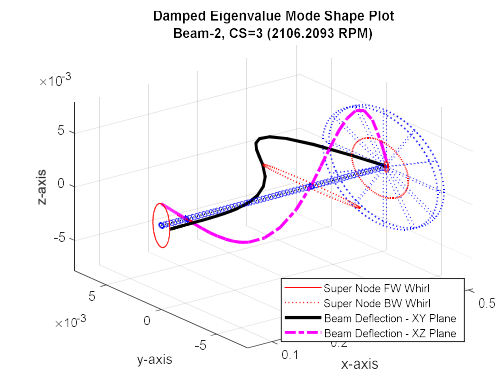
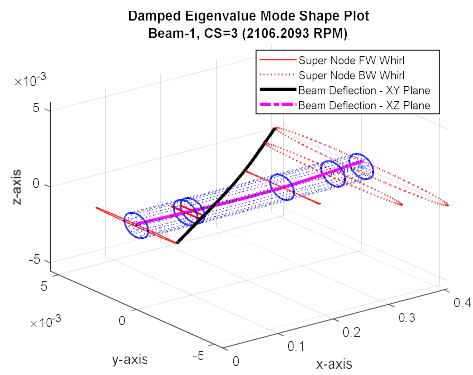
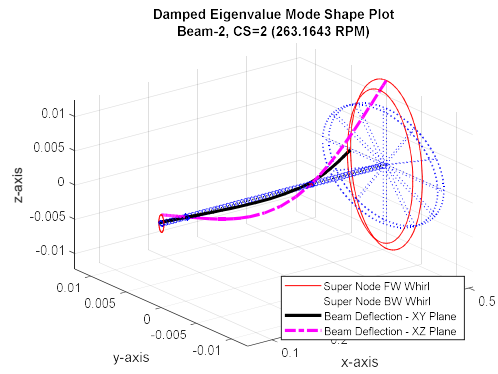
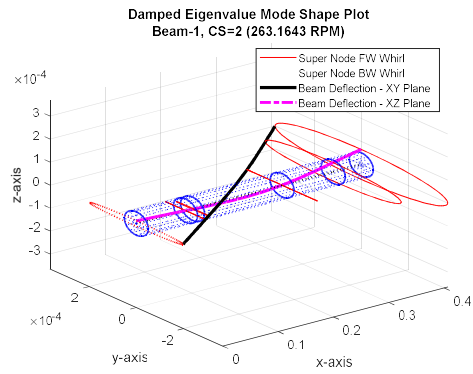
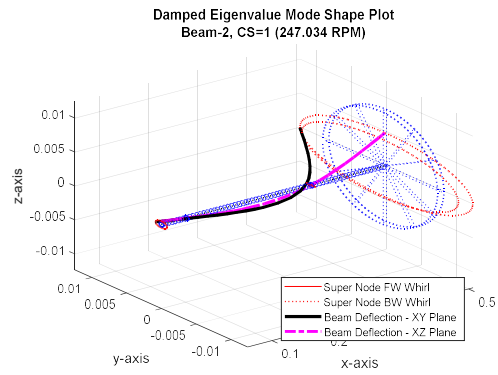
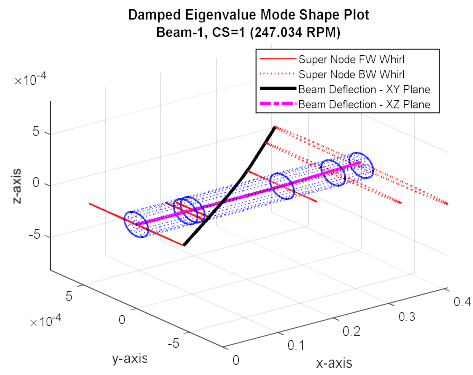


Figure App-N-4 Demonstration Mode Shape Plot – Hybrid (SFD+SQP) Optimum

Biographical Information

Mr. Hauser earned his B.S. in Mechanical Engineering at Texas A&M University in 1983. Since that time, he has worked in industry with focus on the design of complex machinery including gas compressors, engines and medical devices; returning to school to earn his M.S. in Mechanical Engineering from The University of Texas at Arlington in 2015. Key areas of interest relate to optimization of the design process and the development of methods to reduce both time and cost required to bring products to market while maximizing design quality. His continued part-time pursuits in academia to pursue a PhD in Mechanical Engineering are intended to further that effort.

References

-
- ¹ Vance, John M., Fouad Y. Zeidan, and Brian Murphy. Machinery vibration and rotordynamics. John Wiley & Sons, 2010.
 - ² Zu, Jean Wuzheng. "Self-adjoint and non-self-adjoint spinning Timoshenko beam systems." (1994).
 - ³ Lee, Chong-Won, et al. "MODAL-ANALYSIS OF A DISTRIBUTED PARAMETER ROTATING SHAFT." *Journal of Sound and Vibration* 122.1 (1988): 119-130.
 - ⁴ Lee, Chong-Won. "A complex modal testing theory for rotating machinery." *Mechanical Systems and Signal Processing* 5.2 (1991): 119-137.
 - ⁵ Ouisse, Morvan, and Emmanuel Foltête. "Experimental modal analysis of non-self-adjoint systems: inverse problem regularization." *Structural Dynamics*, Volume 3. Springer, New York, NY, 2011. 1251-1260.
 - ⁶ Jha, A. K., P. Dewangan, and M. Sarangi. "Model updating of rotor systems by using Nonlinear least square optimization." *Journal of Sound and Vibration* 373 (2016): 251-262.
 - ⁷ Dimarogonas, Andrew D. *Vibration for engineers*. Prentice Hall, 1996.
 - ⁸ Childs, Dara, and Dara W. Childs. *Turbomachinery rotordynamics: phenomena, modeling, and analysis*. John Wiley & Sons, 1993.
 - ⁹ Newkirk, B. L. "Shaft whipping due to oil action in journal bearings." *General Electric Review* 28 (1925): 559-568.
 - ¹⁰ Gunter Jr, Edgar J. "Dynamic stability of rotor-bearing systems." (1966).
 - ¹¹ Rankine, WJ Macquorn. "On the centrifugal force of rotating shafts." *Van Nostrand's Eclectic Engineering Magazine* (1869-1879) 1.7 (1869): 598.
 - ¹² Dunkerley, Stanley. "On the whirling and vibration of shafts." *Philosophical Transactions of the Royal Society of London*. A 185 (1894): 279-360.
 - ¹³ Stodola, Aurel. *Steam turbines*. Рипол Классик, 1905.
 - ¹⁴ Jeffcott, Henry Homan. "XXVII. The lateral vibration of loaded shafts in the neighbourhood of a whirling speed.—The effect of want of balance." *The London, Edinburgh, and Dublin Philosophical Magazine and Journal of Science* 37.219 (1919): 304-314.
 - ¹⁵ Yoon, Se Young, Zongli Lin, and Paul E. Allaire. *Control of surge in centrifugal compressors by active magnetic bearings: Theory and implementation*. Springer Science & Business Media, 2012.
 - ¹⁶ Bonfitto, Angelo, Andrea Tonoli, and Mario Silvagni. "Sensorless active magnetic dampers for the control of rotors." *Mechatronics* 47 (2017): 195-207.
 - ¹⁷ Lund, J. W. "Sensitivity of the Critical Speeds of a Rotor to Changes in the Design." *Journal of Mechanical Design* 102.1 (1980): 115-121.
 - ¹⁸ Rajan, M., et al. "Optimal placement of critical speeds in rotor-bearing systems." *Journal of vibration, acoustics, stress, and reliability in design* 109.2 (1987): 152-157.
 - ¹⁹ Huang, Shyh-Chin, and Chin-Ann Lin. "Sensitivity analysis and optimization of undamped rotor critical speeds to supports stiffness." *Journal of vibration and acoustics* 124.2 (2002): 296-301.
 - ²⁰ Liu, Shibing, and Bingen Yang. "Optimal Vibration Reduction of Flexible Rotor Systems by the Virtual Bearing Method." *Journal of Vibration and Acoustics* 140.2 (2018): 021008.
 - ²¹ Shiau, Ting Nung, and Jer Rong Chang. "Multiobjective Optimization of Rotor-Bearing System with Critical Speeds Constraints." *ASME 1991 International Gas Turbine and Aeroengine Congress and Exposition*. American Society of Mechanical Engineers, 1991.
 - ²² Lin, Chi-Wei, and Jay F. Tu. "Model-based design of motorized spindle systems to improve dynamic performance at high speeds." *Journal of Manufacturing Processes* 9.2 (2007): 94-108.
 - ²³ Tehrani, Ghasem Ghannad, and Morteza Dardel. "Vibration mitigation of a flexible bladed rotor dynamic system with passive dynamic absorbers." *Communications in Nonlinear Science and Numerical Simulation* 69 (2019): 1-30.
 - ²⁴ Taghipour, Javad, Morteza Dardel, and Mohammad Hadi Pashaei. "Vibration mitigation of a nonlinear rotor system with linear and nonlinear vibration absorbers." *Mechanism and Machine Theory* 128 (2018): 586-615.

-
- ²⁵ Tehrani, Ghasem Ghannad, and Morteza Dardel. "Mitigation of nonlinear oscillations of a Jeffcott rotor System with an optimized damper and nonlinear energy sink." *International Journal of Non-Linear Mechanics* 98 (2018): 122-136.
- ²⁶ Ribeiro, Eduardo Afonso, Jucélio Tomás Pereira, and Carlos Alberto Bavastri. "Passive vibration control in rotor dynamics: optimization of composed support using viscoelastic materials." *Journal of Sound and Vibration* 351 (2015): 43-56.
- ²⁷ Liu, Shibing, and Bingen Yang. "Optimal placement of water-lubricated rubber bearings for vibration reduction of flexible multistage rotor systems." *Journal of Sound and Vibration* 407 (2017): 332-349.
- ²⁸ Strauß, Frank, Mizuho Inagaki, and Jens Starke. "Reduction of vibration level in rotordynamics by design optimization." *Structural and Multidisciplinary Optimization* 34.2 (2007): 139-149.
- ²⁹ Srinivas, R. Siva, R. Tiwari, and Ch Kannababu. "Application of active magnetic bearings in flexible rotordynamic systems—A state-of-the-art review." *Mechanical Systems and Signal Processing* 106 (2018): 537-572.
- ³⁰ Srinivasan, Sriram, Eric H. Maslen, and Lloyd E. Barrett. "Optimization of bearing locations for rotor systems with magnetic bearings." *ASME 1995 International Gas Turbine and Aeroengine Congress and Exposition*. American Society of Mechanical Engineers, 1995.
- ³¹ Tonoli, A., Amati, N., Bonfitto, A., Silvagni, M., Staples, B., & Karpenko, E. "Design of electromagnetic dampers for aero-engine applications." *Journal of engineering for gas turbines and power* 132.11 (2010): 112501.
- ³² Yao, Hongliang, Zidong Chen, and Bangchun Wen. "Dynamic vibration absorber with negative stiffness for rotor system." *Shock and Vibration* 2016 (2016).
- ³³ Shi, Xiang, and Songye Zhu. "Magnetic negative stiffness dampers." *Smart Materials and Structures* 24.7 (2015): 072002.
- ³⁴ Platus, David L. "Negative-stiffness-mechanism vibration isolation systems." *Vibration Control in Microelectronics, Optics, and Metrology*. Vol. 1619. International Society for Optics and Photonics, 1992.
- ³⁵ Correa, Dixon M., Carolyn Conner Seepersad, and Michael R. Haberman. "Mechanical design of negative stiffness honeycomb materials." *Integrating Materials and Manufacturing Innovation* 4.1 (2015): 10.
- ³⁶ Untaroiu, Costin D., Paul E. Allaire, and William C. Foiles. "Balancing of flexible rotors using convex optimization techniques: optimum min-max LMI influence coefficient balancing." *Journal of Vibration and Acoustics* 130.2 (2008): 021006.
- ³⁷ Helfrich, Reinhard, and Nils Wagner. "Application of optimization methods in rotor dynamics." *Proceedings of the 9th IFToMM International Conference on Rotor Dynamics*. Springer, Cham, 2015.
- ³⁸ Deep, Kusum, et al. "A real coded genetic algorithm for solving integer and mixed integer optimization problems." *Applied Mathematics and Computation* 212.2 (2009): 505-518.
- ³⁹ Chelouah, Rachid, and Patrick Siarry. "Genetic and Nelder–Mead algorithms hybridized for a more accurate global optimization of continuous multimimima functions." *European Journal of Operational Research* 148.2 (2003): 335-348.
- ⁴⁰ Fan, Shu-Kai S., Yun-Chia Liang, and Erwie Zahara. "A genetic algorithm and a particle swarm optimizer hybridized with Nelder–Mead simplex search." *Computers & industrial engineering* 50.4 (2006): 401-425.
- ⁴¹ Kao, Yi-Tung, and Erwie Zahara. "A hybrid genetic algorithm and particle swarm optimization for multimodal functions." *Applied Soft Computing* 8.2 (2008): 849-857.
- ⁴² Huang, Jingjing, Longxi Zheng, and Qing Mei. "Design and optimization method of a two-disk rotor system." *International Journal of Turbo & Jet-Engines* 33.1 (2016): 1-8.
- ⁴³ Bettebghor, D., Blondeau, C., Toal, D., & Eres, H. (2013). Bi-objective optimization of pylon-engine-nacelle assembly: weight vs. tip clearance criterion. *Structural and Multidisciplinary Optimization*, 48(3), 637-652.
- ⁴⁴ Marler, R. T., & Arora, J. S. (2010). The weighted sum method for multi-objective optimization: new insights. *Structural and multidisciplinary optimization*, 41(6), 853-862.
- ⁴⁵ Chen, Ting-Yu, and Bo Ping Wang. "Optimum design of rotor-bearing systems with eigenvalue constraints." *ASME 1992 International Gas Turbine and Aeroengine Congress and Exposition*. American Society of Mechanical Engineers, 1992.
- ⁴⁶ Svanberg, Krister. "The method of moving asymptotes—a new method for structural optimization." *International journal for numerical methods in engineering* 24.2 (1987): 359-373.
- ⁴⁷ Pugachev, Alexander O. "Application of gradient-based optimization methods for a rotor system with static stress, natural frequency, and harmonic response constraints." *Structural and Multidisciplinary Optimization* 47.6 (2013): 951-962.

-
- ⁴⁸ Pugachev, A. O., Sheremetyev, A. V., Tykhomirov, V. V., Shpilenko, O. I. "Structural Dynamics Optimization of Rotor Systems for a Small-Size Turboprop Engine." *Journal of Propulsion and Power* 31.4 (2015): 1083-1093.
- ⁴⁹ Longxi, Zheng, Jia Shengxi, and Huang Jingjing. "Numerical and Experimental Study on the Multiobjective Optimization of a Two-Disk Flexible Rotor System." *International Journal of Rotating Machinery* 2017 (2017).
- ⁵⁰ Lin, Y., L. Cheng, and T. P. Huang. "Optimal design of complex flexible rotor-support systems using minimum strain energy under multi-constraint conditions." *Journal of Sound and Vibration* 215.5 (1998): 1121-1134.
- ⁵¹ Palazzolo, A. B., Bo Ping Wang, and W. D. Pilkey. "Eigensolution reanalysis of rotor dynamic systems by the generalized receptance method." ASME 1982 International Gas Turbine Conference and Exhibit. American Society of Mechanical Engineers, 1982.
- ⁵² Palazzolo, Alan B., Bo Ping Wang, and Walter D. Pilkey. "A receptance formula for general second-degree square lambda matrices." *International Journal for Numerical Methods in Engineering* 18.6 (1982): 829-843.
- ⁵³ Shan, Songqing, and G. Gary Wang. "Survey of modeling and optimization strategies to solve high-dimensional design problems with computationally-expensive black-box functions." *Structural and Multidisciplinary Optimization* 41.2 (2010): 219-241.
- ⁵⁴ Bandler, J. W., Biernacki, R. M., Chen, S. H., Grobelny, P. A., Hemmers, R. H. "Space mapping technique for electromagnetic optimization." *IEEE Transactions on Microwave Theory and Techniques* 42.12 (1994): 2536-2544.
- ⁵⁵ Vanderplaats G (2007) *Multidiscipline Design Optimization*, 1st Edition, Vanderplaats Research and Development Inc.
- ⁵⁶ Fliege J, Svaiter B (2000) Steepest descent methods for multicriteria optimization, *Mathematical Methods of Operations Research*, Vol. 51, No. 3, 479-494.
- ⁵⁷ Zoutendijk, Guus. *Methods of feasible directions: a study in linear and non-linear programming*. Elsevier, 1960.
- ⁵⁸ Banks A, Vincent J, Anyakoha C (2007), A review of particle swarm optimization. Part I: background and development, *Natural Computing* Vol. 6, Issue 4, 467-484
- ⁵⁹ Vesterström J, Thomsen R (2004), A comparative study of differential evolution, particle swarm optimization, and evolutionary algorithms on numerical benchmark problems, *Evolutionary Computation*, CEC2004, Vol. 2, 1980-1987
- ⁶⁰ Laskari E, Parsopoulos K, Vrahatis M (2004) Particle swarm optimization for minimax problems, *Evolutionary Computation* CEC2002, Vol. 2, 1980-1987.
- ⁶¹ Hauser, Bret R., and Bo P. Wang. "Optimal design of a parallel beam system with elastic supports to minimize flexural response to harmonic loading using a combined optimization algorithm." *Structural and Multidisciplinary Optimization* 58.4 (2018): 1453-1465.
- ⁶² Stocki, R., et al. "Robust design optimization of the vibrating rotor-shaft system subjected to selected dynamic constraints." *Mechanical systems and signal processing* 29 (2012): 34-44.
- ⁶³ Hong, Sangwon, et al. "Reliability-based design optimization of axial compressor using uncertainty model for stall margin." *Journal of mechanical science and technology* 25.3 (2011): 731-740.
- ⁶⁴ Lian, Yongsheng, and Nam-Ho Kim. "Reliability-based design optimization of a transonic compressor." *AIAA journal* 44.2 (2006): 368-375.
- ⁶⁵ Su, Changqing, et al. "Reliability sensitivity estimation of rotor system with oil whip and resonance." *Advances in Mechanical Engineering* 9.6 (2017): 1687814017702809.
- ⁶⁶ Kumar, D. (2016). Rotordynamic analysis using 3d elements in fixed and rotating reference frame. ASME 2016 International Mechanical Engineering Congress and Exposition. American Society of Mechanical Engineers. pp. V001T03A017-V001T03A017
- ⁶⁷ Bazoune, A., Y. A. Khulief, and N. G. Stephen. "Shape functions of three-dimensional Timoshenko beam element." (2003): 473-480.
- ⁶⁸ Robert, D. Cook, et al. "Concepts and applications of finite element analysis." John Wiley & Sons Inc (2002), pg 84.
- ⁶⁹ Nelson, H. D. "A finite rotating shaft element using Timoshenko beam theory." *Journal of mechanical design* 102.4 (1980): 793-803.
- ⁷⁰ Mindlin, R. D., and H. Deresiewicz. Timoshenko's shear coefficient for flexural vibrations of beams. No. TR-10. COLUMBIA UNIV NEW YORK, 1953.
- ⁷¹ Rouch, K. E., and J-S. Kao. "A tapered beam finite element for rotor dynamics analysis." *Journal of Sound and Vibration* 66.1 (1979): 119-140.
- ⁷² Labuschagne, Anneke, NF Janse van Rensburg, and A. J. Van der Merwe. "Comparison of linear beam theories." *Mathematical and Computer Modelling* 49.1 (2009): 20-~~24~~9

-
- ⁷³ Dong, S. B., C. Alpdogan, and E. Taciroglu. "Much ado about shear correction factors in Timoshenko beam theory." *International Journal of Solids and Structures* 47.13 (2010): 1651-1665.
- ⁷⁴ Cowper, G. R. "The shear coefficient in Timoshenko's beam theory." ASME, 1966.
- ⁷⁵ Hutchinson, J. R. "Shear coefficients for Timoshenko beam theory." *TRANSACTIONS-AMERICAN SOCIETY OF MECHANICAL ENGINEERS JOURNAL OF APPLIED MECHANICS* 68.1 (2001): 87-92.
- ⁷⁶ Greenhill, L. M., W. B. Bickford, and H. D. Nelson. "A conical beam finite element for rotor dynamics analysis." *Journal of Vibration, Acoustics, Stress, and Reliability in Design* 107.4 (1985): 421-430.
- ⁷⁷ Nelson, H. D., and J. M. McVaugh. "The dynamics of rotor-bearing systems using finite elements." *Journal of Engineering for Industry* 98.2 (1976): 593-600.
- ⁷⁸ Choi, S. H., C. Pierre, and A. G. Ulsoy. "Consistent modeling of rotating Timoshenko shafts subject to axial loads." *Journal of vibration and acoustics* 114.2 (1992): 249-259.
- ⁷⁹ Zorzi, E. S., and H. D. Nelson. "Finite element simulation of rotor-bearing systems with internal damping." *Journal of Engineering for Power* 99.1 (1977): 71-76.
- ⁸⁰ Logan, D. L. "A First Course in the Finite Element Method, Thomson." Toronto, ON (2007).
- ⁸¹ Przemieniecki, Janusz S. *Theory of matrix structural analysis*. Courier Corporation, 1985
- ⁸² Schwibinger, P., and R. Nordmann. "Influence of torsional-lateral coupling on stability behavior of geared rotor systems." (1987).
- ⁸³ Hariharan, Parasuraman, and Dara W. Childs. "Solving problems in dynamics and vibrations using MATLAB." Department of Mechanical Engineering Texas A & M University College Station (2014): 11-21.
- ⁸⁴ Hauser, Bret R. "Optimal Design of a Parallel Beam System with Elastic Supports to Minimize Flexural Response to Harmonic Loading." (2015).
- ⁸⁵ Hauser, Bret R., and Bo P. Wang. "Design optimization of a rotordynamic beam system with elastic supports to minimize flexural responses using a combined optimization algorithm." *Structural and Multidisciplinary Optimization* 58.4 (2019): 1453-1465.
- ⁸⁶ Maute, K., Nikbay, M., & Farhat, C. (2003). Sensitivity analysis and design optimization of three-dimensional non-linear aeroelastic systems by the adjoint method. *International Journal for Numerical Methods in Engineering*, 56(6), 911-933.
- ⁸⁷ Hall, M. C., Cacuci, D. G., & Schlesinger, M. E. (1982). Sensitivity analysis of a radiative-convective model by the adjoint method. *Journal of the Atmospheric Sciences*, 39(9), 2038-2050.
- ⁸⁸ Martins, J. R., Alonso, J. J., & Reuther, J. J. (2005). A coupled-adjoint sensitivity analysis method for high-fidelity aero-structural design. *Optimization and Engineering*, 6(1), 33-62.
- ⁸⁹ Othmer, C. (2014). Adjoint methods for car aerodynamics. *Journal of Mathematics in Industry*, 4(1), 6.
- ⁹⁰ Chen, T. Y., & Chi, T. M. (2010). On the improvements of the particle swarm optimization algorithm. *Advances in Engineering Software*, 41(2), 229-239.
- ⁹¹ Shahbazi, K. (2005). An explicit expression for the penalty parameter of the interior penalty method. *Journal of Computational Physics*, 205(2), 401-407.
- ⁹² Kosmatka, J. B. "An improved two-node finite element for stability and natural frequencies of axial-loaded Timoshenko beams." *Computers & Structures* 57.1 (1995): 141-149.
- ⁹³ Bazoune, A., and Y. A. Khulief. "A finite beam element for vibration analysis of rotating tapered Timoshenko beams." *Journal of Sound and Vibration* 156.1 (1992): 141-164.
- ⁹⁴ Yokoyama, T. "Free vibration characteristics of rotating Timoshenko beams." *International Journal of Mechanical Sciences* 30.10 (1988): 743-755.
- ⁹⁵ Friedman, Z., and John B. Kosmatka. "An improved two-node Timoshenko beam finite element." *Computers & structures* 47.3 (1993): 473-481.
- ⁹⁶ Blevins, Robert D., and R. Plunkett. "Formulas for natural frequency and mode shape." *Journal of Applied Mechanics* 47 (1980): 461.
- ⁹⁷ Chen, S. S. (2016) Constrained Particle Swarm Optimization, v1.31.4, BSD License Copyright ©. <https://www.mathworks.com/matlabcentral/fileexchange/25986-constrained-particle-swarm-optimization>
- ⁹⁸ Orban, F. "Damping of materials and members in structures." *Journal of Physics: Conference Series*. Vol. 268. No. 1. IOP Publishing, 2011.